



<https://theses.gla.ac.uk/>

Theses Digitisation:

<https://www.gla.ac.uk/myglasgow/research/enlighten/theses/digitisation/>

This is a digitised version of the original print thesis.

Copyright and moral rights for this work are retained by the author

A copy can be downloaded for personal non-commercial research or study,
without prior permission or charge

This work cannot be reproduced or quoted extensively from without first
obtaining permission in writing from the author

The content must not be changed in any way or sold commercially in any
format or medium without the formal permission of the author

When referring to this work, full bibliographic details including the author,
title, awarding institution and date of the thesis must be given

Enlighten: Theses

<https://theses.gla.ac.uk/>
research-enlighten@glasgow.ac.uk

PHOTOPOLARIMETRIC ANALYSIS

OF EARLY-TYPE STARS

by

Paul A. McGale, B.Sc.

Thesis

submitted to the

University of Glasgow

for the degree of

Ph.D.

ProQuest Number: 10991888

All rights reserved

INFORMATION TO ALL USERS

The quality of this reproduction is dependent upon the quality of the copy submitted.

In the unlikely event that the author did not send a complete manuscript and there are missing pages, these will be noted. Also, if material had to be removed, a note will indicate the deletion.



ProQuest 10991888

Published by ProQuest LLC (2018). Copyright of the Dissertation is held by the Author.

All rights reserved.

This work is protected against unauthorized copying under Title 17, United States Code
Microform Edition © ProQuest LLC.

ProQuest LLC.
789 East Eisenhower Parkway
P.O. Box 1346
Ann Arbor, MI 48106 – 1346

All things began in order, so shall they end, and so shall they begin again; according to the ordaines of order and mystical mathematics of the city of heaven.

- Sir Thomas Browne

Only when the form is quite clear to you will the spirit become clear to you.

- Robert Schumann

Everything is the sum of the past and nothing is comprehensible except through its history.

- Teilhard de Chardin

Music, whatever sound and structure it may assume, remains meaningless noise unless it touches a receiving mind.

- Paul Hindemith

PREFACE

Very recently it has been noticed that whenever a Be star has been photometrically well observed, the light curves seem to exhibit a double wave form with unequal maxima and/or minima. The minima of these light curves are often found not to be symmetrically spaced in phase. Usually it is spectrometry and photometry that are engaged in the modelling of such phenomena. The major proposal of this thesis is that these light curves are caused by a co-rotating light scattering atmospheric bulge controlled or created in some way by a magnetic field. Such a scenario produces a phase dependent polarization. A canonical model is causally developed leading to the second proposal that polarimetry is more important than photometry and should be lifted from the backyard of techniques and given a more central role.

The numerous new procedures designed here for analysing polarimetric data in terms of the proposed model show that indeed polarimetry is a very powerful diagnostic tool, leading to information on stellar inclination, periodicity, co-latitude of the scattering bulge and its optical depth, and the sense of rotation.

The availability of measurements for model adoption (i.e. the combination of polarimetric, photometric and magnetometric data) was found to be unfortunately rather limited, but it does thus give exciting scope for observational programs.

The work of this thesis was carried out in co-operation with Dr. D. Clarke.

The contents of the chapters are as follows, the original work appearing in Chapters 2, 3 and 4.

Chapter 1: Introduction to the phenomenon of the Be stars and a review of typical papers concerning the polarimetry of early-type stars.

Chapter 2: Review and enhancement of techniques for variability searching. Construction of a simple polarimetric point source/point

scattering stochastic model extendable to periodicity. Development of several new analytical techniques for use in the application of the model to polarimetric data.

Chapter 3: Searching for fluctuations in the polarization of several Be stars. Assiduous study of data relating to X Persei and σ Ori E in terms of the scattering bulge model.

Chapter 4: Comparison of a photospheric spot and extended but localized scattering region model to extensive UBV data on EM Cep.

Chapter 5: Conclusions of the thesis and suggestions for future work.

Where extended mathematical proofs are required the facility of an appendix has been invoked. Several FORTRAN77 programs were developed to carry out model fitting to data and listings of some of them appear in Appendix E. When these programs were used it was assumed that they were error free, even although extensive debugging procedures were carried out.

At the time of writing three of the chapters have produced four completed papers (authors Clarke and McGale):

Temporal Polarization Variations of Be Stars

- I. Models Based on Stochastic Behaviour, Astron. and Astrophys. (in press) (1986a)
- II. Model Fitting of Polarimetric Data, Astron. and Astrophys. (accepted) (1986b)
- III. The Polarimetric Behaviour of X Persei, Astron. and Astrophys. (submitted) (1986c)

Double Periodicity in Be Stars. IAU Coll. 92 "Physics of Be Stars" (in press) (1986d)

I wish to extend thanks to Professor A. E. Roy for the use of the facilities of the Department of Astronomy which, in the last few weeks, has become the Department of Physics and Astronomy. The friendliness of the Department's members through both my undergraduate and

postgraduate years have helped make my stay an enjoyable and rememberable one. Thanks are particularly directed towards the personnel, past and present, of the University Observatory (Dr. Brian G. Stewart, Mr. W. Edgar and Mr. R. Loney) for their general friendship, and finally to Mrs. Margaret Morris for her by no means minor contributions towards the technical aspects of the thesis production and her immaculate typing of it.

In the true theatrical tradition the best is kept till last. The subject of the thesis was suggested by Dr. D. Clarke and his constant enthusiasm was a sustaining influence. It is a pleasure to acknowledge his assistance.

During the period of this work I was supported by a S.E.R.C. studentship grant.

Paul A. McGale

30 September 1986

University of Glasgow

C O N T E N T S

Preface	i
Summary	iv
<u>Chapter 1</u> - INTRODUCTION	
1.1 About Be Stars	2
1.2 Scope of Variability	4
1.3 Polarimetry of Early-Type Stars	5
1.4 Relating Polarimetry and Photometry	9
1.5 Aim	10
<u>Chapter 2</u> - DETECTING POLARIMETRIC VARIATIONS, STOCHASTIC POLARIMETRIC MODELS AND THEIR FITTING TO DATA	
2.1 Preamble Regarding Polarimetric Variations	12
2.2 Normality Testing	13
2.3 Regression/Correlation	16
2.4 Welch Testing	17
2.5 The Search for Variability	18
2.6 Preamble on Models Based on Stochastic Behaviour	19
2.7 The Model Geometry	20
2.8 A Preliminary Exploration of Possible Polarimetric Variations	23
(a) Equatorial Break-up	24
(b) Oblique Rotator	24
2.9 Geometry Assessment Based on Random Observations	26
(a) The Truly Random Model	26
(b) Restricted Models with Random Globules	27
(c) <i>Ad Hoc</i> Restricted Models	28
2.10 Preamble to Model Fitting of Polarimetric Data	29
2.11 Further on the Model Equations	31
2.12 Data Reduction Procedures	33
2.13 The q , u Density Distribution	35
(a) Investigation by Taking Moments	35
(b) Chi-Square Testing	40
2.14 Polarimetric Periodicities	42
(a) Introduction	42
(b) Application of Fourier Coefficients	43
(c) Correlation of the Polarization Position Angle	46
(d) Correlation of the Sign of u	47
2.15 Postamble	49
<u>Chapter 3</u> - ANALYSIS OF SOME POLARIMETRIC DATA	
3.1 Introduction	52
3.2 Reduction of η Cep, β Cas, 55 Cyg, γ Cas and ζ Tau Data	52
3.3 Reduction of β Vir, 2H Cam and 28 ω CMa Data	59
3.4 The Polarimetric Behaviour of X Persei	64
(a) Introduction	64
(b) A Cursory View of the Data and Model Inference	66

CONTENTS, continued ..

(c)	Analysis of the Data Density Distribution	69
(d)	The Short-Term Temporal Changes	72
(e)	Investigation of Periodicities	73
(f)	Determination of the Rotation Period	76
(g)	Concluding Discussion	80
3.5	A Comment on the Polarimetry of HDE 226868	84
3.6	The Polarimetric Behaviour of σ Ori E	86
(a)	Introduction	86
(b)	The Measurements	88
(c)	Analysis of the Data	89
(d)	Conclusions	92

Chapter 4 - ASPECTS OF PHOTOMETRY

4.1	Introduction	97
4.2	Model Geometries	99
4.3	The Photometric Behaviour of EM Cep	103
(a)	Introduction	103
(b)	Fitting the Photospheric Spot Model	104
(c)	Fitting the Scattering Oblique Rotator Model	106
(d)	Conclusion	107

Chapter 5 - CONCLUSIONS

5.1	Conclusions	110
5.2	Suggestions for Future Work and Discussion	111

Appendices

A	Correlation Coefficient Percentage Levels	114
B	Moments	123
C	Least Squares Treatment of a Co-Rotating Globule	129
D	Polarimetric Data on HDE 226868 and σ Ori E	140
E	Two FORTRAN77 Program Listings	146

<u>References</u>	154
-------------------	-----

SUMMARY

Over the past few years it has been shown that some (single) early-type stars display polarimetric variability, with the data distributed in the normalized Stokes plane above the usual experimental noise. Presently, in this thesis, a simple point source/point scattering model is developed, which can mimic these distributions. It is found that they should always exhibit at least one axis of symmetry, this being the projection of the stellar equatorial plane onto the sky. In addition the model is extended to involve the effects of stellar rotation and schemes are proposed for investigating the underlying loci in the distributions which lead to determination of stellar periods.

Polarimetric data for particular stars are not always plentiful and may not be suitable for full model application. Plotting of data in the (q, u) plane may prove to be informative, compared to more common polarization, time and position angle, time presentations, for cursory inspection in the light of differing shapes of loci expected from particular scattering geometries. After consideration of instrumental stability by investigation of standard stars, various tests can be applied, normality, regression/correlation, and Welch, to search simply for fluctuations within the polarimetric data.

When measurements prove to be extensive enough for model adoption, special procedures are needed, and indeed various approaches are developed. Data can be treated as a density distribution if it is thought that the polarigenic mechanism is random in local stellar azimuth or just that the nature of the observational sampling has induced a resultant randomness.

The method of moments allows for correction of instrumental noise and, after consideration of any possible interstellar contribution, enables the stellar inclination to be estimated depending on the angle at which the direction of maximum data spread occurs to the equatorial

line, i.e. the line that joins the centre of gravity of the measurements to the tip of the interstellar vector. If this direction is parallel to the equatorial line, equatorial localized events are inferred and if perpendicular then the scattering takes place at polar latitudes of the star under study.

A Chi-square test in conjunction with Monte Carlo simulations allows full model application by considering the probability distributions of sectorized data, which may also have been weighted according to experimental error.

Often stellar intrinsic periodicity may be expected to emerge from data and so needs to be treated as a time-series. The most obvious tool for periodicity searching is the method of least squares and it has been supplemented here by a powerful F-statistic. Two other procedures are also proposed. One test considers the correlation of the polarization position angle with that expected from a model of chosen geometry and periodicity. Secular and stochastic effects may also be present in data, and these may be overcome by investigating the sign (i.e. +ve or -ve) of the observed u and again comparing to artificially generated data of some chosen model, quantifying the result via the continuous curve approximation to the binomial distribution.

The techniques for variation searching are applied to polarimetric data on the Be stars ζ Tau, γ Cas and 28 ω CMa which are all found to exhibit fluctuations of some kind (i.e. over particular timescales).

Extensive polarimetric data on X Persei were available and conclusions as to its nature, an oblique rotator, are drawn as well as the discovery of a rapid periodicity and the physical and geometric parameters of the applied oblique rotator model.

The oblique rotator scenario (i.e. the obliqueness of the location of the polarigenic mechanism to the stellar rotational axis) seemed to

fit the helium rich star σ Ori E, even with a relative paucity of data, particularly well, with its polarization, light and magnetic field all varying in a synchronous manner consistent with the model.

It is also proposed that in considering any polarimetric model it should be possible to predict the form of the light curve through the total intensity Stokes parameter. The oblique rotator scenario as well as a photospheric spot model are fitted to comprehensive UB_V photometric data of the helium rich star EM Cep. The statistical study shows that both models explain the behaviour of the data equally well; under particular circumstances (geometric) the two models can produce essentially identical results. It is judged that such a situation must apply in this case.

Finally, it is concluded that polarimetry should be given a more central role to play in the investigation of early-type stars. The scattering dipole-oblique rotator model, seen as an atmospheric bulge(s) seems to fit the helium rich (B1→B2.5), helium weak (B2.5-B6) and Ap stars particularly well and so the three techniques polarimetry, photometry and magnetometry should be given equal credence in considering such a model since relevant forms can be predicted and hence tested. Actually investigation via polarimetry alone can reveal most of the required parameters, *viz.* stellar inclination, rotation period, co-latitude of the scattering mechanism (magnetic pole?) and its optical depth, and the sense of stellar rotation.

* The nomenclature of "rich" and "weak" refers to the strength of the helium lines at classification dispersion (as used by, e.g., Underhill & Doazan (1983)).

CHAPTER 1. INTRODUCTION

1.1 About Be Stars

1.2 Scope of Variability

1.3 Polarimetry of Early-Type Stars

1.4 Relating Polarimetry and Photometry

1.5 Aim

CHAPTER 1. Introduction

1.1 About Be Stars

Although the title of the thesis may imply that a survey of the photopolarimetry of the early-type stars is about to be undertaken, this is not strictly the case. There will be a heavy bias towards a subgroup, *viz.* the Be stars. These are noted for their extraordinary variability over a wide range of parameters and time-scales, and hence draw attention to themselves as subjects worthy of investigation. As pointed out in the narrative below not all of the related recorded phenomena are unique to Be stars. Some of the Be observational traits can be readily associated with the rest of the early-type stars. Also, Be stars are notoriously difficult to classify spectrally and hence within the thesis title a hint of caution lies! Firstly, I shall elaborate on the phenomena that give rise to the requirement of a special category that is the Be stars.

Since their discovery, the first being γ Cas, in 1866 by A. Secchi, Be stars have been studiously observed over a wide range of wavelengths. They make up about 20% of all B stars and peak at type B2-B3. The normal B stars were the epitome of classical stellar modelling, i.e. having few lines in their visual spectrum. The Be stars, by their very nature, disturbed such a view and were cited as a simple illustration of the effect of an extended atmosphere/envelope brought about by rotational instability inducing mass loss. It is now well known, through space observations (in UV, X-ray), that both B and Be stars have a mass flux and so rotational effects cannot be solely responsible for the extended atmosphere. The stellar winds of the Be stars require, therefore, excursions into cool regions of dimensions able to produce observable emission lines in the visible spectral region.

The general taxonomy of Be implies that the spectrum is that of

Table 1.1.1

An illustration of the resultant problems of Be star spectral
classification (from Harmanec 1983)

VARIOUS ESTIMATES OF THE SPECTRAL TYPE OF KX And (HD 218393)

A5p	HD catalogue
A ve	Merrill (1930)
B9p	Harper (1937)
B3e	Swings and Struve (1940)
B8e	Beals (1951)
B8 Ia	Herman <i>et al.</i> (1959)
B6pe shell	Schmidt-Kaler (1967)
B2 V-IIIe	Doazan and Peton (1970)
B3e + K1 III	Polidan (1976)
B0 IV-IIIe	Hubert-Delplace and Hubert (1979)

any B-type with H I Balmer emission. More specifically, a Be star manifests itself by showing time variability in a large range of parameters, *viz.* line spectrum, continuous spectrum, radial velocity, polarization, etc., but not necessarily on similar time-scales. Such wide-ranging fluctuations are unusual for stars near the main-sequence, and cannot be wholly explained by subtle physical and/or geometrical changes.

Be stars are known to undergo a gradual B \rightarrow Be/shell transition, of which γ Cas is an oft-quoted example, the shell spectrum being one of absorptions which are narrow and deep in both Balmer and singly-ionized metal lines. Such transmogrifications take place on very short time-scales (years, decades) compared to an evolutionary sequence. Usually there is an infra-red excess as well as an ultra-violet excess or deficiency. UV observations reveal spectra of high ionization lines (CIV, NV, etc.) indicating signs of mass outflow - which incidentally may be variable. Singularly, all these properties are not unique to Be stars. Many OB supergiants display similar UV spectra, as could be said of the line spectra of late B and A type supergiants, to the shell spectrum. Other emission line stars, e.g. τ Tauri, are familiar with the transition phenomenon.

There is a consensus that Be stars are fast rotators due to the high $V_{eq} \sin i$ (projection of the equatorial velocity onto the sky; i the inclination of the stellar rotation axis with respect to the line of sight) values recorded for them. However the technique used to derive $V_{eq} \sin i$ for Be stars is susceptible to a wide range of influences (see, e.g., Doazan and Thomas, 1983). As a result, $V_{eq} \sin i$ values must be considered as highly uncertain quantities.

Similarly the spectral classification of Be stars suffers the harassment of contamination of relevant lines by the Be envelope, making the process a little subjective. Table 1.1.1 clearly shows the

consequences and, as I have found myself, this is certainly not an unique example!

The picture of a Be star at present, then, is an object with mass in the range $2M_{\odot}$ to $20M_{\odot}$ and an effective temperature of 1×10^4 K to 3×10^4 K, with an extended slowly moving outer atmosphere ($5R_{*}$ to $15R_{*}$) having subionized regions relative to its photosphere and a variable mass flux. They are thought to be young and moving through the first stages of evolution of a star relatively rapidly.

1.2 Scope of Variability

Throughout this thesis I shall define, in accordance with Harmanec (1983), the period of variability to be:

- (i) Long-term if duration is of years to tens of years,
- (ii) Medium-term " " " several days to months,
- (iii) Rapid " " " 0.1^d to several days, and
- (iv) Ultra-Rapid " " " minutes.

Due to observational (technical) bias, the long-term fluctuations are usually spectroscopic, though not all are periodic. Most medium-term changes, as seen by spectroscopy and photometry, seem to be associated with binaries. The rapid variations are generally of small amplitude for Be stars, and are well recorded by photometry. The cause of rapid variations may be any one of or combination of some type of pulsation, contact eclipsing binaries or rotation. The periodicity of this last variability can be difficult to detect as monitoring is unavoidably on time-scales comparable to the actual period itself, with the end result producing false cycles. Batten (1973) has given a scholium on the generation of spurious periods. The ultra-rapid variations are at the moment testing the state of the art detectors and the observationalists' awareness of various noise sources. This thesis will mainly be concerned with rapid type variations.

1.3 Polarimetry of Early-Type Stars

Little has been said here about polarimetry; this sadly reflects its usage in the modelling of Be stars, which so far has been dominated by results from spectroscopy and photometry.

The first Be star to have been discovered to exhibit an intrinsic linear polarization was γ Cas (again!), in 1959 by A. Behr. Although a direct polarization may be measured, this has an added component caused by the interstellar matter between star and observer. Only the variability, by either wavelength or time, of the intrinsic polarization allows it to be discerned from any assumed constant interstellar contribution - which may not be well known. The discovery of linear interstellar polarization, by J. S. Hall and W. A. Hiltner, preceded that of Behr's finding by ten years.

As to be expected several scenarios followed to try and interpret how such an intrinsic linear* polarization might be produced.

In order to explain the polarization of the eclipsing binary β Lyr, Shakhovskoi (1964) proposed that the simplest way for polarization to be produced would be to have the stellar radiation scattered by particles contained in a volume that is not spherically symmetrical with respect to the observer. Later Coyne and Kruszewski (1969) suggested a model in which the intrinsic polarization of the Be stars is caused by electron scattering (which is wavelength independent) in the envelope, whose geometry is aspherical with respect to the observer, the variation of polarization with wavelength being mainly due to continuous absorption by hydrogen.

To a certain extent the intensity of the $H\alpha$ emission represents the electron density in the envelope if it is optically thin. It is worth noting, however, that a variation in the polarization strength

*From now on "polarization" by itself will infer "linear polarization"

(Be stars have typically a low degree of polarization in the continuum, $\sim 1\%$) may not be reflected in the H α emission lines, as these are thought to be formed at distances much further out ($\sim 15R_*$) than those at which the polarization is generated ($\sim 2R_*$) (see Poeckert and Marlborough 1977, 1978a, 1978b). Fluctuations in the position angle of the polarization imply changes in the geometry of the envelope. So, at this point the greatest contribution that polarization can make to the modelling of Be stars is in the geometry of the extended outer atmosphere.

Not until 1977 was this contribution properly quantified. However, notable exceptions up to this point are the works of Shakhovskoi (1975) and Capps *et al.* (1973). Both authors considered the Be envelope as an extended disk separate from the source star. Approximations such as a point source star and an optically thin envelope for scattering were made. The situations were then studied in a particular case, *viz.* the disk being observed edge-on, and Shakhovskoi showed that here the scattered radiation alone would give a polarization maximum of $1/3$.

Brown and McLean (1977) showed that, after Thomson scattering in an axisymmetric, circumstellar envelope, the polarization, p , observed in the continuous radiation of the Be stars is given by $p = 2\bar{\tau}(1-3\gamma)\sin^2 i$ where; $\bar{\tau}$ is the optical depth of the electron scattering averaged over solid angle, as seen from the source star; γ is the envelope flattening factor; i , as before, is the angle between the star's rotational axis (or axis of envelope symmetry) and the line of sight, *i.e.* the inclination. Obviously measuring p alone does not allow the individual parameters $\bar{\tau}$, γ , i to be separated. However, if it can be assumed that the rotation axes of Be stars are randomly orientated (in which case the intrinsic polarization position angles should be random), the statistical distribution of $p = 2\bar{\tau}(1-3\gamma)$ can be

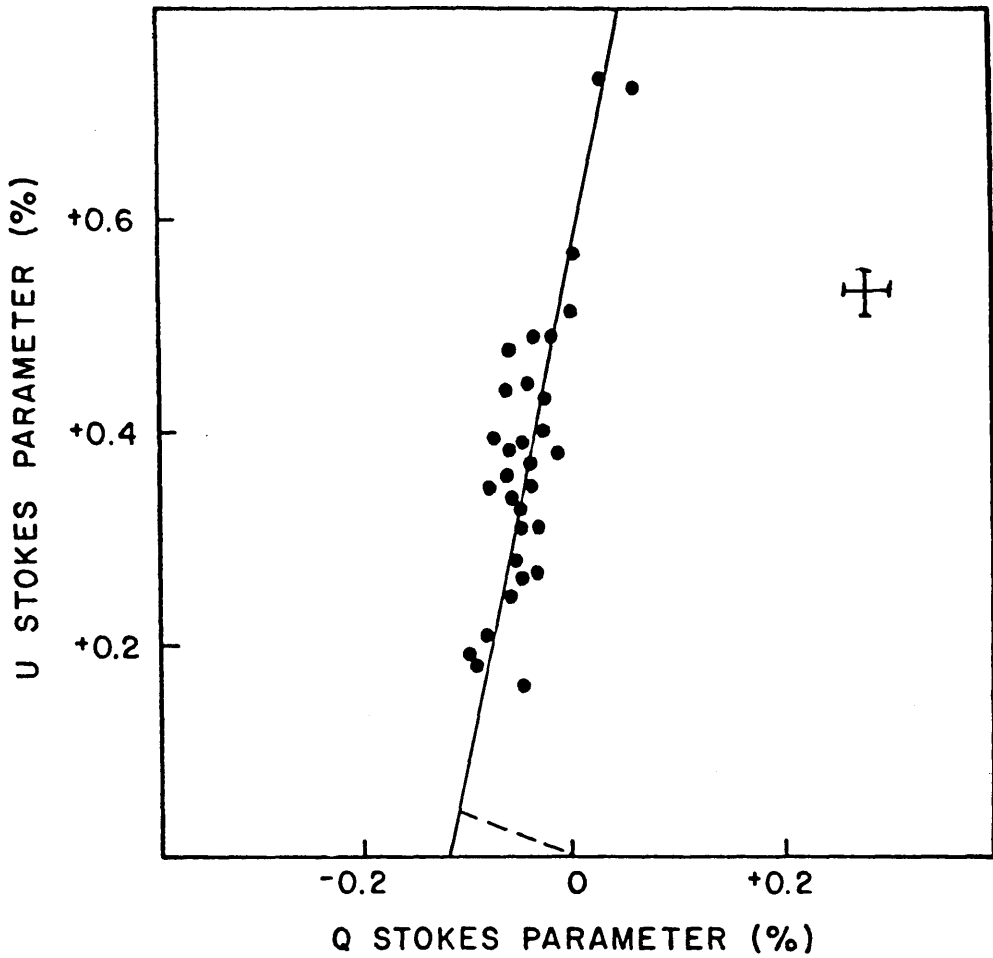


Fig. 1.3.2 B measurements of ω Ori. These were taken over an interval of 6 months from 1979 to 1980. The typical measuring error is shown as a cross and the dashed line denotes the interstellar polarization direction. (After Hayes 1980).

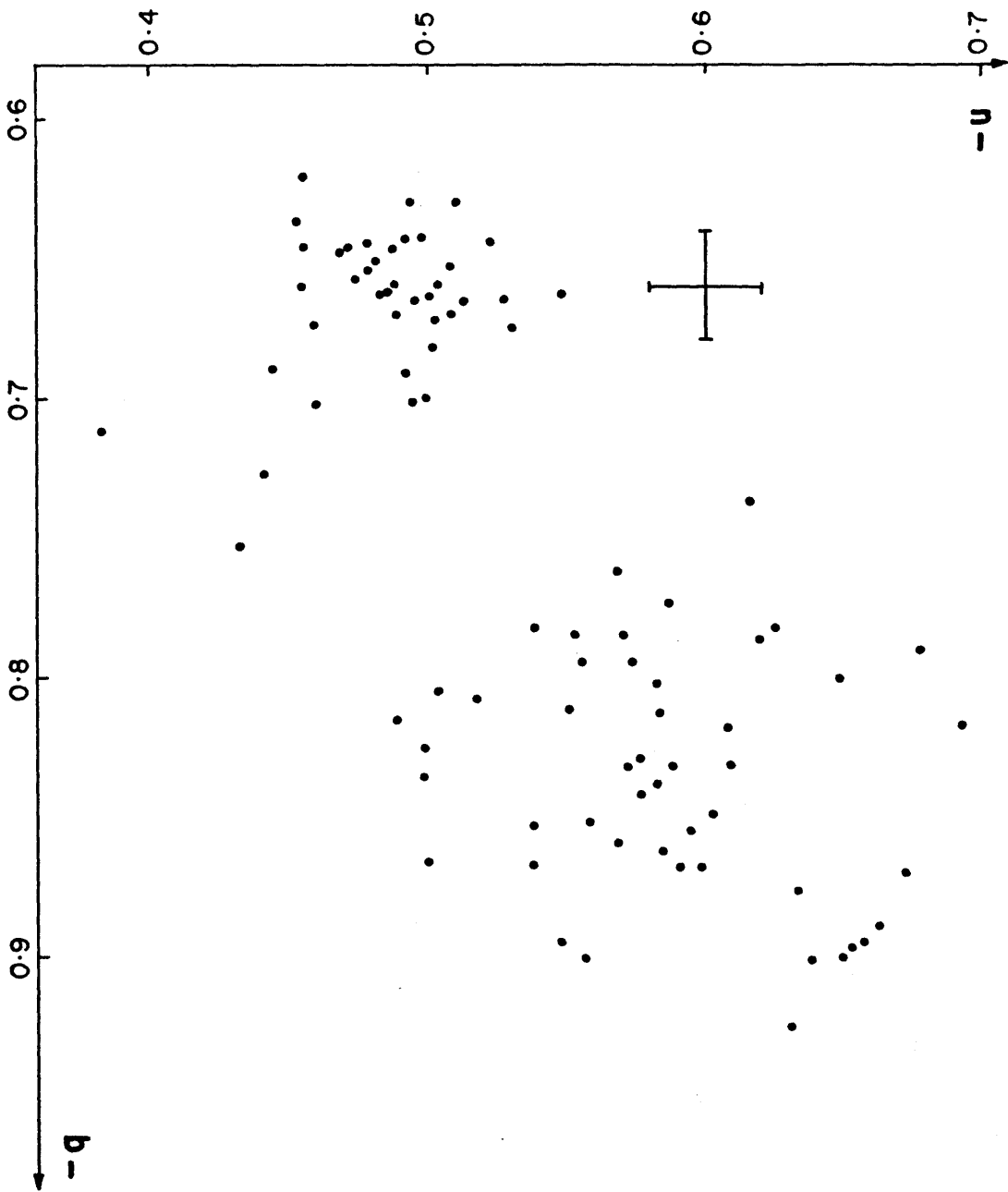


Fig. 1.3.1 The B observations of Y Cas, taken by Piirola (1977) on 3 nights in 1973 and 1 night in 1977, plotted in the normalized Stokes parameter plane. The cross represents the reported typical measuring error.

determined from the distribution of the observed p , since the probability distribution of $\sin^2 i$ can then be known.

From a study of a sample of 67 Be stars, McLean and Brown (1978) found that most of them were not only seen to have large $V_{eq} \sin i$ values but also very small polarizations. Hence the implication is that the majority of Be stars have quasi-spherical atmospheres and not highly flattened disk-shaped envelopes as had been presupposed. However the validity of this result must be questioned due to the high uncertainty in determining $V_{eq} \sin i$ as mentioned in Section 1.1.

The intrinsic polarization exhibited by Be stars is not a peculiar feature. It is often observed in many other emission-line stars, e.g. Herbig's Ae/Be stars, the Wolf-Rayet and Of stars, and the late-type supergiants.

As hinted earlier, Be stars can exhibit temporal variability in their polarization. In Fig. 1.3.1 the B wide-band polarimetric observations of γ Cas (B0.5 IVe) by Piirola (1979) have been plotted in the normalized Stokes parameter (q , u) plane; the wisdom of which will become apparent as the thesis unfolds (usually it is the polarization and its position angle that are plotted against time). This star seems to exhibit both rapid and long-term variations, as the measurements taken on three nights in 1973 are well removed from those on the night in 1977, and at the same time real changes (i.e. above the instrumental noise) are reported in both groups. Piirola attributes the changes as being due to inhomogeneities and instabilities in the rotating circumstellar envelope.

Fig. 1.3.2 displays the B wide-band measurements of ω Ori (B2 IIIe) by Hayes (1980) over the interval October 1979 to March 1980. There is an obvious well defined linear pattern to the changes, and Hayes claims them to be ordered (in terms of time) as well as of rapid type. Hayes attributes the fluctuations to a variable mass loss rate.

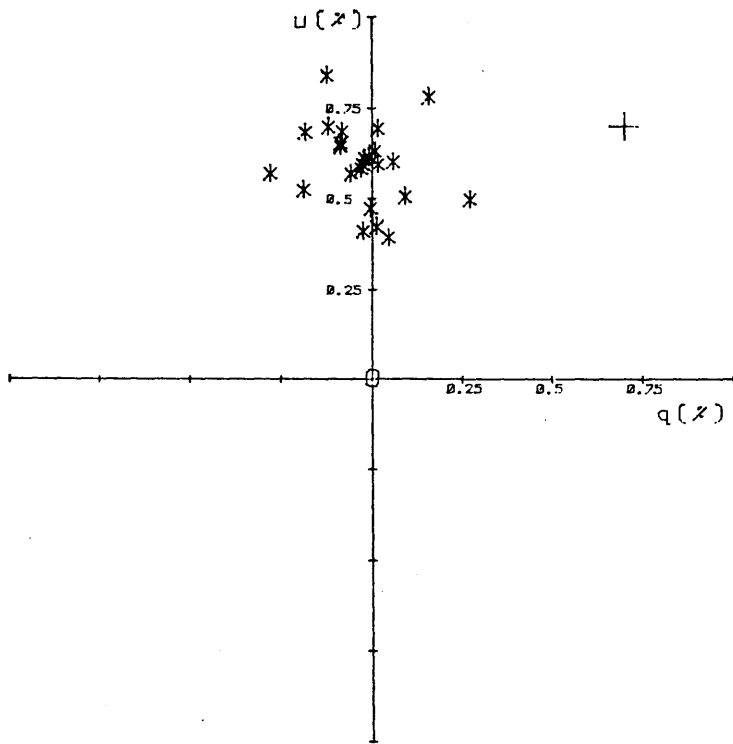


Fig. 1.3.5 The 24 3600/500Å measurements of ϕ Per taken over the period 1966 to 1975 (from Coyne and McLean 1975). The cross represents the reported typical measuring error.

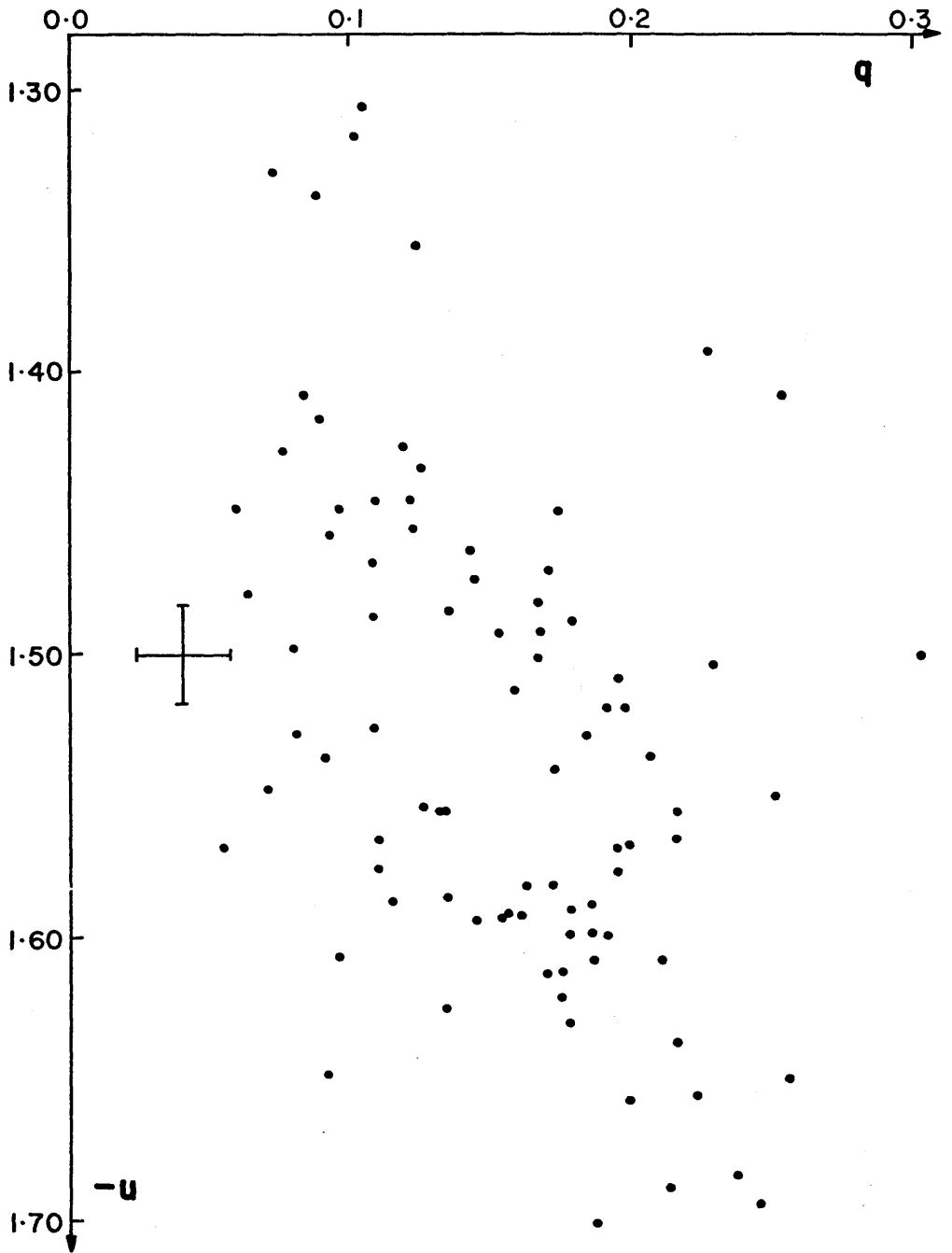


Fig. 1.3.4 From observations taken during 2 months in 1976 and 5 months in 1978, by Hayes(1984) of α Cam in the B band, the (q,u) measurements are plotted. The estimated measuring error was reported as 0.017%.

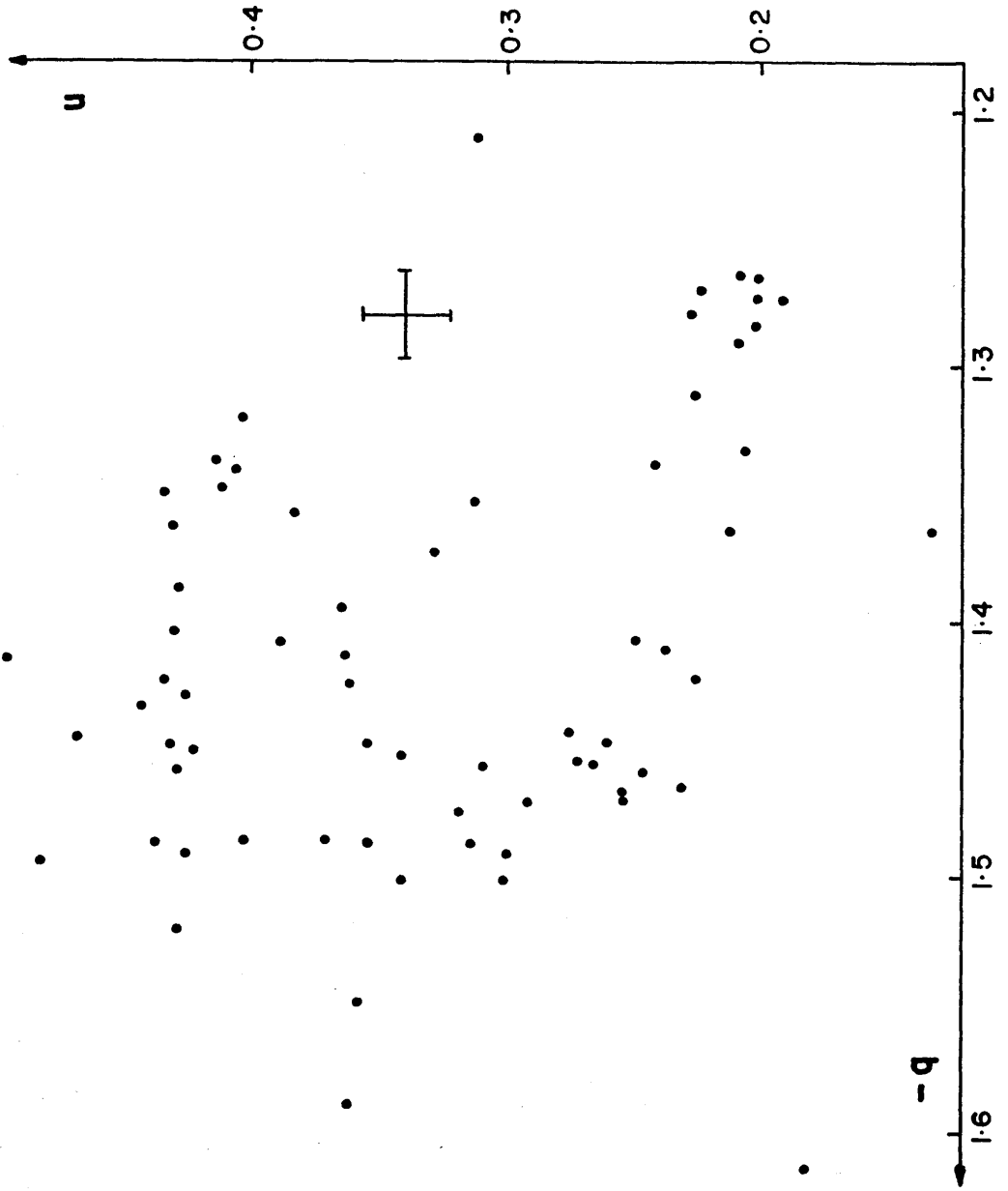


Fig. 1.3.3 The (q,u) observations from 4 months in 1976 and 5 months in 1978 of κ Cas. These were recorded by Hayes (1984), in the B-band, and he reports the typical measuring error to be 0.017%.

According to Hayes and Guinan (1984) these collinear changes are still apparent in this star.

Hayes (1984) has also performed observations on the early-type supergiants κ Cas (B1 Ia) and α Cam (O9.5 Ia), and they are shown in the (q, u) plane in Figs. 1.3.3 and 1.3.4 respectively. The data were recorded from several months in 1976 and 1978. Both stars are claimed to exhibit rapid fluctuations; the changes seem neither to be stochastic nor strictly periodic. Hayes also attributes them to be due to variable mass loss in the extended stellar atmospheres.

Coyne and McLean (1975) have looked at the star ϕ Per (B0 IV-Ve+?) over a wide range of wavelengths and band widths. The measurements at 3600/500 Å are plotted as Fig. 1.3.5. The base line of the 24 observations is from 1966 to 1975 and stochasticity is obviously apparent. Coyne and McLean attribute changes in electron density and/or temperature as the cause.

Immediately it can be seen that the forms of the variations are not homogeneous. Since the presences of the loci are essentially explained by the same attributives (and assuming them to be correct interpretations) the differences must be due, in part, to geometry. Without wanting to be too polemical, most of the arguments proposed by the relevant authors to substantiate the shape of any of the above loci, have been overly qualitative.

In this thesis I would like to present some ideas on how a locus in the (q, u) plane could be produced, and to give various new and novel methodologies that can be used in their analysis. The objective is to determine the geometry of the system whence it came, as well as investigating physical parameters (e.g. for variations in the optical depth at which the scattering is taking place). The scheme will be applicable for treating the data both as density distributions to cover stochastic effects and as a time sequence to search for periodicities.

It would seem that the astronomer's working principle is "There's no variability without periodicity", and his motto is "If there's a variability, let's determine its periodicity." One scenario in which polarimetric periodicity could emerge, would be from a binary system - scattering from a co-rotating cloud of electrons. The majority of observations relating to such a phenomenon have been performed by J. C. Kemp's group (e.g. see their work on AO Cas (Rudy and Kemp (1976)), σ Ori E (Kemp and Herman (1977)), Cyg X-1 (Kemp *et al.* (1978)) with the slightly more definitive (*cf.* Rudy and Kemp (1978)) theoretical work being done by Brown *et al.* (1978). It is noted that Buerger and Collins (1970) carried out detailed radiative transfer calculations for contact binary systems. The encounter of the observations with the theory and subsequent analyses was the subject of a thesis by Aspin (1981).

Another scenario could be the consequence of an oblique rotator, where cones of material are in co-rotation with a star, at an angle relative to the spin axis of the star (Clarke and McGale (1986c)). Polarimetrically this is a new idea and is explored further in Chapter 3 of this thesis.

1.4 Relating Polarimetry and Photometry

The inclusion of a discussion on photometry in this thesis is the result of a windfall of the total intensity Stokes parameter. A short discussion follows.

Percy (1982) has listed a dozen Be stars which display rapid photometric variations. There are several possibilities that could be responsible for these continuum fluctuations (note that they all taunt periodicity!)

- 1) Eclipses in a close binary system (e.g. Lynds (1959a))
 - 2) Photospheric spots (e.g. Torres and Ferraz Mello (1973))
 - 3) Radial pulsations
 - 4) Non-radial pulsations
 - 5) Oblique rotator (e.g. Harmanec (1984)).
- } e.g. Lesh and Aizenman (1974)

In considering any polarimetric model it should be possible to predict the form of the relative light curve, the scattered radiation detected as a polarization being apparent photometrically as an intensity modulation. So it can be seen that it might be possible to eliminate some of the mechanisms 1 to 5 by observing in both polarimetry and photometry. It is of course appreciated that other information from, e.g., radial velocity, spectroscopy, may also help in model selection. In the end, though, what is needed if any star system is to be modelled *in toto* is coverage of the broadest wavelength range, enabling investigation at a variety of optical depths.

The concept of the oblique rotator as a photospheric phenomenon, really possibility 2 above, or as a scattering phenomenon is considered fully in Chapter 4.

1.5 Aim

The aim of this thesis is to:

- 1) Present a scheme that may be used to search simply for variations in polarimetric data.
- 2) Introduce stochastic polarimetric models that mimic, superficially at least, (q, u) loci found for some early-type stars.
- 3) Give some means of quantitatively analysing loci, in terms of statistical significance of fit.
- 4) Reinforce that polarimetry and photometry are relatable through the notion of an oblique rotator.
- 5) Qualify the above by the analysis of polarimetric data on η Cep, β Cas, 55 Cyg, γ Cas, ζ Tau, β Vir, 2H Cam, 28 ω CMa, X Per, HDE 226868 (Cyg X-1?) and σ Ori E, and photometric data on EM Cep.

It is hoped that the thesis may contribute towards making these most variable of all variable stars a little less phenomenological and a little more noumenonological.

CHAPTER 2. DETECTING POLARIMETRIC VARIATIONS, STOCHASTIC
POLARIMETRIC MODELS AND THEIR FITTING TO DATA

- 2.1 Preamble Regarding Polarimetric Variations
- 2.2 Normality Testing
- 2.3 Regression/Correlation
- 2.4 Welch Testing
- 2.5 The Search for Variability
- 2.6 Preamble on Models Based on Stochastic Behaviour
- 2.7 The Model Geometry
- 2.8 A Preliminary Exploration of Possible Polarimetric Variations
- 2.9 Geometry Assessment Based on Random Observations
- 2.10 Preamble to Model Fitting of Polarimetric Data
- 2.11 Further on the Model Equations
- 2.12 Data Reduction Procedures
- 2.13 The q , u Density Distribution
- 2.14 Polarimetric Periodicities
- 2.15 Postamble

CHAPTER 2. Detecting Polarimetric Variations, Stochastic Polarimetric Models and Their Fitting to Data

2.1 Preamble Regarding Polarimetric Variations

Before considering stellar polarimetric data in relation to models, and models themselves, a discussion on searching for variability within such measurements is given.

Two terms that are often connected with data of any kind are accuracy and precision. Accuracy is a measure of certainty whereas precision is a measure of observational consistency. In performing any statistical test, precision is assumed great enough such that hypothesis failures/passes can be regarded as due to intrinsic variations within the data and that failures/passes are not caused by an unstable recording device. This is a very important general statement but it is sometimes forgotten with a result that false variability (more often in photometry than in polarimetry) is carelessly reported. All too often insufficient time and effort is put into the monitoring of standard stars to check on instrumental stability.

In polarimetry one way of investigating precision is to study stars that are classed as polarimetric standards, i.e. stars whose polarization (p), if any, and position angle (θ) are constant in time and wavelength. Serkowski (1974, pp.168-170) has listed such a set of stars. The non-polarized standards also allow the presence of any polarization induced by the detector and telescope combination to be ascertained. The polarized standards on the other hand are favourable for the finding of the orientation of the instrumental frame relative to the equatorial frame. It is generally taken that the positive q -axis, of the Stokes parameter equatorial frame, corresponds to the direction of celestial north, whilst the u -axis is rotated 45° north through east relative to the q -axis. The instrumental frame is an

arbitrary plane of measurement and is controlled by one of the elements of the polarimeter. So, if data are to be compared between observers, a standard reference is required - as is the purpose of the equatorial frame.

In investigating the precision of an instrument via polarimetric standards, analysis can be carried out in the instrumental frame. The q and u measurements (treated as independent parameters) of such stars would be expected to be normally distributed for high photon counts (at least above 100 per integration), have no correlation with time and be significantly non-variant in time. The time-base of stability should be tested on time-scales similar to those used in searching for suspect variability in program stars. Clarke and Stewart (1986) have given a method that may be used to elucidate the presence of any instrumental polarization. Clarke and Stewart also suggest that it is better to work with q and u rather than p and θ , since values of p are usually biased, even after having debiasing procedures applied.

2.2 Normality Testing

In the case of limiting noise (i.e. photon counting) a polarimetric standard would be expected to exhibit q and u measures which are normally distributed about means \bar{q} and \bar{u} respectively. This hypothesis can be tested by investigating the skewness and kurtosis of the two distributions. Skewness describes the symmetry of a distribution and is defined to be the average value of $(X_j - \mu)^3$, i.e. the third moment about the population mean. The mean value of $(X_j - \mu)^4$ is called the kurtosis; this quantity relates the width of a distribution and has also been described as a test of unimodality versus bimodality. To render skewness and kurtosis independent of scale, they are divided by powers of $(X_j - \mu)^2/n$. The resulting ratios of moments are known as the coefficient of skewness, γ_1 , and the coefficient of kurtosis, β_2 , where the sample estimates are given by

$$\hat{\gamma}_1 = \frac{m_3}{m_2^{3/2}} \quad \hat{\beta}_2 = \frac{m_4}{m_2^2}$$

$$\text{and } m_r = \sum_{j=1}^n \frac{(x_j - \bar{x})^r}{n} ; \quad \begin{array}{l} \bar{x} = \text{the sample mean} \\ x_j = j^{\text{th}} \text{ observation} \\ n = \text{number of observations} \end{array} \quad (2.2.1)$$

For the normal distribution $\gamma_1 = 0$ and $\beta_2 = 3$. In a distribution that has $\gamma_1 > 0$, the low values of "x" are concentrated towards its mean, and if $\beta_2 > 3$ the tails are longer than a Gaussian of the same m_2 . So if $\hat{\gamma}_1$ and $\hat{\beta}_2$ can be calculated for any data set, a confidence may be set on whether they follow the pattern of a normal distribution or not. Brooks (1984) has produced improved tables of percentage points of γ_1 and β_2 for samples from 3 of up to 125 points. Thereafter relevant critical values may be calculated using the unbiased estimators \hat{g}_1 and \hat{g}_2 of γ_1 and β_2 respectively where

$$\hat{g}_1 = \pm c \left[\frac{6n(n-1)}{(n-2)(n+1)(n+3)} \right]^{\frac{1}{2}} \quad (2.2.2)$$

$$\hat{g}_2 = 3 \pm c \left[\frac{24n(n-1)^2}{(n-3)(n-2)(n+3)(n+5)} \right]$$

and n as before is the number of points in the sample under study with c being the ordinate of the percentage point to be calculated (e.g. c = 1.96 corresponds to the 95% confidence limit).

The bias refers to the denominator used in calculating the moments. Taking n as the divisor, the moment is termed a bias estimator and an unbiased estimator if n-1 is used instead. There is little difference between the two if n is large ($> \sim 120$). Whilst \hat{g}_1 gives a good approximation to γ_1 , \hat{g}_2 is rather poor until $n \sim 1000$; this is because the distribution of kurtosis is skew.

Skewness in itself is an important test. A failure in q and/or u may relate to a time drift in the measurements or the presence of a point or points unusually well departed from the sample's mean, these being termed outliers or glitches, caused by a sudden change in the

noise characteristics or an astrophysical fluctuation. It is therefore useful to know how good are skewness and kurtosis at detecting glitches.

The power of skewness and kurtosis can be investigated by carrying out Monte Carlo simulations on the distributions of skewness and kurtosis. A program of the following nature would be required:

- (i) Sample (n times) from a normal distribution of mean zero and unit variance (i.e. $\sigma^2 = 1$).
- (ii) Add a glitch of $k\sigma(k\epsilon R^+)$ to one of the sample points.
- (iii) Calculate $\hat{\gamma}_1$ and $\hat{\beta}_2$ and store.
- (iv) Repeat for another 2000 data strings of length n .
- (v) Order the values of $\hat{\gamma}_1$ and $\hat{\beta}_2$ and take the 11th and 1990th points for the 99% confidence limits and the 51st and 1950th for the 95% confidence limits of γ_1 and β_2 .
- (vi) Repeat another 50 times, so that the mean 99% and 95% confidence limits of γ_1 and β_2 with standard errors can be found.
- (vii) Repeat for another value of n .

Such a program was constructed in conjunction with the Numerical Algorithms Group's routines G05CCF, G05DDF and M01ANF. G05CCF sets the random number generator routine to a non-repeatable starting position. G05DDF returns a pseudo-random number taken from a normal distribution of user specified mean and standard deviation. M01ANF allows the vectors, in this case, of $\hat{\gamma}_1$ and $\hat{\beta}_2$ to be sorted into ascending order. The numbers 2000 and 50 were chosen after inspection of the simulations of a related nature by Jones (1969) and Brooks (*loc. cit.*). They are a compromise between allowable computing time and the requirement that the investigated levels actually are those levels to within approximately $\pm 0.5\%$. The standard errors derived for the present simulation are comparable with those in the tables of Brooks. The glitch, k , was made to range from 0.0 to 5.0 with a resolution of 0.1,

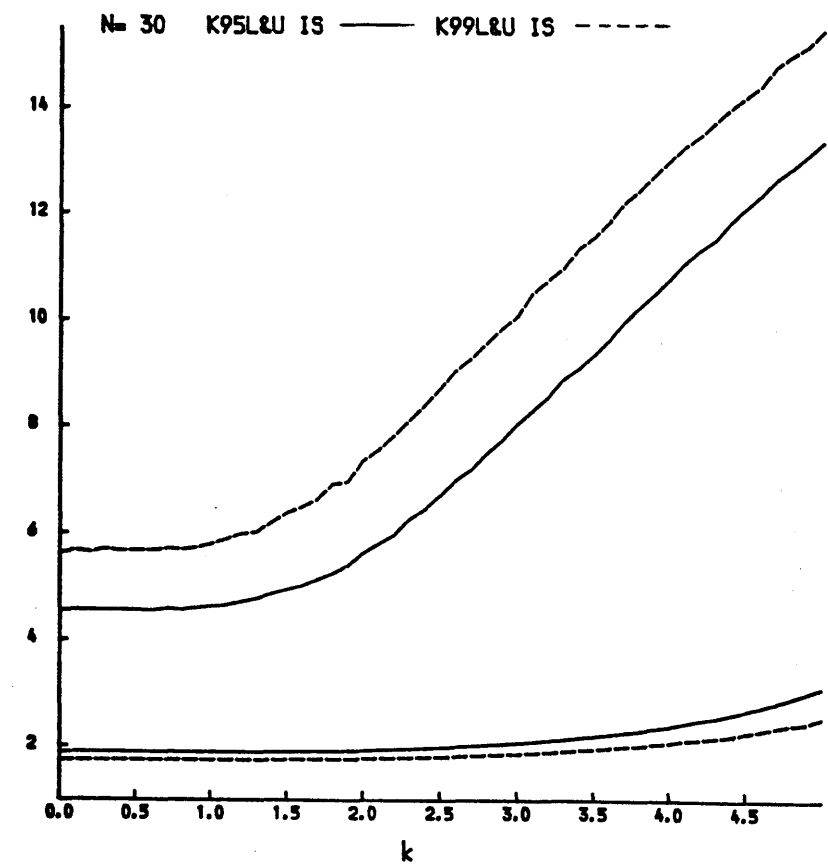
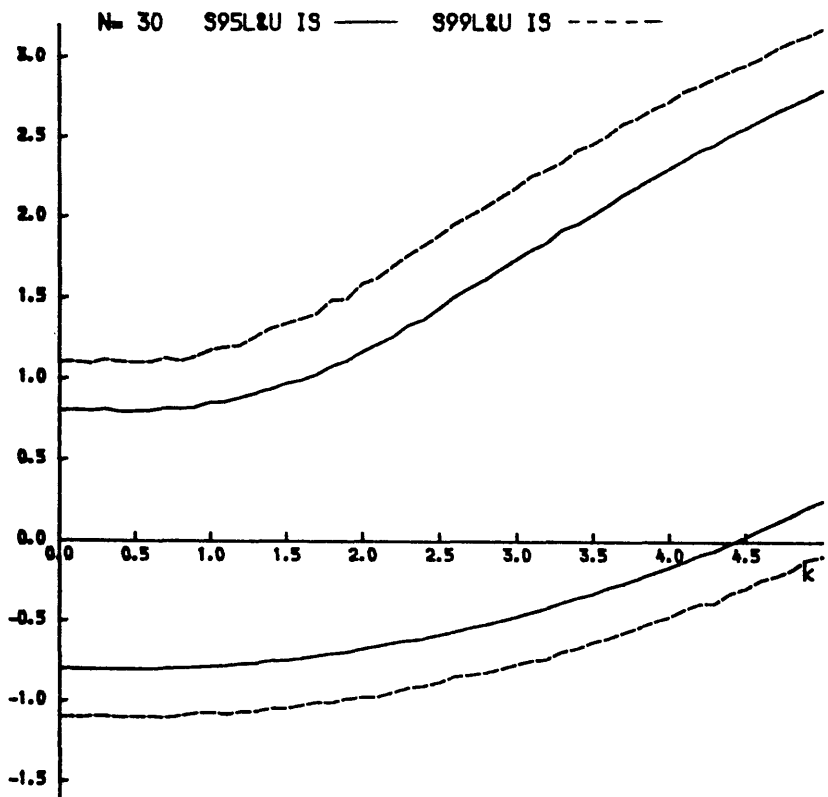


Fig. 2.2.1(g)

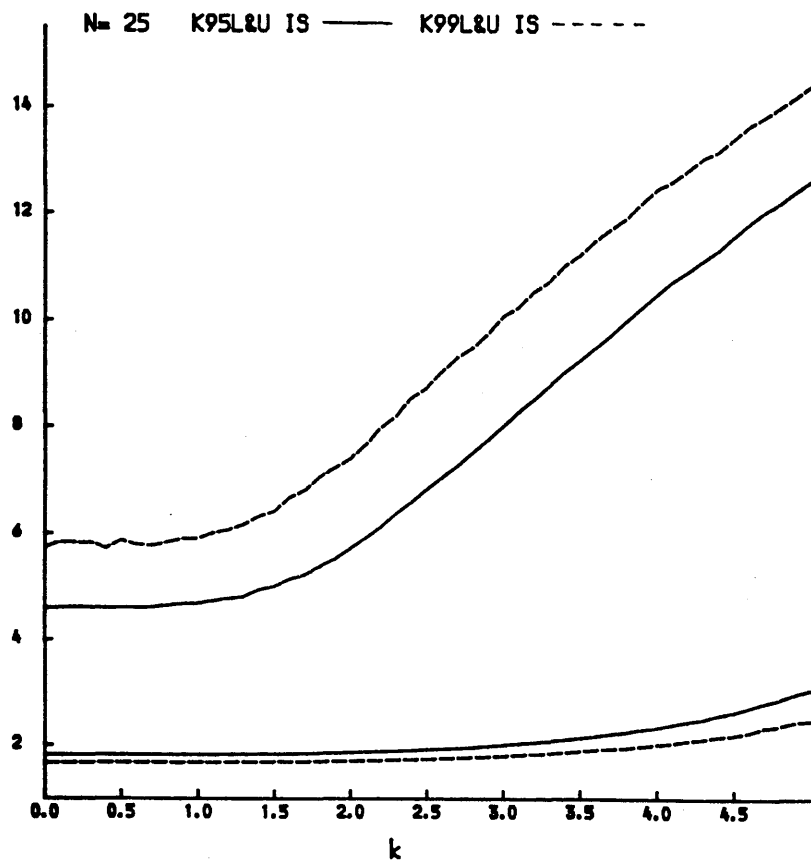
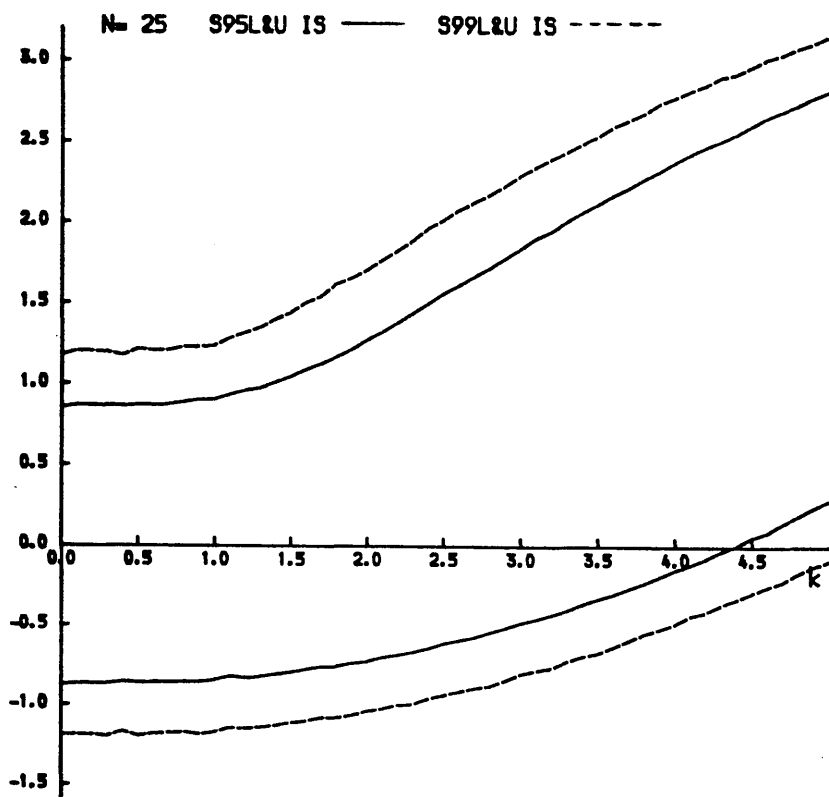


Fig. 2.2.1(f)

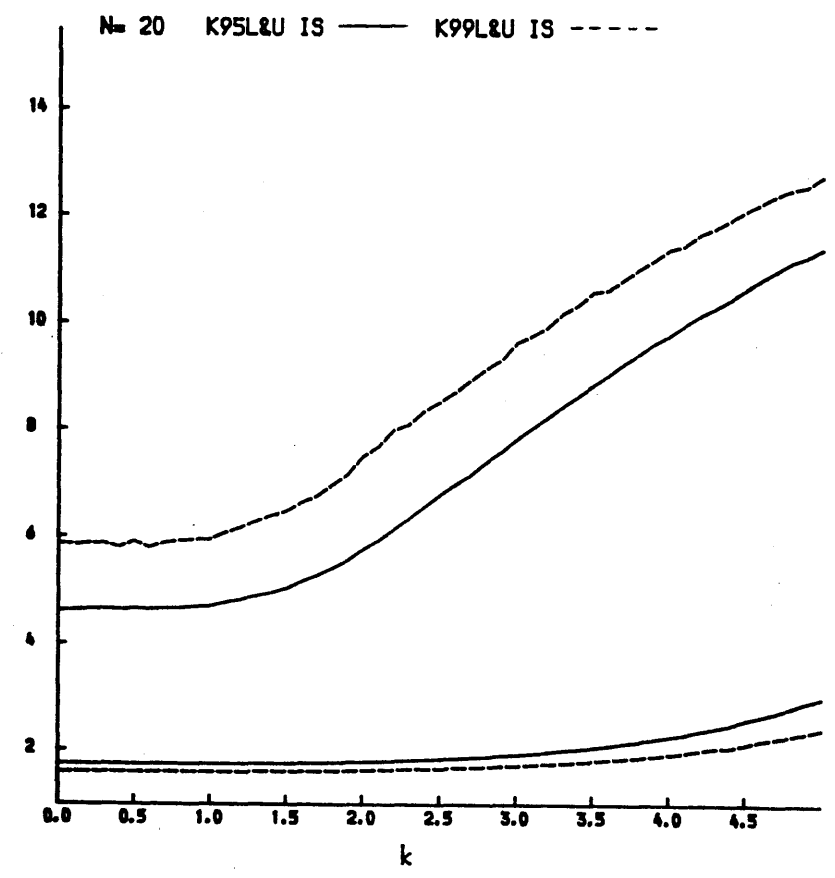
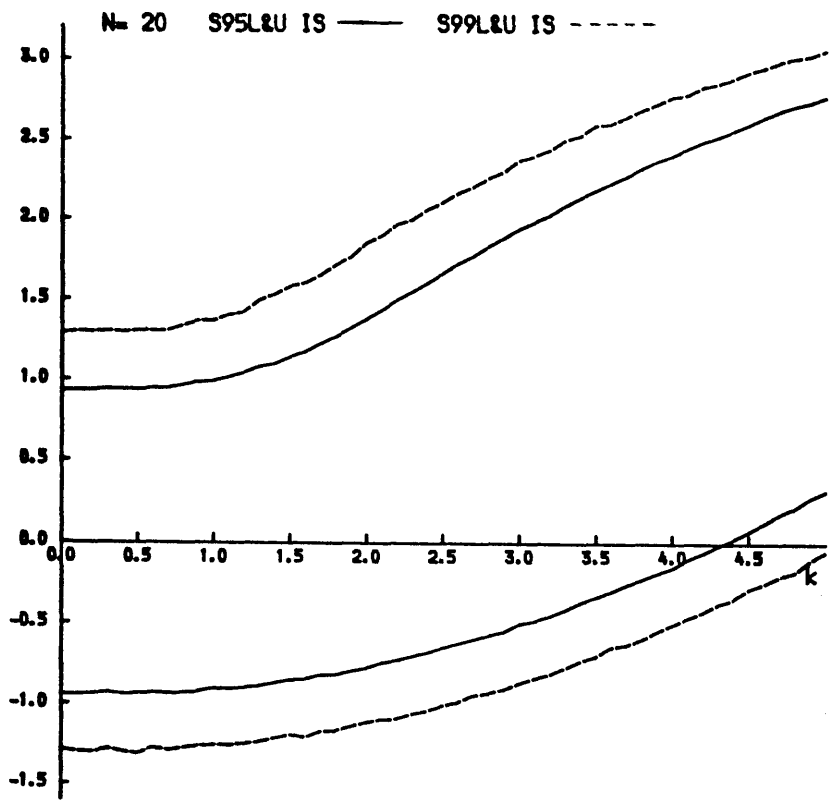


Fig. 2.2.1(e)

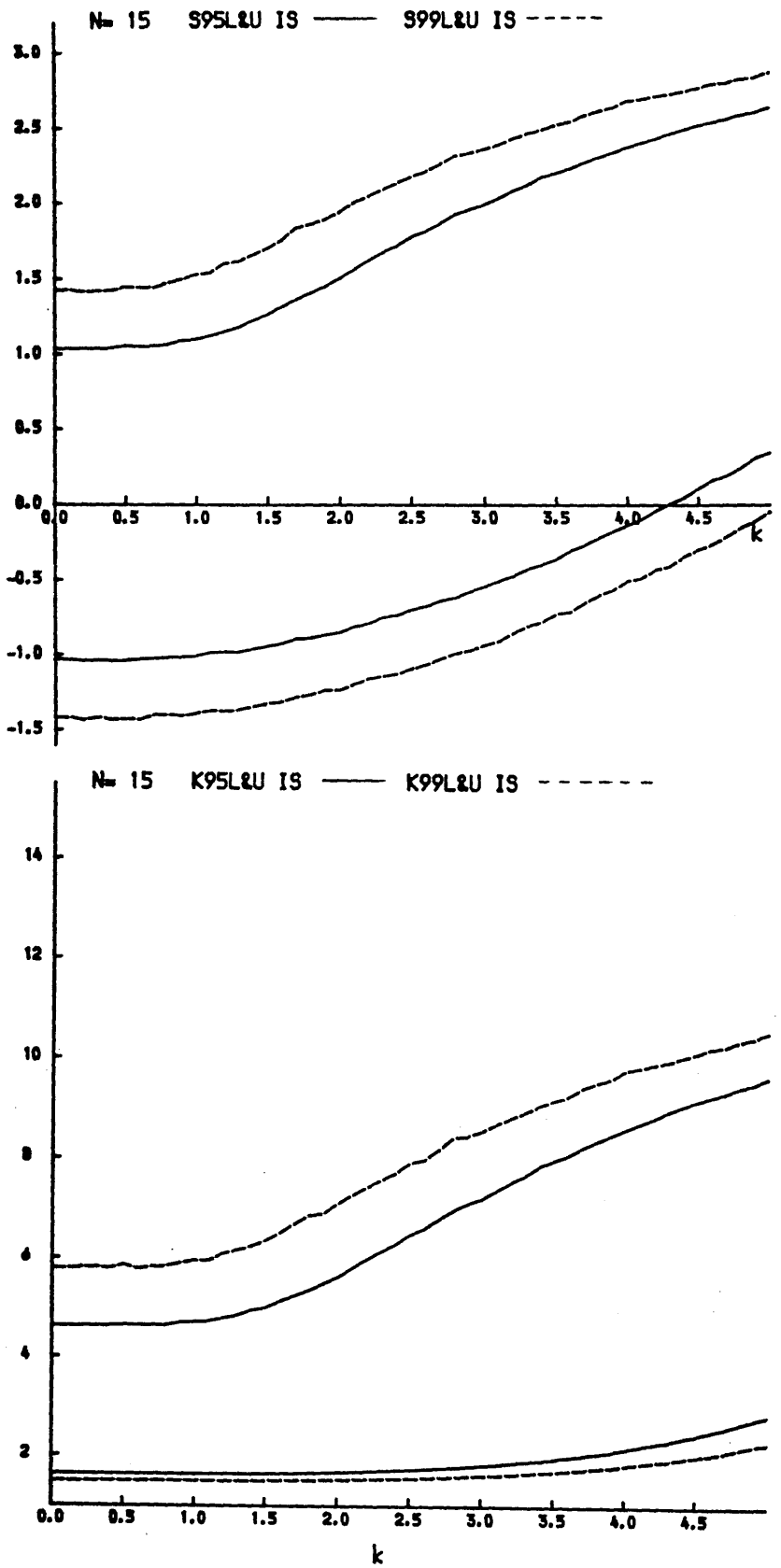


Fig. 2.2.1(d)

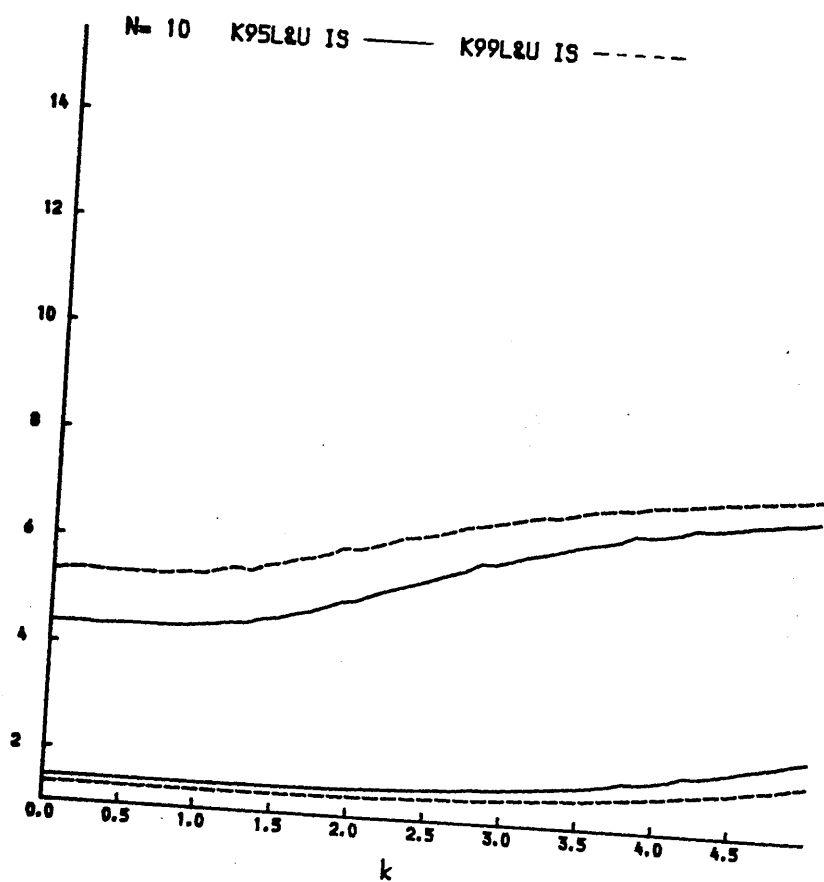
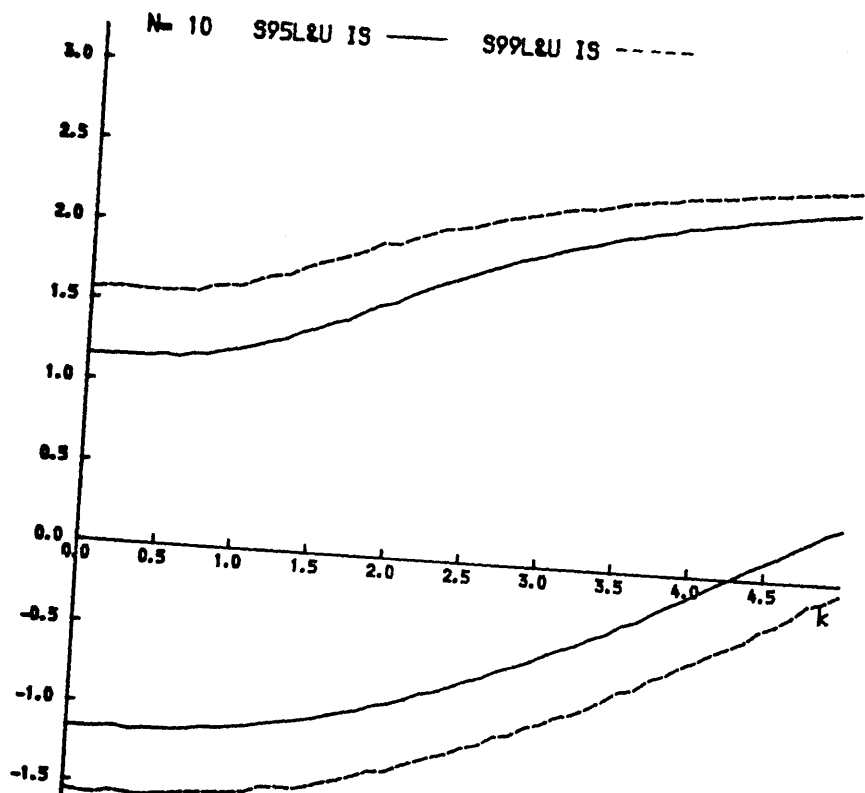


Fig. 2.2.1(c)

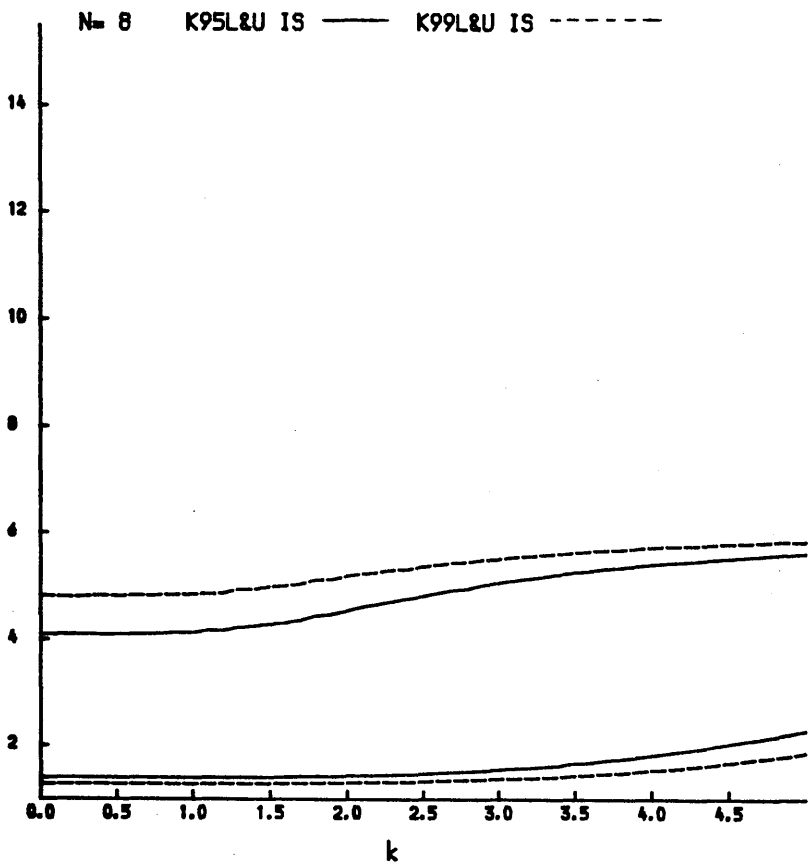
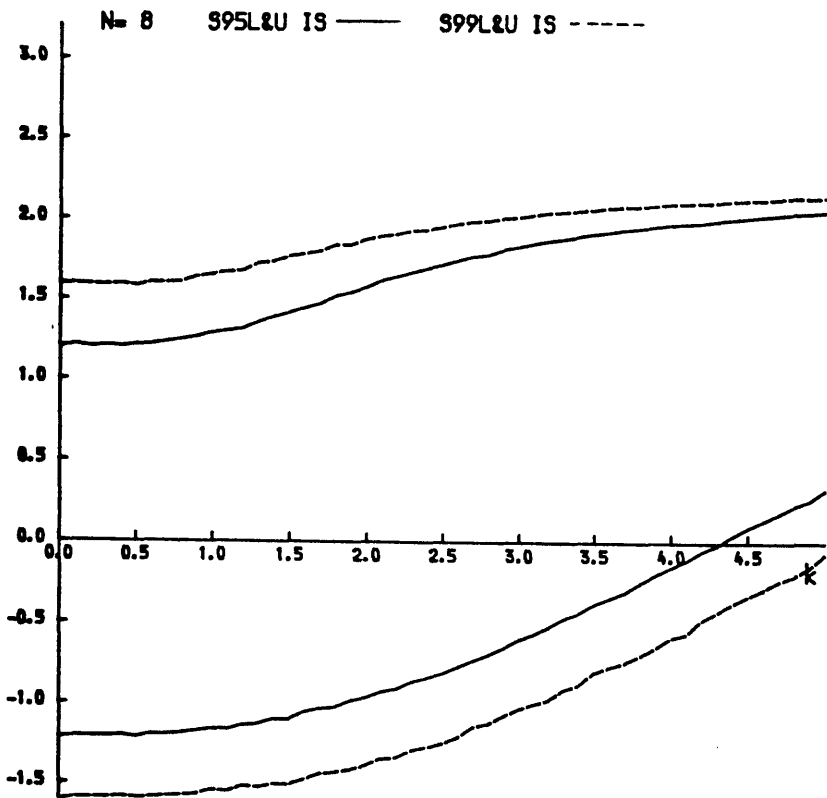


Fig. 2.2.1(b)

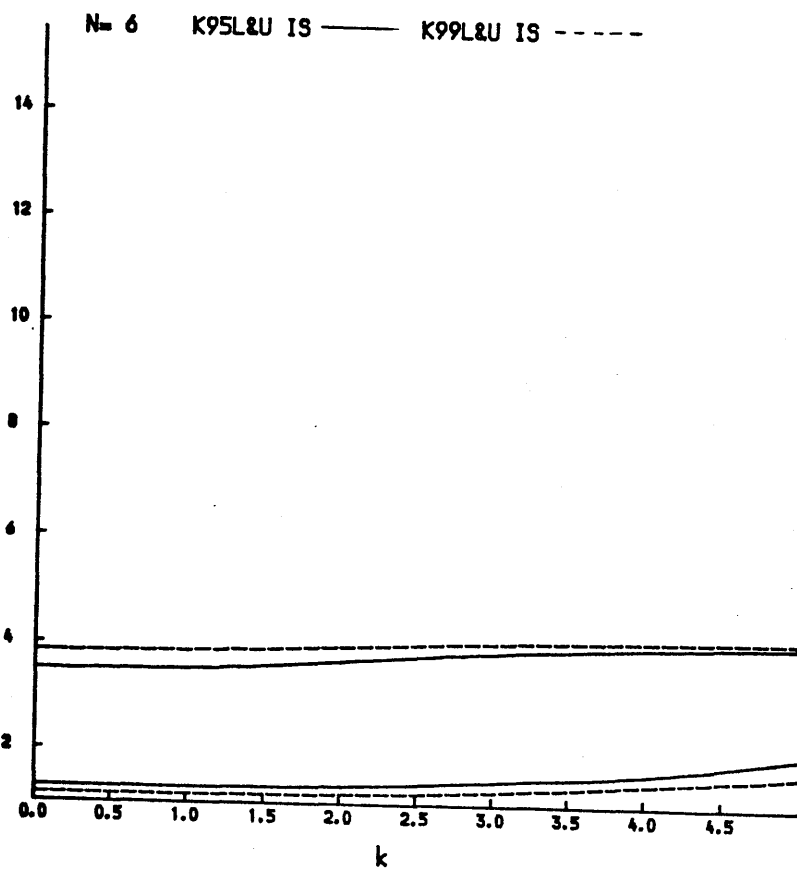
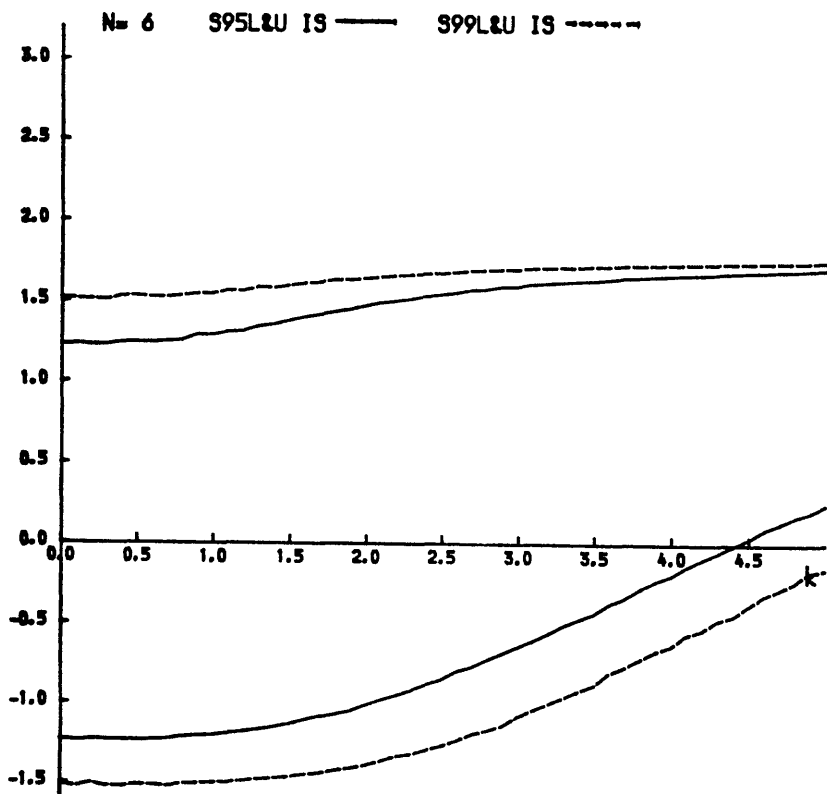


Fig. 2.2.1(a)

The behaviour of the 95% and 99% confidence intervals of skewness (upper) and kurtosis (lower) with a glitch of k added to a sample of N points from a normal distribution of zero mean and unit variance.

with the number of points in the sample covering 4(1)10 and 15(5)30. The results for $n=6,8,10,15,20,25$, and 30 are displayed as Figures 2.2.1(a)-(g). The graphs reveal (when the lines begin to curve) at what value of k , for some n , do skewness and kurtosis appreciate the presence of a glitch. Obviously the larger the sample the easier it is to detect an outlier as is confirmed from the graphs. Theoretically it is possible to calculate skewness with as few as 3 points and kurtosis with 4, but Figs. 2.2.1(a)-(g) imply that the minimum number of points needed for a reliable normality test is a little larger. With at least a sample size of 10 a confident result would be expected.

2.3 Regression/Correlation

A method of sighting coherent drifts in q or u is to perform sample linear regressions of q and u on time (T). As an example consider q and T . The equation of the sample regression can be written as

$$\hat{q} = a + bT \quad (2.3.1)$$

where \hat{q} is the estimate of q at time T ; the object - to derive the sample estimates a and b , a the interception of the q -axis and b the gradient in the (T, q) plane, the usual technique of least squares being applied to the estimates (e.g. see Barford (1967), Ch. 3). Having carried out the fitting procedure, the null hypothesis that the population regression line has zero slope, i.e. the means of q are unrelated to time, can be tested. This may be done by comparing the value of b/S_b (S_b is the sample estimate of the standard error of b) to a table of percentage points of the t distribution with $(n-2)$ degrees of freedom (df).

The line described by

$$\hat{T} = a' + b'q \quad (2.3.2)$$

can also be fitted, enabling the population correlation coefficient (ρ) to be estimated by the sample correlation coefficient (r), where

$$r = |\sqrt{bb'}| \quad (2.3.3)$$

Its value can then be compared with the comprehensive percentage levels with ndf for the correlation coefficient given in Appendix A. So, the null hypothesis that $\rho = 0$ is easily tested at the required degree of significance.

As with the sample linear regression, the correlation coefficient may be regarded only as an indicator of the strength of a linear (in this case) relationship between two variables and not proof that they are actually correlated. Justification of the causality of "X" to "Y" needs to come from external sources. Essentially the two tests are identical, although it should be noted that the mathematical model of linear regression requires the X in $Y = a + bX$ to be known without error. This condition will be violated in the situation of fitting Equation (2.3.2), making b' a bias estimator of the population gradient. It is not a totally insurmountable problem, however (see, e.g., Snedecor and Cochran, Sec. 9.14, 1980). So the linear regression, in particular circumstances, is perhaps a more powerful test for searching for drifts, in so much as its robustness is less challenged in relation to correlation.

2.4 Welch Testing

The Welch test (e.g. see Brown and Forsyth, 1974) is useful for searching for variability that is not necessarily coherent with time. Data can be divided into groups to form a set of means and variances. The null hypothesis that all the population means are equal is testable. The tables that can be used to check the significance of equality are the F tables, since the Welch statistic (W) is approximately distributed as an F statistic if the null hypothesis is true. W requires only that the observations within any group are Gaussian.

Brown and Forsyth suggest that the critical values of W are valid

for groups containing as low as 5 observations, remembering that they have to be normal. So in using skewness and kurtosis to check on the normality before proceeding with the Welch test, this limit will rise slightly if a chance reduction in the power of W is to be avoided.

2.5 The Search for Variability

Reduction of data on program stars may also be carried out in the instrumental frame. In order, though, to make any variations immediately more relatable to the star (assuming it to be responsible for them!), analysis could be done in a plane where changes in q correspond to changes in intrinsic polarization and with wavelength (if position angle is assumed colour independent), and fluctuations in u to intrinsic position angle - a (p, θ) frame. This would necessitate evaluation of any interstellar contribution (a difficult problem) and knowledge of the relevant intrinsic position angle. McLean and Clarke (1979) have cited various methods whereby interstellar components can be resolved. The intrinsic position angle may be approximated in the form of a weighted mean of all relating observations providing a "snapshot" of the angle in time.

A scheme to search simply for polarimetric variations in the data of stars could be:

- i) Observe polarimetric standards.
- ii) Perform normality, regression and Welch procedures on the data of the standards.
- iii) If stability is evident at some chosen level - proceed.
- iv) Test for instrumental polarization using non-polarized standards.
- v) Compare the position angle(s) of the polarized standard(s) with its (their) value(s) in the equatorial plane.
- vi) Derive interstellar contribution for program star.
- vii) Rotate measurements of program star to a (p, θ) frame.

viii) Perform normality, regression and Welch tests.

ix) Write paper, with the q and u measurements tabulated in the equatorial frame!

If in studying the polarimetric standards an accurate value of the variance from photon counting statistics (the limiting noise) can be ascertained, then step ii) can be missed out. Hayes (1980), for example, performs a χ^2 test on the variances of program star data to see if they significantly exceed that expected from photon counting statistics. Further parameters relating to the instrument usually need investigating as well, such as the wavelength dependence of the retarder used, the effective wavelength of the filter-detector (photomultiplier) combination, and instrumental depolarization. All in all, "detection" of false variability should be avoided if steps i) to viii) are adhered to, directly or in principle. The problems regarding stability, unfortunately, do not end there; other considerations include, for example, the effects of atmospheric seeing, a non-uniformly sensitive cathode of a photomultiplier. Stewart (1984) has explored further these and other related problems.

The achievement of higher and higher polarimetric precision is a never ending story.

2.6 Preamble on Models Based on Stochastic Behaviour

Eventually variations of any kind need to be modelled if an understanding as to why they occur is to be found. As illustrated in Chapter 1, temporal fluctuations in early-type stars, particularly Be stars, of p are common, the behaviour being complex and covering a range of time-scales. The polarimetric changes could be either well ordered or stochastic or demonstrate a periodicity or even a combination of these traits.

Both slow global changes and periodicities may be detected by examining coherent movements of the "time-path" through the data when

plotted in the normalized Stokes parameter plane. However, sometimes the data distribution is "apparently random" from which an underlying random behaviour for the polarigenic mechanism is inferred. Randomness in polarimetric measurements has been qualitatively described by Lupie (1983) in terms of vector changes with no preferred position angle relative to the centre of gravity of the data point distribution with a range of magnitudes.

In this thesis the way the stochastic behaviour affects the data distribution is more rigorously explored with a view to determining models for recorded data of Be and other early-type stars. The geometry described in Brown, McLean and Emslie (1978) is adapted to allow the investigation of the polarimetric effects of localised concentrations of electrons acting as scattering globules, these perhaps being superimposed on the level produced by a general average distribution of an extended axisymmetric atmosphere.

2.7 The Model Geometry

Whilst it is appreciated that polarimetric variability could also in some cases be modelled via e.g. binaries, non-radial pulsators, the evidence that B and Be stars exhibit a mass loss (variable for Be stars), suggests the scenario of the scattering of the stellar radiation by an enhancement/bulge of free electrons detached from the stellar photosphere as an attractive starting point. The scatterers need not necessarily be limited to free electrons, as symmetrical scatterers (e.g. H_2 molecules) have the same scattering angle dependence. Further, a stochastic globule model could be easily extended to cover periodicity if the bulge is allowed to co-rotate.

The approach below to the investigation of the polarigenic effects of scattering globules is, although simplistic, basic. It is assumed that the initial unpolarized radiation originates from a point source star and that the polarization is produced by an assembly of free

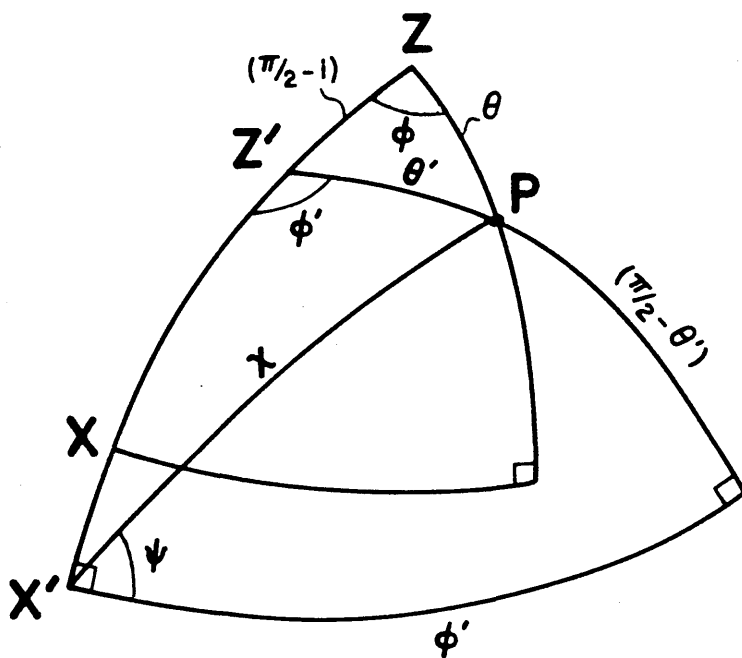
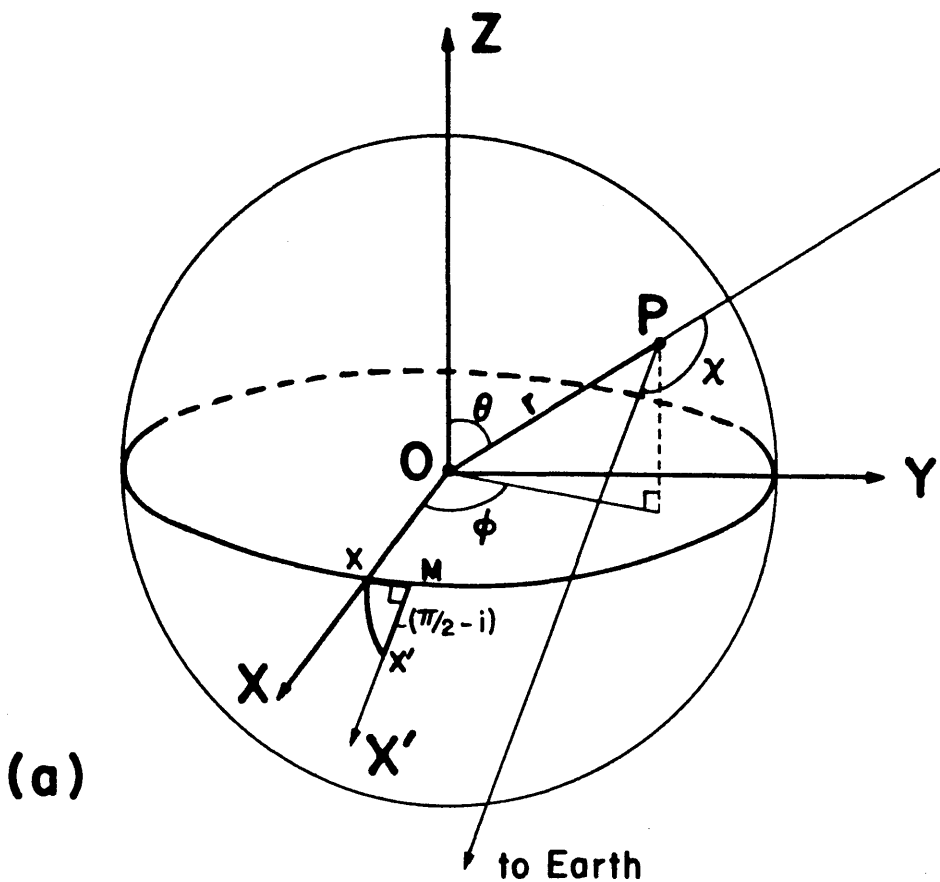
electrons considered to act as a point scatterer. In reality the globule is likely to be placed at distances comparable with the stellar photospheric radius, with the geometry involving a spread in the scattering angles tending to reduce the polarization with respect to the effect of a point source/point scatterer; a similar end result would be expected if the scatterer was no longer considered to be a point.

In addition, the electron concentration in the globule may provide a non-optically thin situation with multiple scattering reducing the emerging polarization. As already indicated in Chapter 1, the extended atmosphere also produces a polarization, some of this flux possibly entering the globule and influencing the resultant.

Thomson scattering is wavelength independent. Temperature influences the ratio of the number of absorbing (wavelength dependent) atoms to the number of scattering electrons *ergo* affecting the optical depth, τ_0 , especially at lower temperatures (i.e. below ionization temperatures). Therefore, τ_0 can be wavelength dependent, hence inducing a wavelength reliance to the polarization. Emission adds to the dilution of the polarization at higher temperatures, if the emission itself is presumed to be unpolarized.

In comparing models with real data, such effects then may need to be incorporated; nonetheless the models should give insight to the interpretation of observational material.

Consider two sets of Cartesian co-ordinates, one (X,Y,Z) associated with the preferred axes of the local stellar geometry (e.g. Z might be the spin axis of the star, or XY might be the plane of the equatorial bulge of an axisymmetric extended atmosphere) the other (X',Y',Z') being dependent on the observer's position; the emitting



(b)

Fig. 2.7.1 The stellar point source is at O and P is a general scattering region providing a scattering angle χ . Stellar (X, Y, Z) and observer (X', Y', Z') co-ordinates have O as a common origin and are uncoupled by the inclination i (arc XZ') of the star's rotation axis (OZ), whilst OX' is the direction to Earth. The stellar co-ordinates (r, θ, ϕ) of P can be related to χ through its observer spherical co-ordinates (r', θ', ϕ') .

star is at their common origin O ; the line of sight to Earth is OX' . The relative orientation of the two frames (see Fig. 2.7.1(a)) is given by the great circle arc xx' which may be resolved into the great circle arcs xm and mx' . In the description below, the value of the fiduciary azimuthal angle corresponding to the arc xm is unimportant and arbitrary and for convenience is taken as zero as in Fig. 2.7.1(b). The arc mx' corresponds to $(\frac{\pi}{2}-i)$ where i is the inclination of the stellar pole to the line of sight.

If P is considered as a globule of free electrons, the flux scattered towards the Earth is

$$\frac{I_* \sigma_0 n}{r^2} (1 + \cos^2 \chi) \quad (2.7.1)$$

with a polarized component given by

$$\frac{I_* \sigma_0 n}{r^2} \sin^2 \chi \quad (2.7.2)$$

where I_* is the unpolarized isotropic intensity of the point source star, σ_0 the scattering cross section efficiency of a single free electron, n the number of electrons at P , a distance r from the star and χ the scattering angle. The scaling factor $\frac{\sigma_0 n}{r^2}$ represents the total solid angle subtended by the electrons as seen from the star and is the scattering optical depth (i.e. τ_0) of the globule. By referring the polarized component to the reference plane which is set at an angle Ψ to the local scattering plane, the Stokes vector of the polarization may be written as

$$\begin{bmatrix} I \\ Q \\ U \end{bmatrix} = I_* \tau_0 \begin{bmatrix} 1 + \cos^2 \chi \\ \sin^2 \chi \cos 2\Psi \\ \sin^2 \chi \sin 2\Psi \end{bmatrix} \quad (2.7.3)$$

with the direction of Q corresponding to the projection of the stellar equator on the sky, this being referred to as the *equatorial line*.

From the geometry depicted in Fig. 2.7.1 the following relationships are readily established:

$$\begin{aligned}\frac{X'}{r} &= \sin\theta' \cos\phi' = \cos\chi \\ \frac{Y'}{r} &= \sin\theta' \sin\phi' = \sin\chi \cos\psi = B \\ \frac{Z'}{r} &= \cos\theta' = \sin\chi \sin\psi = C\end{aligned}\quad (2.7.4)$$

By adding the direct contribution of the star to the scattered intensity and using the identities above, having related them to the local stellar frame through spherical triangle ZZ'P, the observed Stokes vector for the linear polarization may be written as:

$$\begin{bmatrix} I \\ Q \\ U \end{bmatrix} = I_* \begin{bmatrix} 1 + \tau_o(1 + \cos^2\chi) \\ \tau_o(B^2 - C^2) \\ 2\tau_o BC \end{bmatrix}\quad (2.7.5)$$

where $B = \sin\theta \sin\phi$

and $C = \cos\theta \sin i + \sin\theta \cos\phi \cos i$

Since $I_* \gg I_* \tau_o(1 + \cos^2\chi)$, we may write the observed normalized Stokes parameters as:

$$\begin{aligned}q &= \frac{Q}{I} = \tau_o(B^2 - C^2) \\ u &= \frac{U}{I} = 2\tau_o BC\end{aligned}\quad (2.7.6)$$

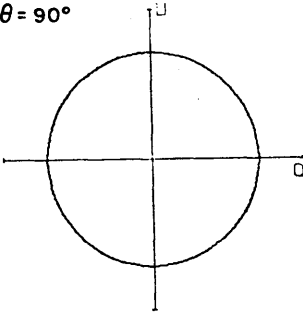
It may be noted that the forms of Equations (2.7.6) are applicable to all forms of Rayleigh scattering which has the same angular dependence as for free electrons.

2.8 A Preliminary Exploration of Possible Polarimetric Variations

The application of Equations (2.7.6) depends to a large degree on the underlying astrophysical processes involved in the generation and evolution of the globules and on the variety of *ad hoc* geometries that are considered. However, insight into possible polarimetric behaviour

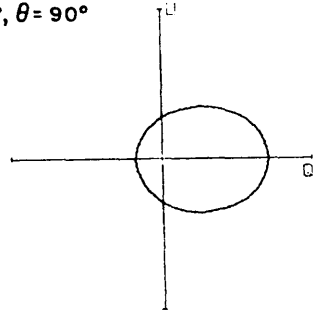
$i = 0^\circ, \theta = 90^\circ$

(a)



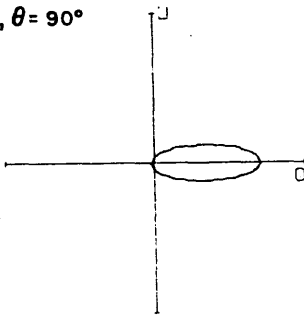
$i = 60^\circ, \theta = 90^\circ$

(b)



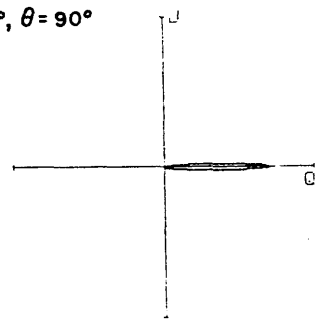
$i = 80^\circ, \theta = 90^\circ$

(c)



$i = 88^\circ, \theta = 90^\circ$

(d)



$i = 60^\circ, \theta = 90^\circ$

(e)

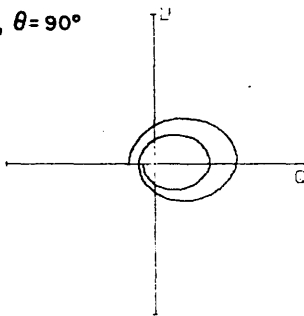


Fig. 2.8.1 For a globule in orbit about a stellar equator ($\theta=90^\circ$) the shape described in the (q,u) plane departs from a circle, to an ellipse, to a straight line as the inclination, i , of the star takes values from 0° to 90° .
(e): Dissipation of the globule during its orbit may produce spiral type figures.

can be gained by first considering two simple scenarios involving globules in orbit about the star at constant latitude.

2.8(a) Equatorial Break-up Because of high $V_{eq} \sin i$ values associated with Be stars, proposals for sporadic ejection of material from the stellar equator have a long history; references to the topic can be found in Peters (1976).

For an equatorially ejected globule, the polarization locus can be investigated from Equations (2.7.6) by setting $\theta = \frac{\pi}{2}$ and allowing ϕ to take all possible values from 0 to 2π . Figure 2.8.1 displays the behaviour for a range of inclination values, the amplitudes of the q , u values depending on the size of the globule and its distance from the stellar point source. It can be seen that the locus varies from a circle, through an ellipse to a straight line as i changes from 0 to $\frac{\pi}{2}$.

In reality, such regular loci are unlikely to be maintained. As the globule evolves, perhaps increasing its distance from the star and dissipating, the polarization locus would match this evolution. A possible schematic temporal development is shown in Fig. 2.8.1(e), the degree of spiralling being dependent on the dissipation rates and the stellar rotation period. The situation may be even more complicated as more than one globule and of differing strengths may be simultaneously present at different longitudes.

2.8(b) Oblique Rotator The photometric behaviour of some Be stars has been interpreted in terms of an oblique rotator model (see Harmanec, 1984) and this proposal may be extended to describe polarization variations. For example a magnetic pole might influence a concentrated outflow of material with globules which follow the field lines. If the magnetic pole is oblique to the rotational pole by the angle θ then, during its lifetime, the scattering globule is also at co-latitude θ . For a dipole field, two spots in the form of N and S poles are simultaneously present providing means for outflow and inflow

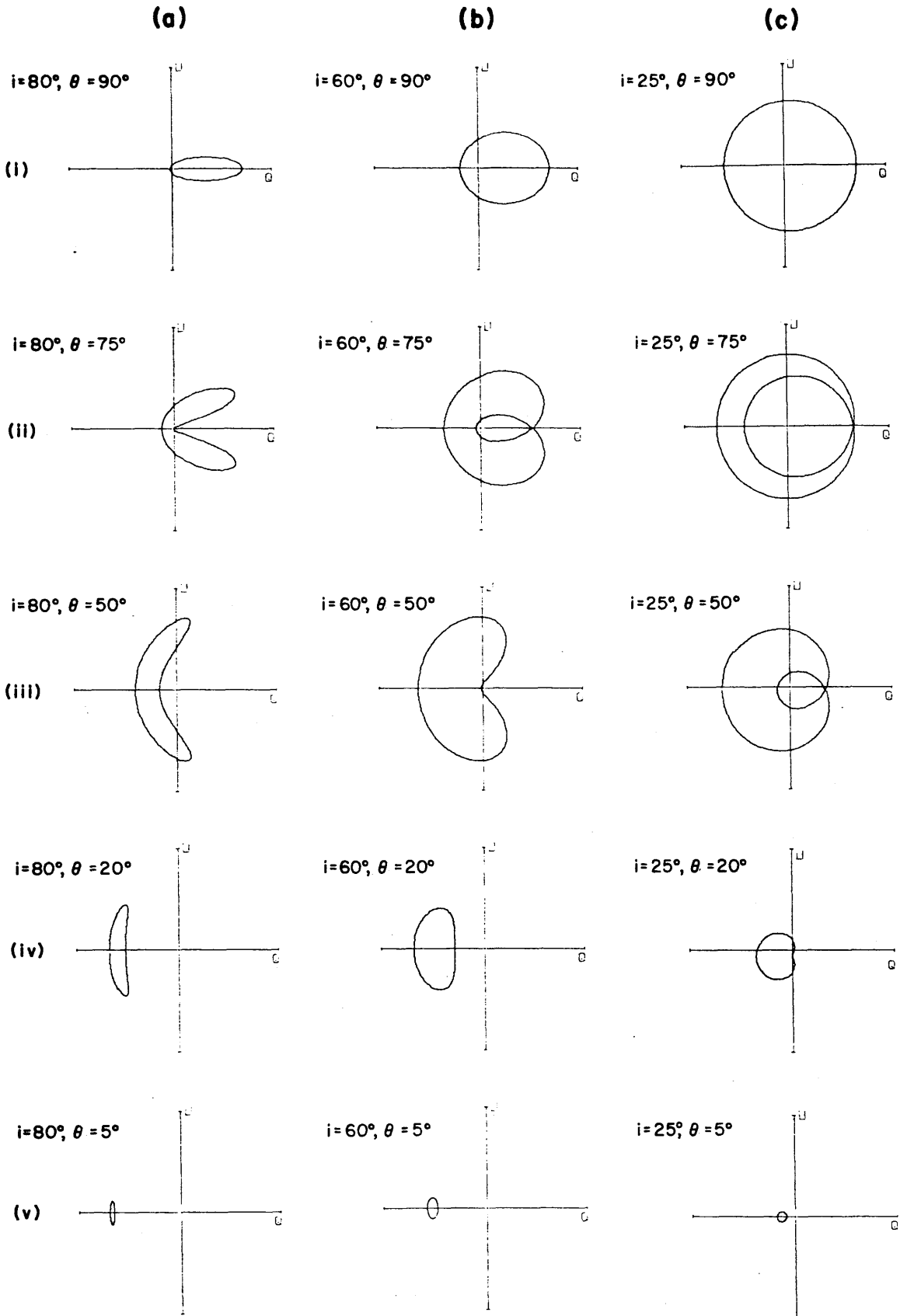


Fig. 2.8.2 In the scenario of a classical oblique rotator, an orbiting globule at angle θ from the rotational pole provides a wide range of (q,u) loci. As θ is varied from 90° (equatorial zone) to 5° (polar zone), the loci change from ellipses, to double-loops, to renal shapes, to near ellipses, their appearance depending on i . It can be seen that the loci always have at least one axis of symmetry, i.e. the q -axis being the projection of the equatorial plane on the sky; for the extreme case of $\theta=90^\circ$, the major axis is parallel to the equatorial line and for θ close to zero the major axis is orthogonal to this line.

of scattering material. However, as the scattering geometry is symmetric, the overall effect can be equated to a single globule at either pole and the subsequent discussion is therefore couched in terms of there being just one active region. This assumes that two globules, one at either pole, have a difference in ϕ of exactly $\pm\pi$, and that one globule has a co-latitude of θ and the other a co-latitude $\pi - \theta$.

Figure 2.8.2 displays the behaviour of polarimetric loci for a range of θ and i values. For a given inclination, the θ dependence shows that, starting at $\theta = \frac{\pi}{2}$ (i.e. on the equator), the pattern varies from being elliptical to a double loop, to a renal shape, to a near ellipse as θ approaches 0 (i.e. the pole). It may be noted that for these two physical extremes of θ , the major axes are orthogonal and that for $\theta = \frac{\pi}{2}$, the pattern encompasses the origin while for $\theta = 0$, it does not. In all cases, the locus has at least one axis of symmetry, this being the equatorial line.

Comparison may be made between the double looped pattern (see, for example, Fig. 2.8.2(b-iii)) and the data for σ Ori E (Kemp and Herman, 1977). In view of the observational evidence of a magnetic field periodicity (Landstreet and Borra, 1978), the magnetic oblique rotator model is an attractive alternative to the interactive binary model which has been applied to the data.

Again, in practice, the temporal behaviour will be more complicated than outlined by the simple theory above. For example the globule's radial distance will change continuously and the cloud will dissipate; several globules may be present simultaneously. The geometry might be complex in that the globules could emerge within a coned volume around the magnetic pole, hence making θ come from an interval. Indeed there may be a continuous stream in the cone with the occasional globule. Nonetheless, investigation of polarimetric data as outlined below provides means for investigating underlying geometries.

2.9 Geometry Assessment Based on Random Observations If it can be considered that at any given time the observed polarization is generated by a single globule, then, for a given value of i , the position of the data point in the q, u plane depends on the size of the globule, its distance from the star and its co-ordinates θ, ϕ . Neglecting the effects of the usual experimental noise, if it can be shown that n, r, θ and ϕ are independent of each other, the probability of observing the first normalized Stokes parameter in the range q to $q + \Delta q$ is given by

$$P(q | n, r, \theta, \phi) \Delta q = P(n) \Delta n \cdot P(r) \Delta r \cdot P(\theta) \Delta \theta \cdot P(\phi) \Delta \phi$$

Similarly for the second parameter (2.9.1)

$$P(u | n, r, \theta, \phi) \Delta u = P(n) \Delta n \cdot P(r) \Delta r \cdot P(\theta) \Delta \theta \cdot P(\phi) \Delta \phi$$

These Equations in combination with Equations (2.7.6) provide the Stokes plane data density distribution. Hence it is the underlying behaviour of the various probabilities associated with the sizes of the globules, $P(n)$, and with their geometric positions $P(r)$, $P(\theta)$, $P(\phi)$ which controls the probability distributions of the normalized Stokes parameters.

Again it may be noted that this approach is perhaps too simplistic to expect exact modelling. In real situations it is likely that the four probability distributions will not be completely independent. For example $P(n)$ is likely to depend on $P(r)$, particularly if the measurement sampling occurs during the evolution of a globule; similarly $P(n)$ may depend on $P(\theta)$. Nonetheless it is instructive to perform the exercise with the simplification of probability independence and this is done briefly below for some special model cases.

2.9(a) The Truly Random Model As mentioned earlier, reports on stellar polarimetric behaviour occasionally make reference to

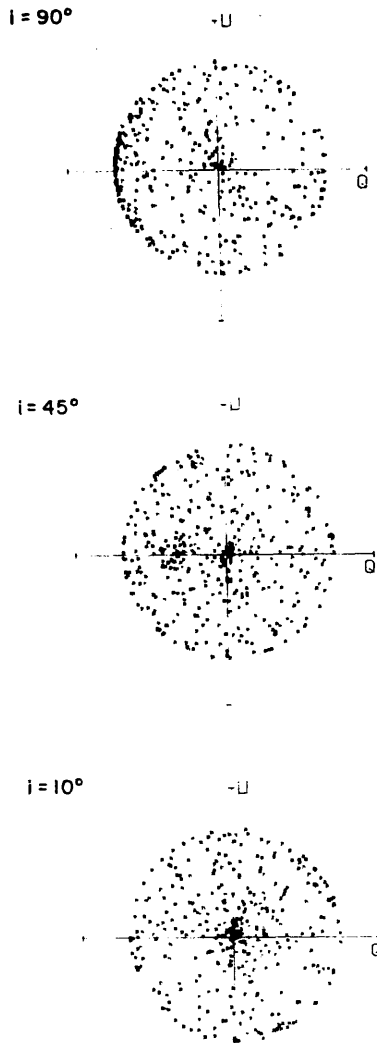


Fig. 2.9.1 For a given value of τ_0 with angular co-ordinates θ, ϕ coming from constant probability distributions between $0 \rightarrow \pi$ and $0 \rightarrow 2\pi$ respectively, the locus produced in the (q, u) plane is a circle, the density distribution being influenced by i .

time-paths in the data when plotted in the q, u plane; the term *random* is sometimes used to describe the pattern when no regular periodicity is detected or any other correlation with time is observed. However, the density distribution of the data in the q, u space is never assessed quantitatively and compared with what might be the expected behaviour of true random effects. Indeed, truly random effects in the star do not get translated into random data distributions in the q, u plane.

In terms of the scattering geometry, the truly random case occurs when $P(\theta)$ and $P(\phi)$ are constant for all values of θ (0 to π) and ϕ (0 to 2π). Figure 2.9.1 displays computer generated data for this case with various values for i and with both $P(n)$ and $P(r)$ set at unity at particular values of n and r . From a cursory view it might be thought that a distribution of globules over θ and ϕ as outlined above would give rise to q, u density distributions which are independent of i , as the random position of the globule has no significance in respect to this parameter. However, the scattering geometry does involve i and it is this contribution to the polarigenic mechanism that gives rise to the apparent biasing. For the above scenario, the Stokes plane density distribution depends on the probability distributions of B and C (see Equation (2.7.6)). As these latter terms use trigonometrical functions involving θ, ϕ and i as variables, biased density functions automatically ensue.

2.9(b) Restricted Models with Random Globules For the models involving equatorial break-up or the active spot (oblique rotator) as outlined earlier, a specific value is assigned to θ , so adding a restriction to the q, u density distribution. However all values of ϕ may still be considered to have equal probability either because that is the statistical nature of the globule generation or, in the case of a spot source following the rotation of the star, because of random

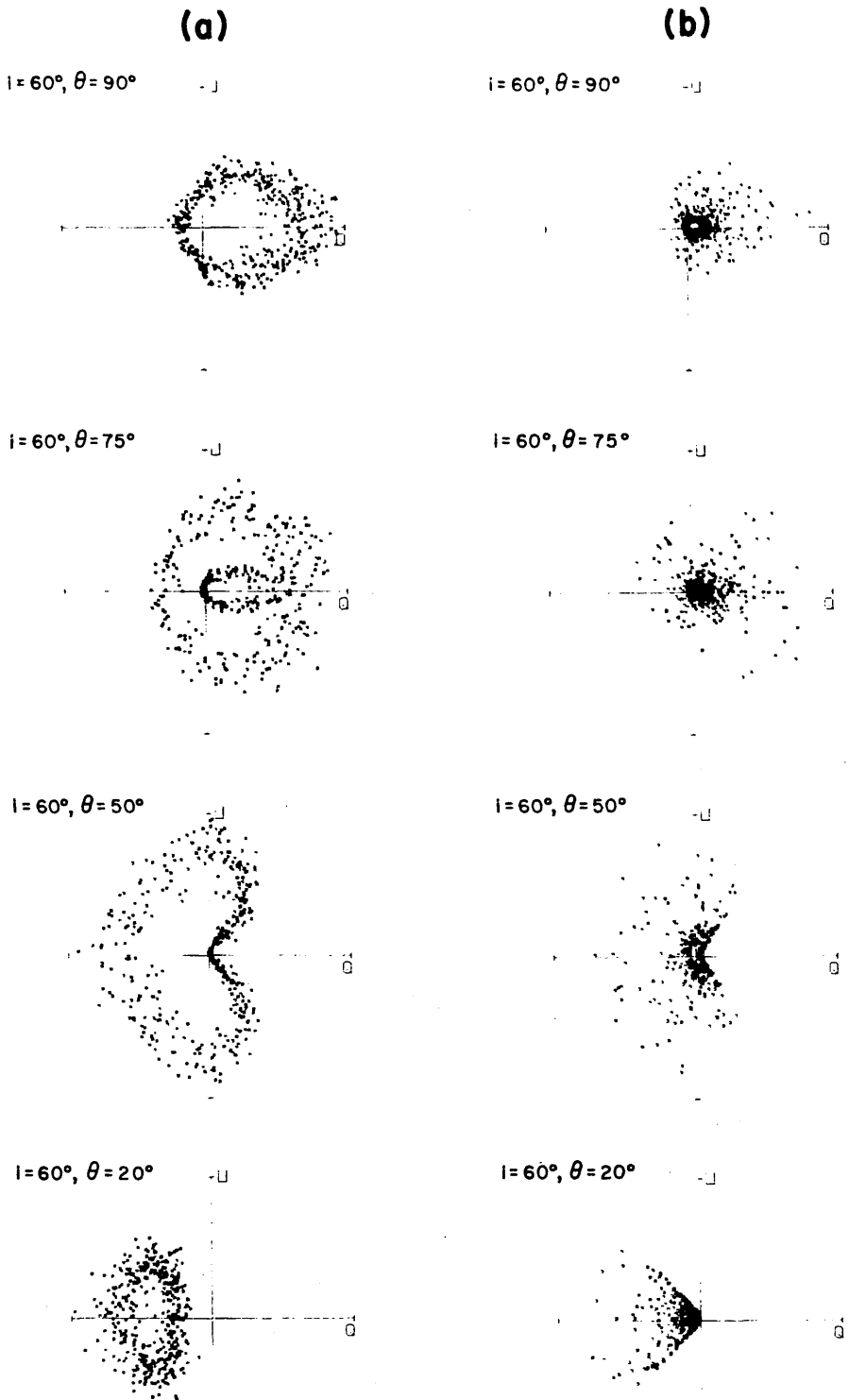


Fig. 2.9.2 (a) Using the same stellar geometries as Fig. 2.8.2(b) but introducing a Gaussian distribution for the size (n) of the globules and random values of ϕ , the basic data patterns are aberrated, the strength of the effect depending on the position on the periphery. (b) Introducing a restricted flat probability distribution for r but keeping n fixed, the data₂ patterns display density distributions reflecting the $1/r^2$ dependence of the scattering.

sampling in time by the observer. By assigning probability distributions to n and r , computer generated q , u density distributions may again be developed. Figure 2.9.2(a) depicts the result for the case where $P(n)$ has been given a normal distribution with $P(r)$ being unity at a particular value of r whereas Figure 2.9.2(b) shows the effect of $P(r)$ having a uniform distribution, but letting $P(n)$ be unity for a chosen value of n . The chosen geometries are the same as for Fig. 2.8.2 and the underlying behaviour patterns are clearly seen in Fig. 2.9.2(a) between the fuzzy boundaries resulting from the introduction of the $P(n)$ distribution. Because of the $1/r^2$ dependence of the strengths of the observed polarization parameters, the introduction of any reasonable function for $P(r)$ results in a bias to the density distributions with respect to the origin. As can be seen from Figure 2.9.2(b), the outer boundaries of the underlying patterns are more fuzzy than their inner edges. The effect increases as θ tends to the pole, gradually deforming the locus to a cone.

It may be noted that where the geometry provides larger polarization values, the data points become more spread, this reflecting that, with the chosen probability distributions, the departures from the underlying pattern reflect fractional changes to the polarization.

The magnitude of the data spread depends on the variance of the $P(n)$ function in relation to the mean value of n . If the variance is relatively large then open patterns tend to fill in with data points from one part of the underlying pattern overlapping the points from another part. Nonetheless, all of the density distributions produce at least one axis of symmetry which, if determined, provides the equatorial line for the star.

2.9(c) Ad hoc Restricted Models A more realistic model situation ensues if, in addition to the randomness of ϕ , the values of θ are

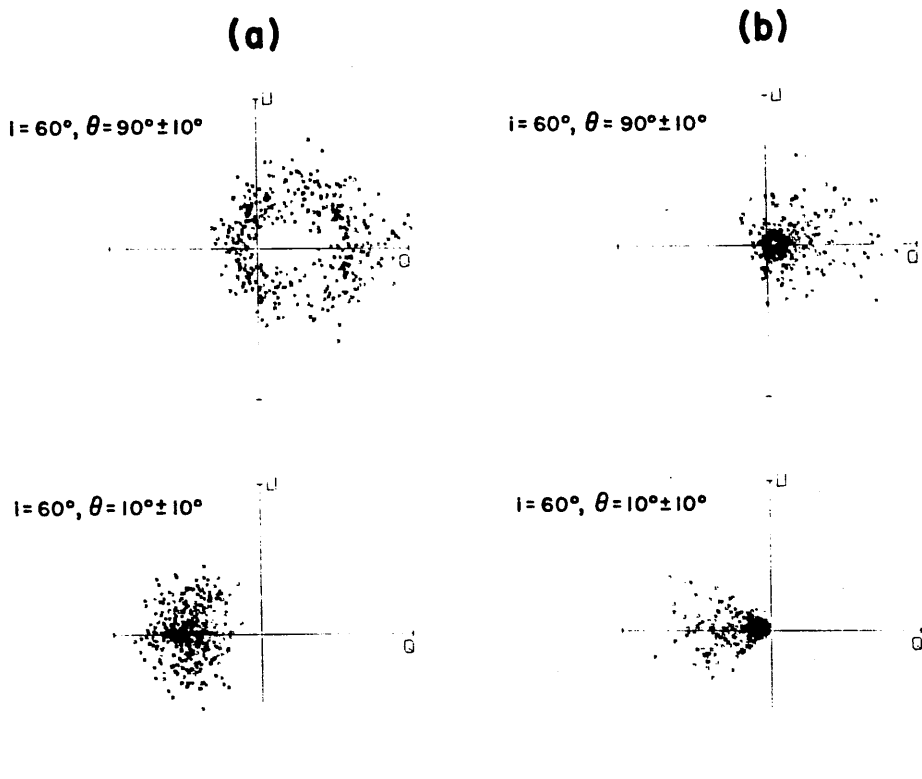
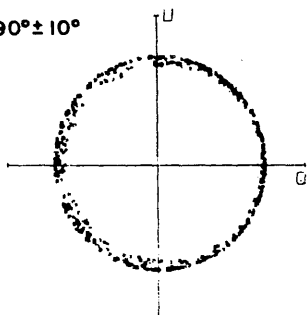


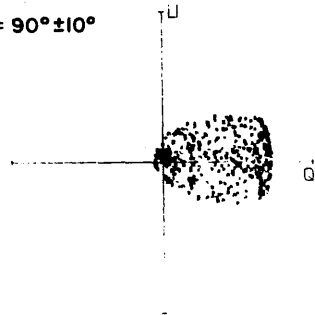
Fig. 2.9.4 (a) Introducing a normal distribution for the size (n) of the globules but otherwise applying the same constraints on the other parameters as in Fig. 2.9.3, the loci are similar, but with removal of sharp boundaries (*cf.* Fig. 2.9.2(a)).

(b) Restoring n to a unique value and letting r come from a restricted flat distribution, but otherwise using the same parameters as (a), the patterns produced are similar to those of Fig. 2.9.2(b).

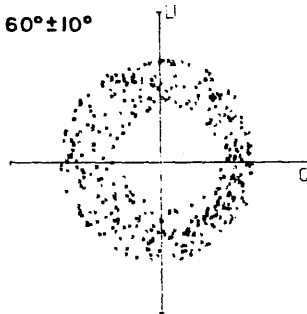
$$i = 10^\circ, \theta = 90^\circ \pm 10^\circ$$



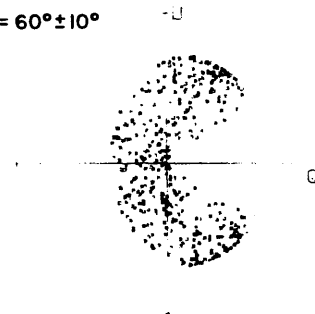
$$i = 80^\circ, \theta = 90^\circ \pm 10^\circ$$



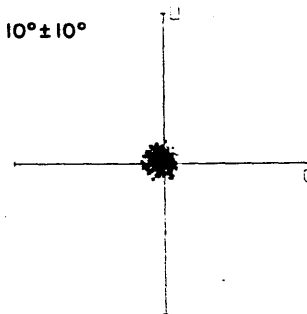
$$i = 10^\circ, \theta = 60^\circ \pm 10^\circ$$



$$i = 80^\circ, \theta = 60^\circ \pm 10^\circ$$



$$i = 10^\circ, \theta = 10^\circ \pm 10^\circ$$



$$i = 80^\circ, \theta = 10^\circ \pm 10^\circ$$

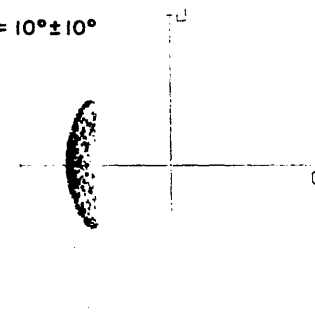


Fig. 2.9.3 Examples of data distributions for the case where θ has a flat distribution within a small interval ($\pm 10^\circ$) for given values of i , τ_0 , and random values of ϕ .

allowed to lie in a restricted range. In this way, for example, the effect of an outflow of material from a magnetic pole on the surface of a rotating star might be investigated by ascribing globules to the limits of a cone.

Figure 2.9.3 gives examples of the restricted cone model with a range of values of i . Both n and r are given unique values just to show how the introduction of a spread in θ tends to fill in the density distributions. With the addition of a normal $P(n)$ distribution (Fig. 2.9.4 - set (a)), the sharp limits of the q, u density distribution disappear, providing a behaviour which, at a superficial level, mimics real data. Giving $P(n)$ a singular value and allowing $P(r)$ to be a uniform distribution, Fig. 2.9.4(b) ensues. The degree of deformation of the expected q, u loci given by various particular values of i and θ , is consistent with the results of section 2.9(b).

It may be again noted that the computer generated data always produce at least one axis of symmetry related to the equatorial line. In the comparison of data for the equatorial flow in relation to a polar outflow it can be seen that the major axes of the elliptical or near-elliptical distributions are parallel to and perpendicular to the equatorial line respectively. Hence, even a cursory examination of data should indicate any preference of geometry for the outflow.

2.10 Preamble to Model Fitting of Polarimetric Data

Sections 2.7 to 2.9 showed that if sufficient measurements are made of stars which display fluctuations of polarization, quantitative analysis of the density distributions of the data in the q, u plane may provide insight into the geometries and size distributions of the globules which give rise to the variations. Such studies would be particularly relevant in helping to decide on the basic causes of other rapid variations (photometric and spectral) as to whether they result from rotating inhomogeneities, non-radial pulsations or the presence of

a close companion.

This suggests the need to compare the recorded q and u probability functions with the basic models and their equivalent computer generated data, with a view to isolating the key underlying astrophysical processes and geometries. Data reduction and processing techniques will be required, and the description of these follows.

With the ideas on mechanisms for producing polarimetric variability in mind and with the intent of evaluating the parameters associated with the best fit of the stochastic globule model to a set of measurements, i.e. determining the basic geometry of the situation and the sizes and evolution of the globules, a variety of approaches to the analysis of polarimetric data are presented.

Any previous general temporal polarimetric analysis has been applied in relation to periodicity searching and the establishment of geometries associated with interactive binaries (for example, see Brown, McLean and Emslie, 1978). In this thesis, new approaches to temporal data analysis will be presented and, in addition, other novel schemes will be demonstrated that concentrate on the distribution of the q , u values without recourse to the times of measurement, allowing for situations where there is no underlying periodicity or where it might be assumed that if any periodicity is present, the observational scheme imposes a randomness to the sampling.

Before applying the analyses described below, it is assumed that statistical tests will have first been undertaken to demonstrate that the distribution of measured values in the q , u plane represent real fluctuations above the experimental noise; such tests to see if the spread of points is greater than that expected from experimental and photon shot noise are described in the polarimetric work of Kemp and Barbour (1983) and Hayes (1984) for example, or a scheme of the type described in Section 2.5 carried out.

2.11 Further on the Model Equations

Equations (2.7.6) may be written as:

$$q = \tau_o (a_o + a_1 \cos\phi + a_2 \cos 2\phi) \quad (2.11.1)$$

$$u = \tau_o (b_1 \sin\phi + b_2 \sin 2\phi)$$

where $a_o = \sin^2 i \left(\frac{3}{2} \sin^2 \theta - 1 \right)$

$$a_1 = -\frac{1}{2} \sin 2\theta \sin 2i$$

$$b_1 = \sin 2\theta \sin i$$

$$a_2 = -\frac{1}{2} \sin^2 \theta (1 + \cos^2 i)$$

$$b_2 = \sin^2 \theta \cos i$$

In practice the application of these equations is made complicated for four reasons, it being convenient to introduce them in the following order. Firstly, there is likely to be an intrinsic polarization from the global extended atmosphere. This situation has been modelled for the optically thin axisymmetric case by Brown and McLean (1977) and provides an offset, q_A , in the first parameter only. Secondly, the stellar equatorial line will, in general, be rotated relative to the instrumental measuring frame which in turn is normally relatable to the standard celestial equatorial frame. Thirdly, there may be an interstellar polarization affecting both normalized Stokes parameters. Usually its value, q_I , u_I , is expressed in the standard celestial equatorial co-ordinate frame or instrumental frame. Relating the overall situation to the chosen reference frame by using the Mueller calculus (see Clarke and Grainger, 1971), Equations (2.11.1) may be written as:

$$q_{*j} = q_I + (q_A + \tau_o (a_o + a_1 \cos\phi_j + a_2 \cos 2\phi_j)) \cos 2\Omega - \tau_o (b_1 \sin\phi_j + b_2 \sin 2\phi_j) \sin 2\Omega + n_{qj} \quad (2.11.2)$$

$$u_{*j} = u_I + (q_A + \tau_o (a_o + a_1 \cos\phi_j + a_2 \cos 2\phi_j)) \sin 2\Omega + \tau_o (b_1 \sin\phi_j + b_2 \sin 2\phi_j) \cos 2\Omega + n_{uj}$$

where Ω is the rotation (positive) of the stellar equatorial line to the reference frame and the subscript j refers to the values associated

with the j^{th} measurement. More correctly, for the general stochastic model, τ_0 should also be subscripted to allow for its variability. In most of the analytical procedures it is assumed to be constant. Fourthly, as indicated in Equations (2.11.2), the measurements carry the usual experimental noise which in the optimum case is set by photon shot noise. To a good approximation, it can be assumed that the experimental noise behaves as though it is additive to the underlying polarization, i.e. it is not a fractional noise. Its values n_{q_j} and n_{u_j} can be considered to be taken from a probability distribution, say from normal distributions with zero mean and standard deviations σ_q and σ_u . For the proposed schemes of analysis, it is assumed that the data are fairly homogeneous in terms of noise strength with each of the values of q and u carrying the same uncertainty ($\sigma_q = \sigma_u$).

If the globule is in co-rotation with the star and Equations (2.11.2) are being considered with a view to determining periodicities, they can be modified by replacing with $(2\pi\nu t + \epsilon)$ where ν is the rotational frequency and ϵ the phase relative to some epoch, say the time of the first measurement in the data stream. Terms involving $2\pi\nu$ may be defined as contributors of the fundamental and those with $4\pi\nu$ the harmonic. Values of ν may be positive or negative depending on the sense of rotation of the star; a positive value corresponds to a left-to-right rotation as seen by the observer.

Hence

$$\begin{aligned}
 q_*(t_j) = & q_I + (q_A + \tau_0(a_0 + a_1 \cos(2\pi\nu t_j + \epsilon_f) + a_2 \cos(4\pi\nu t_j + \epsilon_h))) \cos 2\Omega \\
 & - \tau_0(b_1 \sin(2\pi\nu t_j + \epsilon_f) + b_2 \sin(4\pi\nu t_j + \epsilon_h)) \sin 2\Omega + n_{q_j}
 \end{aligned}
 \tag{2.11.3}$$

$$\begin{aligned}
 u_*(t_j) = & u_I + (q_A + \tau_0(a_0 + a_1 \cos(2\pi\nu t_j + \epsilon_f) + a_2 \cos(4\pi\nu t_j + \epsilon_h))) \sin 2\Omega \\
 & + \tau_0(b_1 \sin(2\pi\nu t_j + \epsilon_f) + b_2 \sin(4\pi\nu t_j + \epsilon_h)) \cos 2\Omega + n_{u_j}
 \end{aligned}$$

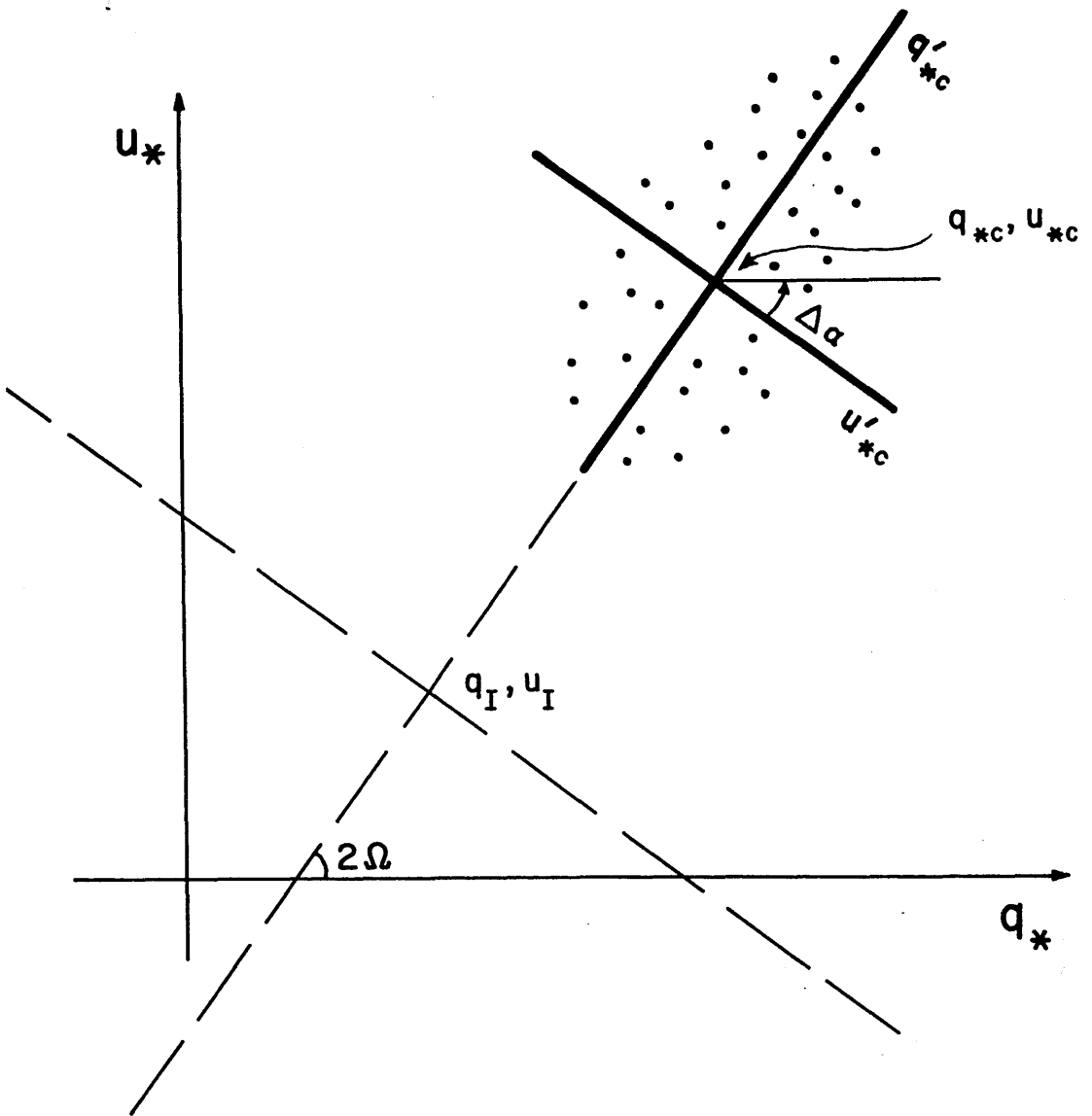


Fig. 2.11.1 Stellar intrinsic normalized Stokes parameter axes are translated and rotated (2Ω) relative to the instrumental axes (q_*, u_*) by the interstellar components (q_I, u_I). A set of axes parallel to the intrinsic axes but with origin on the centre of gravity of the data (q_{*c}, u_{*c}) are used to investigate their distribution by the method of moments, and by χ^2 tests (sector width $\Delta\alpha$); periodicity may also be investigated by the method of least squares, by correlation of the position angle, α , and by correlation of the sign of u'_{*c} .

where t_j refers to the time of the individual measurements and ϵ_f and ϵ_h refer to the planes of the fundamental and harmonic respectively; in this model $\epsilon_h = 2\epsilon_f$. An example of the behaviour of Equations (2.11.3) with noise is depicted in Figure 2.11.1. Some idea of how the data pattern would change according to the stellar geometry (i, θ) can be obtained by considering Figs. 2.8.1 and 2.8.2, adding an offset intrinsic polarization, rotating the co-ordinate frame, taking points at random on the locus and adding an experimental noise.

Even if the experimental noise is small, rather than following clearly defined loci, values from the stochastic globule model and real measurements provide data densities with a spread that is influenced by the probabilities associated with the various model parameters $(\theta, \phi, \tau_0$ - see Section 2.9). The analytical techniques described below address the problem of fitting the recorded data density distribution to the stochastic model.

2.12 Data Reduction Procedures

Some points on reducing data have been raised before by previous workers but not in a unified way as is done here.

Equations (2.11.2) and (2.11.3) may be used to various degree to provide information about stellar systems. In the first place they may be considered solely in connection with periodicity searches with either or both Stokes parameters being investigated. The amplitudes of the q and u fundamental and harmonic frequency components might be evaluated independently and compared to ascertain the basic geometric coefficients (i, θ) of the system and its orientation Ω relative to the instrumental reference frame. Ultimately the best model fit might be investigated incorporating the combination of the fundamental and its harmonic simultaneously for both Stokes parameters, with the appropriate phase restraints, as necessary.

Another approach might involve determination of the basic geometry

of the star ignoring the times of measurement, involving only the behaviour of the q, u data density distribution.

The chief difficulty in performing any data analysis is the decoupling of the model parameters (i, θ) from those introduced by the observer (Ω , and ϵ if relevant). If any of the parameters can be determined prior to the main analysis, especially Ω , the model fitting procedures are greatly simplified.

Valuable insight to the situation should be available if the interstellar polarization is known before the main analysis (see Section 2.5). Its position (q_I, u_I) in the reference frame provides an origin for the intrinsic polarization (see Fig. 2.11.1).

Knowledge of the intrinsic origin is particularly useful for making preliminary assessments of the data by looking for characteristic patterns as described in Sections 2.7 to 2.9, this being particularly valid if it can be assumed that the times of observation have imposed a randomness on the values of ϕ . Assuming that the measurements constitute a large sample taken randomly with respect to any underlying periodicity, their centre of gravity (q_{*C}, u_{*C}) may be defined as (cf. Equations (2.11.3)):

$$q_{*C} = q_I + (q_A + \tau_0 a_0) \cos 2\Omega \quad (2.12.1)$$

$$u_{*C} = u_I + (q_A + \tau_0 a_0) \sin 2\Omega$$

Hence if the interstellar polarization can be estimated accurately, its offset can be subtracted allowing the orientation of the stellar equatorial line to be determined, since q_{*C} and u_{*C} should lie on this line; the direction of the centre of gravity of the data distribution relative to the intrinsic origin corresponds to the equatorial line. With knowledge of Ω , model fitting could be undertaken more directly.

Comment on the underlying nature of Equations (2.11.3) has previously been made by Brown *et al.* (1978). They have clearly demonstrated that the fundamental and the harmonic treated separately represent elliptical figures. With the nomenclature here, the fundamental ellipse has its major-axis parallel to the u -axis of the stellar frame, while the harmonic ellipse is parallel to the q -axis, the eccentricities depending on the inclination. The relative size of the ellipses depends on the position of the globule in the stellar system. A strong fundamental ellipse indicates a globule nearer to the pole while a strong harmonic indicates a globule closer to the equator.

If there is an obvious eigendirection in the data density distribution, this corresponds to the major-axis of one of the ellipses (fundamental or harmonic) described above. Thus the value of Ω is determined with ambiguity, i.e. the preferred axis corresponds to Ω or $\Omega + \frac{\pi}{4}$, remembering that angles are doubled when plotted in the q, u plane.

More quantitative investigations along these lines form part of a more general approach to model fitting from which all of the geometric parameters - those associated with the star and its geometric aspect - automatically emerge. This scheme is now presented below.

2.13 The q, u Density Distribution

2.13(a) Investigation by Taking Moments A first approach to the investigation of the data density distribution can be made by projecting the measurements along various axes and examining their distribution in the form of a histogram. Comparison might be made of the histogram profile with computer generated data via Equation (2.11.1). For convenience the axes might be made to pass through the centre of gravity of the data, the measurements having been transformed to the centre of gravity frame to provide new values given by $q'_{*c} = (q_* - q_{*c})$ and $u'_{*c} = (u_* - u_{*c}) - c\delta$. Equations (2.11.2) and (2.12.1). By

rotating the centre of gravity frame, the various projected frequency distributions might be examined and the direction along which the maximum spread occurs might be termed the major principal axis (MPA).

It can be seen from Equation (2.11.1) that q and u will have maxima. In the case of the q parameter, this occurs when $\phi=0$ but for u , the required value of ϕ depends on the choice of u_1 and u_2 . The relative magnitude of the q and u maxima also depends on the underlying model parameters and if an elongation is seen in the data, its direction corresponds to either the q or u axis. Thus by estimating the direction along which positions of the data extrema lie to determine the MPA, it may be seen from Equations (2.11.2) that Ω can be deduced but with ambiguity (Ω or $\Omega + \frac{\pi}{4}$), depending on the underlying values of i and θ , as already described above in relation to the equatorial and polar ellipses.

A more quantitative statistical approach can be applied by taking various moments $m_{(k)}$ about the centre of gravity, here the moment being defined for N data points (cf. Section 2.2) as:

$$m_{(k)q} = \frac{1}{N} \sum_{j=1}^N (q_{*j} - q_{*c})^k ; \quad m_{(k)u} = \frac{1}{N} \sum_{j=1}^N (u_{*j} - u_{*c})^k \quad (2.13.1)$$

The incorporation of the centre of gravity of the data points q_{*c} , u_{*c} into the definitions automatically forces the first moment to be zero.

The second moment gives a measure of the spread of the data, defining the population variance, and it can be used for assessing the presence of eigendirections and determining the stellar equatorial line. Further, the second moment can be used for establishing i , if it can be shown that θ has a value from either the equatorial or polar zones.

If the reference frame for the measured Stokes parameters is

rotated through an angle α , the data can be transformed to the new frame by applying the appropriate Mueller matrix to Equations (2.11.2) to give:

$$\begin{aligned} q_{*j} = & q_1 \cos 2\alpha + u_1 \sin 2\alpha + n_{qj} \cos 2\alpha + n_{uj} \sin 2\alpha \\ & + (q_A + \tau_o(a_o + a_1 \cos \phi_j + a_2 \cos 2\phi_j)) \cos 2(\Omega - \alpha) \\ & - \tau_o(b_1 \sin \phi_j + b_2 \sin 2\phi_j) \sin 2(\Omega - \alpha) \end{aligned} \quad (2.13.2)$$

$$\begin{aligned} u_{*j} = & -q_1 \sin 2\alpha + u_1 \cos 2\alpha - n_{qj} \sin 2\alpha + n_{uj} \cos 2\alpha \\ & + (q_A + \tau_o(a_o + a_1 \cos \phi_j + a_2 \cos 2\phi_j)) \sin 2(\Omega - \alpha) \\ & + \tau_o(b_1 \sin \phi_j + b_2 \sin 2\phi_j) \cos 2(\Omega - \alpha) \end{aligned}$$

By taking the second moments in the new frame, in the limit for a large sample, it may be shown that:

$$\begin{aligned} m_{(2)q\alpha} = & \frac{\tau_o^2}{2} ((a_1^2 + a_2^2) \cos^2 2(\Omega - \alpha) + (b_1^2 + b_2^2) \sin^2 2(\Omega - \alpha)) \\ & + \sigma_q^2 \cos^2 2\alpha + \sigma_u^2 \sin^2 2\alpha \end{aligned} \quad (2.13.3)$$

$$\begin{aligned} m_{(2)u\alpha} = & \frac{\tau_o^2}{2} ((a_1^2 + a_2^2) \sin^2 2(\Omega - \alpha) + (b_1^2 + b_2^2) \cos^2 2(\Omega - \alpha)) \\ & + \sigma_q^2 \sin^2 2\alpha + \sigma_u^2 \cos^2 2\alpha \end{aligned}$$

(See Appendix B for proof).

Hence the second moments take on maxima and minima when $\alpha = \Omega$ or $\Omega + \frac{\pi}{4}$, depending on the relative magnitudes of $(q_1^2 + q_2^2)$ and $(u_1^2 + u_2^2)$. For example, for the equatorial case, $a_1 = b_1 = 0$ and $a_2 \geq b_2$ and the maximum of $m_{(2)q\alpha}$ occurs when $\alpha = \Omega$; for the polar case, $a_2 = b_2 = 0$ and $b_1 > a_1$, giving the maximum of $m_{(2)q\alpha}$ at $\alpha = \Omega + \frac{\pi}{4}$. Thus the ambiguity of determining Ω already mentioned in earlier general discussions is clearly identified. However, if the direction of the interstellar polarization is known with reasonable confidence, the ambiguity might be resolvable. With noisy measurements it may also be noted that the eigendirections will be difficult to identify if the underlying model

provides $(a_1^2 + a_2^2) = (b_1^2 + b_2^2)$. It may also be noted that the test is strictly valid only if $\sigma_q = \sigma_u$, so making the effects of noise independent of the choice of the co-ordinate frame. A check on whether the maximum and minimum variances are statistically significantly different can be made by the usual F-test (see Snedecor and Cochran, Sec. 6.12, 1980).

As previously mentioned, the inclination can also be derived by the second moments when θ is approximately polar or equatorial.

Case (1) Polar ($\theta \rightarrow 0^\circ$)

Here the correct orientation of the reference frame is obtained when $\alpha = \Omega + \frac{\pi}{4}$ thus:-

$$m_{(2)}_{q\alpha} = \frac{\tau_0^2}{2} (b_1^2 + b_2^2) + \sigma_q^2 \cos^2 2\alpha + \sigma_u^2 \sin^2 2\alpha \quad (2.13.4)a$$

$$m_{(2)}_{u\alpha} = \frac{\tau_0^2}{2} (a_1^2 + a_2^2) + \sigma_q^2 \sin^2 2\alpha + \sigma_u^2 \cos^2 2\alpha$$

Now for any relevant distribution under study, at α the maximum variance (V_2) should occur (i.e. parallel to u-axis) and simultaneously a minimum variance (V_1) in the orthogonal direction (i.e. parallel to q-axis); these variances will correspond to $m_{(2)}_{q\alpha}$ and $m_{(2)}_{u\alpha}$ respectively. Since σ_q^2 and σ_u^2 are known, these two added variances are easily subtracted from V_1 and V_2 . So, and remembering $a_2 = b_2 = 0$:

$$V_2 - (\sigma_q^2 \cos^2 2\alpha + \sigma_u^2 \sin^2 2\alpha) = \sigma_2^2 = \frac{\tau_0^2}{2} b_1^2 = \frac{\tau_0^2}{2} \sin^2 2\theta \sin^2 i \quad (2.13.4)b$$

$$V_1 - (\sigma_q^2 \sin^2 2\alpha + \sigma_u^2 \cos^2 2\alpha) = \sigma_1^2 = \frac{\tau_0^2}{2} a_1^2 = \frac{\tau_0^2}{8} \sin^2 2\theta \sin^2 2i$$

$$\text{i.e.} \quad i = \cos^{-1} \left[\frac{\sigma_1}{\sigma_2} \right] \quad (2.13.5)$$

Although $a_2 = b_2 = 0$ only occurs when there are no variations (i.e. $\theta = 0$),

Estimated Inclination vs. True Inclination

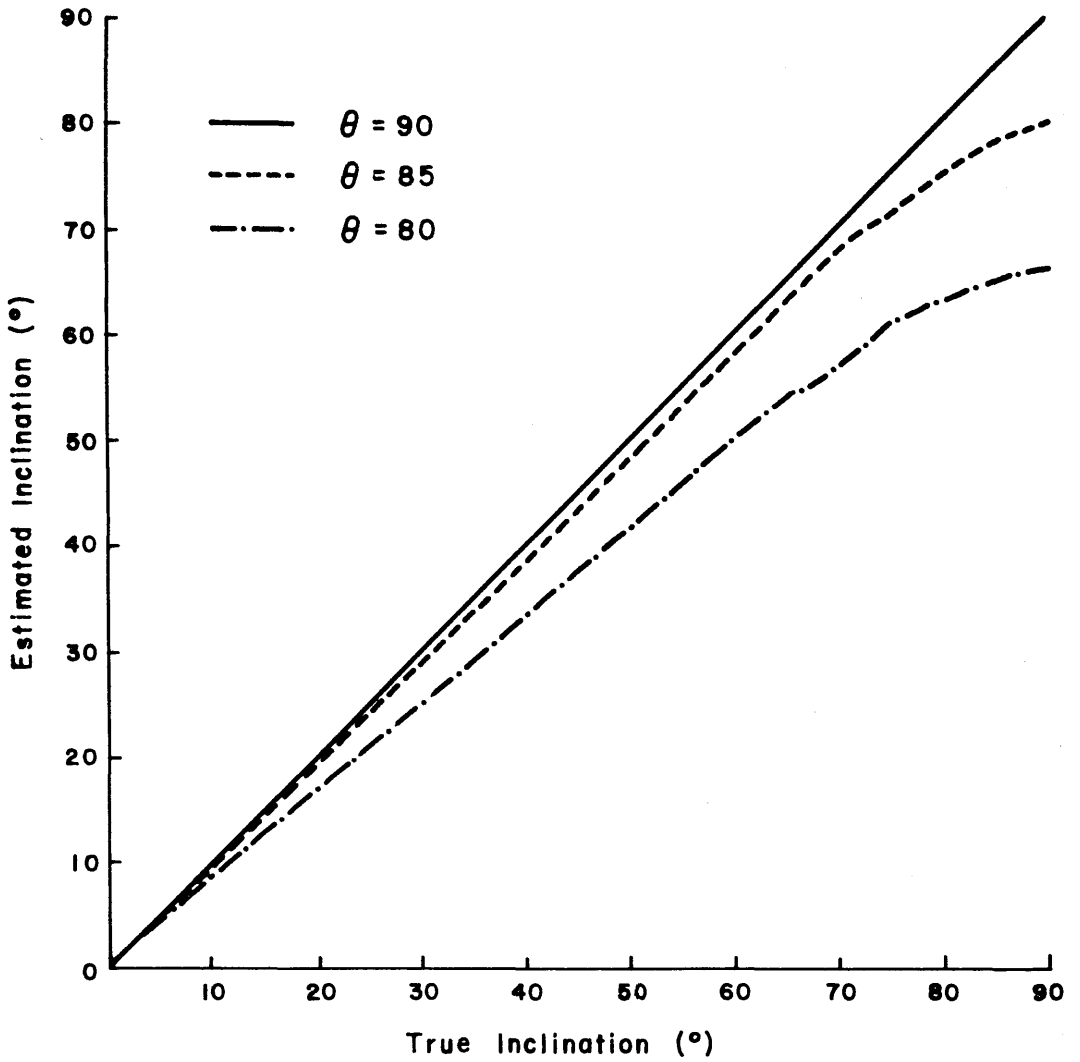


Fig. 2.13.2 For a star showing variations about its equatorial zone, the inclination may be derived by forming the ratio of the second moments. The formula can be used to give a reasonable estimation of the stellar inclination until $\theta < 80^\circ$.

Estimated Inclination vs. True Inclination

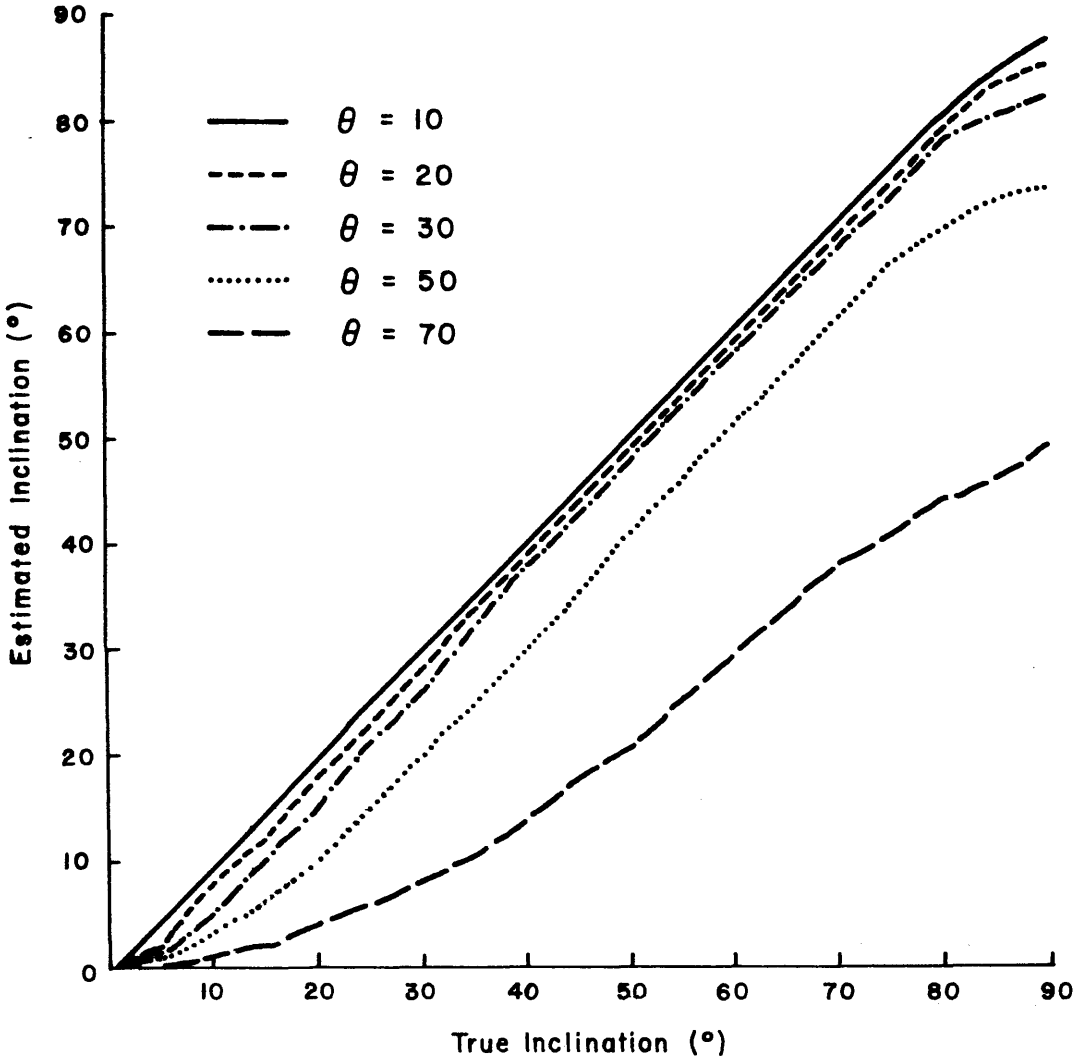


Fig. 2.13.1 When it can be demonstrated that a star is showing variations from its polar regions, the stellar inclination can be estimated by taking the ratio of the second moments. The estimation holds good until $\theta > 30^\circ$.

Fig. 2.13.1 shows how well the approximate formula (Equation (2.13.5)) holds for various values of θ . There appears to be an insignificant underestimation in i , until $\theta > 30^\circ$.

Case (2) Equatorial ($\theta = 90^\circ$)

At $\alpha = \Omega$, correct orientation is achieved, Equation (2.13.3) becoming:

$$m_{(2)q\alpha} = \frac{\tau_0^2}{2} (a_1^2 + a_2^2) + \sigma_q^2 \cos^2 2\alpha + \sigma_u^2 \sin^2 2\alpha \quad (2.13.6)$$

$$m_{(2)u\alpha} = \frac{\tau_0^2}{2} (b_1^2 + b_2^2) + \sigma_q^2 \sin^2 2\alpha + \sigma_u^2 \cos^2 2\alpha$$

So for any related distribution under study, noting that $a_1 = b_1 = 0$, and applying the corrections for experimental noise as in Case (1):

$$V_2 - (\sigma_q^2 \cos^2 2\alpha + \sigma_u^2 \sin^2 2\alpha) = \sigma_2^2 = \frac{\tau_0^2}{2} a_2^2 = \frac{\tau_0^2}{8} \sin^4 \theta (1 + \cos^2 i)^2 \quad (2.13.7)$$

$$V_1 - (\sigma_q^2 \sin^2 2\alpha + \sigma_u^2 \cos^2 2\alpha) = \sigma_1^2 = \frac{\tau_0^2}{2} b_2^2 = \frac{\tau_0^2}{2} \sin^4 \theta \cos^2 i$$

$$\text{i.e.} \quad i = \cos^{-1} \left[\frac{\sigma_2}{\sigma_1} - \left[\frac{\sigma_2^2}{\sigma_1^2} - 1 \right]^{\frac{1}{2}} \right] \quad (2.13.8)$$

Note in Equation (2.13.8) that since $\sigma_2^2 \geq \sigma_1^2$, i has only one solution. Fig. 2.13.2 reveals the adequacy of the approximation of i , for differing θ values. Fig. 2.13.2 suggests reasonable estimates of i are got for θ down to $\approx 80^\circ$.

In both cases, if experimental noise is not removed, the value of i derived would be further underestimated. Errors on i may be calculated by considering confidence intervals on the population variances of the sample variances V_1 and V_2 . Further, V_1 and V_2 can be ratioed by the variances of the experimental noise to check if V_1 and V_2 are above the instrumental error (cf. Section 2.5) via the F-test.

The third moment describes the asymmetry of any distribution and it can be seen from Figs. 2.8.2 or from Equations (2.11.2) that the stellar equatorial line provides an axis of symmetry for the general model. Thus by adjusting the value of α until the minimum value of $m_{u_\alpha}^{(3)}$ is obtained (zero for a large data sample), Ω is determined uniquely. The power of the third moment for determining the stellar equatorial axis is best for models away from the extremes of the equatorial and polar cases, particularly the former, which for the exact case provides an indeterminacy. As can be readily seen from Fig. 2.8.2, $m_{q_*}^{(3)}$ is zero when $i=0^\circ$ or $=90^\circ$. However, the ambiguity is resolved by noting that the difference between $m_{q_*}^{(2)}$ and $m_{u_*}^{(2)} = \Delta M^{(2)}$ is zero at $i=0^\circ$, but not at $\theta=90^\circ$.

2.13(b) Chi-Square Testing One of the standard procedures for model fitting is the application of the χ^2 -statistic to compare the data with values engendered by the theoretical model. For the exercise here, the data should be transformed to the centre of gravity frame. If the value of Ω is known with the data set already expressed in the stellar co-ordinate frame, Equation (2.11.2) would be used with Ω equal to zero. Classes may be constructed by dividing the data, q'_{*c} , u'_{*c} , into a set of sectors of angular width $\Delta\alpha$ (see Fig. 2.11.1). According to Cochran (1952), the number of classes for comparison by the χ^2 -test should be moderate (10-25) and have equal interval. Since χ^2 works best with classes containing a larger rather than smaller sample, a convenient division might involve 10 sectors each of width 36° .

The observed probability (p_j) for the number of data points in the j^{th} sector is given by the ratio of the number of points in that sector to the total number of points, N , constituting the data. Again using Equation (2.11.2), the expected probability (P_j) can be calculated by Monte Carlo methods according to the chosen model parameters i , θ (and Ω if necessary) and the selected probability distribution for ϕ , an

obvious one being that all values of ϕ are equally probable. The initial value of τ_0 can be taken as unity since scale is not important in the comparison. For testing that τ_0 might be varying, a variety of distributions for n and r can be applied, either in combination or singularly, depending on the proposed globule production mechanism and evolution.

Comparison of p_j with P_j may be made through the statistic

$$\chi^2 = N \sum_{j=1}^{10} \frac{(p_j - P_j)^2}{P_j} \quad (2.13.9)$$

It is then possible to test the null hypothesis, H_0 : Can the observations be regarded as randomly drawn from the theoretical distribution? The value of χ^2 can then be compared with the appropriate tables to assess the statistical significance of any fit. Since the computed values of the P_j 's represent estimates for the true probability distribution for the model, the degrees of freedom are (10-2) rather than (10-1). Accordingly the critical value of χ^2 for rejection at the 5% level is =15.51, for example. The parameters which produce the minimum value of χ^2 from Equation (2.13.9) provide the best model fit. Hence the most appropriate values of i , θ , and Ω (if necessary) are determined with a calculated significance. The sharpness of the minimum value of χ^2 will depend on the number of sectors chosen in relation to the total number of data points and the underlying values of i and θ not to mention the quality of the data used itself; in practice the number of sectors might be varied to achieve the sharpest minimum, i.e. to obtain the narrowest range of acceptable model fits.

Since the apexes of the sectors are at the origin of the centre of gravity frame, it will be appreciated that the chances of a data point in this vicinity lying in any particular sector are greatly dependent

on the experimental noise. To reduce the error on the observed probabilities, weighting might be applied to the data. One possible scheme might remove all points within a specified radius from the origin and recalculate χ^2 after amending the value of N. Without knowing the value of τ_0 (which cannot be found by this method), it is very difficult to assign a value to the standard deviations of the experimental noise, if their effect is to be included in the calculation of P_j , from Equation (2.11.2). A rule of thumb might be, however, let the standard deviations of n_q and n_u be comparable with the amplitudes of a_1 , a_2 , b_1 and b_2 predicted by the values of i and θ under study.

2.14 Polarimetric Periodicities

2.14(a) Introduction Polarimetric periodicity may be caused by scattering from material in co-rotation within a binary system or by a scattering zone revolving with a single star. Equations describing the first situation have been developed by Brown *et al.* (1978) and several binaries have been analysed in terms of their canonical model (e.g. Brown *et al.* - *loc. cit.* Rudy and Kemp, 1978). In terms of polarimetry, a single rotating star with an enhanced scattering region is equivalent to a special case of the binary model and is represented by Equations (2.11.3). It is taken that the globule acts as the polarigenic mechanism, with the variability caused by stellar rotation, the globule being attached in some way to the stellar photosphere. In this investigation of how the periodicities can be determined from the data, the discussion is couched in terms of single stars rather than binary systems, appreciating that additional observational material, such as radial velocity variations or a light curve, may be applied to help decide on the fundamental nature of the variability.

In the discussion below, Equations (2.11.3) are investigated with a view to obtaining values for the periodicity, phase and geometric

coefficients with emphasis on quantifying the statistical significance of the fits of the model parameters. The application of the method of determining Fourier coefficients (Section 2.14(b)) makes no pretence of being new but a brief discussion of this topic is presented for completeness. Two other novel data treatments will then be presented, the last one being appropriate to situations in which the effective globule scattering strength, τ_0 , displays temporal fluctuations or in which the strength of the contribution from the axisymmetric atmosphere exhibits changes.

Again, any analysis is simplified if Ω is already known and the problem is made easier if the value of the phase ϵ can be assumed, say from independent measurements such as a light curve or a radial velocity curve. If the phase is being determined directly by the period analysis, it is important to remember that for any overall best fit a unique value is required such that $\epsilon = \epsilon_h = 2\epsilon_f$. As a consequence of expressing the behaviour of q with cosine functions and that of u with sine functions (see Equations (2.11.1)), and using sine-wave fitting routines to both q and u , the oscillations in the stellar equatorial frame of the fundamental frequency for the two parameters should appear to be out of phase by $\pm\frac{\pi}{2}$; the same constraint also applies to the harmonic.

If analysis of the data density distribution has been applied as outlined above in Section 2.13, suggestions might ensue for domains in which i and θ lie, allowing model fits to be confined within limits, so reducing the overall computing time for period searches.

2.14(b) Application of Fourier Coefficients Various approaches have been made in connection with binary star studies to detect periodicities and to apply them to determine the stellar geometry. In some cases the periodicity taken for the model fitting is obtained from photometric or spectroscopic observations.

By expanding Equations (2.11.3) the polarimetric oscillations may be expressed by:

$$q_*(t_j) = q_0 + q_1 \cos 2\pi v t_j + q_2 \sin 2\pi v t_j + q_3 \cos 4\pi v t_j + q_4 \sin 4\pi v t_j \quad (2.14.1)$$

$$u_*(t_j) = u_0 + u_1 \cos 2\pi v t_j + u_2 \sin 2\pi v t_j + u_3 \cos 4\pi v t_j + u_4 \sin 4\pi v t_j$$

Kemp's group (Kemp *et al.*, 1976, Kemp *et al.*, 1978) have used an autocorrelation technique to determine the polarization power periodogram. Significant periods were then fitted by least squares to allow determination of the Fourier coefficients which were translated into geometric parameters describing the stellar system (Kemp and Barbour, 1983).

Brown *et al.* (1978) have shown that the Fourier coefficients can be related to i , Ω and ϵ , and they may be written as:

Fundamental

Harmonic

$$\left[\frac{1 + \cos i}{1 - \cos i} \right]^2 = \frac{(u_1 + q_2)^2 + (q_2 - u_2)^2}{(u_1 - q_2)^2 + (u_2 + q_1)^2}$$

$$\left[\frac{1 + \cos i}{1 - \cos i} \right]^4 = \frac{(u_3 + q_4)^2 + (q_3 - u_4)^2}{(u_3 - q_4)^2 + (u_4 + q_3)^2}$$

(2.14.2)

$$\Omega = \frac{1}{4} \left[\tan^{-1} \left(\frac{u_1 - q_2}{u_2 + q_1} \right) + \tan^{-1} \left(\frac{u_1 + q_2}{q_1 - u_2} \right) \right]$$

$$\Omega = \frac{1}{4} \left[\tan^{-1} \left(\frac{u_3 - q_4}{u_4 + q_3} \right) + \tan^{-1} \left(\frac{u_3 + q_4}{q_3 - u_4} \right) \right]$$

$$\epsilon_f = \frac{1}{2} \left[\tan^{-1} \left(\frac{u_1 - q_2}{u_2 + q_1} \right) - \tan^{-1} \left(\frac{u_1 + q_2}{q_1 - u_2} \right) \right]$$

$$\epsilon_h = \frac{1}{2} \left[\tan^{-1} \left(\frac{u_3 - q_4}{u_4 + q_3} \right) - \tan^{-1} \left(\frac{u_3 + q_4}{q_3 - u_4} \right) \right]$$

As a_1 , b_1 , a_2 and b_2 , are relatable to the Fourier coefficients, the value of θ may be determined using either the q or the u parameters as follows:

$$\text{By } q_* : \theta = \tan^{-1} \left[\frac{2a_2 \sin 2i}{a_1(1 + \cos^2 i)} \right] \quad \text{By } u_* : \theta = \tan^{-1} \left[\frac{2b_2 \tan i}{b_1} \right] \quad (2.14.3)$$

Brown *et al.* (1978) noted that the alternative forms associated with the fundamental and harmonic serve as a consistency check. In later papers the fitting of the canonical model to the data has been investigated (Simmons, Aspin and Brown, 1980, Aspin, Simmons and Brown, 1981) in terms of a χ^2 statistic. This work showed that the normal experimental noise produces uncertainties to the model parameters which are larger than those predicted by the formal error treatment and, in addition, the determined values from the fit carry bias.

A least-squares fit can be applied to Equations (2.14.1). This may be done on the fundamental and harmonic separately for each of the Stokes parameters. Alternatively, an overall model fit might be considered by determining the least-squares values of the mean level and the coefficients of the fundamental and harmonic simultaneously with the imposition of the required phase between the fundamental and harmonic. Whether the method of least squares is applied to the components individually or to a unified fitting procedure (i.e. to the model), the significance of the fit can be assessed according to the calculated F-value. For the least-squares fit the F-value for q_* , say, is given by (see Daniel and Wood, 1980):

$$F = \frac{R_q^2}{1 - R_q^2} \cdot \frac{(N - K - 1)}{K} \quad (2.14.4)$$

where R_q^2 is the multiple correlation coefficient squared and represents the fraction of the total variation accounted for by the fitted equation, N = number of data points and K = number of unknowns (excepting the constant (DC) term, *viz.* q_0 in this example);

$$R_q^2 = 1 - \frac{\sum_j (q_{*j} - Q_{*j})^2}{\sum_j (q_{*j} - \bar{q}_{*j})^2}$$

where Q_{*j} is the fitted equation value for the j^{th} data point and q_{*j} the mean of q_{*j} . The F-value can be compared with tabled values using K as the numerator and $(N-K-1)$ as the denominator for the degrees of freedom to give a joint test of the null hypothesis that all the coefficients are zero against the alternative that the equation, as a whole, produces a significant reduction in the total sum of squares. In the light of possible biasing effects the alternative hypothesis may be preferred for testing the significance of a period. Indeed any period search might be effected by determining the F-values and the results presented by plotting the F-values against v . (A full least squares treatment on Equations (2.14.1) appears in Appendix C).

2.14(c) Correlation of the Polarization Position Angle As already emphasised, the establishment of the parameters for the best fit for the canonical model requires both Equations (2.11.3) to be satisfied simultaneously and this can be achieved by comparing the variations of the position angle of the polarization with that generated by the model using the proposed parameters. Because of the uncertainties in any estimate of the interstellar polarization, and as the value of the constant term of the intrinsic polarization is unknown, the correlation is best performed in the frame whose origin is the centre of gravity of the data.

As outlined above in Section 2.12, the transformation might provide a reasonable value for Ω or a value might be obtained by determining the MPA, in which case the equations might be simplified by applying the appropriate rotation to the co-ordinate frame. No matter the orientation of the frame, the azimuths of the data given by $\alpha'_j = \tan^{-1}(u'_j/q'_j)$ may be compared with those, $\alpha'_{jm} = \tan^{-1}(u'_{jm}/q'_{jm})$, generated by the model according to Equations (2.11.3) with chosen values for i and θ .

It may be noted that in determining the α 's, the factor τ_0 cancels

and therefore need not be known. However, the method requires the factor to be constant, as must q_A , to maintain the position of the centre of gravity of the data distribution from which the azimuths are referred.

For any selected frequency, the value of its phase may be adjusted over a range of 2π until the best correlation is achieved. The significance of any particular frequency and phase may be calculated from correlation confidence tables (see Appendix A and cf. Section 2.3). The best model match may be considered when the values i and θ maximise the correlation between the azimuths of the calculated data. Alternatively the gradient given by α'_j/α'_{jm} being closest to unity, which should also intersect the origin for $\Omega=0$, provides a criterion. The exercise should be repeated after adjusting the values of i and θ used to determine the values of α'_{jm} with a view to maximising the correlation. Only if Ω is known may the phase, ϵ , be determined.

It will be appreciated that in performing the correlation the limits of α'_n and α'_j both run from zero to 2π . One of the problems of applying the method is that a value of α'_m close to 0° , for example, may equally be represented by one α'_j value either close to 0° or 360° according to the individual measurement error. If the latter occurs for a particular point, this distorts the correlation. The final result becomes less meaningful the greater the noise. However, the problem can be reduced by weighting the data. For example, those points which provide α'_m close to 0° or 360° might be discarded or data points which are close to the centre of gravity of the distribution might be removed because of the uncertainty in their α'_j value.

2.14(d) Correlation of the Sign of u In setting up the model, account has been duly made of the contribution to the polarization from the global effect of the extended atmosphere. For the rotation axisymmetric case discussed here, this intrinsic polarization is

contained in the q parameter of the stellar equatorial frame and is expressed in Equations (2.11.3) as q_A . Many Be stars exhibit slow secular polarization variations as though this component is subject to change, causing the centre of gravity of the data distribution to drift along the q -axis, making the implementation of all the above data reduction methods less precise.

In the stellar equatorial frame, any global changes affecting the scale but not the geometry have no effect on the value of u . Direct comparison of the u -data with individually predicted values from Equation (2.11.3) may be considered. However, this will not be effective if τ_0 is also noisy.

One way to deal with variable q_A or noisy τ_0 is to consider the u parameter in the stellar equatorial frame as having two states: positive and negative. Based on predictions by Equations (2.11.3), according to a chosen frequency and starting epoch, the number of successes of matching the signs of the u 's from the model with the time indexed real data values can be determined. The statistical significance of this number can be ascertained according to the binomial distribution appropriate to the number of data points, the number of successful matches and the probability of a match, P , for the random condition ($P=0.5$; + or - being equally probable).

Again by applying a series of discrete frequencies to generate model u values and using a series of starting epochs to allow adjustment of phase, significant periods may be selected. The procedure may be weighted by discarding u values close to zero, these having a greater probability of carrying the wrong sign as a result of experimental noise or ill determined Ω . The analysis is performed best if an accurate value for Ω has been obtained and the axes rotated correctly so as to concentrate purely on the stellar equatorial frame u parameter. Checks might be made on the validity of Ω by making

adjustments to its value and reinvestigating the correlation.

2.15 Postamble

It is now possible to present a scheme, following Sections 2.11 to 2.14, that furthers the approach outlined in Section 2.5. The design below is applicable to any substantial polarimetric data indicating intrinsic variability:

i) Obtain an estimate for any interstellar polarization either from field stars and/or from the data themselves.

ii) By projecting the data onto various axes, check its statistical normality by taking moments and use the method of moments to search for eigendirections (related to preferred stellar axes) - Section 2.13(a). Information from this might be used directly in subsequent analyses or the derived axes can be compared with those obtained from the more comprehensive data fitting routines.

iii) Having reduced the data to a centre of gravity frame, investigate the data density distribution, comparing it (χ^2 tests) with computer generated data according to various model parameter distributions and noise - Section 2.13(b).

iv) If some coherence is suspected in the variability, investigation of the time-path of the data points or parts of the time-path, particularly if the intrinsic origin is known, might be informative. Visual inspection might allow variation of n , r or ϕ to be deciphered or more quantitative comparisons might be applied by correlation measures of the time dependent vectors.

v) Should periodicity be suspected, apply appropriate search routines to the data, combining the results for the q ,

u parameters according to the dictates of any proposed model. This might be done by taking heed of the phases associated with the periodicities in q and u, or by correlation of the polarization position angle - Sections 2.14(b) and 2.14(c). A period fitting procedure involving an investigation of u only (subject to it being defined in a stellar co-ordinate frame) may be applied if the data appear noisy as a result of variability of the scattering strength of the globule - Section 2.14(d).

Whereas the guidelines given in Section 2.5 can be applied to polarimetric data in general, it must be borne in mind that the steps above are related to a particular model.

CHAPTER 3. ANALYSIS OF SOME POLARIMETRIC DATA

3.1 Introduction

3.2 Reduction of η Cep, β Cas, 55 Cyg, γ Cas and ζ Tau Data

3.3 Reduction of β Vir, 2H Cam and 28 ω CMa Data

3.4 The Polarimetric Behaviour of X Per

3.5 A Comment on the Polarimetry of HDE 226868

3.6 The Polarimetric Behaviour of σ Ori E

CHAPTER 3. Analysis of Some Polarimetric Data

3.1 Introduction

This Chapter concerns applications of the polarimetric stochastic globule model and demonstrates the schemes outlined in Sections 2.5 and 2.15. Data sets that are not substantial enough (e.g. recorded over a few nights only) to warrant an assiduous study are investigated with the intention of searching for glitches and time drifts as well as noting the direction in which they occur. If the glitches/time drifts are seen to predominate along any particular course, e.g. parallel to or orthogonal to the p vector, inferences such as a change in scattering strength or geometry may be drawn. For extended data sets, these are analysed with a view to determining the geometry and physical properties of the stellar system involved, *viz.* i , θ , τ_0 as well as any periodicity associated with the fluctuations and to estimate or give an upper bound to the electron number density of the polarigenic mechanism.

The analysed data comprised measurements by Dr. D. Clarke and Mr. A. Brooks on η Cep, β Cas, 55 Cyg, γ Cas and ζ Tau acquired on the 24" (Morgan) and 42" telescopes at Lowell during September 1982 and on β Vir, 2H Cam and 28 ω CMa taken by myself and Dr. Clarke at La Palma on the 40" JKT, realized by a successful PATT application. Observations on X Per, HDE 226868 and σ Ori E were taken from papers of Prof. J. Kemp's group.

3.2 Reduction of η Cep, β Cas, 55 Cyg, γ Cas and ζ Tau Data

These stars were observed through narrow-band interference filters (FWHM $\sim 10\text{\AA}$) at $H\beta$ (4870\AA) and Ca II K (3955\AA) using the Glasgow University Polarimeter/Photometer (GUPP) as described by Clarke and Brooks (1984). The procedure adopted for reduction of the data, *i.e.* those observations recorded in any one observing session, was:

- i) calculate the mean values of the normalized Stokes parameters (NSP) for the data run under study, treating q and u independently.
- ii) test the data for normality
- iii) perform linear regressions on the whole of the data run and on individual groups brought about by subdividing the data into, e.g., halves, thirds, etc., until the time-base of any one class is not less than approximately 30 mins.
- iv) examine the equality of the means of these groups.

Sections 2.2 - 2.4 can be referred to for the stated null hypotheses which need to be failed at greater than above some limit, say that of 95%, for significant results to be implied. For the case of non-polarized standards the projection method (Clarke and Stewart, 1986) was used to search for any possible instrumental polarization, again at the 95% limit. The stars η Cep and β Cas were observed to ascertain the level of instrumental polarization and 55 Cyg to get the rotation needed to the standard equatorial frame from the frame of measurement.

η Cep (HD 198149, $m_V = 3.59$, KO IV, $\alpha_{1950} = 20^h 43^m 16^s$, $\delta_{1950} = +61^\circ 38' 39''$)

This non-polarized standard (Serkowski p. 168, 1974) was monitored for 1 night on the 42", the data train being ~ 2 hrs. long, with a typical integration time of around 20^s .

At H β , the mean values of the NSP were found to be:

$$\bar{q} = -0.005\% \pm 0.023\%$$

$$\bar{u} = 0.017\% \pm 0.024\%$$

both coming from normal distributions. No instrumental polarization was apparent. No relationship of q with time was found but u showed a correlation at 95% over the entire length of the data run. Carrying out the Welch procedure on q then on u revealed time variability (at

95%) in both q and u between 2 groups of 1 hour duration, 4 x 30 mins. classes, and for u only 3 groups of 40 mins. base-line each.

At Ca II K the measured mean values were

$$\bar{q} = -0.082\% \pm 0.062\%$$

$$\bar{u} = 0.016\% \pm 0.060\%$$

the data exhibiting behaviour recognised as Gaussian, with no instrumental polarization surfacing. No correlation of q with time was evident although for u the first half of the data (≈ 1 hr) showed a significant result at the 95% limit. Welch testing on grouped data revealed no significant variability in either q or u.

β Cas (HD 432, $m_V = 2.42$, F5 IV, $\alpha_{1950} = 0^h 6^m 30^s$, $\delta_{1950} = +58^\circ 52' 27''$)

This star is also recognised as a non-polarized standard (Serkowski 1974). It was observed for 1 night on the 24", over a time interval of about $2\frac{1}{2}$ hrs., a typical integration being 20^s .

At H β the recorded averages of q and u were:

$$\bar{q} = -0.008\% \pm 0.023\%$$

$$\bar{u} = -0.034\% \pm 0.023\%$$

with their distributions passing normality testing. The values of q and u and their standard errors suggest there is no instrumental polarization. The data collected in the first hour showed a strong correlation (99%) of q with time and there was a 95% limit hypothesis failure for one group (40 mins. in length) of u data. Testing the equality of the means formed by the classed data, showed that both q and u were non-variant.

The mean values at Ca II K were

$$\bar{q} = -0.010\% \pm 0.028\%$$

$$\bar{u} = 0.042\% \pm 0.028\%$$

Whilst q were found to behave normally, u exhibited a skewness at 95%, but not at 99%. The polarization test was then required to be

carried out at the 99% confidence limit - no instrumental polarization being the conclusion. Neither q nor u showed any relationship with time, suggesting perhaps that the skewness of u was due to glitches rather than a steady drift in time. Scintillation noise might have been the culprit although indications are that the limiting error was dominated by photon counting statistics. On subdividing the data and performing the regression and Welch test analysis - no significant failures of the null hypotheses were found.

55 Cyg (HD 198478, $m_V = 4.89$, B3 Ia, $\alpha_{1950} = 20^h 47^m 14^s$, $\delta_{1950} = +45^\circ 55' 40''$)

According to Serkowski (1974), this star is a polarized standard with $\lambda_{\max} = 5300\text{\AA}$, $p_{\lambda_{\max}} = 2.8\% \pm 0.1\%$, and $\theta_{\lambda_{\max}} = 3^\circ \pm 1^\circ$. However, Hsu and Breger (1982) suggest that it is not a standard star as they claim to have found fluctuations in both p and θ (this information coming too late for the Lowell observing run).

A $3^{h.2}$ run was recorded on the 24", a typical integration time being $\sim 20^s$.

At H β , the measured mean values of q and u were

$$\bar{q} = -0.240\% \pm 0.047\%$$

$$\bar{u} = -2.760\% \pm 0.048\%$$

which imply $\bar{p} = 2.7\% \pm 0.05\%$. Using Serkowski's empirical interstellar polarization law, *viz.*

$$p(\lambda) = p(\lambda_{\max})[\exp -1.15 \ln^2(\lambda_{\max}/\lambda)] \quad (3.2.1)$$

the expected polarization should be $\doteq 2.8\% \pm 0.1\%$ which agrees well with \bar{p} . Both q and u pass normality testing. No (t, q) or (t, u) correlations were found except for one group (of 30 min. duration) of u data at the 95% limit. Neither q nor u exhibited any variations as seen by Welch testing.

7 Colour Polarization Measurements of γ Cas (9434Å \rightarrow 3413Å)

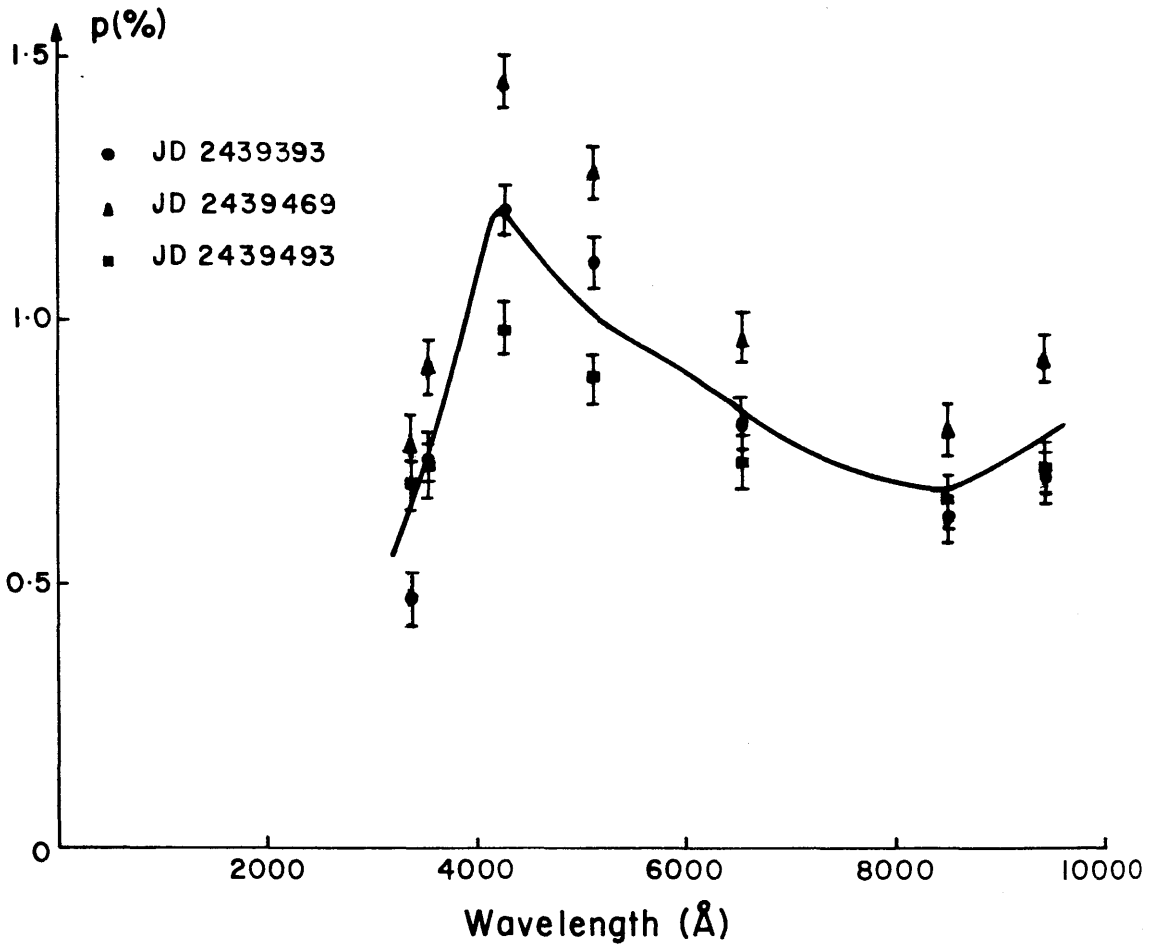


Fig. 3.2.1 Three sets of seven colour measurements of γ Cas taken by Coyne(1975). The curve is a schematic mean, showing that the form of the polarization wavelength dependence does not conform to that expected from a pure interstellar component.

For Ca II K the data supplied

$$\bar{q} = -0.410\% \pm 0.057\%$$

$$\bar{u} = -2.556\% \pm 0.055\%$$

which imply $\bar{p} = 2.6\% \pm 0.06\%$. This compares with the expected value of $P_{(3955)} = 2.5\% \pm 0.1\%$. Both q and u pass normality testing. No failures of the correlation or equality of means null hypotheses were found, with the exception of one group of u data (36 mins. duration) which showed a relationship with time at the 95% limit.

In summary, the study of the polarimetric standards (via normality and Welch tests), in the instrumental frames, suggests that any variations (i.e. equal to or above 95% limits) found within the data on γ Cas and ζ Tau are likely to be real (that is, intrinsic to the star), especially if they are found over time-scales of a few hours. However, for the measurements recorded at $H\beta$ on the 42", Welch test failures would need to occur at greater than or above the 99% limit if they are to be confidently considered as due to intrinsic changes. Only for η Cep (42", $H\beta$) does there appear to be the consistency of where there are correlations of q or u with time (albeit at the 95% limit) are there failures of the Welch test; yet the strong correlation (99% limit) exhibited by the first half ($\cong 1\frac{1}{4}$ hrs.) of the q parameter of the β Cas $H\beta$ measurements induces no inequality of the means formed by the former and latter halves of the data. No corrections for instrumental polarization will be required. The following analyses of γ Cas and ζ Tau are performed in the equatorial frame, their interstellar values not being known accurately enough to warrant reduction in their stellar frames.

γ Cas (HD 5394, $m_V = 1.6-3.0$, B0.5 IVe, $\alpha_{1950} = 0^h 53^m 40^s$, $\delta_{1950} = +60^\circ 26' 47''$)

Fig. 3.2.1 is a plot of 3 sets of 7 colour measurements taken by Coyne (1975) and displayed in a (λ, p) frame. The mean

Table 3.2.1

Polarization log of γ Cas, in equatorial co-ordinates, taken at the Lowell 42" and 24" (Morgan) telescopes during Sept. 23 - Sept. 31 1982. Times are in UT.

Typical integration for 1 measurement to form the mean values was less than 20^s.

<u>Date</u>	<u>WaveLength</u>	<u>Telescope</u>	<u>$\bar{q}(\%) \pm \Delta q(\%)$</u>	<u>$\bar{u}(\%) \pm \Delta u(\%)$</u>
23.9.82	H β (4870Å)	42"	-0.638 \pm 0.008	-0.494 \pm 0.008
6 ^h 19 ^m 29 ^s to 9 ^h 41 ^m 27 ^s	Ca II K (3955Å)	42"	-0.659 \pm 0.009	-0.537 \pm 0.009
24.9.82	H β	42"	-0.637 \pm 0.011	-0.404 \pm 0.011
6 ^h 18 ^m 31 ^s to 8 ^h 46 ^m 56 ^s	Ca II K	42"	-0.654 \pm 0.012	-0.445 \pm 0.011
30.9.82				
0 ^m 41 ^s to 7 ^h 10 ^m 3 ^s	Ca II K	24"	-0.701 \pm 0.017	-0.531 \pm 0.019
31.9.82	H β	24"	-0.666 \pm 0.032	-0.425 \pm 0.036
2 ^h 27 ^m 13 ^s to 4 ^h 43 ^m 14 ^s	Ca II K	24"	-0.625 \pm 0.030	-0.596 \pm 0.032

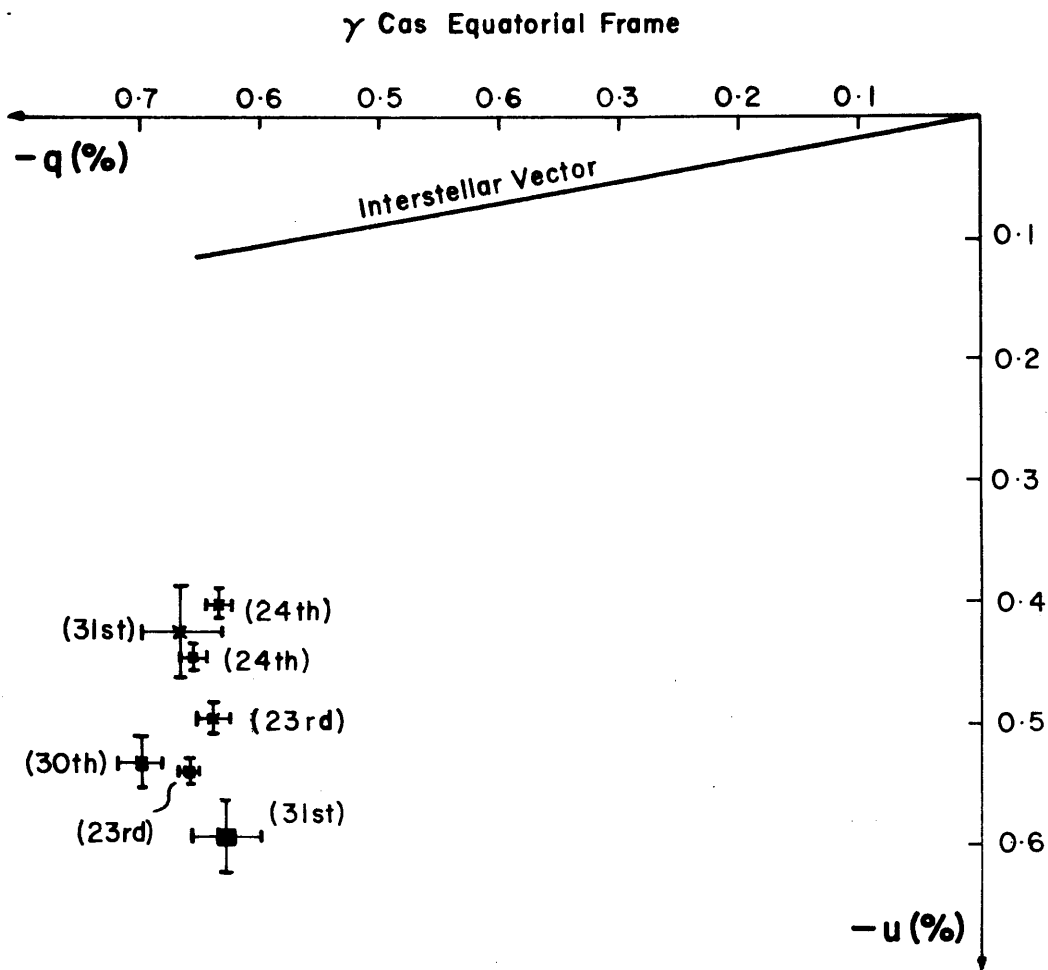


Fig. 3.2.2 The average (q,u) values, in the equatorial frame, from several observing runs on γ Cas between Sep 23 and 31 1982 (*- $H\beta$, \blacksquare -Ca II K, the numbers correspond to the date of the run).

polarization-wavelength curve clearly shows that this star exhibits an intrinsic polarization. The data taken with GUPP were recorded over 3 nights from Sept. 23 - Sept. 31 and the mean values of q and u for each run are displayed in Fig. 3.2.2, along with the interstellar component (McLean and Clarke, 1976 - Table 1).

At $H\beta$, on 1 night (31st) there was a 99% failure of the Welch test by the u parameter, the data being divided into 4 \sim 30 min. groups. From the approximate interstellar position, these changes would correspond to fluctuations in intrinsic p rather than intrinsic θ . As evident from Fig. 3.2.2, a change is apparent between the 3 nights on which the measurements were taken, in a direction indicating a variation in p , the strongest fluctuations being between the 23rd and 24th - i.e. a rapid-type change.

At Ca II K, on 1 night (24th) there was a significant (99%) Welch failure when the q 's, i.e. approximately θ , were binned into 5 groups of 30 mins. width. Among data sets from individual observing runs, the strongest Welch test result occurred between the two nights 23rd and 24th, in a direction related to p . Comparison of the other nights was not possible due to technical problems.

The Sept. 23-24 variation seen in both $H\beta$ and Ca II K were of the same significance (slightly stronger in Ca II K, the noise in both colours being equivalent) and indicate a correlation of movement in the q, u plane. The mean values of the polarimetric data for the observing run are presented in Table 3.2.1.

ζ Tau (HD 37202, $m_V = 2.9-3.0$, B1 I Veishell, $\alpha_{1950} = 5^h 34^m 39^s$, $\delta_{1950} = +21^\circ 6' 50''$)

This shell star is well known as a member of a spectroscopic binary with a period of $132^d.9735$, and is reported to exhibit rapid-type variations in its polarimetry (Clarke and McLean, 1976) and photometry (Pavlovski, 1983).

Table 3.2.2

Polarization log of ζ Tau, in equatorial co-ordinates, taken at the Lowell 42" and 24" (Morgan) telescopes during Sept. 22 - Sept. 30 1982. Times are in UT.

Typical integration for 1 measurement to form the mean values was less than 20^s.

<u>Date</u>	<u>Wave length</u>	<u>Telescope</u>	$\bar{q}(\%) \pm \Delta q(\%)$	$\bar{u}(\%) \pm \Delta u(\%)$
23.9.82	H β (4870 \AA)	42"	0.475 \pm 0.028	1.309 \pm 0.028
11 ^h 33 ^m 19 ^s to 12 ^h 11 ^m 30 ^s	Ca II K (3955 \AA)	42"	0.511 \pm 0.030	1.426 \pm 0.026
25.9.82	H β	24"	0.604 \pm 0.025	1.051 \pm 0.024
9 ^h 27 ^m 12 ^s to 11 ^h 38 ^m 46 ^s	Ca II K	24"	0.660 \pm 0.022	1.271 \pm 0.024
28.9.82	H β	24"	0.565 \pm 0.021	1.123 \pm 0.022
8 ^h 26 ^m 5 ^s to 12 ^h 7 ^m 20 ^s	Ca II K	24"	0.620 \pm 0.021	1.347 \pm 0.020
29.9.82				
?	Ca II K	24"	0.581 \pm 0.025	1.336 \pm 0.025

ζ Tau Equatorial Frame

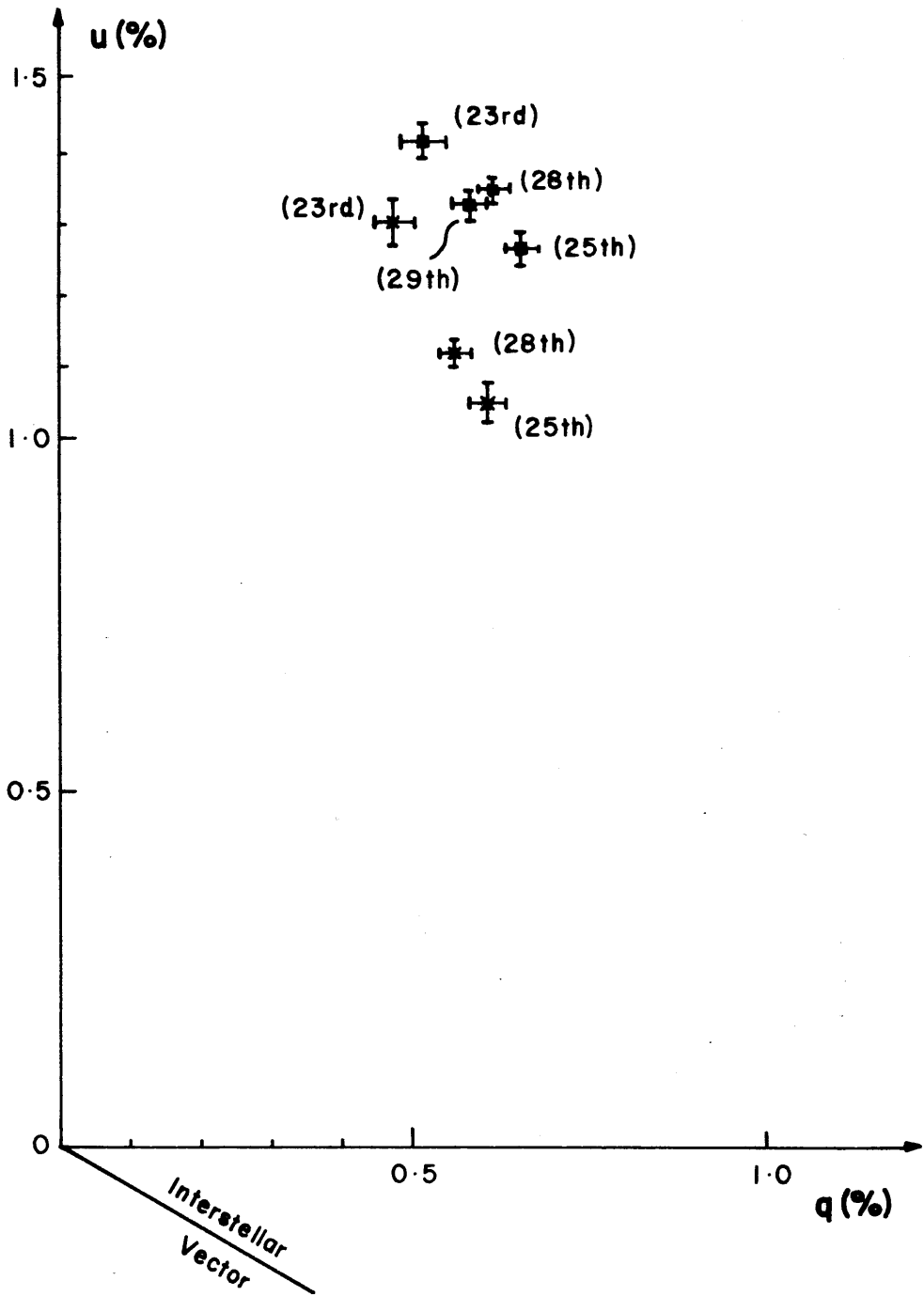


Fig. 3.2.3 Average (q,u) values, in the equatorial frame, of several observing runs on ζ Tau between Sep 23 and 29 1982 (*-H β , □-Ca II K, the numbers correspond to the date of the run).

The mean values of the data recorded over 4 nights between 23rd and 29th are plotted as Fig. 3.2.3 along with the approximate interstellar value again taken from McLean and Clarke (1976).

The unfortunate position of the interstellar contribution in the (q, u) plane does not make q and u immediately realizable as intrinsic p and θ , unlike the γ Cas situation. So, any variation found in q , say, could correspond to a change in either p or θ , although the tendency is for u to p and q to θ .

At $H\beta$, there are apparently no changes as seen by Welch testing over intervals of up to 4 hours (the longest run) resolving down to $\sim \frac{1}{2}$ hr. However, there are very strong fluctuations (i.e. $> 99\%$ limit) over at least a period of 2 days in both q and u , especially between the 23rd Sept. and 25th Sept. runs. These two observing nights were done on different telescopes but indications are that the variations are not due to systematic errors as the data of later nights seem to exhibit a "recovery" to the position in the (q, u) plane of the first night's (i.e. 23rd) measurement.

As with $H\beta$, for Ca II K there are no changes evident over intervals of up to 4 hrs. resolved down to $\frac{1}{2}$ hr. There are again, though, night to night fluctuations (especially between 23rd and 25th), but these are not as strong as (i.e. do not fail the Welch test at as high a significance) the $H\beta$ variations, although the direction of change correlates and the noise (i.e. experimental errors) in the two colours is comparable.

Table 3.2.2 records the values of the means displayed in Fig. 3.2.3.

In summary, both γ Cas and ζ Tau exhibit rapid type fluctuations which, from the above short observing run cannot be shown to be periodic. For γ Cas, changes are evident over a few hours and seem to be irregular in parameter (i.e. p or θ) and time, Its night to night

variations show through equally well in H β and Ca II K. However, for ζ Tau the night to night fluctuations are more evident in H β than in Ca II K - possibly due to observing events at differing optical depths, with no variations being evident over hour timescales.

3.3 Reduction of β Vir, 2H Cam and 28 ω CMa Data.

As previously mentioned, observation of these stars was made possible through a successful PATT application for time on the 40" JKT, using the People's Photometer (PP) in polarimetric mode at the Roque de los Muchachos Observatory. The run took place between the 9th and 15th of January 1985, and was unfortunately dogged by bad weather and technical problems.

The PP is described in "The People's Photometer User and Technical Manual (No. 58)" available from the RGO. Briefly, in relation to its polarimetric mode, the instrument contains a half-wave ($\lambda/2$) plate which is rotated once in 960ms. The plate modulates incidental light as a sine-wave, with 1 cycle being a quarter of the mechanical frequency. A Foster prism acts both as a beam-splitter and as an analyser. The optical path is split into two - an undeviated beam and an orthogonal one - and these arrive at two photomultipliers after encountering the desired colour filters, in this case the narrow-band to intermediate-band (Glasgow) filters. The output signal $A(\phi)$, for linear polarization takes the form

$$A(\phi) = I + Q\cos 4\phi + U\sin 4\phi \quad (3.3.1)$$

where ϕ is the position angle of the fast axis of the $\lambda/2$ plate and I, Q, U are the coefficients to be derived by regression analysis. Equation (3.3.1) is sampled for 10ms, 96 times over 1 mechanical rotation of the retarder. After an optional number of revolutions, the values of the NSP are calculated for that particular integration.

The gist of the scientific case for support described an application of the stochastic globule model at an early stage of its

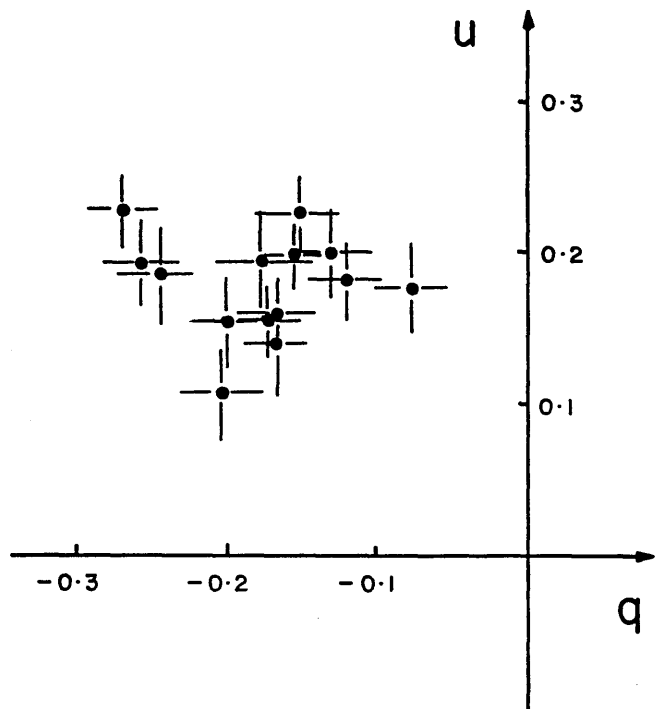


Fig. 3.3.1 Variable Polarization at 4269\AA of $28\ \omega\ \text{CMa}$ during 1983 Apr 29 - May 9 (GUPP at SAAO - 0.75m).

development. Intuitively, for a star displaying mass loss around its equatorial regions, any local scattering will cause polarization measurements to exhibit circular symmetry in the (q, u) plane if the star is seen pole-on. A straight line in the (q, u) plane would be evident if a similar star was to be observed equator-on (cf. ω Ori ? Hayes, 1980). Obviously an intermediate case would be expected to produce an elliptical distribution.

Preliminary (q, u) measurements of 28ω CMa at 4269\AA taken with GUPP at SAAO by Clarke and Brooks (Fig. 3.3.1) during 1983 April 29 - May 9, indicate that there are significant, but unequal, variations in orthogonal directions. So, further observations might help better define the apparent (q, u) distribution enabling perhaps the value of the stellar inclination to be estimated along with the scale of the mass loss (globules).

During a polarimetric observing run standard stars need also to be measured, β Vir (instrumental polarization) and 2H Cam (relative orientation of co-ordinate frames) fulfilling the role here.

β Vir (HD 102870, $m_V = 3.80$, F8 V, $\alpha_{1950} = 11^{\text{h}} 48^{\text{m}} 5^{\text{s}}$, $\delta_{1950} = +2^{\circ} 2' 47''$)

This star is listed by Serkowski (1974) as a non-polarized polarimetric standard. Monitoring on several nights and at a variety of wavelengths (7 from $4269/40\text{\AA}$ to $6790/130\text{\AA}$), was typically for 20 mins., with an integration for single measurements usually being ≈ 50 revs. From the 18 data sets recorded, analysis in the instrumental frame revealed that q behaved as Gaussian consistently, but there were 5 normality failures for u, these being equally spread between beam, wavelength and passband. Possible instrumental polarization was recorded at wavelengths/passbands 4269/40 and 6385/92. At 5020/70 indications were for instrumental polarization but, as the data behaved in a non-normal fashion, such hypothesis

Table 3.3.2

Polarization measurements of 2H Cam and α Leo (with polaroid).
 For 2H Cam typical error on p is less than 0.03% and $0^\circ.4$ for θ .
 For α Leo the error on p is less than 0.04% and $0^\circ.09$ for θ .
 Δ corresponds to the maximum difference in each column.

<u>Wavelength/ Passband(\AA)</u>	<u>2H Cam</u>		<u>α Leo</u>	
	<u>p(%)</u>	<u>$\theta(^\circ)$</u>	<u>p(%)</u>	<u>$\theta(^\circ)$</u>
4269/40	3.39	29.5	96.89	93.0
4860/50	3.57	29.2	99.23	94.6
4870/10			99.64 99.64	94.5 94.5
5020/70	3.62 3.58	32.4 32.4	98.30	95.3
5320/30	3.57	31.8	98.10	96.6
6385/92			98.20	100.5
6790/130	3.28	37.9	97.62	100.8
$\Delta = 2521$	$0.34\% \pm 0.04\%$	$8^\circ.7 \pm 0^\circ.6$	$2.75\% \pm 0.05\%$	$7^\circ.8$

Table 3.3.1

Polarimetric record of the behaviour of β Vir during 1985 Jan 9-15
 (People's Photometer - JKT). N = number of integrations in data set,
 * = testing not possible. Y - YES, N = NO.

<u>Wavelength/ Passband (Å)</u>	<u>Dates</u> N	<u>Polarized (?)</u>	<u>Means Equal (?)</u>
4269/40	9.1.85 (11)	Y	u fails at 95%
	12.1.85 (36)	Y	
	13.1.85 (27)	N	
4860/50	9.1.85 (20)	N	Y
	13.1.85 (23)	N	
	14.1.85 (14)	N	
4870/10	9.1.85 (17)	N	u fails at 95%
	14.1.85 (20)	N	
	14.1.85 (24)	*	
5020/70	12.1.85 (36)	*	*
	13.1.85 (27)	*	
5320/70	9.1.85 (11)	*	*
	14.1.85 (20)	N	
6385/92	9.1.85 (11)	Y	*
	14.1.85 (24)	*	
6790/130	9.1.85 (20)	N	Y
	13.1.85 (23)	N	
	14.1.85 (14)	N	

examination was not strictly practicable.

Welch testing, where possible, was carried out between data sets of the same wavelength, which may have been recorded hours or days apart. Two failures at the 95% limit were noted for u at 4269/40 and 4870/10. Table 3.3.1 is a résumé of the analysis.

2H Cam (HD 21291, $m_V = 4.42$, B9 IA, $\alpha_{1950} = 3^h 25^m 0^s$, $\delta_{1950} = +59^\circ 46' 5''$)

This star is a polarized standard and, according to Serkowski (1974), $\lambda_{\max} = 5300\text{\AA}$, $p_{\lambda_{\max}} = 3.5\% \pm 0.1\%$, and $\theta_{\lambda_{\max}} = 115^\circ \pm 1^\circ$. Analysis by Hsu and Breger (1982) tends to support the criterion notion, and they refine the parameters further; $\lambda_{\max} = 5210\text{\AA} \pm 30\text{\AA}$, $p_{\lambda_{\max}} = 3.53\% \pm 0.02\%$, and $\theta_V = 116^\circ.6 \pm 0^\circ.2$.

During the present observing run, the star was observed at 5 wavelengths, from 4269/40 to 6790/130, the time-base of any one data set being typically 20 mins., with an integration time ≈ 50 revs. Welch testing was possible at only one of the wavelengths, *viz.* 5020/70, which passes, as at all the others only 1 set of measurements was available. Alone at 4269/40 do the data exhibit non-normality, with q skew and u kurtos.

It is important to check whether the $\lambda/2$ plate used is achromatic or not. This was done by placing a sheet of polaroid over the sky baffle of the JKT and observing a bright star - α Leo. Table 3.3.2 shows how p and θ (in the instrumental frame) change with wavelength for 2H Cam and a polaroid obstructed α Leo (no correction for instrumental polarization has been applied and demonstrates that the variations behave in a correlated manner, i.e. an alteration in θ for 2H Cam is mirrored by α Leo). The maximum differences over wavelength for 2H Cam in p and θ were $0.34\% \pm 0.04\%$ and $8^\circ.7 \pm 0^\circ.6$ respectively, whilst for α Leo the figures are $2.75\% \pm 0.05\%$ and $7^\circ.8$. The manufacturers claim that the optic axis of the retarder changes within

the entire spectral region by only $\pm 2^\circ$, but this is not obviously the case. The polaroid sheet used seems to be wavelength dependent, evident by the strength of emergent polarization.

For 2H Cam, its position angle is colour independent, the apparent variation coming from the employed retarder. Using Equation (3.2.1) and the Hsu and Breger parameters, between wavelengths 6790\AA and 4269\AA the difference in p should be $\sim 0.1\%$. For the measurements here, the difference is also $\sim 0.1\%$. The maximum value of p recorded was $3.62\% \pm 0.03\%$ (at 5020/70) which is not significantly departed from $3.53\% \pm 0.02\%$.

In relation to the analysis of the 28 ω CMa data, β Vir and 2H Cam suggest that the reduction be done in an instrumental frame, as the evidence for a wavelength dependent/independent polarization is uncertain. Any Welch failures will be considered significant only if above the 99% limit. If needed, the correction to the equatorial frame is $83^\circ.2$ at 5320\AA , noting that the dispersion about this wavelength for θ from the polaroid experiment can give the rotation required at other colours.

28 ω CMa (HD 56139, $m_V = 3.52-4.18$, B2-3 IV-Ve, $\alpha_{1950} = 7^h 12^m 47^s$, $\delta_{1950} = -26^\circ 41' 5''$)

This star has become quite prominent in Be literature through the work of Baade (1982a, 1982b), who claims to have found cyclic RV, line profile and V/R variations with a period of 1.37 days, but apparently there are no (or little) corresponding light changes. The V/R and RV refer to the relative intensity of the violet and red components of the double H I Balmer emission, and RV to radial-velocity. Baade has modelled this star as a non-radial pulsator. There may be in fact be two eclipsing binaries involved in this system (Harmanec 1983) comprising two B stars.

The PP measurements were taken at 3 wavelengths, *viz.* 4269/40,

28 ω CMa - Instrumental Frame

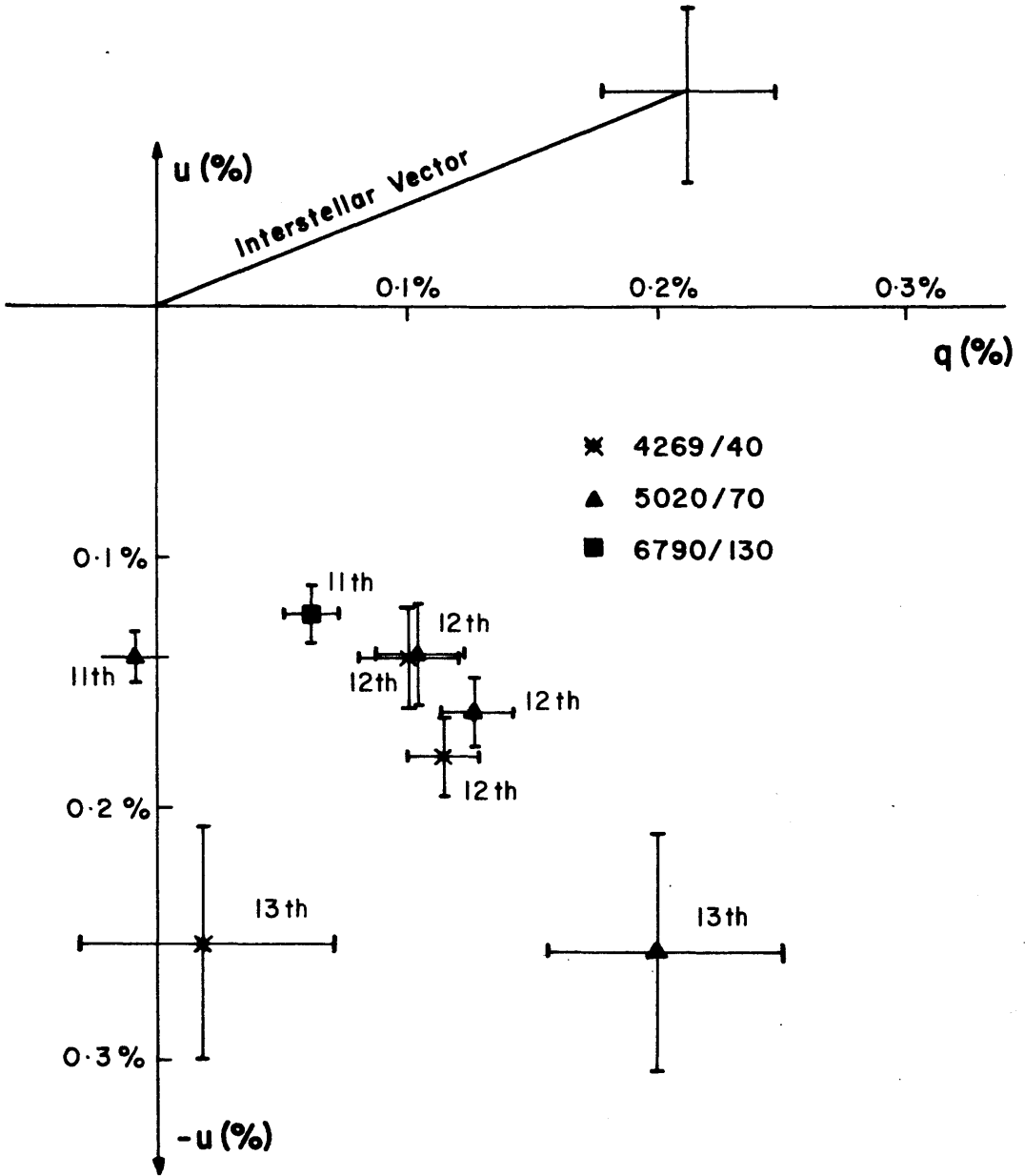


Fig. 3.3.2 The average (q,u) values, in the instrumental frame, from several observing runs on 28 ω CMa during 1985 Jan 11 - 13 (*-4269Å, Δ-5020Å, ■-6790Å, numbers refer to date of run).

Table 3.3.3

The polarimetric behaviour of 28 ω CMa during Jan 11 - 13 1985.
 Times are in UT. Y - YES, N - NO.

<u>Wavelength/ Passband(\AA)</u>	<u>Date</u>	<u>Normal (?)</u>	<u>Means Equal (?)</u>
4269/40	12.1.85 22 ^h 42 ^m 15 ^s to 0 ^h 57 ^m 57 ^s	u skew	
	12.1.85 1 ^h 9 ^m 9 ^s to 3 ^h 14 ^m 45 ^s	q skew	q : Yes u : Poss.
	13.1.85 2 ^h 52 ^m 34 ^s to 3 ^h 22 ^m 59 ^s	Y	
5020/70	11.1.85 0 ^h 21 ^m 49 ^s to 3 ^h 37 ^m 53 ^s	q kurtos	
	12.1.85 22 ^h 42 ^m 15 ^s to 0 ^h 57 ^m 57 ^s	q skew & kurtos u kurtos	
	12.1.85 1 ^h 9 ^m 9 ^s to 3 ^h 14 ^m 45 ^s	q skew	q : ? u : Y
	15.1.85 2 ^h 52 ^m 34 ^s to 3 ^h 22 ^m 59 ^s	Y	
6790/130	11.1.85 0 ^h 21 ^m 49 ^s to 3 ^h 37 ^m 53 ^s	q kurtos	

5020/70 and 6790/130⁰. A typical run lasted 2 hrs. on which time-scale, and shorter, no variations were found via Welch testing. At 4269/40⁰ 3 data sets were available, 2 being essentially contiguous and the other recorded on the following night. For the contiguous data sets, in one q exhibited skewness as did u in the other. For the 4 data sets at 5020/70, q was non-Welch examinable as they behaved non-normally, with u showing constancy. Only 1 data set was available at 6790/130, for which q displayed a kurtosis. Table 3.3.3 is a log of the behaviour of the measurements, and Fig. 3.3.2 records the mean positions of the data in the instrumental frame. The approximate interstellar vector is also shown.

The field-star polarization pattern for 28 ω CMa, using 27 stars within a $\pm 5^\circ$ region from the catalogues of Krautter (1980), Klare and Neckel (1980), Mathewson and Ford (1970), Serkowski, Mathewson and Ford (1975) and Hall (1958), implies that the mean interstellar (IS) position as $\theta_{IS} = 94^\circ \pm 10^\circ$ and the mean polarization extinction per unit distance modulus as $\bar{p}/(m-M) = 0.034 \pm 0.005$. The absolute magnitude of 28 ω CMa has been estimated from Allen (1955) as -2.9 giving $m-M \doteq 6.7$ which implies that $\bar{p}_{IS} = 0.23\% \pm 0.035\%$. The values of q_{IS} and u_{IS} can be transformed from the equatorial to instrumental (IF) frames by the relations:

$$\begin{aligned} q_{IS} &= p \cos 2(\theta_E - 83) \\ u_{IS} &= p \sin 2(\theta_E - 83) \end{aligned} \tag{3.3.1}$$

where θ_E is the position angle in equatorial co-ordinates.

The non-Gaussian behaviour of the recorded data has made searching for variations through Welch difficult and inconclusive, although the non-normality itself implies fluctuations within some of the individual data sets especially for the q parameter which would, according to the IS position, correspond to θ . Any apparent changes of the means of the measurements do seem to be correlated in direction in the (q, u) plane

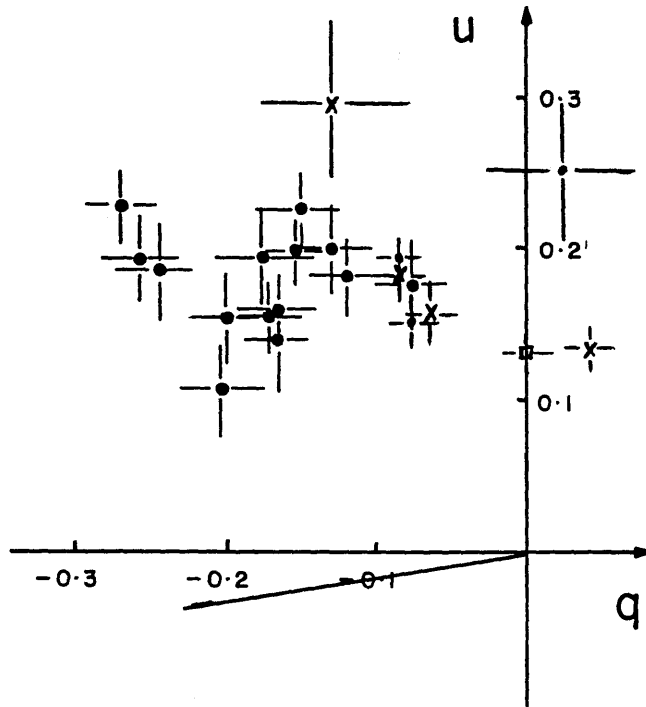


Fig. 3.3.3 Variable polarization at 4269\AA (.) of $28\ \omega$ CMa during 1983 Apr 29 - May 9 (GUPP at SAAO - 0.75m) and at 4269\AA , 5020\AA (x), and 6790\AA (\square) between Jan 8 -14 1985 (People's Photometer - JKT - La Palma). The full line represents the interstellar polarization.

with wavelength. Lastly, the 5020/70, 4269/40 and 6790/80 data have been added to those in Fig. 3.3.1 to produce Fig. 3.3.3 to show that there still appears to be a coherence to the polarimetric variations over an interval of about 2 years.

3.4 The Polarimetric Behaviour of X Persei

3.4(a) Introduction

X Per (HD 24534, $m_V = 6.0-6.6$, 09.5 Vpe-Bone, $\alpha_{1950} = 3^h 52^m 15^s$, $\delta_{1950} = +30^\circ 54' 1''$)

This star has been given a Be spectral classification and, according to Moffat, Haupt and Schmidt-Kaler (1973), its characteristics are normal for that category. Following proposals that it corresponds to the position of one of the X-ray sources (3U 0352+30) recorded by the Uhuru satellite, it has been the focus of several studies (see Underhill and Doazan, 1982, for references and general discussion). Support to the identification of it emitting X-rays has come from observations made with the Copernicus and Ariel 5 satellites (White, Mason and Sandford, 1976) which provided evidence of periodicity at 13.9 mins. and 11/22 hrs. According to Weisskopf *et al.* (1984), the 13.9 mins. variation has been fully established whereas the longer periods have not been confirmed; Weisskopf *et al.* (*loc. cit.*) claim positive identification from the high resolution imaging provided by the HEAD 2/Einstein satellite. It is now generally accepted that like γ Cas, X Per is a low luminosity source in the hard X-ray region (Underhill and Doazan, *loc. cit.*).

Several efforts to link optical and X-ray measurements have been made and have failed, but a 13.9 min. fluctuation in the H α line has been reported by Mazeh, Treffers and Vogt (1982). It may be noted that one paper (Henricks and van den Heuvel, 1977) cites Liller's (1975) work on the He II 4686 line as providing positive evidence for an identification while another (Mazeh *et al.*, *loc. cit.*) lists it under

the "no confirmed detection" category.

Using spectral archives of half a century, Hutchings *et al.* (1974) (see Hutchings, Crampton and Redman (1975) for listings of the source material) have determined an orbital period of 580^d which has since been incorporated into all the model proposals. Following more intensive spectrometric studies in 1975-76 by Hutchings (1977), the radial velocities appeared to be noisy, making the 580^d periodic variation less marked. Reservations on the validity of this periodicity emerge from the analysis here but full comment will not be made until later.

Optical polarization was investigated for X Per by Baud and Tinbergen (1972) who found no evidence of any circular component but suggested that the linear might be variable, this also being claimed by Wolf (1972). In an attempt to estimate the relative intrinsic and interstellar components of the polarization, Clarke and McLean (1975) made measurements at the H α and H β emission lines. Other polarization observations have been made by Kemp and Wolstencroft (1973), Avery, Michalsky and Stokes (1973) and values are given in the catalogues of Hiltner (1954), Hall (1958) and Behr (1959). A substantial polarimetric programme has been undertaken by Kemp and Barbour (1983) - KB - and it is with these results that this section is concerned.

From their extensive study of X Per, KB claim to have detected a phase-locked polarization pattern with a period (580^d) associated with the documented radial velocity curve. Following analysis which provided values for the Fourier coefficients for this period and the harmonic (290^d), an inclination of 79° was calculated for the binary system according to the theory (e.g. see Brown, McLean and Emslie, 1978) which assumes that a localised co-rotating cloud of scattering electrons is present. However, over and above the cyclic variation, the measurements reveal fluctuations of an apparently stochastic

nature, these dominating the temporal polarimetric behaviour.

Here the KB data are assessed comprehensively in the light of Sections 2.7 to 2.9 and according to the scheme outlined in Section 2.15 with investigations of the data density distribution and searches for rapid-type periodicities. The results of the analyses lead to the proposal that X Per is an oblique rotator with the period, the inclination of the rotational pole and the position of the active region relative to the stellar pole being evaluated. It is also suggested that the previously deduced periods (290^d and 580^d) used with proposed binary models correspond to a beat and its undertone resulting from the data sampling.

3.4(b) A Cursory View of the Data and Model Inference

The data have been taken directly from Table 1 (KB) which lists 400 measurements of X Per in the V-band ($5530/850\text{\AA}$). Typical accuracies of 0.030% for q and 0.035% for u are reported. The material mostly provides a single set of values per night, but occasionally two observations were undertaken up to 6 hours apart. Polarimetric changes are obviously present on these short time-scales.

The magnitude of the noisy behaviour may be appreciated by subtracting the underlying periodic terms determined by KB from their tabulated data. This exercise shows how little the periodic terms account for the overall polarimetric behaviour which is apparently dominated by stochastic effects either from within the star or by experimental noise. It was therefore decided to undertake an overall independent fresh appraisal of the situation.

A value for the interstellar polarization was obtained from analysis of the polarization pattern of field stars. For X Per, 16 stars are within a $\pm 5^\circ$ area in the catalogues of Hall (1958) and Behr (1959) resulting in $p_{IS} = 0.99\% \pm 0.16\%$ and $\theta_{IS} = 69^\circ \pm 11^\circ$, these values being comparable with those obtained by KB. This interstellar

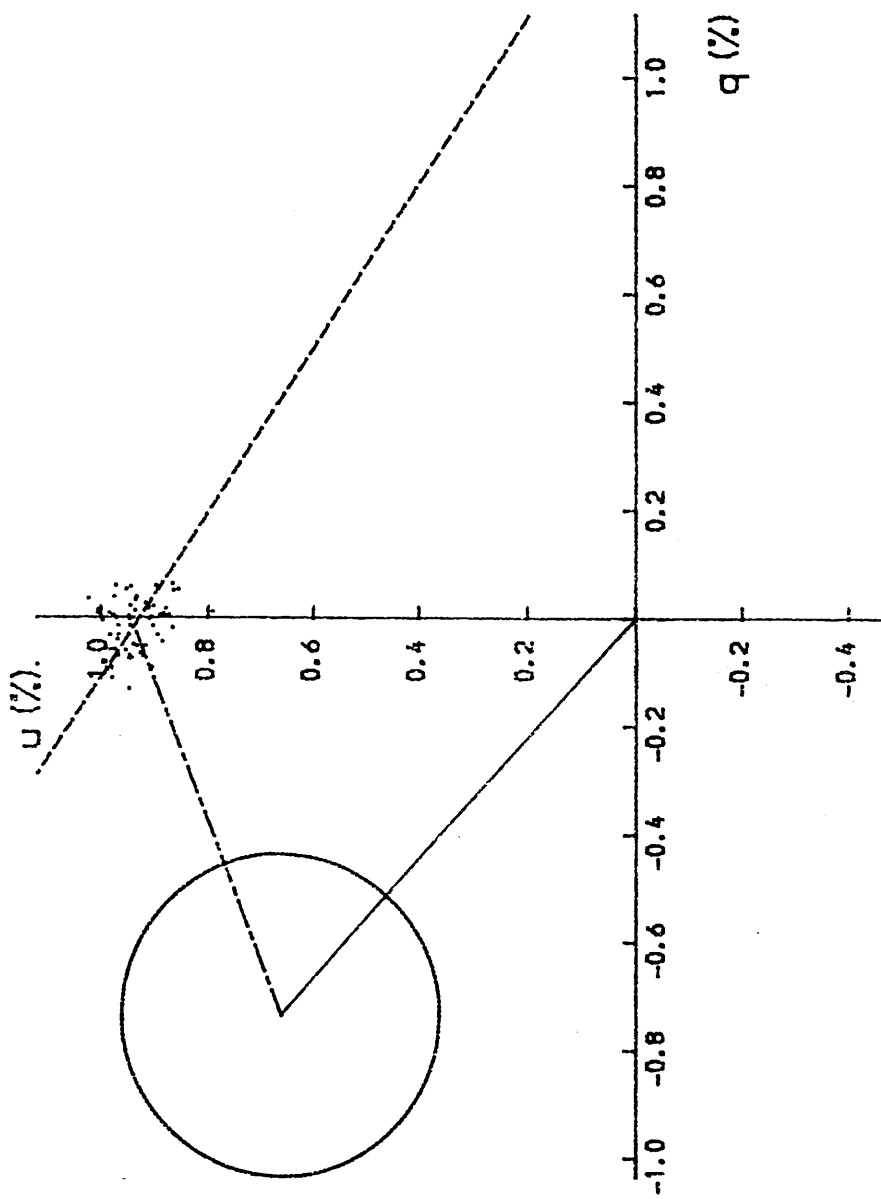


Fig. 3.4.1(b)

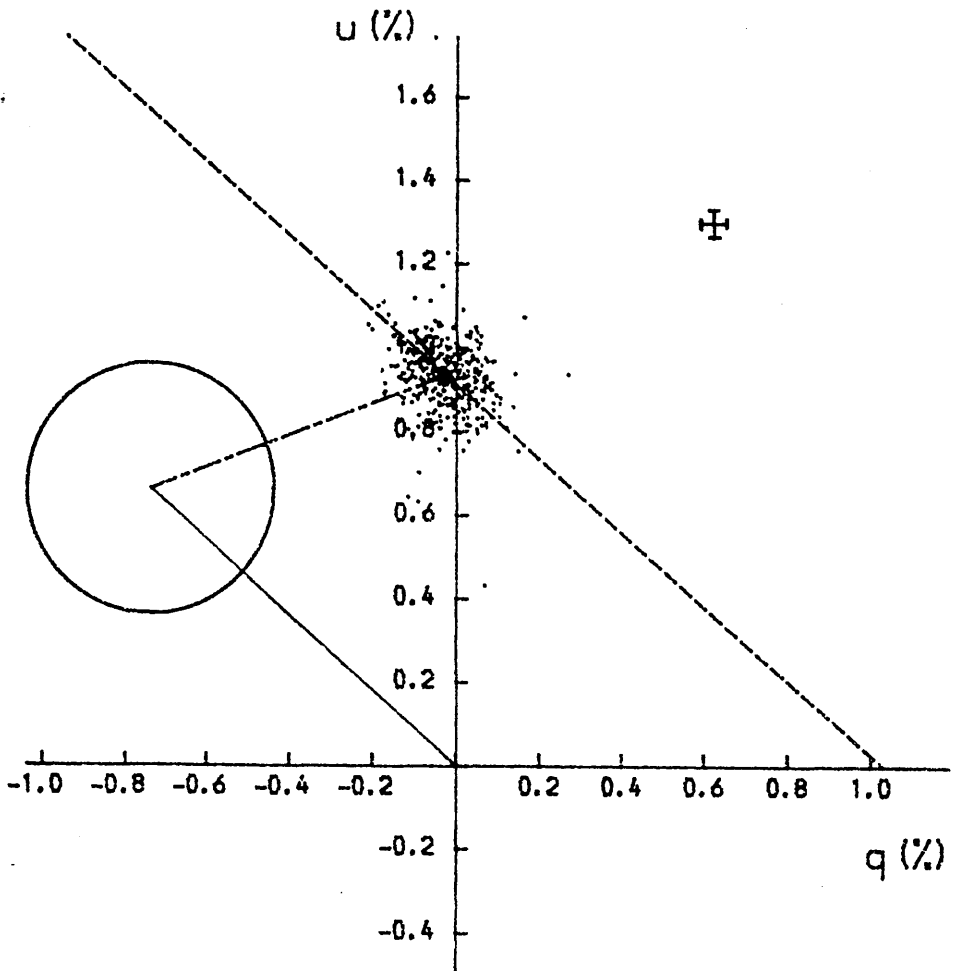


Fig. 3.4.1(a)

Plot of KB's data - all values (a) and 15-day time-averages (b). The centres of the circles correspond to the mean interstellar value, with radius equal to 1σ . The dashed line (---) passing through the circle centre is the stellar intrinsic line, the other dashed line (-----) being the MPA. The straight edge of the D-shape clearly seen in (b) is approximately normal to the intrinsic line. An error box typical of an individual measurement is indicated in (a).

value with its standard error zone is plotted in Figs. 3.4.1(a) and 3.4.1(b). The distribution of KB's tabulated data is displayed in Fig. 3.4.1(a) and the line joining the interstellar point to the mean of the measurements may be considered as the intrinsic (equatorial) line of the star, the interstellar point acting as the origin of the intrinsic frame. The distribution of the data suggests that there is an underlying steady state intrinsic polarization which drifts slowly, particularly noticeable between one observing season and the next, and an additional short-term noisy component.

In a discussion of their data, KB combined the individual measurements into averages over 19-day intervals and demonstrated that the meaned (q, u) values provided a distribution with preferred axes or eigendirections (see KB, Fig. 3). They made special comment on this but elaborated no further as to an interpretation.

Averaging of the data was re-applied here with a range of time windows and it was found that the distinctive (q, u) distribution commented on by KB was apparently best defined when the means were taken over a 15-day interval and these are plotted in Fig. 3.4.1(b). It may be noted that the straight line boundary to the data distribution is perpendicular to the intrinsic line. For the limits to the (q, u) distribution of the basic data (Fig. 3.4.1(a)), there is similarity to the pattern presented in the lower part of Fig. 2.9.4(a) and also a hint that the locus forms a cone whose apex is roughly along the stellar intrinsic direction.

The data were also investigated by taking moments (Section 2.13(a)). Both the original data and the 15-day means reveal that the direction along which maximum variance (MPA) occurs, is perpendicular to the stellar intrinsic line (to within 1° for the complete data set). The F-test performed on the maximum and minimum (orthogonal) variances showed that they are significantly different at better than the 1%

level, so confirming the non-circularity of the distribution in the (q, u) plane. The difference is not related to the small difference in KB's measurement accuracies of q and u .

This cursory inspection of the data immediately gives four hints which, as well as directing a more detailed analysis, can be used to reveal something about the geometric and physical properties of the "events" causing the polarimetric variations:

1. The fact that the data distribution has identifiable eigendirections suggests that the polarimetric behaviour is relatable to preferred axes (equatorial line).
2. The orthogonality of the MPA to the intrinsic line suggests that the globule source (or extended atmospheric bulge) occurs in polar regions rather than close to the equator (cf. Figs. 2.8.2(b)). Hence the MPA corresponds to the direction of the u -axis of the intrinsic stellar frame rather than q .
3. The presence of a straight edge to the boundary of the data when they are time-averaged reinforces point 2 and promotes a non-low inclination for the system (cf. Figs. 2.8.2(a)iv, (b)iv and (c)iv). An overall "D-shape" is very apparent.
4. The suggested appearance of a coned boundary to the tabulated data (cf. Fig. 3.4.1(a)) implies a possible variation of globule size, a range of globule distance from the source or a convolution of these two effects. The disappearance of coning and the establishment of the straight edge to the data limits when measurements are combined over longer periods (~ 15 days) suggests that two controlling factors with different time-scales may influence the apparent polarimetric behaviour. Again point 2 is reinforced (cf. Figs. 2.9.2 and 2.9.4).

Table 3.4.1

Determination of i from the method of moments

Form of data	No. of values	i (degrees) (uncorrected)	i (degrees) (corrected)
All data	400	44	47 ± 7
Outliers (>3.5 σ) removed	397	39	42 ± 8
15-day time average	66	46	48 ±15
19-day time average	56	48	50 ±15

The effect of forming the ratio of moments with and without (corrected) the influence of the measurement noise is clearly apparent.

3.4(c) Analysis of the Data Density Distribution

Introduction

A cursory examination of both the original data and the time-averaged values reveals that the q , u distributions are primarily influenced by the three parameters i , θ and noise (some of it possibly from τ_0) with the values of ϕ being considered as equally probable. Choosing ϕ to have a probability distribution which is constant within the range 0 to 2π does not restrict the possibility that there is an active region, say a magnetic pole, acting as the source (or sink) for the globules at any particular ϕ . Since the star rotates, the method of observation induces a distribution for ϕ , the values appearing to be random whether they are individual or time-averaged.

Two approaches have been investigated with a view to obtaining quantitative geometry of the X Per system. Generally the full data set was used but, in some cases, modified forms have been applied. Examination of the data shows that there are a few points which have large deviations from the centre of gravity of the distribution; some of the analyses have been made on reduced data sets with outliers ($> 3.5\sigma$ in either q or u) removed. Other treatments have taken time-averaged data.

Moments

From Section 2.13(a) it was seen that for the case where θ has a polar value and for a constant value of τ_0

$$R = m_{(2)q} / m_{(2)u} \doteq \frac{1}{\cos^2 i}$$

The results of the exercise of determining R , listed in Table 3.4.1 for different data treatments, show that the inclination of the system is fairly well defined with a value of i between 42° and 50° .

The values of R are calculated from sample variances which are

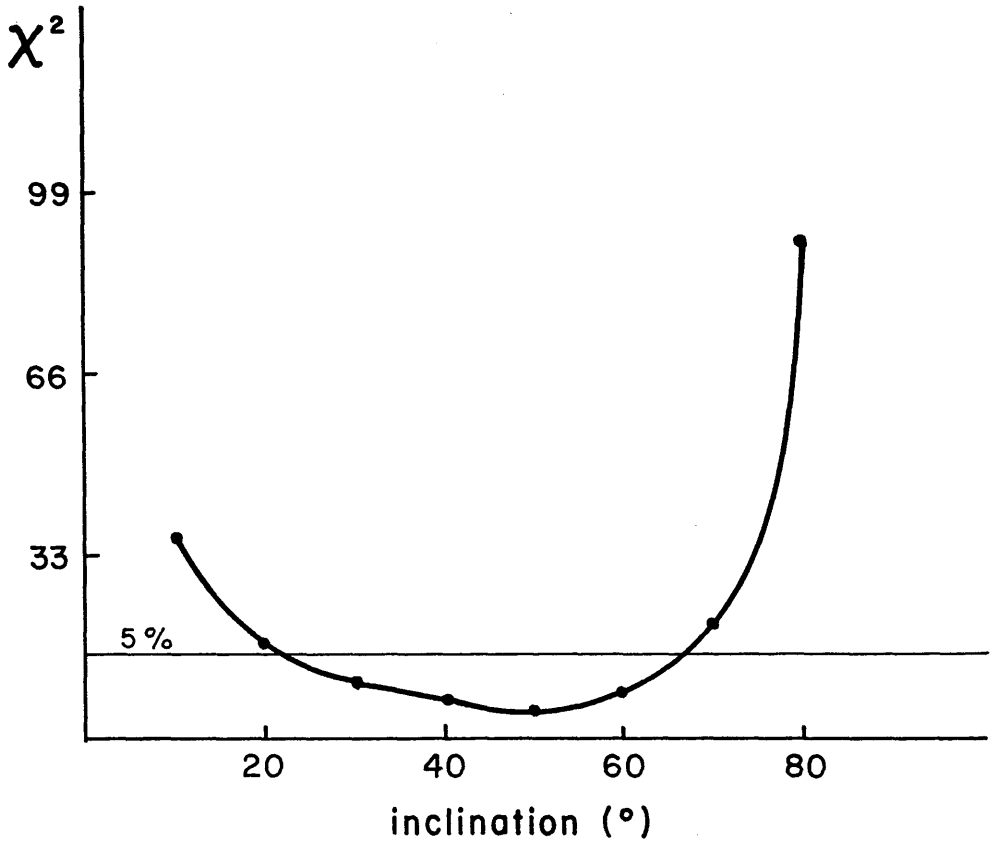


Fig. 3.4.2 Variation of χ^2 with inclination for $\theta=15^\circ$ depicting the minimum at 50° with significant fits (at 5%) from 23° to 67° , the data being time-averaged over 15 days. Very similar curves are obtained for $\theta=10^\circ$ and 20° and for other data assemblies.

estimates of the population variances (σ^2) and the tabulated uncertainties of i correspond to the 95% confidence interval on σ^2 . These were obtained using the χ^2 statistic, assuming normal data and taking half the difference between the upper and lower bounds of the confidence interval.

The F-values for the distributions in the directions of maximum and minimum variance are larger than expected from purely experimental noise indicating that "events" in the star are affecting the data in both directions, this giving confidence to the pursuit of further analytical procedures.

The value of Ω determined for each data treatment to maximise R is used appropriately in all the subsequent analyses.

Chi-Square Investigations

Following the procedures outlined in Section 2.13(b), the best fitting of χ^2 was applied to the data (again after various treatments and with rotation effected to the stellar equatorial frame) for given model geometries. Minimum χ^2 (see Fig. 3.4.2) occurs when the data are time-averaged over 15 days and compared with an artificial distribution generated with the parameters $i = 50^\circ$, $\theta = 5^\circ$ or 10° or 15° and with all values of ϕ equally probable. The insensitivity of θ for polar events to the model fitting is to be expected. Suppose a unique figure were to be formed in the (q, u) plane by choosing a particular i and θ and letting ϕ take all values from 0 to 2π , then by varying θ alone and repeating the exercise, a set of roughly concentric figures would be seen, especially for the mid-range values of i (e.g. cf. Fig. 2.8.2b(iv) and (v)). This consequence is reflected in the above result and holds until $\theta = 20^\circ$, thus giving an upper bound to its value. If i had been extremely high or low (e.g. 80° or 10°), the lack of distribution concentricity for the different values of θ would be marked and more precise information on this parameter would have

emerged. For $\theta = 15^\circ$, the estimation of i is at its best such that $i = 50^\circ \begin{smallmatrix} +17^\circ \\ -27^\circ \end{smallmatrix}$, the limits coming from the testing of H_0 , that the observations can be considered as being randomly drawn from the distribution generated by the model.

The data in their full form did not give a significant fit for the model parameters (i, θ) considered above. However, on removal of the outliers, significant fits emerged again. The cause of these wild points which give rise to the apparent coning commented on in Section 3.4(b) point 4 was investigated by considering the possible contribution of the parameter τ_0 in the model. Applying a variety of reasonable distributions for n and r provided significant fits only when the outliers were again removed and their origin remains obscure. This also shows that the apparent coning of the data points commented on under point 4 has no statistical significance.

A question now arises as to why time-averaging with a particular interval (15 days) provides the minimum χ^2 value and maximises the model fit. Certainly the effect of time-averaging would appear to reduce a noise from the system, probably the experimental (photon) noise. Another response would be to say that there is some kind of periodicity in the production of, or the appearance of, the polarimetric events, with a typical life span of 15 days. However, since the χ^2 -test explores randomness, it might be that the time-averaging process at this interval provides values of ϕ for each averaged data point which are more random than for the individual measurements, this constraint on ϕ being implicit to the model.

If the apparent behaviour for the generation of the globules requires ϕ to be random, this would imply that the active zone is in the form of an annulus with an angle $\sim 15^\circ$ relative to the stellar (rotational) pole. Astrophysically, this situation is overly artificial. However, as already outlined above, random ϕ is readily

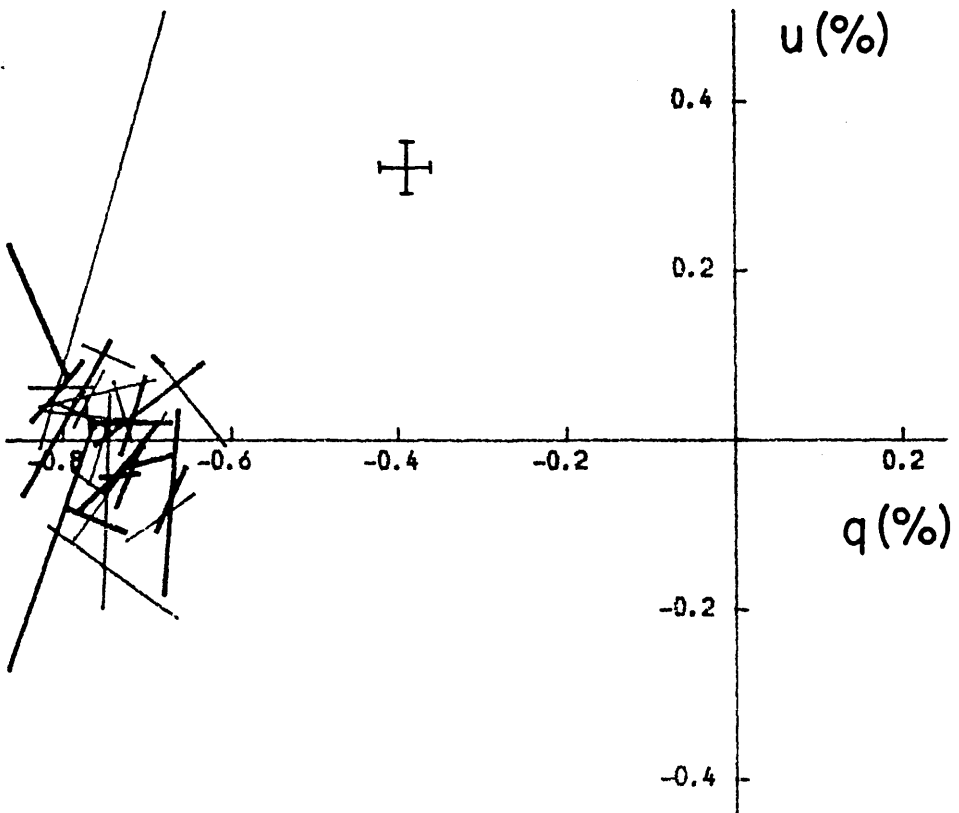


Fig. 3.4.3 The vector plots of measurements taken hours apart provide an elongatory appearance; heavy lines indicate that the second measurement from the pair is nearer the line $u=0$ (stellar intrinsic frame). An estimate for the uncertainty of the positions of the vector tips is depicted by an error cross.

mimicked by an active region in rotation about the stellar pole but whose polarigenic effect is sampled randomly with time. If this represents the underlying situation, consideration of the times of measurements should lead to the detection of rotation and a determination of the period. Before this is done, the behaviour of the short-term changes is discussed.

4.3(d) The Short-Term Temporal Changes

KB's data table includes some measurement pairs which were obtained just a few hours apart during the course of a single night. Inspection of these data reveals that the observed polarization may change substantially over such time intervals giving the impression of a stochastic behaviour and the question might be asked as to whether the hour-to-hour changes reflect some form of short-term globule evolution.

The notion of evolution may be investigated by analysis of the vectors defined by the initial and final positions in the (q, u) plane for the data pairs. For example, if the dominant trend of any short-term development is for the globule to maintain a constant latitude but move radially outwards from the star, the effect of increasing distance would weaken the observed polarization (Equation 2.7.6) causing the vector to be directed towards the line $u=0$, intersecting it at a point corresponding to the intrinsic origin; conversely, if the motion is towards the star, the polarimetric path would be away from the origin. Changes in the number density of the electrons within the globule would also produce similar effects.

Fig. 3.4.3 displays the vectors obtained from KB's data pairs plotted in the intrinsic axial frame of X Per. According to the evolutionary scheme outlined above it is expected that the vectors would converge or diverge with the origin of the frame acting as a focus, but it is immediately apparent that this is not the case. The

evolutionary scenario suggests that, for example, the moduli of the vectors describing the data pairs would depend in some way on the time interval between the two measurements, according to the dynamical influences acting on the globules. However, no correlation was found and, in addition, no relationship was found between the gradients of the vectors and the time intervals between the measurement pairs.

The distribution of the vectors in Fig. 3.4.3 exhibits an elongated appearance along the stellar u direction, the pattern being consistent with a set obtained by taking starting and finishing points, according to the elapsed interval along a closed locus (cf. Fig. 2.8.2) defined by Equation 2.11.3; a locus with the same D-shape obtained from the 15-day time-averaged values would provide the effect if it were executed on a short-time scale, say ~ 1 day.

It would seem appropriate to search for frequencies in the range covered by expected stellar rotation periods. Rather than doing this only to the measurement pairs, all the data have been included in the assessment.

3.4(e) Investigation of Periodicities

Introduction

The power spectrum analysis of KB has covered the short period range and the only peaks that are apparent are around 12^h and 24^h . If any stellar periodicity is present, it must be associated with these values. However KB dismiss these power peaks as being aliases caused by the sampling intervals, commenting that the 44 nights with measurement pairs serve to a certain degree to suppress this aliasing, although not completely. It may be noted that the calculated polarimetric power as plotted by KB takes no account of the relative phases of q and u .

If a stellar rotation period is contributing to these power peaks, it might be thought impossible to disentangle it from aliasing effects.

Although periodic analysis of each of the normalized Stokes components treated independently may be prone to the introduction of false periodicities, consideration of polarigenic models imposes phase relationships between the components; period searches based on the detection of an underlying model automatically incorporate these phasal constraints and suppress any aliasing. As it turns out, according to the tests described below, it is demonstrated that any spurious periodicities introduced by the particular sampling intervals and length of data run are below significant levels in each of the parameters separately, even without applying the constraints of their combination.

Least Squares Sine-fit

According to the analysis earlier of the data density distribution, the value of θ is small with i in the mid-range which, by Equations (2.11.3), suggests that the fundamental frequency should dominate the oscillatory behaviour of the NSP's. Although not providing the best values for the model, the single periodicity search was undertaken to check the detailed form of the power spectrum as presented by KB and to investigate the problems of aliasing, if any. This was done using a least squares fitting routine on the data after transforming it to the stellar equatorial frame with origin at the centre of gravity of the data. The fitted parameters were a constant (to allow for any systematic error of the co-ordinate origin) and the amplitude and phase of a sine-wave.

A series of discrete frequencies, ν , corresponding to a range of periods from $23^h(0^m.001)25^s$ was applied. F-values (397 data points, outliers removed, with 2 & 394 degrees of freedom) of 4.8 and greater indicate a confidence of fit at or above the 99% limit. As might be expected in consideration of the large number of trial fits (i.e. 2000), several periodicities produced F-values above the 99% confidence

limit, but the zone from about $23^{\text{h}}.75$ to $24^{\text{h}}.15$ provided an envelope within which a comb of peaks appeared (see Fig. 3.4.4) with very strong significance. Since the variation in q has been expressed as a cosine and that of u by a sine, the sine-wave fitting procedure requires the restraint of the phase difference between q and u to be either $\pm \pi/2$. For this condition set within 1σ , the periods for the best fit were not the exact ones which gave the highest F -values. A similar search around 12 hours again provided periods but when the $\pm \pi/2$ phase constraint was applied, none complied. This gave strength to the notion that the period of ~ 24 hours is the fundamental with the period of ~ 12 hours being the first harmonic.

As a check on the influence of the sampling intervals on the forcing of spurious periods, data based on $i = 45^\circ$ and $\theta = 10^\circ$ were generated via Equation (2.11.2), allowing ϕ to be chosen at random between 0 and 2π . Using random values in association with the tabulated times of the real observations, a period search was undertaken. The significance of the period fits over the interval $23^{\text{h}}.5$ to $24^{\text{h}}.5$ was much the same as to be expected from data having no underlying period, indicating that the form of the data run in no way introduces spurious periodicities (see Fig. 3.4.4). Similar tests were applied after assembling computer generated data with particular values of ν and ϵ . For these simulations, the period search rapidly identified the chosen ν and ϵ , but lower and higher frequencies (i.e. side-lobes) were also detected, albeit at a lower statistical significance. Thus the patterns of the frequency spectrum obtained from the real data are consistent with the detection of a stellar periodicity ~ 24 hours and the accompanying side-lobe aliases.

Three different approaches have been made to determine the best period and, where applicable, the stellar geometry and these are now presented.

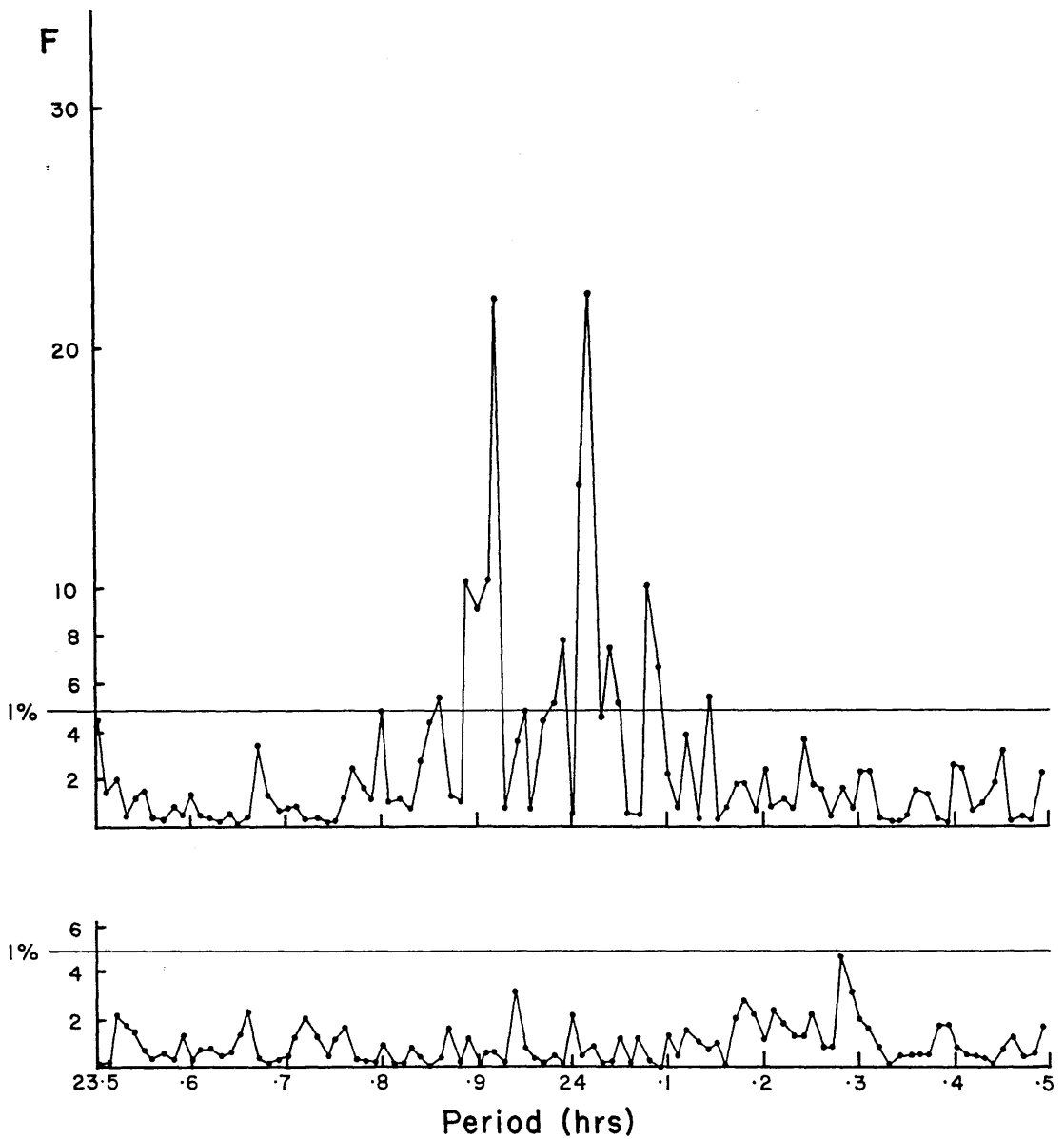


Fig. 3.4.4(a)

The periodograms (F-value of sine fit) for q'^{*}_c --(a)-- and u'^{*}_c --(b)-- over the interval 23.5(0.01)24.5 (in hours) reveals highly significant frequencies. For comparison (lower part of figures), the similar functions for random q'^{*}_c and u'^{*}_c with assigned KB timings illustrates that sampling does not introduce any significant false periodicity in this range. The 1% significance level is depicted in all cases.

3.4(f) Determination of the Rotation Period

Least Squares Fundamental and Harmonic Fit

In a similar manner as outlined in the preceding section, a least squares fitting procedure was applied to determine the coefficients for a constant level and amplitudes and phases for the fundamental and harmonic simultaneously; a grid of frequencies corresponding to periods between $23^{\text{h}}.5$ and $24^{\text{h}}.5$ was investigated. According to the degrees of freedom, the F-value for the 99% confidence limit was 3.5. In addition to the consideration of the F-values for the various fits, restraints that the phase difference between q and u should for the fundamental be $\pm \pi/2$ and for the harmonic be $\pm \pi/4$, each to within 1σ , were applied. As it happened no frequency passed these strict criteria combinations - unsurprisingly due to ill defined harmonic phases.

Comment has already been made that for the i and θ values determined by treating the data as being random in ϕ , the fundamental period is dominant over the first harmonic. For the periods providing the highest F-values for q, the error of the amplitude of the harmonic is larger than its determined value, while for u the error/amplitude ratio is about one half, so reflecting the insignificance of the harmonic to the model fit and confirming the small value of θ . By relaxing the restraints for the harmonic in view of its low signal-to-noise, the two most significant periods to emerge were:

	F-values	Fundamental $\Delta\epsilon = \pm\pi/2$	Harmonic $\Delta\epsilon = \pm\pi/4$
$23^{\text{h}}.924$ to $23^{\text{h}}.926$	q=6 u=12	+ at $\leq 1\sigma$	+ at 2.5σ
$23^{\text{h}}.991$	q=7 u=5	+ at $\leq 1\sigma$	+ at 2.5σ

Hence the most significant fit gives a positive (from left to right) stellar rotation period of $23^{\text{h}}.924$ with phase ($\phi = 0^\circ$) at JD $2,443,376.3 \pm 0.1$. From the determined coefficients, the parameters for the fundamental provide an inclination of $i = 52^\circ \pm 12^\circ$, the harmonic giving a value with little statistical significance. By combining the results from the q and u parameters, the weighted value of $\theta = 22^\circ \pm 13^\circ$. Similarly the weighted value for the scattering optical depth of the globule $\tau_0 = 0.065\% \pm 0.024\%$ which compares with $-0.032\% \pm 0.017\%$ for the constant value (a_0 in Equation 2.11.1). The global atmospheric contribution is difficult to decouple from the constant effect of the globule because of the large uncertainty on the interstellar value. After fitting the determined parameters to the data, the residuals were tested for normality. Both parameters provided mean residuals of zero; the u parameter residuals behaved as a normal distribution and the q parameter displayed a slight positive kurtosis. The tests proved the adequacy of the model fit.

At the period $23^{\text{h}}.924$ the fundamental amplitudes of q and u are $0.023\% \pm 0.005\%$ and $0.037\% \pm 0.006\%$ respectively, the harmonic amplitudes being insignificant. From Section 3.4(b) it was seen that the typical measuring errors were $\sim 0.03\%$ per data point. To confirm that the presence of noise is not influencing the production of spurious periodicities because of sampling, as in the preceding sub-section, computer generated data with $i = 52^\circ$, $\theta = 22^\circ$ and ϕ random were produced assigning KB's times of measurement but adding noise equivalent to the experimental error. This required that the noise had zero mean with standard deviation equal to $0.55(=\sin 2\theta \sin i)$, being the appropriate scaled value for $\tau_0 = 1$. Using a grid of $23^{\text{h}}.5(0^{\text{h}}.01)24^{\text{h}}.5$ for the periods, no fits greater than or equal to the 1% significance level emerged. This confirmed that neither the sampling, nor the experimental noise, nor their combination is responsible for the

detected short-term periodicity in X Per.

Another artificial data file similar to that above was generated with ϕ made cyclic with a period of $23^{\text{h}}.92$. Again using the same scheme for the period search, the most significant period emerged at $23^{\text{h}}.92$ in compliance with the model constraints. The amplitudes of the fundamental for q and u were 0.36 ± 0.04 and 0.60 ± 0.04 respectively, implying that $i = 53^\circ \pm 6^\circ$, $\theta = 20^\circ \pm 6^\circ$, $\tau_0 = 1.10 \pm 0.02$ and $a_0 = -0.6 \pm 0.2$. All these results agree well with the input values, showing that any noise induced biasing of deduced parameters is small and that this should also apply to the parameters obtained from the real data.

It can be seen that the signal-to-noise of the amplitudes for the real data is ~ 5 and ~ 10 for the artificial data. This suggests that a large proportion of the residual variations are from experimental error but the small discrepancy may reflect possible lack of homogeneity in the quality of the real data relative to the artificial data, or that there is noise within the star, or that for the artificial data the fit is made to the self-same model, there being no assumption that the applied model is exact.

It is also important to check on how well the model describes the recorded data. The goodness of fit was investigated by testing the significance of the multiple correlation coefficient squared, R^2 , this parameter measuring the fraction of the total sum of squares of the variations accounted for the fitted equation. For the period $23^{\text{h}}.924$, $R^2_q = 0.06$ and $R^2_u = 0.11$ indicating that only a small (though still significant) part of apparent variations are directly accountable to the mechanism proposed by the model.

Although the detected periodicity has a high statistical significance, giving a basic stellar geometry which is consistent with that derived from the model with the time element ignored, a large part

of the variability of the data is not accounted for directly. However, as demonstrated above, it is again suggested that these residual fluctuations are mainly due to measuring errors from photon noise, rather than inadequacies of the admittedly simplistic model. It is because of the large number of measurements over repeated periods that the underlying nature of the variable polarization shows through.

Correlations of the sign of u

Following the procedure outlined in Section 2.14(d) with the data rotated to the stellar frame, a series of discrete frequencies was applied (periods $23^{\text{h}}.5(0^{\text{h}}.01)24^{\text{h}}.5$ and phase steps of $0^{\text{h}}.1$) to generate model u values and using a series of starting epochs to allow adjustment of phase, significant periods were searched for using the statistic of the binomial distribution. For the model with $i = 45^\circ$ and $\theta = 10^\circ$, the success maximum occurred at $23^{\text{h}}.90$. After removal of the outliers ($>3.5\sigma$), the 397 values produced 276 sign correlation successes, providing a 7.73σ detection of the period and phase, the significance being based on the continuous curve approximation for the binomial distribution. By removing data with u values within $\pm 0.035\%$ of zero, i.e. within one standard deviation of a measured u parameter in KB's instrumental frame, the number of successes was 192 out of 254 ($\equiv 8.09\sigma$ detection). Obviously the experimental errors (photon-noise) are masking the underlying behaviour of the star. The resulting epoch for all these tests covered the range JD 2,443,376.21 to 2,443,376.23 (cf. phase from previous sub-section). The highest significance achieved on searching for spurious periods, with artificially generated KB-time assigned data, was less than 3σ .

Correlation of the polarization Position Angle

The data have been analysed according to the proposed method of Section 2.14(c), the 99% confidence limit for the sample correlation coefficient being zero is 0.1291.

Setting i and θ according to the values immediately above, a series of discrete frequencies (periods from $23^{\text{h}}.5(0^{\text{h}}.01)24^{\text{h}}.5$ with discrete phases at resolution $0^{\text{h}}.05$) was applied and correlations between α'_m and α'_j performed.

The best gradient (0.42 ± 0.06) provided a period of $23^{\text{h}}.92$ with phase at JD 2,443,376.95, whilst the best correlation (0.34) provided a period of $23^{\text{h}}.98$ with phase at JD 2,443,376.79. The intercepts (α'_j) at these conditions are $112^\circ \pm 11^\circ$ and $115^\circ \pm 10^\circ$ respectively; the 99% confidence interval on the population correlation coefficient, ρ , is $0.21 \leq \rho \leq 0.44$, for which the value of 1 is obviously not included. These shortcomings set doubts on either Ω being determined correctly or on the significance of the results themselves. The polarization variability is small in relation to the experimental noise associated with each data point and because of the low signal-to-noise the method may suffer from the problems outlined in Section 2.14(c). For this reason, less weight should be applied to the determined phase in relation to the results of the two preceding sub-sections.

Again as a check on possible aliasing, model data were generated and selected at random to replace the binned real measurements. When the period search on the α -correlation was performed, several v/ϵ combinations provided correlations beyond the 99% confidence interval, as was to be expected in relation to the number of trial fits, but none matching the significance of the two periods described above.

3.4(g) Concluding Discussion

Analysis by means of a stochastic model of extensive data by KB of X Per suggests that the polarimetric fluctuations are caused by globules of electrons or a fairly well defined bulge in the extended atmosphere in the polar regions of this star which offers a non-low inclination. Both the analysis of the Stokes plane data density distribution and the fitting of a model involving stellar rotation

provide consistent results showing that $i = 50^\circ \pm 10^\circ$ with the co-latitude, θ , of the polarigenic zone $\sim 15^\circ$ to 20° . The range of values for θ represents a ball-park estimate based on the χ^2 and least squares fitting, it being difficult to quantify any weighted value with the associated errors.

The time-averaged data produced well formed D-shapes implying that the globules (or bulge), as represented by τ_0 , are fairly constant on time-scales of ~ 15 days. A study of data taken during single nights did not reveal evolution of τ_0 , but suggests that stellar rotation is the dominant effect in explaining the apparently short-term "stochastic" polarimetric variations.

After checking the little effect that the average sampling interval and the limited data window have on producing false periodicity around 24 hrs. in the q and u parameters and having shown that, in any case, any aliasing is suppressed by performing a periodicity search in their combination according to the dictates of the stellar rotation model, a period of $23^{\text{h}}.95 \pm 0^{\text{h}}.05$ emerges, the value within the error bounds being dependent on the method chosen to fit the equations representing the model. The value of the epoch corresponding to $\phi=0^\circ$ is also slightly sensitive to the method of implementing the equations for the model to the data but the suggested value is JD 2,443,376.2 \pm 0.1.

The periodicity and geometry determined for X Per suggest that it is an oblique rotator, with the possibility that magnetic poles are enhancing the number density of electrons. From the value of θ , the obliquity would be taken as 15° with an upper bound of 20° . This discovery has great importance in its own right but the particular value of the rotation period is also significant for the interpretation of all other data related to the star.

Firstly, taking the interpretation by KB of their polarimetric

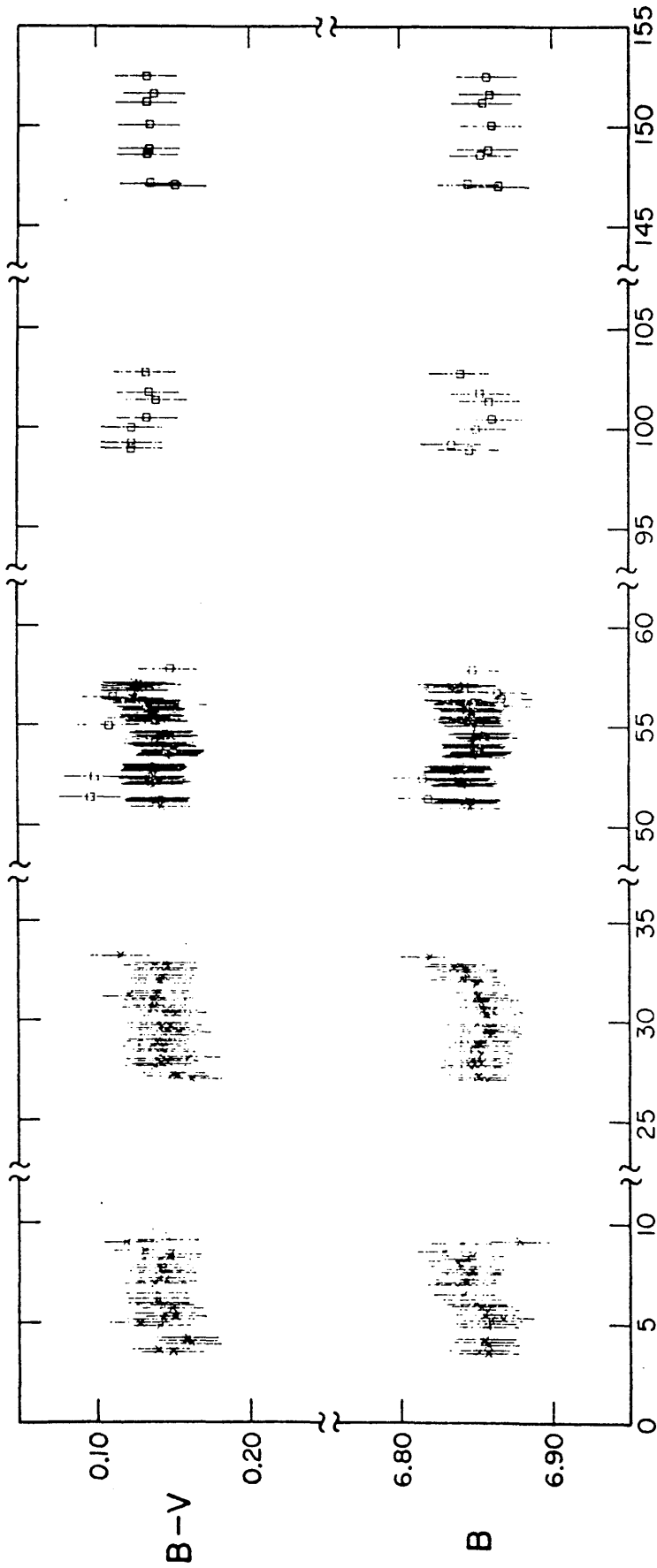
data, the enigma of the D-shape, noted by KB when the data are time-averaged, is resolved. Because of the closeness of the rotation period to the average sampling interval, within a time-averaged interval, say 15 days, there is only a small change of phase. Nightly observations over a short span are equivalent to repetitive measurements, the time-averaged values providing a more accurate estimate for that particular phase of the rotation. Fifteen days represents the best interval for obtaining an accuracy which then allows the apparent progression to be noted from one time average to the next. The inclusion of measurement pairs from a single night make the 15-day averages noisy. Of course the D-shape obtained by the 15-day average is the same as obtained when the data are used individually in the assembly; it is just that it is apparently more distinctive by smoothing out the noise.

Secondly an alternative explanation is also available for the long term periodicity detected by KB. Because the real period of the stellar polarimetric variation is close to 24 hrs., its sampling with an average interval of ~ 1 day will automatically generate beats. For a beat period of 290 days to be produced, sampling at 24 hrs. requires an underlying period of $23^{\text{h}}.917$ to be present, this being remarkably close to the discovered rotation period reported here. It is therefore suggested that KB's 290 day period and the longer one (~ 580 days) correspond to a beat and its first undertone.

The question is also immediately raised as to the reality of the 580 day radial velocity period determined by Hutchings *et al.* (1974). Examination of the data used to obtain their radial velocity curve reveals that they typically comprise three measurements per observing season over a few weeks, so imposing that any detected periodicity will be longer than one year. Again it is proposed that the 580 day velocity period corresponds to twice the beat period which itself, at

290 days, is too short to show from the form of their data train. It is interesting to note that, following more intensive spectroscopic activity in the middle 1970's, interpretation of the radial velocity data has become harder to interpret. From measurements of a variety of lines, no coherent picture emerges in terms of a binary model. According to Hutchings (1977), existence of the 580 day period still stands in the Balmer absorption velocities but the period is not clearly seen in either the He I or Balmer emission, this being hard to reconcile for a binary system. If the misidentification of the true period is taken for granted, it is therefore suggested that Balmer absorption and the polarimetric mechanism occur at the same atmospheric level. It may also be noted that a complementary analysis of archived spectra of X Per by Cowley *et al.* (1972) concluded that if the star is involved in a binary system it is likely that the period lies between a few weeks to several months; the difficulty of locating and measuring truly stellar features makes the question of a possible binary system difficult to establish. Another argument against the 580 day period comes from Penrod and Vogt (1985) who claim that the variations reported by Hutchings *et al.* (1974) are spurious and are caused by asymmetric and variable emission components hiding in the absorption profiles.

For the determined rotation period and assumed size of the photosphere of X Per ($\sim 6R_{\odot}$), the estimated equatorial velocity is 305 kms^{-1} , giving a $V_{\text{eq}} \sin i = 235 \text{ kms}^{-1}$. After a reassessment of the emission contamination, Hutchings (1977) provides a consistent determination of $250 \pm 25 \text{ kms}^{-1}$; the value of $V_{\text{eq}} \sin i$ given by Penrod and Vogt (1985) is $213 \pm 20 \text{ kms}^{-1}$. By inverting the relation for τ_0 (see Equation 2.11.1) and taking a conservative estimate of the scattering height above the photosphere as $2R_*$ (see Section 1.3), the upper bound for the electron number density is found to be $\sim 10^{12} \text{ cm}^{-3}$.



HOURS ELAPSED FROM J.D. 2442431.5

Fig. 3.4.5 Photoelectric photometry of X Per starting at 0^h UT 1975 Jan 19. Crosses, points obtained at Leuschner Observatory; squares points obtained at Lick Observatory. There is a hint that the B-band is exhibiting a periodic minimum consistent with a \approx 24hr cycle. (Reproduced from Morgan, Bowyer, and Penegor 1976 - Fig. 1).

According to the same model which has been fitted here to the polarimetric data, it is predicted that rotation will provide a light curve with the fundamental and its harmonic present. There have been many papers which confirm that X Per exhibits brightness changes, but of particular note are the results of Margon, Bowyer and Penegor (1976) who performed extensive photometry on five consecutive nights. (Figure 3.4.5 reproduces their light curve of X Per in the B band). Although they suggest that their measurements do not reveal night-to-night variability, examination of their graphed data suggests that a B-band minimum was occurring each night and that the periodicity of this would not be inconsistent with a value of just less than 24 hours.

No concrete suggestions are made here in relation to the generation of the X-rays but as the present situation is unsatisfactory as to modelling involving a compact object within the system (Weisskopf, *et al.*, 1984), the introduction of there being a coherent magnetic field (see Underhill (1983) related to magnetic activity in the atmospheres of early-type stars) might allow new proposals to be made to the suggestion by Doazan (see Underhill and Doazan, 1982) that the X-rays are associated with coronal activity.

3.5 A Comment on the Polarimetry of HDE 226868

(HDE 226868, $m_v = 8.9$, B0 Ib, $\alpha_{1950} = 19^h 56^m 29^s$, $\delta_{1950} = +35^\circ 3' 35''$)

On visual inspection HDE 226868 has the guise of a single star, but it is actually a short period spectroscopic binary. Interest arose in the system when the X-ray source (4U 1956+35) was discovered to emanate from the same position in the sky. (Bolton (1971, 1972) and Webster and Murdin (1972)). CYG XR-1 has been synonymous with HDE 226868 ever since. For X-rays to be emitted it is generally thought that some sort of compact object is involved. Obviously then it is important that the masses of the stars in the binary should be sought. For this, the value of the orbital inclination is needed; the

mass of the primary, i.e. the visual component, can be estimated from its spectral type, leaving only the mass of the secondary to be ascertained straightforwardly from the usual mass function and with it, an opinion as to its type.

It may be reasonable to expect in such a system that the primary gets influenced to such an extent by the secondary as to cause it to have either an excessive mass loss (forming an accretion disk) or a tidal distortion, the effect being observed, one way, as a modulating intrinsic polarization.

With such a scenario in mind, Kemp's group (Nolt, *et al.* (1975), Kemp, Southwick and Rudy (1976), Kemp *et al.* (1978) and Kemp *et al.* (1979)) decided to undertake a polarimetric campaign on the system with a view to determining i . Upper limits have been placed on i from analysis of its light-curve and through the absence of X-ray eclipses (see Bolton (1975) *loc. cit.*), the boundary being at about 60° .

After monitoring in the V band (see Appendix D for a comprehensive listing of the data) over 3 years (June 1975 - December 1978), Kemp *et al.* (1979) claimed to have found a polarization component modulated over a $5^{\text{d}}.6$ interval, synchronized with the $5^{\text{d}}.6$ radial velocity period, and calculated that the inclination lay between 60° and 70° , *ergo* conflicting with the suppositions on i above. However, Simmons, Aspin and Brown (1980) applied a χ^2 technique to the V band data (as opposed to the least squares approach) and showed that the error on i is grossly underestimated, and revised i to lie in the interval $30^\circ \leq i \leq 85^\circ$.

On observing a 9th magnitude star, even on a 61cm reflector and using wide-band filters, instrumental noise is obviously going to contribute to a significant part of any variability recorded in data (it was in this case the important effect of instrumental noise that Kemp ignored in calculating i and its error). The method of moments

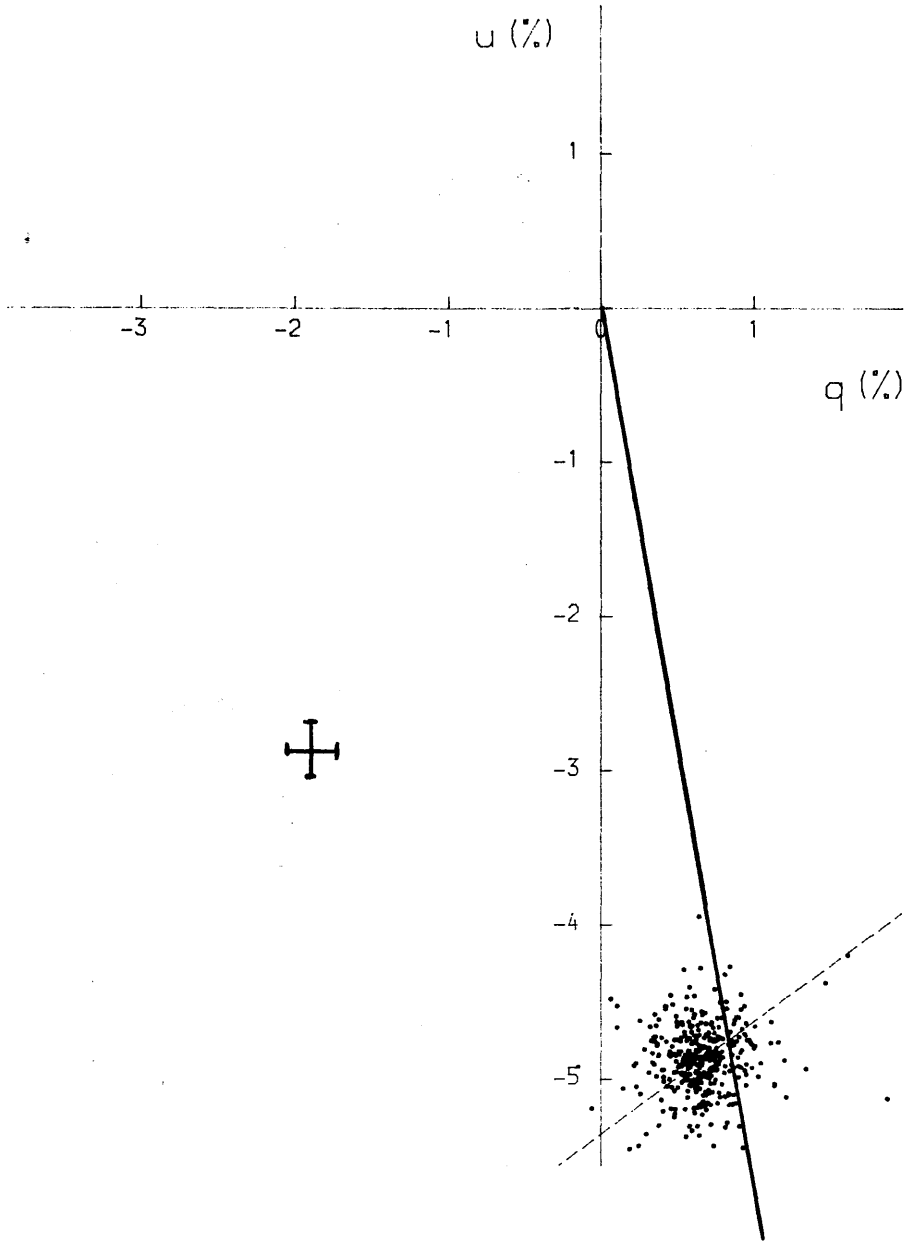


Fig. 3.5.1 The V-band data of Kemp's group plotted in the equatorial frame. The dashed line (-----) represents the MPA. The circular form of the measurements make eigendirections difficult to identify. The typical error on a single data point is indicated (the cross), as is the approximate interstellar direction (the full line).

(special cases (1) and (2) in Section 2.13(a)) can directly account for noise and so may be a particularly useful tool in such a situation. Applying this technique to the data, the maximum variance (σ_x^2) was found to be 0.04263%² and the minimum (σ_N^2) 0.03497%². The two variances, occurring at orthogonal directions, give $F = \sigma_x^2 / \sigma_N^2 = 1.22$, which compares with ~ 1.2 - the 5% significant level. So it can be seen that there are no immediately identifiable eigendirections (see Fig. 3.5.1). According to Kemp, the typical measuring error in either q or u was $\sim 0.15\%$ (i.e. $\sigma_e^2 = 0.0225$), which implies $\sigma_{x'}^2 = \sigma_x^2 - \sigma_e^2 = 0.0201$ and $\sigma_{N'}^2 = 0.0125$, hence now $F = 1.6$. Therefore employing the noise corrected second moments and their χ^2 mean error estimates, gives i to be $\sim 61^\circ \pm 6^\circ$ if the scattering region is near or in the orbital plane or $\sim 38^\circ \pm 8^\circ$ if nearly perpendicular to it. Unfortunately analysis of the field star polarization pattern or the 6 colour measurements of Gehrels (1972) do not reveal the interstellar value in the HDE 226868 direction, so no indication as to the co-latitude of the scattering mechanism is forthcoming.

Carrying out a periodicity search over the interval 5 hrs. to 40 hrs. in steps of $0^h.01$, revealed no fits of significance approximately comparable to a $5^d.6$ fit.

On the whole the experimental noise seems to prevent any hope of deriving any fundamental information, i.e. i, θ , from the data, the one exception being the $5^d.6$ polarimetric periodicity.

3.6 The Polarimetric Behaviour of σ Ori E

(HD 37479, $m_V = 6.7$, B2 V, $\alpha_{1950} = 5^h 36^m 16^s$, $\delta_{1950} = -2^\circ 37' 38''$)

3.6(a) Introduction

This object can be considered as the prototype of a small class of helium rich stars, and it has been extensively studied. A discussion on the results of various observations can be found in Underhill and

Doazan (1982, p. 159). It exhibits a diversity of rapid-type phenomena - the light curve, He I lines, H α emission, magnetic field and polarization all seem to vary with a period of about 1.19 days.

Two genera of model have been proposed to explain what has been observed. Kemp and Herman (1977) - KH - suggested that σ Ori E is a member of a mass transfer binary system, after discovering a modulated polarization synchronous with the light period. They derived the orbital inclination to be $\sim 76^\circ$. The lack of radial velocity variations, which Bolton (1974) had shown were less than 4 km s^{-1} , work against the binary hypothesis, though. Harmanec (1984) has recently pointed out that the light curves of several Be stars behave in a similar manner - σ Ori E being taken as the archetype - and labelled them as oblique rotators. Groote and Hunger (1977) suggested that the star has two helium caps, but again such a model requires radial velocity changes and, further, the secondary minimum of the light curve (Hesser, Walborn and Ugarte (1976)) occurs $0^{\text{P}}.43$ after the primary one and not $0^{\text{P}}.5$ as it would need to be here. Shore and Bolton (1976, 1977, 1982) (as referenced in Harmanec (1984)) offered a magnetic oblique rotator explanation in which the helium abundant region is concentrated at the magnetic equator in the form of a band. Landstreet and Borra (1978) - LB - in considering their version of a magnetic oblique rotator, suggested that optically-thin localized gas clouds act as absorbing and/or scattering mechanisms, and attribute the lack of observed radial velocity variations as being due to non-robust measuring procedures. LB's model explains the recorded phenomena well, except for the H α variability, which may be caused by localisation of out-flowing mass controlled by the magnetic poles, and the phasing of the critical values of the light curve. They estimate the inclination of the rotation axis of the star to be near 90° , it not being possible to calculate the obliqueness of the magnetic pole(s) for such an aspect

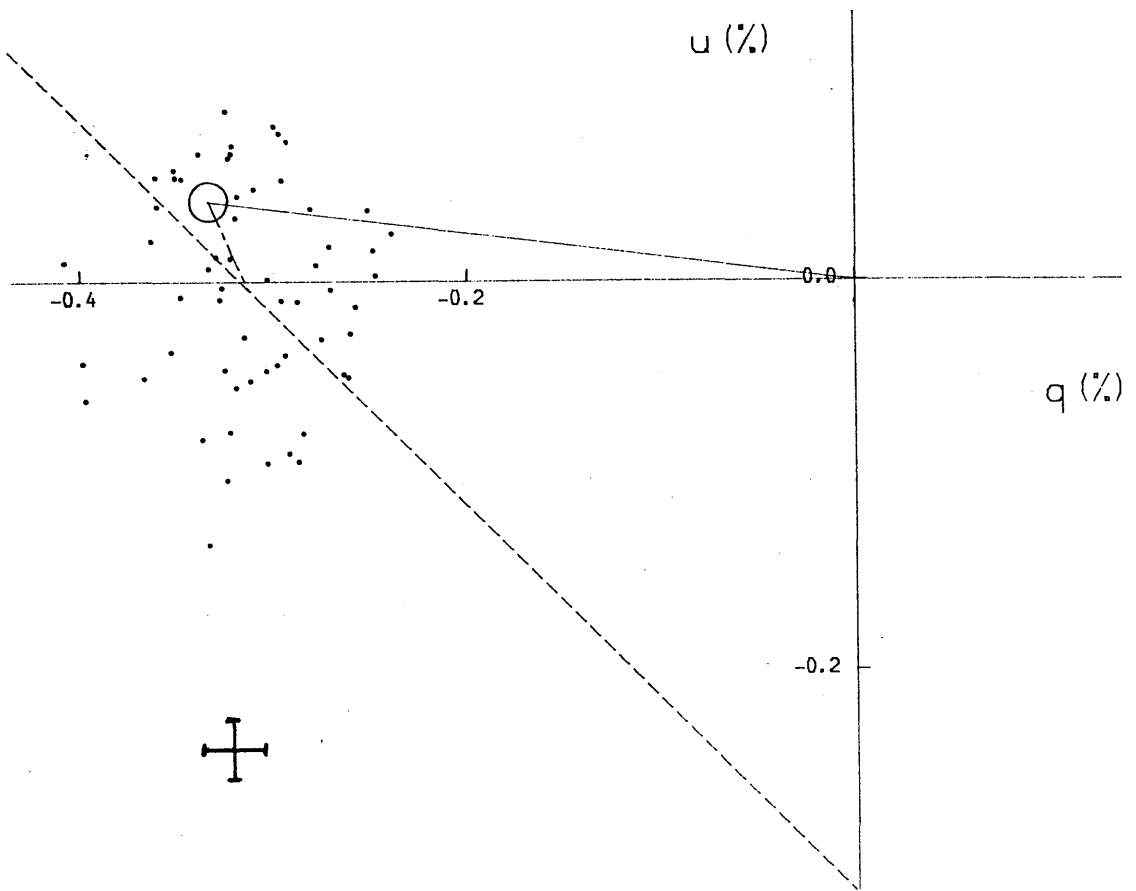


Fig. 3.6.1 Plot of KH's data in the equatorial frame. The circle corresponds to the approximate interstellar position. Note that the dashed line (---), the stellar equatorial line, emanating from the circle is nearly parallel to the MPA (-----). The interpreted error of a single measurement is indicated by the cross.

using their magnetic data alone.

If the gas clouds are considered primarily as scattering mechanisms, then the polarization will vary with the rotation period and also the apparent stellar magnitude.

The oblique rotator model, as described in Section 3.4, is applied to the polarimetric B wide-band measurements of KH below, with a view to deriving the stellar inclination, obliqueness of the magnetic pole, the scattering optical depth and to check if the $1^d.19$ period surfaces in both q and u with appropriate phase constraints. The latter quantity is the severest test for an oblique/rotator scenario. The results of the analysis tend to support and enhance the model of LB.

3.6(b) The Measurements

The 60 B band measurements of KH, taken over 69 days between Jan. 7 - Mar. 17 1977, are listed in Appendix D; up to 5 points were recorded on any one observing night. It is unclear as to what is the error on a single measure, but it has been interpreted as 0.015% in both q and u . This seems a little small in comparison to the values quoted in Kemp and Barbour (1983) ($\sim 0.03\%$) for observations on X Persei, which is a star of similar magnitude to σ Ori E, since the same telescope and filters (V) of similar band-pass were used. KH estimated the interstellar polarization (p_{IS}) to be 0.335% (no error available) and $\theta_{IS} = 86^\circ.5 \pm 0^\circ.5$ from the group of stars in which σ Ori E is known to be a member.

Fig. 3.6.1 shows the B measurements in the equatorial (q, u) plane, along with the interstellar value and the direction of maximum spread (i.e. variance) in the data (MPA). It is immediately obvious from the figure that the MPA is almost parallel to the equatorial line, implying that the scattering material lies near the equatorial regions of the star and that the harmonic components of Equations (2.11.2) and/or (2.11.3) should dominate the oscillations.

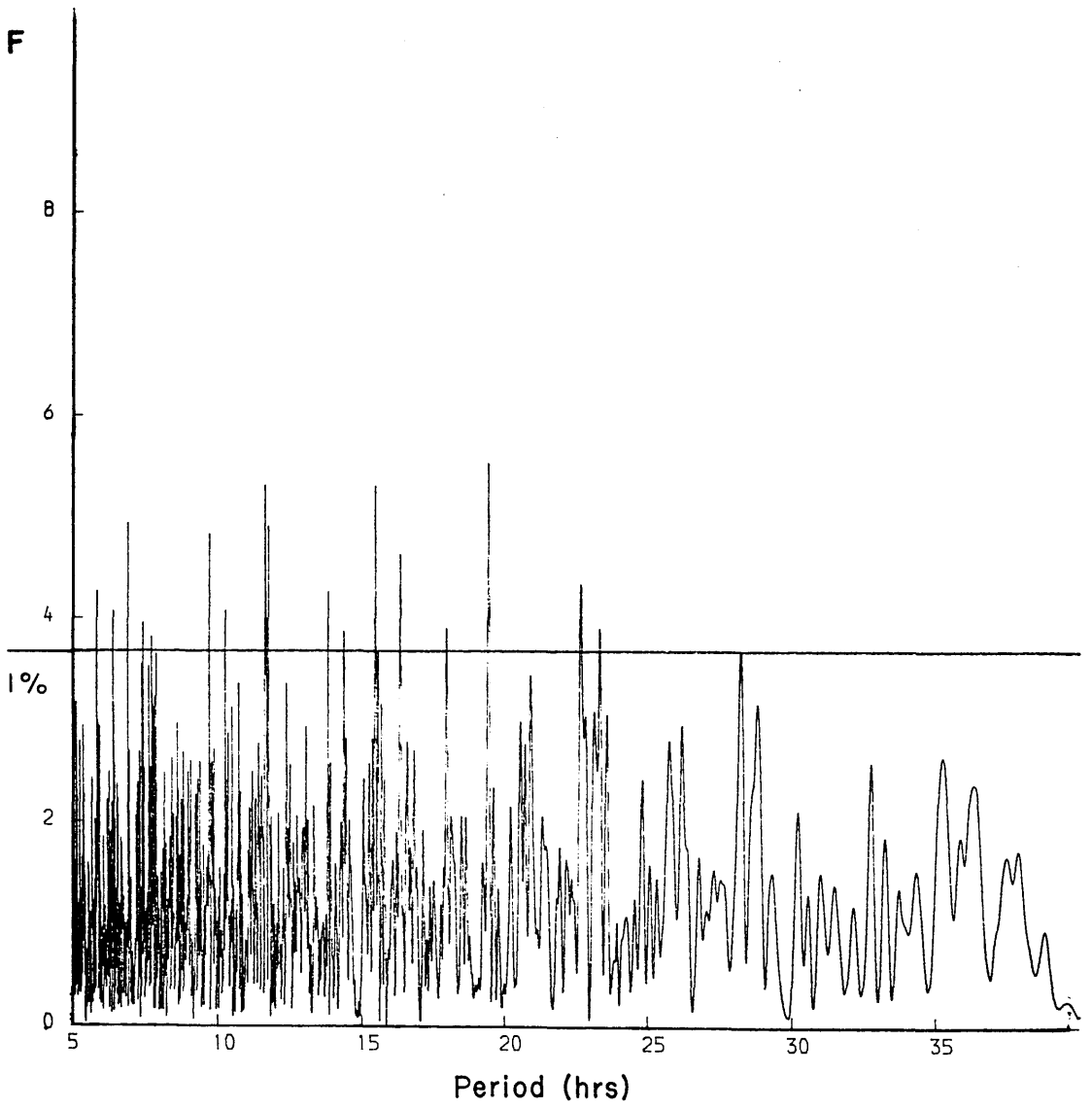


Fig. 3.6.2(b)

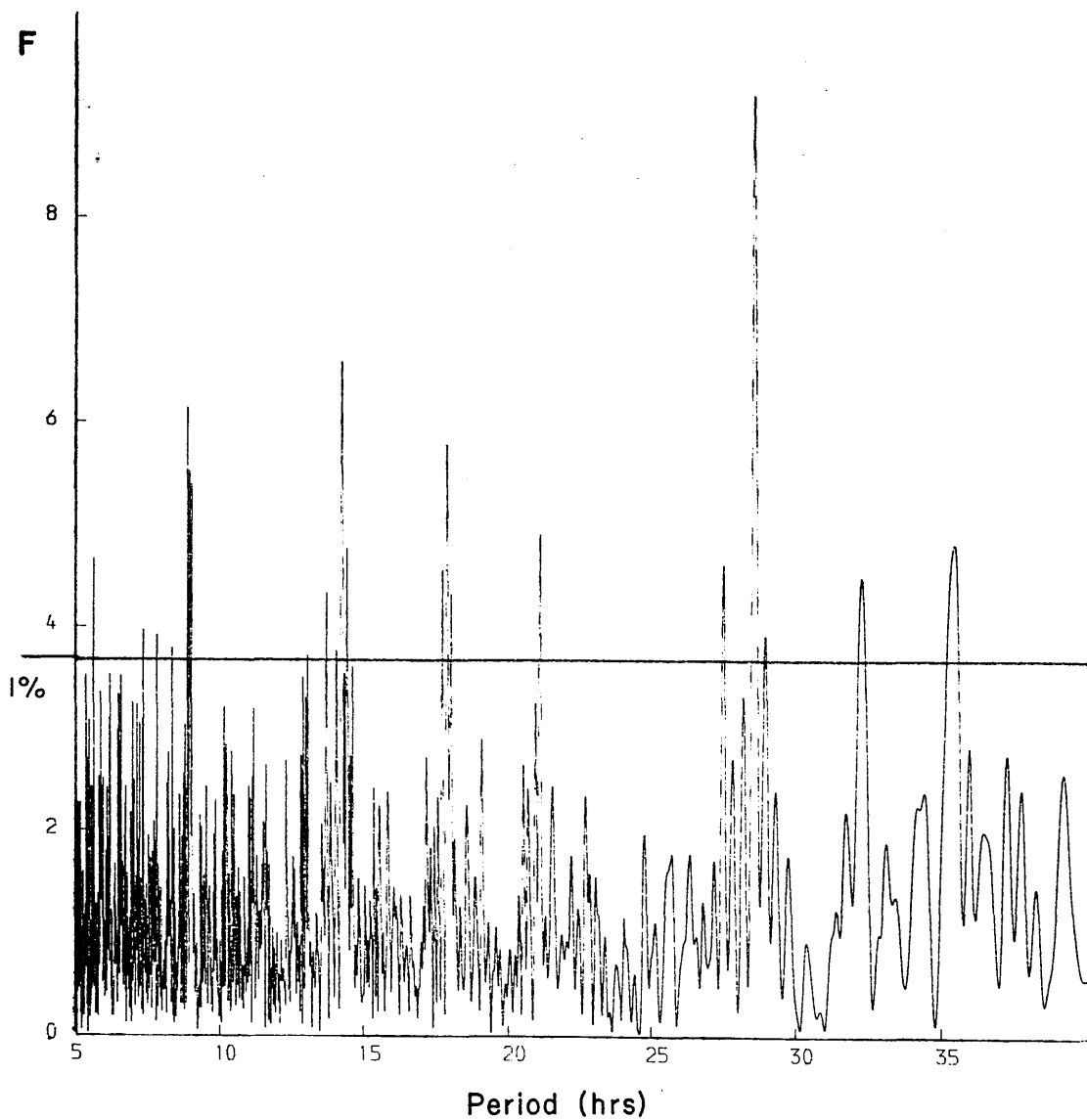


Fig. 3.6.2(a)

The periodograms for q'_{*c} --(a)-- and u'_{*c} --(b)-- over the interval $5(0.01)40$ hours. The 1.19^*_{*c} day (28.5hrs) period is very apparent in (a), but not in (b).

3.6(c) Analysis of the Data

Moments

As mentioned above, the direction of the MPA implies $\theta \approx 90^\circ$, and so i can be estimated from the combination of maximum (σ_x^2) and minimum (σ_N^2) variances (see Section 2, Case (2)). The result gives $i = 67^\circ \pm 9^\circ$, the error value being calculated using the mean 95% confidence intervals on the noise corrected second moments by way of the χ^2 statistic. It was assumed that the form of the data sampling was such that ϕ could be treated as a random parameter.

If the experimental (σ_e) has been interpreted correctly then the ratios $F_x = \sigma_x^2 / \sigma_e^2$ and $F_N = \sigma_N^2 / \sigma_e^2$ give 12.8 and 6.4 (cf. $F(5\%) = 1.6$) respectively implying that the periodical form of both q and u should be detectable on fitting a sine-wave comprising a fundamental and harmonic frequency by least squares. However, if the true experimental error is more on a par with that quoted in Kemp and Barbour (1983) ($\Rightarrow F_x = 2.4$), only a significant fit for q should emerge at the expected 1.19 day period. Further, the value of i derived above will have been slightly underestimated.

For the purposes of the analysis below, the value of 2Ω needed for rotation from the instrumental to stellar frames was taken as -76° - calculated using Equation (2.12.1).

Least Squares Fundamental and Harmonic Fit

The power spectrum of KH had shown that in the B measurements, the highest peak occurred at $0^d.595$ (i.e. half of $1^d.19$). Presently a grid of periods $5^h(0^h.01)40^h$ was applied in a co-ordinate system whose origin was the centre of gravity of the data points and whose axes were parallel to those of the stellar equatorial frame, the object being to check if a significant fit occurs at $1^d.19$ in both q and u and to see if the $\pm \pi/2$ and $\pm \pi/4$, to 1σ , phase constraints are conformed to. The resulting periodograms are shown in Fig. 3.6.2.

The most evident peak occurs at $28^{\text{h}}.55$ ($\equiv 1^{\text{d}}.19$) in q , but no fits greater than the 1% level (i.e. $F > 3.7$) are seen in u above 23 hrs. - it being perhaps related to the lack of information concerning the value of the instrumental noise. Re-applying a finer comb of $28^{\text{h}}.54(0^{\text{h}}.001)28^{\text{h}}.57$, still no confident results emerged for u , but the maximum for q ($F = 9.2$) revised the period to $28^{\text{h}}.554$. The F -values can be compared to those tabulated with numerator and denominator degrees of freedom of 4 and 55 respectively. At $28^{\text{h}}.554$, $F_{\text{u}} = 2.1$, $a_1 = 0.023\% \pm 0.008\%$, $a_2 = 0.045\% \pm 0.008\%$, $b_1 = 0.011\% \pm 0.007\%$ and $b_2 = 0.016\% \pm 0.007\%$. The differences between the phases of q and u would be expected to be $\pi/2$ and $\pi/4$ for the fundamental and harmonic respectively. The derived values, in the sense $\epsilon_q - \epsilon_u$ i.e. right to left rotation, were $161^\circ \pm 46^\circ$ (i.e. slightly greater than 1σ) and $45^\circ \pm 15^\circ$. So it can be seen that at $28^{\text{d}}.554$ the polarimetric variability conforms to an oblique rotator model.

Combining a_1 , a_2 , b_1 and b_2 give the weighted means $i = 80^\circ \pm 6^\circ$, $\theta = 85^\circ \pm 4^\circ$, $\tau_0 = 8.7 \times 10^{-4} \pm 1.5 \times 10^{-4}$ and $a_0 = 0.041\% \pm 0.008\%$. (a_1 and b_1 give a meaningless result for i) with phase (i.e. $\phi = 0$) at JD 2,443,150.33 \pm 0.02. No comment can be made as to whether or not there is a general atmospheric contribution (i.e. q_A) as the error on p_{IS} is not available. Simmons, Aspin and Brown (1982) have pointed out that in situations of strong noise, least squares can give a biased (upward) value of i where error will also be underestimated. Since u did not give a significant fit at $28^{\text{h}}.554$ and that its coefficients are comparable to their accuracies imply that such a case exists here. It is important to note, however, that the position of the data is not inconsistent with there being truly high values of i and θ as is supported by the method of moments.

As a check on the effect of sampling and noise on the fitting procedure at $28^{\text{h}}.554$, artificial data were generated with the

parameters $i = 80^\circ$, $\theta = 85^\circ$ and $\tau_0 = 1$, and ϕ random. Noise equivalent to the errors on a_2 and b_2 was added. Running the data set under a grid of periods, $28^h(0^h.001)29^h$, revealed no significant fits superior to the 1% level. Hence neither the sampling nor instrumental noise has had any noticeable effect on the manufacturing of the $28^d.554$ cycle.

Another artificial data set was generated again with $i = 80^\circ$, $\theta = 85^\circ$ and $\tau_0 = 1$, but ϕ was made cyclic with a period of $28^h.554$. Noise was added so that the "signal to noise" ratio of $a_2/\Delta a_2$ was comparable to $a_2/\Delta a_2$ of the real data. The parameters i , θ and τ_0 reproduced quite well giving $i = 68^\circ \pm 8^\circ$, $\theta = 79^\circ \pm 5^\circ$ and $\tau_0 = 1.0 \pm 0.2$.

Correlation of the Sign of u

Since the u parameter appears to be dominated by noise, this method (see Section 2.14(d)) might more readily, compared with regression, identify the $28^h.554$ period in u at a significant level.

The data were rotated to the stellar equatorial frame and the signs of u matched to those of model values generated with a period from the interval $28^h.4(0^h.01)28^h.6$ and a series of starting epochs resolved to $0^h.1$, $i = 80^\circ$ and $\theta = 85^\circ$. The significance of any correlation can be assessed using the continuous curve approximation for the binomial distribution, for which if ϕ can be considered as random will have a standard deviation of $\sigma = 0.5/\sqrt{N}$, where N is the number of data points. The 99% limit for detection is at 2.54σ .

At $28^h.60$, the 60 measurements produced 40 matches ($\equiv 2.4\sigma$). Weighting by removing u values within $\pm 0.015\%$ of zero (i.e. the supposed experimental error) produced 29 successes from the 42 possible ($\equiv 2.3\sigma$) at periods ranging from $28^h.51$ to $28^h.58$. No significant periods were detected.

An artificial data set with the same parameters as used in the least squares section was generated to check if the above fits are superior to that expected from noise alone. Applying a grid of

periods, ranging from $28^{\text{h}}.4(0^{\text{h}}.01)28^{\text{h}}.6$, and phase steps of $0^{\text{h}}.1$, the most significant matching result was equivalent to a 1.9σ detection, on the data produced with ϕ random and a conservative estimate of the scaled experimental noise. This shows that the u parameter of the B band measurements can be equally represented by a distribution governed by uniform ϕ , as one in which ϕ is periodic.

Re the Magnetic Field

Following Stibbs (1950) and Landstreet (1982), and considering the geometry of Fig. 2.7.1, where P would now represent the position of the field vector, it is easy to show that for an oblique dipole rotator, the longitudinal component of the field B_e is described by:

$$B_e = A + B \cos \phi \quad (3.6.1)$$

where $A = \frac{-8}{20} B_p \cos \beta \cos i$, $B = \frac{8}{20} B_p \sin \beta \sin i$, β is the obliquity of the magnetic axis to the rotation axis ($\equiv \theta$) and B_p is the polar field strength.

Equation (3.6.1) is at a maximum when $\phi = 0^\circ$. Fitting the above equation to the 8 magnetic observations of LB with the polarimetric period shows that the epoch of $\phi = 0^\circ$ is at $\text{JD } 2,443,441.77 \pm 0.02 + 1^{\text{d}}.1898$ and hence is correctly synchronous with the polarimetric modulations if the magnetic poles are being considered as the site of the localized (enhanced) scattering.

At $1^{\text{d}}.1898$ the F-value of the least squares fitting of Equation (3.6.1) is 51.2 which compares to the 1% level = 13.3; $A = -0.381 \pm 0.191$ kilogauss and $B = 2.68 \pm 0.26$ kilogauss.

3.6(d) Conclusions

Analysis of a polarimetric B-wide-band data run of moderate length by KH enhances the magnetic oblique rotator model for σ Ori E described by LB. Reduction of the data density distribution by moments implies that the inclination of the stellar rotation axis, i , is equal to $67^\circ \pm 9^\circ$ and that the polarigenic mechanism(s) is/are confined to the

equatorial regions of this star. Consideration of the measurements as a time-sequence result in $i = 80^\circ \pm 6^\circ$, and the co-latitude of the scattering cloud(s) $\theta \sim 85^\circ \pm 4^\circ$ and show an expected rotation period of $28^{\text{h}}.554$ consistent with that of the light curve (see Hesser, Walborn and Ugarte, 1976). The suggested mean value of i by combining the values derived by the moments and least squares methods is then $74^\circ \pm 6^\circ$. It was unclear as to what the value of the experimental error in the data of KH is, it being interpreted as 0.015% for both q and u . The fact that u did not show through at $28^{\text{h}}.554$ in the fitting of a sine-wave comprising fundamental and harmonic frequencies, and the correlation of its sign demonstrated that u could be represented by a non-periodic parameter, implies the value of the true experimental noise to be greater by at least the order of 2. Obviously more data are needed to clarify if u has a significant periodicity at $28^{\text{h}}.554$ or not; but the situation at present would not rebuke i and θ as having high values. Neither the sampling nor the noise seem to have had any noticeable effect on the production of the stated cycle.

If the scattering takes place in a cone of say $\pm 5^\circ$ in extent about θ and ϕ , and at a height of $2R_*$ above the photosphere (see Section 1.3), then the electron number density (n_e) can be given an upper bound. The scattering optical depth was found to be 8.7×10^{-4} and if $R_* = 3.5R_\odot$ (LB) then a conservative estimate of n_e would be $\sim 10^{12} \text{ cm}^{-3}$ for two cones, noting that $n = \tau_0 r^2 / \sigma_0$ - the electron number and that the volume of one scattering region $V = 8R_*^3 \sin\theta d\theta d\phi / 3$. This figure for n_e is not unreasonable (cf. Capps, Coyne and Dyck (1973) analysis of ζ Tau, where they give $n_e \sim 10^{11} \text{ cm}^{-3}$). The number of the last observable Balmer line for σ Ori E gives $n_e \sim 2 \times 10^{12} \text{ cm}^{-3}$ (see LB) which agrees well with that above.

The fitting of a sinusoid gives the epoch of $\phi = 0$ at JD $2,443,150.33 \pm 0.02$, using the phase derived for the harmonic component

of q as this was the one determined with least error. If the polarimetric fluctuations are caused by a co-rotating gas cloud, the same mechanism would also vary the intensity, with the secondary maximum brightness occurring at a JD corresponding to $\phi = 0$ (see Figs. 4.2.2 and 4.2.4). LB give the ephemeris of primary minimum of the light curve as $\text{JD } 2,442,778.819 + 1.19080E$, implying that the middle of the secondary maximum occurs, from their sketch of the modulation (LB - Fig. 1), about $0^{\text{P}}.2$ later, i.e. at $\text{JD } 2,442,779.057 + 1.19080E$. For the photometric and polarimetric variations to be synchronous (using the derived polarimetric period) $(3150.33 - 2779.057)/1^{\text{d}}.1898$ would need to be an integer - which it is to the second decimal place! This result is all the more startling as the polarimetric phase was derived independent of the brightness ephemeris, unlike the analysis of KH and further as the data sampling was "far from optimum". The variation of the longitudinal component of the magnetic field has also been shown to be in phase with the polarimetric modulations. LB have already pointed out that photometric primary minimum is coincident with $B_e = 0$. The strength of the polar field may also be estimated using the relation (Stibbs, 1950) $B_p = 3.3B_e(\text{max})/\cos(\theta-i)$, which gives $10,290\text{gauss} \pm 1201\text{gauss}$ taking θ to be the obliquity of the magnetic pole.

A major problem that the light curve posed the spot oblique rotator model of Groote and Hunger (1977) and LB was that the minima were observed to be separated by $0^{\text{P}}.43$ and not $0^{\text{P}}.5$ as might be expected. Such phase differences are easily explainable, if, again, the polarigenic and photogenic mechanisms are identical. The brightness trend would be described by the equation

$$\tau_0 (A \sin 2i \cos(\omega t + \eta_1) + B \sin^2 i \cos 2(\omega t + \eta_2))$$

where η_1 and η_2 are phases and ω = rotational velocity for scattering. A and B depend on the distribution of the scattering material in and

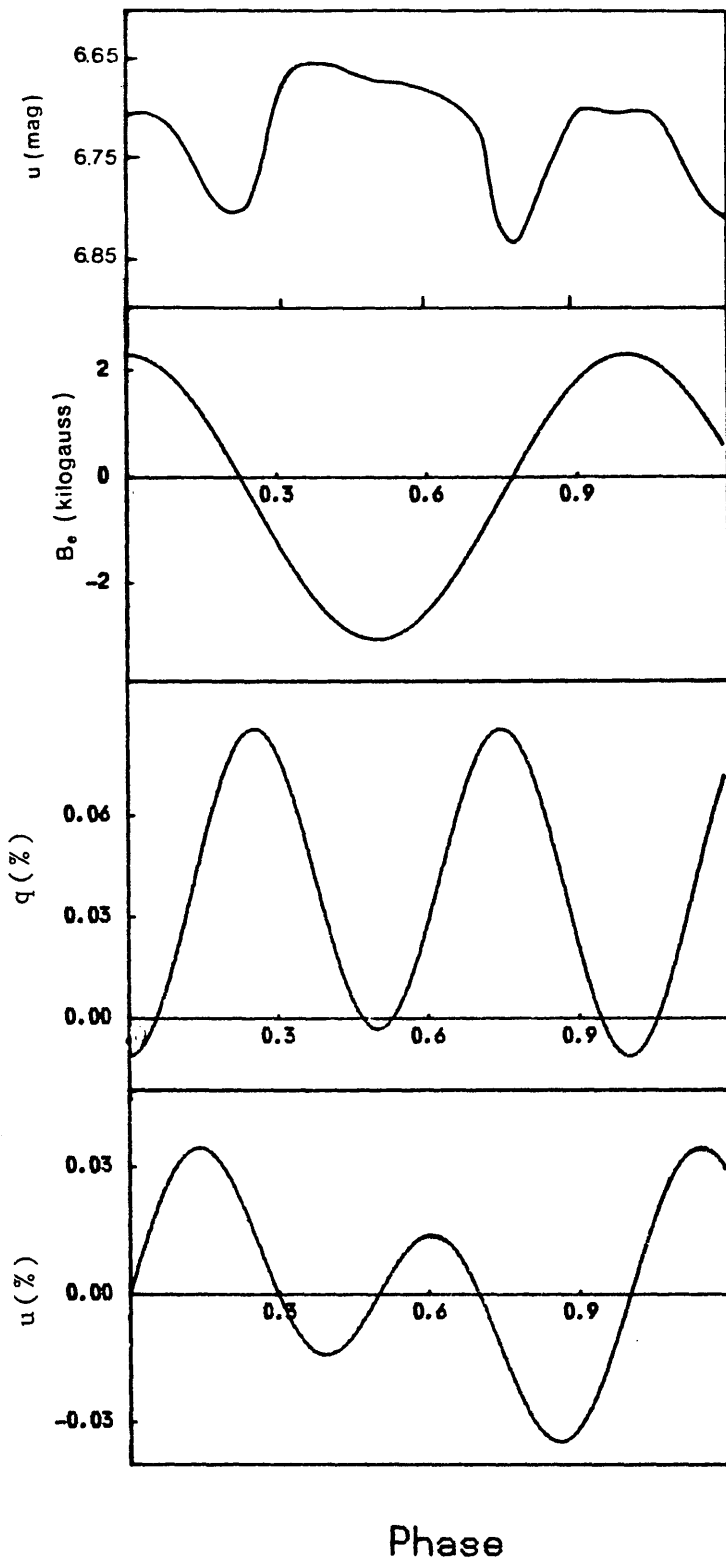


Fig. 3.6.3 Observed variation of σ Ori E as a function of phase. Top to Bottom: Strömgren u magnitude; longitudinal magnetic field strength B_e ; and the normalized Stokes parameters q and u .

out of the equatorial plane. High values of i and θ ($\approx 70^\circ$), (as detected here!), are required for a minima detachment of $\sim 0^{\text{P.4}}$, assuming the relative phases (i.e. η_1 and η_2) to be similar to that found for the q parameter. Fig. 3.6.3 shows the phase relationship of the light curve and the magnetic and polarization variations from an epoch corresponding to $\phi = 0$.

Scattering may also relate the strength of the H α emission since, in optically thin cases, as justified by the low value of τ_0 , it can represent n_e . If n_e is subject to change, e.g. temporal, or with wavelength due to increasing/decreasing absorption, then not only would the emission vary in a correlated manner but τ_0 too. Hence the brightness and polarization would also fluctuate, the effect being observed either as added noise or as a reduction/increase in the photometric and polarimetric amplitudes. The variation in the depth of the minima of the light curves with wavelength, as reported by Hesser *et al.* (1977) may thus in part be explained.

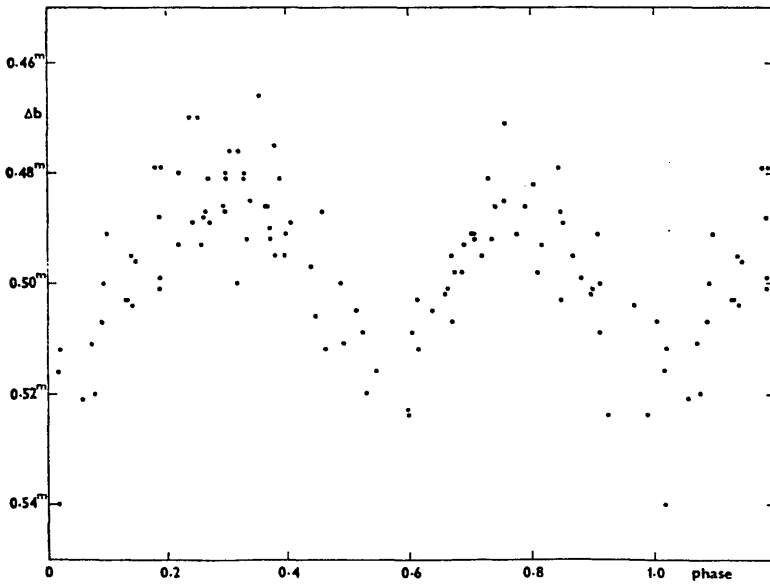
The analysis has revealed an excellent union of polarimetric, photometric and magnetic predictions in considering a co-rotating scattering cloud/bulge model and makes the case of a magnetic oblique (spot) rotator scenario very strong for this star.

CHAPTER 4. ASPECTS OF PHOTOMETRY

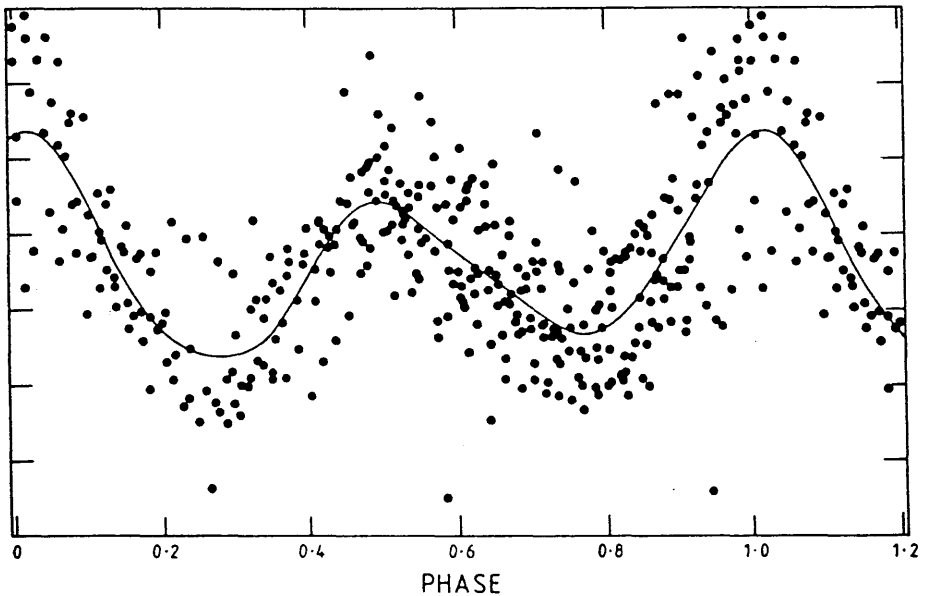
4.1 Introduction

4.2 Model Geometries

4.3 The Photometric Behaviour of EM Cep



Comparison of the phase diagrams of the light variations of LQ And plotted with the periods of 0.310049, and 0.622832 days, the time of mid-minimum HJD 2 443 791-958 corresponding to phase zero in both cases. The b magnitude differences in the sense LQ And - HR 9011 from the data used by Percy (1983) are shown.



Light curve for Ahmed 63. The period is 0.844 day; phase zero is JD 2446000.000. Tick marks are spaced at intervals of 0.01 mag.

Fig. 4.1.1 Examples of Be stars whose light curves exhibit a double-wave form. (Upper after Harmanec 1984 ; Lower after Balona and Engelbrecht 1986).

CHAPTER 4. ASPECTS OF PHOTOMETRY

4.1 Introduction

Recently, it has been noticed that whenever a Be star is photometrically well observed, the light curves seem to exhibit a low-amplitude double-wave form with unequal maxima and/or minima with a period close to that of stellar rotation (~ 1 day) with time asymmetry between minima pairs, e.g. see Fig. 4.1.1. Harmanec (1984) - H - has remarked on the similarity of the rapid cyclic variations of EM Cep, σ Ori E and possibly LQ And. In studying the young cluster NGC 3766, Balona and Engelbrecht (1986) - BE - found that of the seven Be stars observed, four showed the characteristics commented on above and two others revealed variability but of too small an amplitude to derive a period.

Several models have been proposed to explain these strange waveforms but all have some difficulties. One hypothesis is that of a close binary companion, but this would require the secondary to be very close to the primary to give the short periods. Moreover, eclipsing and large radial velocity variations would be expected, these effects not being observed. Another proposal is the non-radial pulsator, but the difficulty that presents itself here is that the periods of such objects are usually less than 0.5 days.

The model favoured by H and BE is one involving some form of spotted disk. According to Evans (1971), "the hypothesis of star spots has a long and dishonourable history", it being one of those rather vague catch-all mechanisms contrivable to explain everything, but still plausible when all around are failing. An early reference is Pickering (1880). Walker (1953) also proposed it to explain the light variations of EW Lac, the first Be star in which such short-period fluctuations were found.

BE suggest that the unequal maxima/minima are caused by two

co-rotating spots diametrically opposed, with one more extensive in area than the other, and variations in the light amplitude which are also detected result from the spots migrating in latitude or changing in size. A problem that arises, though, is that the relative phases of the maxima (for bright spots) would be expected to be $0^{\text{P}}.5$, which they are often found not to be.

Consideration of the total intensity Stokes parameter (I), its relation with the scattering function of the free electron (or any symmetrical scatterer) and the geometry of the oblique rotator (i.e. obliqueness of the "spots" to the stellar rotational axis) reveals that the observed rapid periods and related phenomena can be successfully explained in a simple and non-contrived manner.

For convenience, let us term the spotted disk scenario:- the photospheric spot model (PSM), and the scattering representation:- the scattering oblique rotator model (SORM). The fundamental difference between PSM and SORM is that for the PSM the spots are "on" the stellar surface whereas in SORM the effect takes place above the photosphere and may be related to a bulge in the stellar atmosphere. It may be possible that both situations can result for the same initial mechanism, perhaps radiatively driven outflowing gas channelled through magnetic poles.

Below, the PSM and SORM are both fitted to readily available comprehensive UBV data on EM Cep, which incidentally has been the most extensively studied short-period Be star case, recorded by Rachkovskaya (1975, 1976) - R. It is sad to note, though, the remark made by BE that intensive photometric observations of Be stars are few and far between despite the potential importance they may have to the understanding of the Be phenomenon.

Firstly the geometry and mathematics of both PSM and SORM are briefly described.

4.2 Model Geometries

The most complete mathematical description of a PSM that I have come across appears in a paper by Torres and Ferraz Mello (1973). The geometry they used is essentially that displayed in Fig. 2.7.1, but with the primed and unprimed axes interchanged. It is easy to show that the luminosity, $L(\lambda)$, of an unspotted star, radius R_* and monochromatic flux $F_*(\lambda, \alpha)$ at a point angled α to the line of sight is given by

$$L(\lambda) = \pi R_*^2 F_*(\lambda, 0) (1 - \mu(\lambda)/3) \quad (4.2.1)$$

where λ is the wavelength and $\mu(\lambda)$ the colour dependent coefficient of limb darkening. A spot with limits (θ_1, θ_2) , (ϕ_1, ϕ_2) , monochromatic flux $F_s(\lambda, \alpha)$ having the same $\mu(\lambda)$ as for the star but of greater temperature, contributes to the stellar luminosity causing a magnitude change $\Delta m(\lambda, t)$ relative to an unblemished disk at time t is given by:

$$\Delta m(\lambda, t) = 2.5 \log_{10} [1 + G(\lambda, t)(\beta - 1)] \quad (4.2.2)$$

where

$$G(\lambda, t) = \frac{1}{\pi(1 - \frac{\mu(\lambda)}{3})} \int_{\phi=\phi_1}^{\phi_2} \int_{\theta=\theta_1}^{\theta_2} (1 - \mu(\lambda) + \mu(\lambda) \cos \alpha) \cos \alpha \sin \theta d\theta d\phi$$

and

$$\beta = \frac{F_s(\lambda, \alpha)}{F_*(\lambda, \alpha)}$$

The spot of course affects the observed brightness only when it is on the apparent disk, i.e. $\Delta m(\lambda, t) = 0$ whenever $\cos \alpha < 0$. When the spot is at $\phi = 0$, its effect will be at a maximum and so $G(\lambda, t) = G_{\max}(\lambda)$ which will represent the relative areas of the spot and disk. Hence the amplitude, $A(\lambda)$, of the light curve is

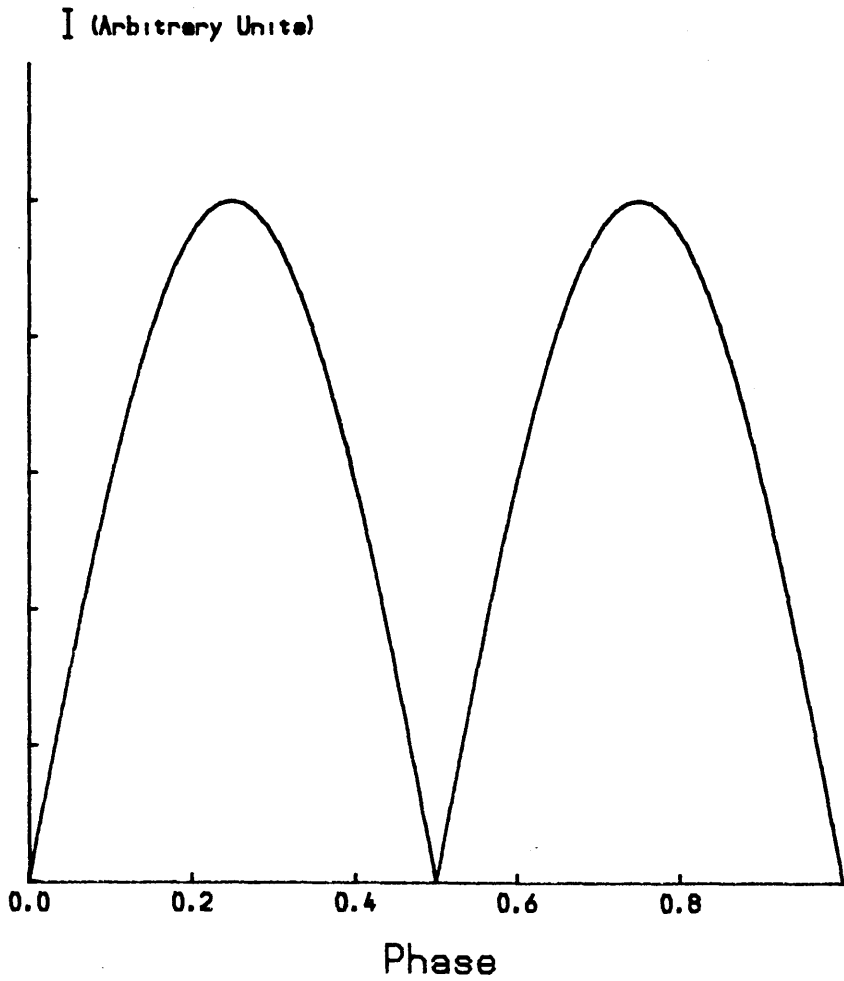


Fig. 4.2.1 The form of the light curve expected from two point like diametrically opposed bright spots co-rotating on a stellar equator. $\phi = 0$ at zero phase.

$$A(\lambda) = 2.5 \log_{10} [1 + G_{\max}(\lambda)(\beta-1)] \quad (4.2.3)$$

Two kinds of parameter are involved here, *viz.* physical (through β) and geometrical (through G). The model is most sensitive to T_* and T_s , the temperatures of the star and spot respectively, the spot co-ordinates and area, and the stellar inclination. Unfortunately Equation (4.2.3) has its parameters convolved such that they cannot be wholly extracted from data fitting, but consideration of the amplitude of variation of the colour indices may help in determining T_* and T_s (T_* can be assumed from spectral type). Limb darkening has little effect. Evans (1971) has stated some obvious principles regarding star spots and they include:

- a) A brighter spot of the same area as a darker spot produces more noticeable effects.
- b) The shape of the light curve will be almost independent of spot shape.
- c) If variations are to be observed, the number of areas of anomalous brightness must be small, counting a localized group as a single spot (i.e. spots are not randomly scattered about the disk).

For $i = 90^\circ$ and two diametrically opposed point-like spots co-rotating on a stellar equator, the resultant light curve may look like that depicted in Fig. 4.2.1. Note the cusp-like appearance as one spot moves into view and the other out of view.

As shown in Section 2.7, in a point source/point scatterer scenario, for a globule of free electrons the flux scattered towards Earth is

$$I_* \tau_0 (1 + \cos^2 \chi)$$

and, using the geometry of Fig. 2.7.1, this can be written as:

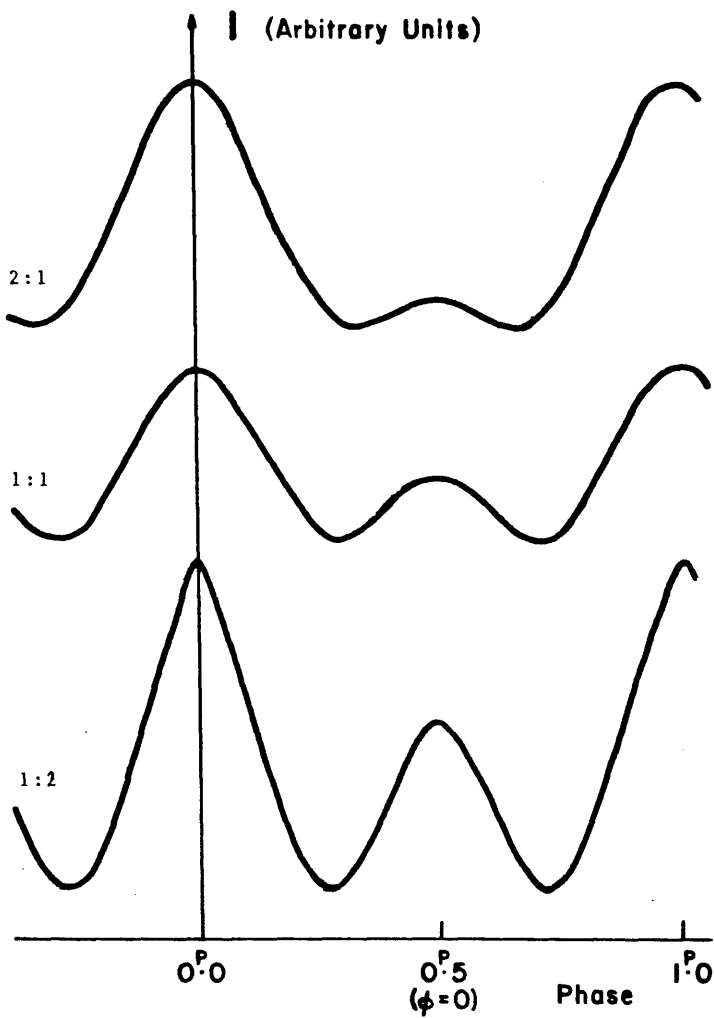


Fig. 4.2.2 The light curves expected from a co-rotating point scattering bulge.

$$I_* \tau_0 (A + B \cos \phi + C \cos 2\phi) \quad (4.2.4)$$

where

$$A = 1 + .5 \sin^2 \theta \sin^2 i + \cos^2 \theta \cos^2 i$$

$$B = -.5 \sin 2\theta \sin 2i$$

$$C = .5 \sin^2 \theta \sin^2 i$$

and since the globule/atmospheric bulge is assumed to be in co-rotation, ϕ can be represented by a periodic term $\nu i z$. $\omega =$ stellar angular velocity and phase ϵ corresponding to the epoch $\phi = 0$.

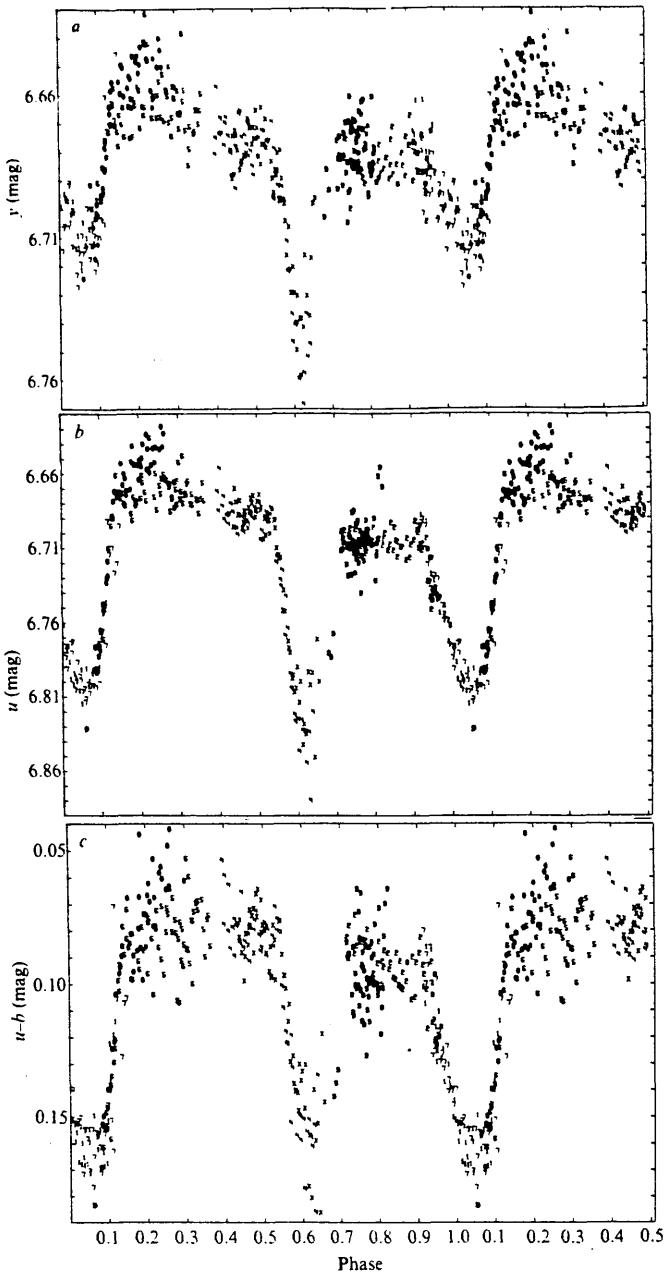
The total intensity thus arriving from the star is equal to:

$$-I_a + I_* (1 + \tau_0 (A + B \cos(\omega t + \epsilon) + C \cos 2(\omega t + \epsilon))) \quad (4.2.5)$$

where I_a is the extinction, depending on τ_0 , along the line of sight, i.e. when $\chi = 0$. I_a may be variable since if the general extended atmosphere is also scattering the incident stellar radiation, there may be a further attenuation when the enhanced scattering zone possibly moves into the line of sight. Equation (4.2.5) is applicable to all forms of Rayleigh scattering. Temperature may invoke a form of wavelength dependence to Equation (4.2.5), as a depletion in the number of free electrons would be expected the cooler the temperature, away from ionization levels.

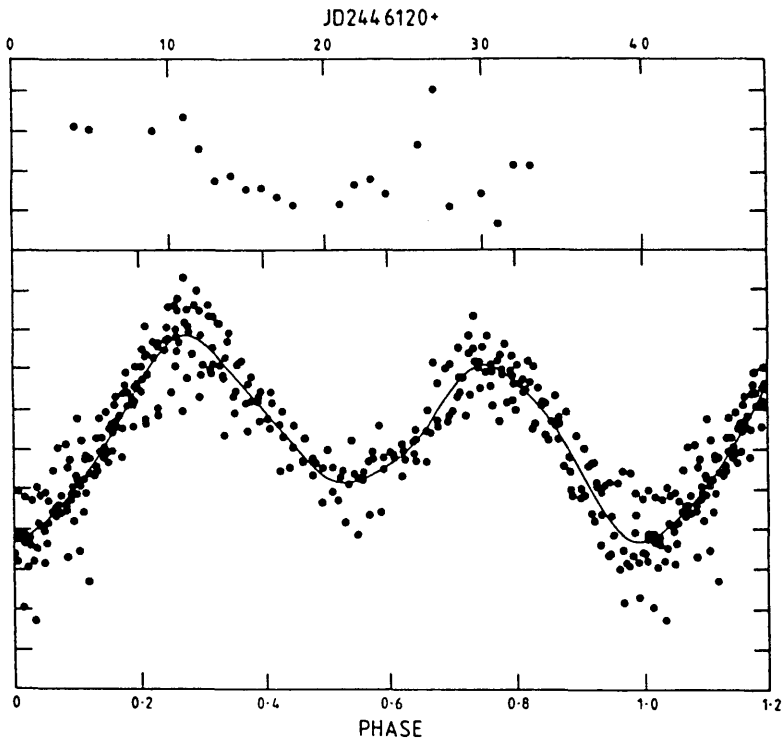
It can be seen immediately from Equation (4.2.5) that if either θ or i equals zero, then there would be no periodic variations, but stochastic changes would still be apparent if τ_0 fluctuates; the amplitudes of the periodic variations would also be variable if τ_0 changes.

Fig. 4.2.2 shows the light curve expected for differing ratios of B:C. For 2:1, 1:1 and 1:2 the separation of the minima are approximately, in terms of fraction of phase, $0^P.33$ & $0^P.67$, $0^P.42$ & $0^P.58$, and $0^P.46$ & $0^P.52$ respectively. The double periodicity

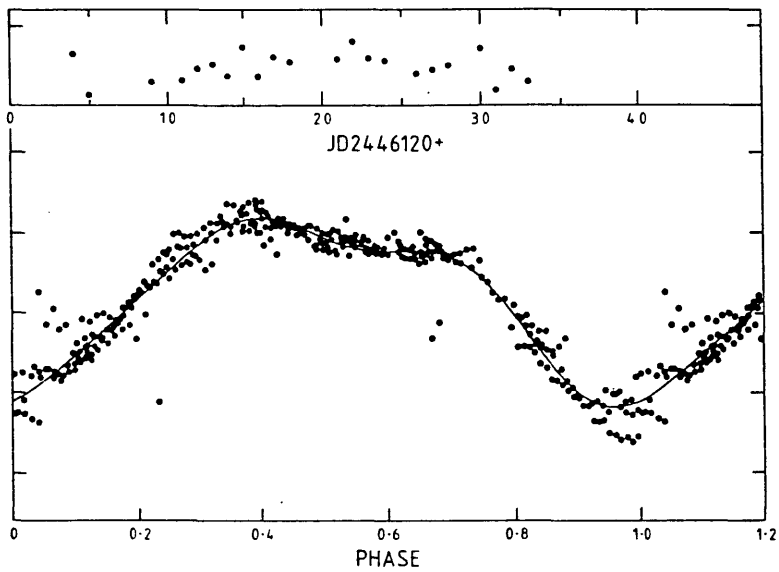


a-c: y , u , and $u-b$ light and colour curves for α Ori E from the 1975-76 data, with 1975 December 28.0 = JD 2442774.5 as zero phase and a period, 1.19082 d, that differs insignificantly from the finally adopted value, 1.19080 d. The symbols serve to distinguish data from different nights: 0-9 correspond to December 28-January 6 and \triangleright to January 7. Because of occasional high humidity during the observations, it is uncertain if some fine details of the light curves (for example, the tendency for night 0 (28 December) to lie somewhat brighter than those of nights 5 or 6 at $\phi \approx 0.2$) arise from stellar variations or to slightly inaccurate differential extinction corrections. The $u-b$ colour is (normally) a reliable temperature indicator for B stars.

Fig. 4.2.4 Taken from Hesser *et al.* (1976).



Top panel, nightly variations of Ahmed 88; bottom panel, light curve of Ahmed 88 with nightly variations removed. The period is 0.946 days; phase zero is JD 2446000.000. Tick marks are spaced at intervals of 0.01 mag in both panels.



Top panel, nightly mean variations of Ahmed 1, bottom panel, light curve of Ahmed 1 with nightly variations removed. The period is 1.739 days; phase zero is JD 2446000.000. Tick marks are spaced at intervals of 0.05 mag in both panels.

Fig. 4.2.3 The above observed double-wave forms (after Balona and Engelbrecht 1986) seem to be well matched by the characteristics of the shape of the predicted light curves for a scattering mechanism as shown in Fig. 4.2.2.

is best seen when the fundamental and harmonic are both significantly present. Note also that only one globule is needed to give a variation throughout the whole of the rotation period; two globules diametrically opposed serve only to enhance the amplitudes. Decoupling of the parameters i and θ from photometry alone is difficult as they are interchangeable (see Equation (4.2.5)). Examination of Figs. 4.2.2 and 4.2.3 shows that the scattering mechanism is successful in explaining the double-wave form related in Section 4.1. However, comparing these curves to the waveform of σ Ori E (Fig. 4.2.4) shows that it is the minima that are unequal rather than the maxima as predicted by the model. The suggestion is that point scattering theory may be a little too simplistic to describe accurately the photometry in every case. The form that Equation (4.2.5) would take, revised for an extended scattering region or source, would be similar to that of Brown *et al.* (1978) - Equation (8) which describes the scattered intensity in an optically thin envelope of arbitrary shape illuminated by point sources:

$$I = I_0(1 + \tau_0(2(1+\gamma_0) + (1-3\gamma_0)\sin^2 i + G\sin 2i \cos(\lambda+\lambda_1) + H\sin^2 i \cos 2(\lambda+\lambda_2))) \quad (8) \text{ or } (4.2.6)$$

where $\lambda_1 - \lambda_2 = \Delta\lambda$, the phase difference between the first and second harmonic contributions (or fundamental and first harmonic in the present terminology)

$$G = (\gamma_1^2 + \gamma_2^2)^{\frac{1}{2}}$$

$$H = (\gamma_3^2 + \gamma_4^2)^{\frac{1}{2}}$$

$$\tau_0\gamma_0 - \tau_0\gamma_4 \quad \text{are moments}$$

λ is local longitude and

i is the inclination of the orbital plane.

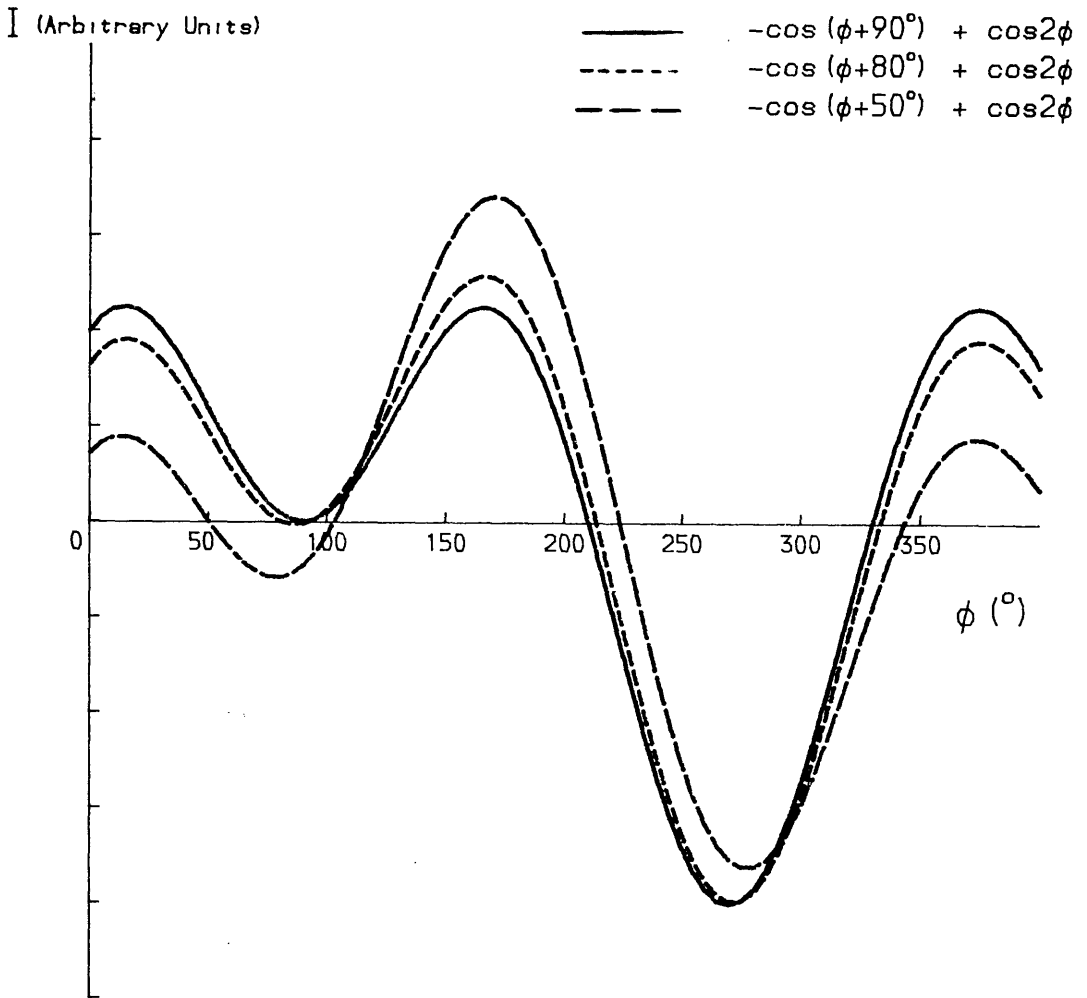


Fig. 4.2.5 The light curve expected from an extended co-rotating scattering bulge. The fundamental and harmonic having various relative phases but the same amplitudes.

Obviously it is θ and ϕ that are affected in considering an extended scattering region (or extended light source), and so by analogy with Equation (4.2.6) the part of Equation (4.2.5) which governs the modulation takes the form:

$$-E \sin 2i \cos(\omega t + \psi_1) + F \sin^2 i \cos 2(\omega t + \psi_2) \quad (4.2.7)$$

again no periodicity being apparent if $E = F = 0$ or $i = 0^\circ$, with harmonic domination in the stellar equatorial plane or if $i = 90^\circ$. Fig. 4.2.5 shows the form of the expected light curves when the amplitude of the fundamental and harmonic are equal for various relative phase differences, and appear to be very favourably relatable to Figs. 4.2.3 and 4.2.4.

4.3 The Photometric Behaviour of EM Cep

(HD 208392, $m_V = 7.1$, B1 IVe, $\alpha_{1950} = 21^h 52^m 22^s$, $\delta_{1950} = +62^\circ 22' 40''$)

(a) From her UBV photoelectric observations spanning 1971 to 1974, R found rapid light variations ($0^d.806196$) with amplitudes ranging from $0^m.10$ to $0^m.05$, and indicated that the star was either a β Cep variable or an oblique rotator (PSM) and not a contact binary as suggested by Lynds (1959a, b) - the discoverer of the fluctuations. She also found that the light was weaker in 1974 by about $0^m.05$, in maximum and minimum than in 1972. Rachkovskaya performed spectrophotometric observations as well ($\lambda\lambda 3600-4900\text{\AA}$, dispersion $\Delta\lambda = 37 \text{\AA}_{mm}^{-1}$, 1971-1974) from which she concluded the spectral type to be B0-8 IV-V and that there is an excess of helium abundance in the atmosphere.

Hubert-Delplace and Hubert (1979) have reported an alternation between B and Be phases on time-scales of years. Rachkovskaya (1980) found no phase-dependent line profile variations in excess of measuring errors. The $H\beta$, $H\gamma$ and He I 4471 profiles measured by Hilditch *et al.* (1982) tentatively show additional absorption near one photometric

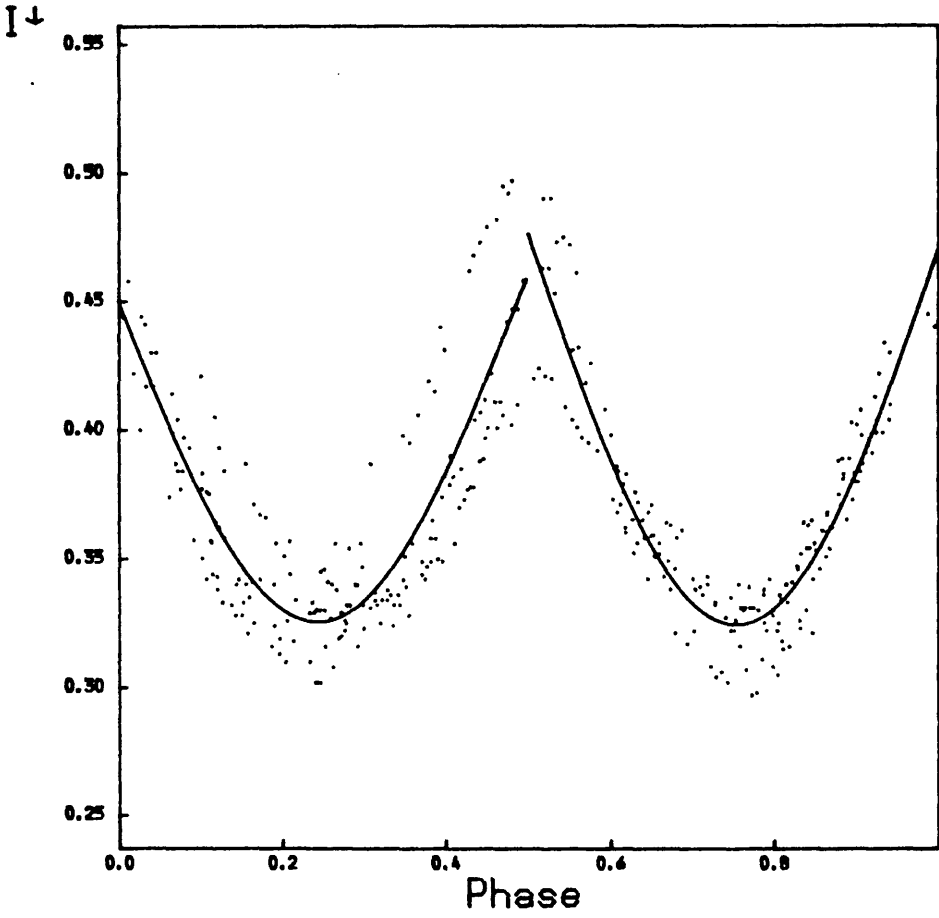


Fig. 4.3.1(e) V-band : J.D. 2442239.3266 - J.D. 2442283.5673

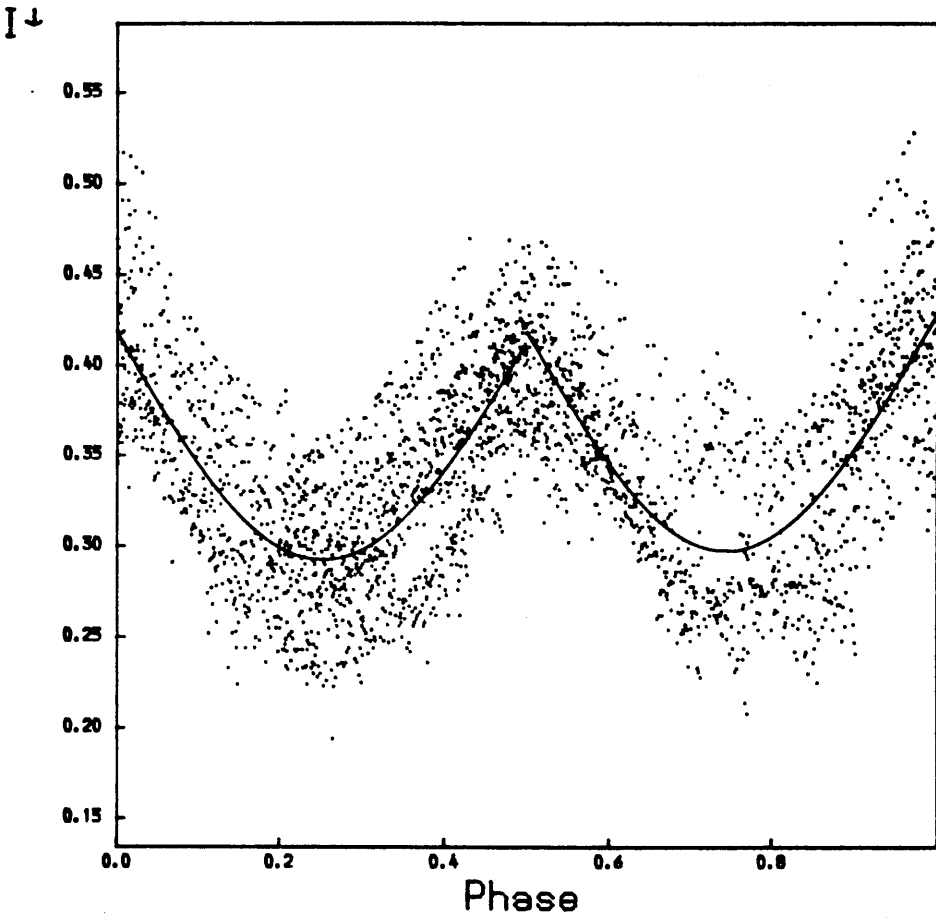


Fig. 4.3.1(d) B-band : J.D. 2441206.233 - J.D. 2442283.5663

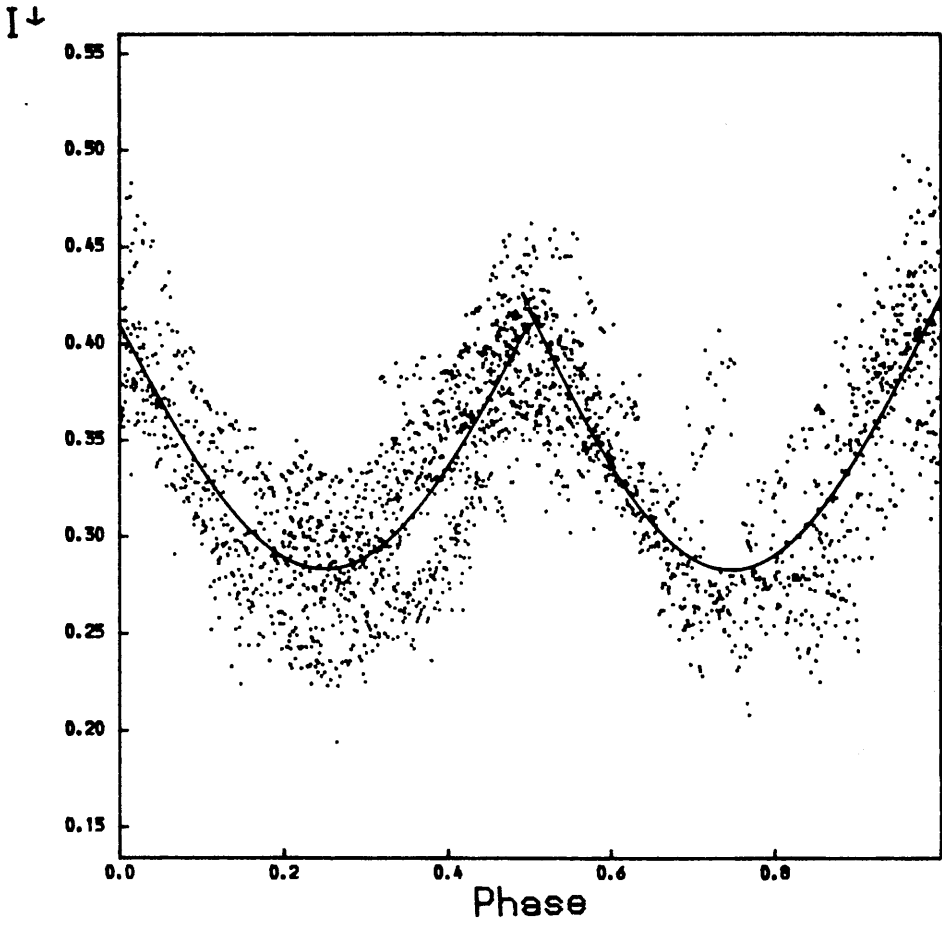


Fig. 4.3.1(c) B-band : J.D. 2441206.233 - J.D. 2441527.554

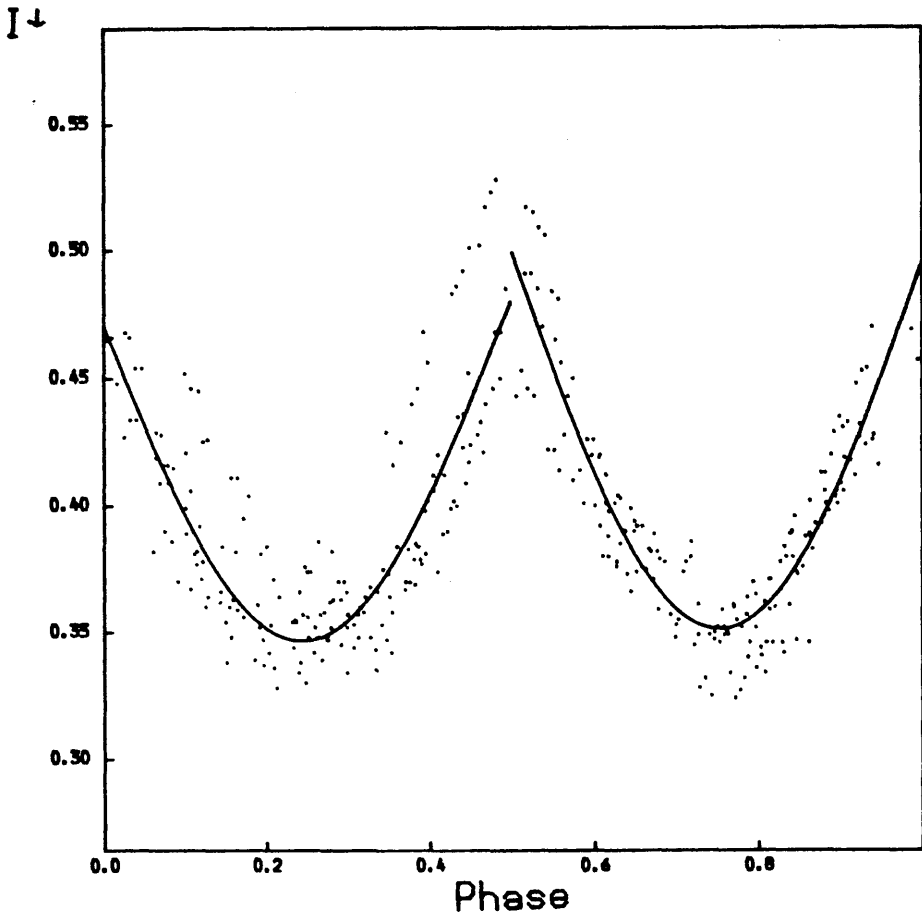


Fig. 4.3.1(b) B-band : J.D. 2442239.3259 - J.D. 2442283.5663

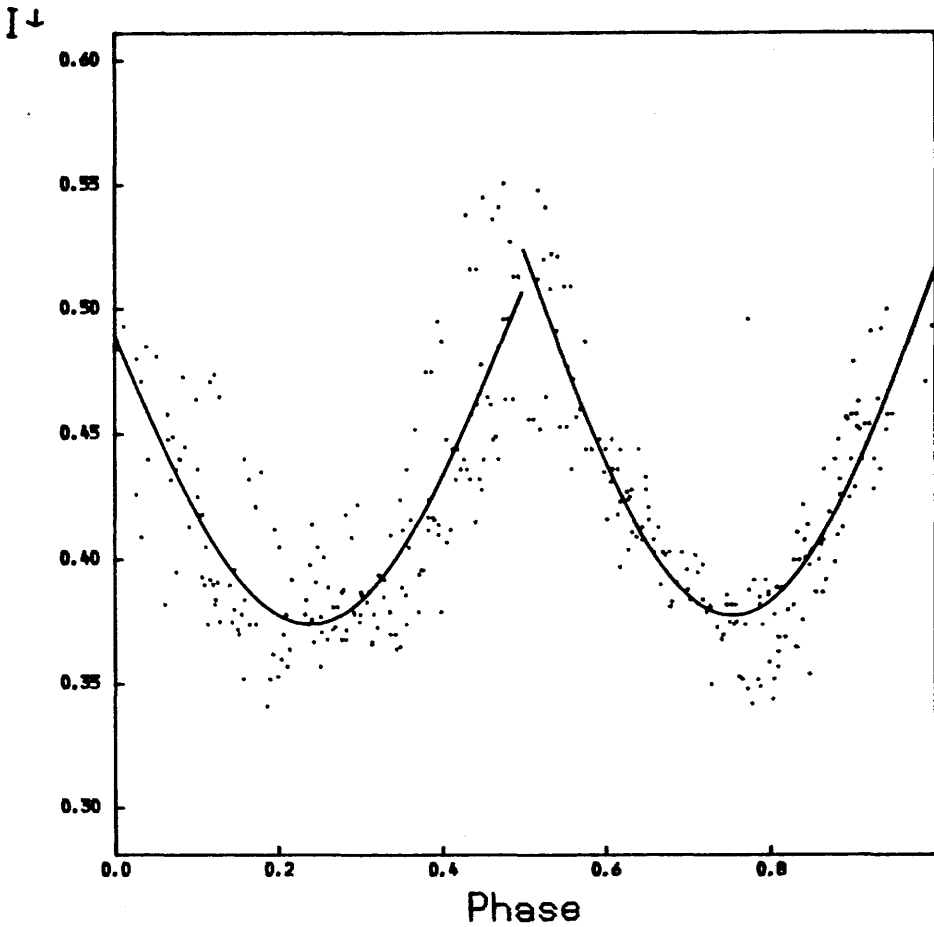


Fig. 4.3.1(a) U-band : J.D. 2442239.3252 - J.D. 2442283.5656

The curves are the best fit, assuming a $0^{\text{d}}.806196$ period, of a PSM to UBV data on EM Cep recorded by Rachkovskaya (1975,1976). The arrow shows the direction of increasing brightness, the divisions being in magnitude. Phase is with respect to the time of measurement of the first data point in each set.

Table 4.3.1

The results of fitting a PSM to UBV photometric data of EM Cep recorded by Rachkovskaya (1975, 1976). A period of $0^d.806196$ was assumed.

<u>Filter</u>	<u>Time Interval (JD)</u>	<u>No. of Points</u>	<u>$0P.0+0P.5$</u>	<u>$0P.5+1P.0$</u>	<u>R²</u>
U	2442239.3252 →2442283.5656	345	DC* Amp* Phase 0.499±0.006 0.125±0.008 184°±1°.5	0.520±0.005 0.142±0.007 359°±1°.1	0.6821
B	2442239.3259 →2442283.5663	355	0.479±0.005 0.129±0.006 182°±1°.2	0.497±0.004 0.146±0.005 359°±1°	0.7612
B	2441206.233 →2441527.554	2353	0.411±0.002 0.128±0.003 180°±0°.6	0.420±0.002 0.137±0.004 1°±0°.6	0.5995
B	2441206.233 →2442283.5663	2708	0.416±0.002 0.124±0.003 179°±0°.7	0.423±0.003 0.126±0.004 2°±0°.8	0.4857
V	2442239.3266 →2442283.5673	348	0.455±0.005 0.130±0.006 182°±1°	0.473±0.004 0.149±0.005 359°±1°	0.7905

* units are magnitude

minimum; they conclude that EM Cep is possibly a non-radial pulsator and not a short period binary. According to H, $V_{eq} \sin i \sim 300 \text{ km s}^{-1}$, this not being high enough to make a $0^{\text{d}}.4$ period with one minimum and maximum in each cycle a possibility - otherwise an unrealistically high rotational velocity would be needed.

The UBV data of R are reanalysed here, as both the PSM and SORM present themselves as attractive scenarios and favour a $0^{\text{d}}.806$ period. Neither model has been applied by previous workers to the measurements; further, the relative goodness of fit can be appraised by examination of the multiple correlation coefficient squared (R^2). From the figures presented in R, it is obvious that the experimental noise ($1\sigma = \pm 0^{\text{m}}.012$) is not totally responsible for the variations within the data.

(b) Fitting the PSM Here the $0^{\text{d}}.806196$ cycle is not challenged. The data were folded into one period and Equation (4.3.1) fitted, *viz.* two dc's, amplitudes and phases, via the method of least squares.

$$I_i = \begin{cases} d_0 + d_1 \sin(\omega t_i + \eta_1) & 0^{\text{P}}.0 \leq t_i < 0^{\text{P}}.5 \\ e_0 + e_1 \sin(\omega t_i + \eta_2) & 0^{\text{P}}.5 \leq t_i < 0^{\text{P}}.5 \end{cases} \quad (4.3.1)$$

A difficulty that arises is that an initial epoch must be chosen such that the data are correctly phased for ease of adapting Equation (4.3.1) i.e. testing for the interval in which the observation taken at time t_i lies. The starting time was derived for each individual measurement set (5 in all) by fitting a sinusoid of period $0^{\text{d}}.806196$ and finding the relative phase of the first data point. If this relative phase has been correctly found, η_1 should equal 180° and η_2 , 0° . For an optimum fit $i = 90^\circ$ is desired. The form of the data when folded on the assumed period fortunately suggests such a geometry. The results are shown in Table 4.3.1 and are displayed graphically as Fig. 4.3.1(a)-(e).

The concurrently taken UVB data indicate that there is a positive correlation between increasing goodness of fit and increasing wavelength (assuming $U \sim 3700\text{\AA}$, $B \sim 4450\text{\AA}$, $V \sim 5500\text{\AA}$). Forming the strict criterion that two means are significantly departed if their absolute difference is greater than three times the square root of the sum of the squares of their errors, an implication is that amplitude is independent of wavelength. Generally, the waves fitted to the first and second half of the period interval have the same dc, amplitude and correct phase. Note also for B, the amplitudes derived for the earlier extended observing run are approximately the same as for the later data train.

For the shorter data sets, when individually subdivided into two groups composed of roughly an equal number of points, it was found that there was a change in η_1 for all three colours. For B a fluctuation in both dc and amplitude was apparent. In V there was a difference between e_1 of the first and second groups. R^2 was seen to decrease between the sets of two classes consistently (in colour). Obviously as well as the rapid cyclic variations there are also medium term fluctuations (~ 10 days) present, which account for the wide spread in the data of the longer run (see Fig. 4.3.1(c)). Similar changes in dc, amplitude and phases are found when the extended B measurements are subdivided into 4 groups of roughly 30 days duration each.

As previously commented, this star appears to have a high inclination ($\sim 90^\circ$) suggested by the _____ obvious _____ rectified sine-wave form, and to exhibit events around its equatorial zones. Taking the effective temperature of a B1 IV spectral type to be 27000°K (e.g. see Underhill and Doazan (1982), Table 3-5) and $\mu_U = 0.666$, $\mu_B = 0.65$ and $\mu_V = 0.644$ (Kopal (1959)) then Equation (4.2.3) can be used to estimate the possible size and temperature of the two diametrically opposed photospheric spots. One possible but not unique set of

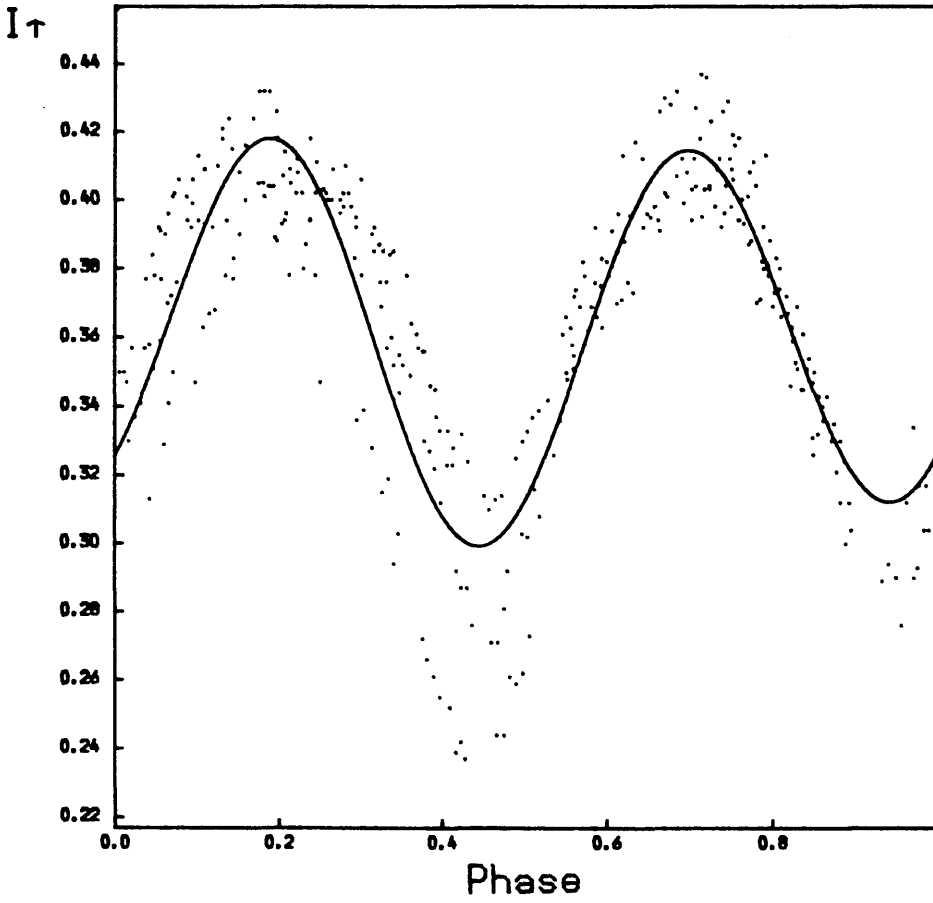


Fig. 4.3.2(e) V-band : J.D. 2442239.3266 - J.D. 2442283.5673

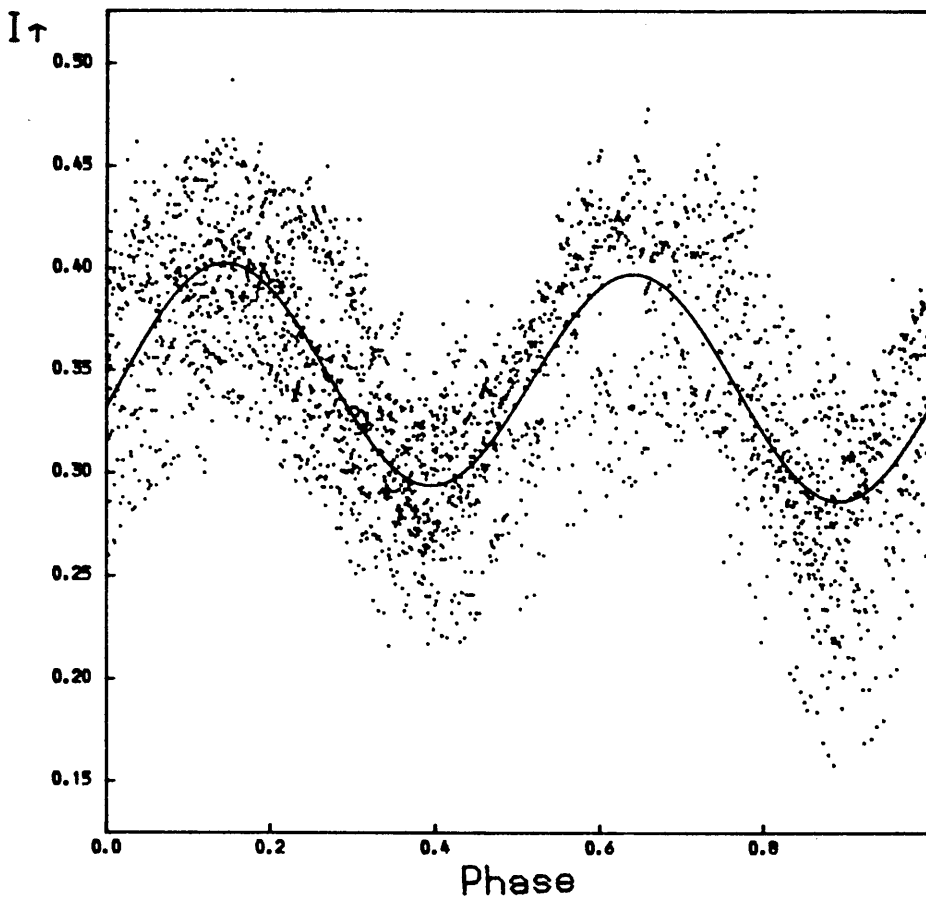


Fig. 4.3.2(d) B-band : J.D. 2441206.233 - J.D. 2442283.5663

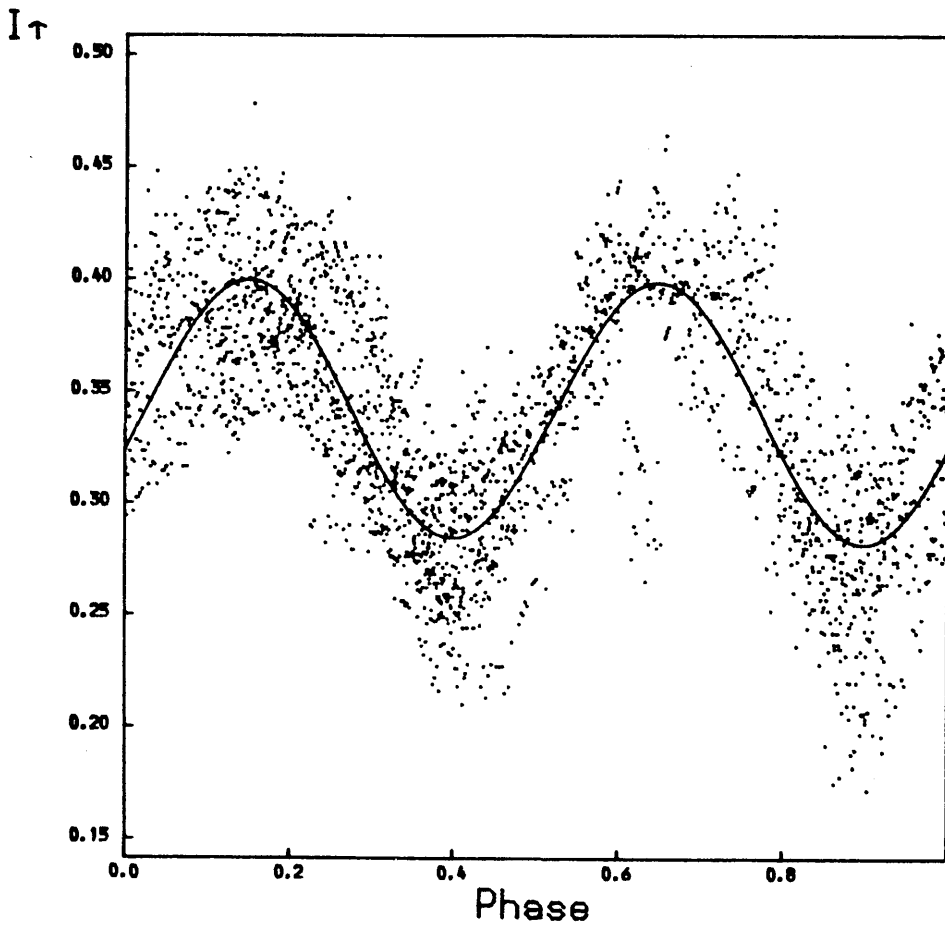


Fig. 4.3.2(c) B-band : J.D. 2441206.233 - J.D. 2441527.554

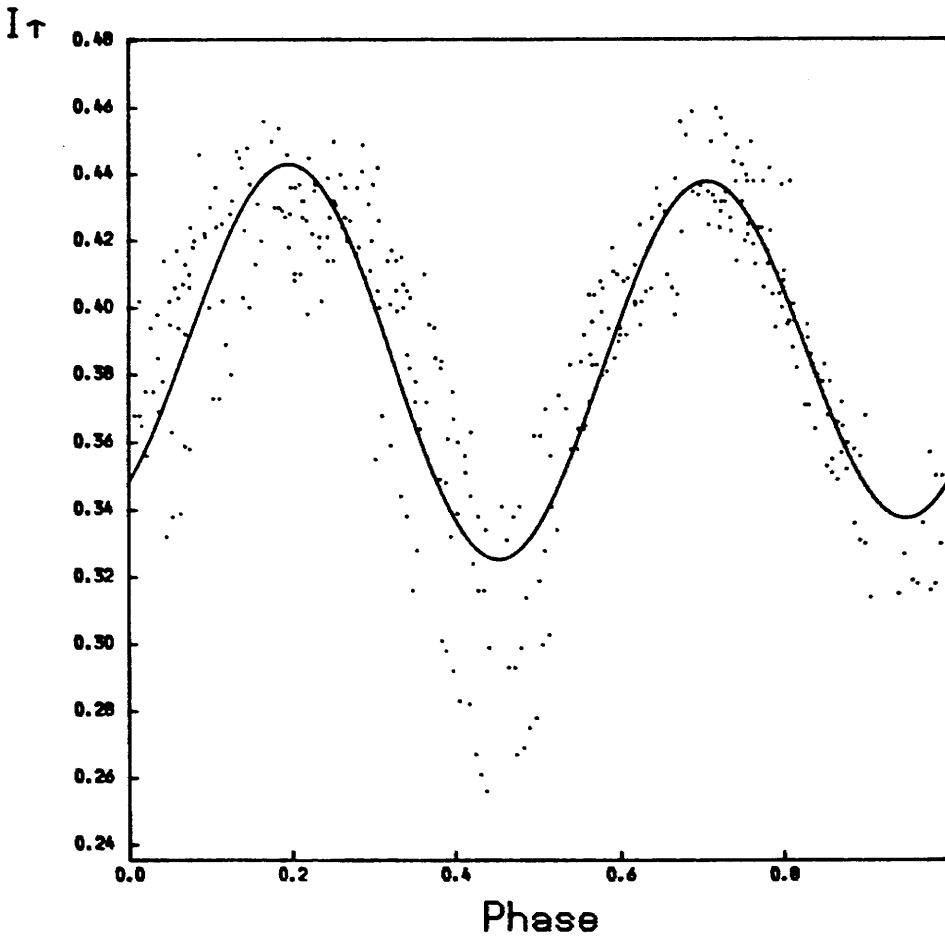


Fig. 4.3.2(b) B-band : J.D. 2442239.3259 - J.D. 2442283.5663

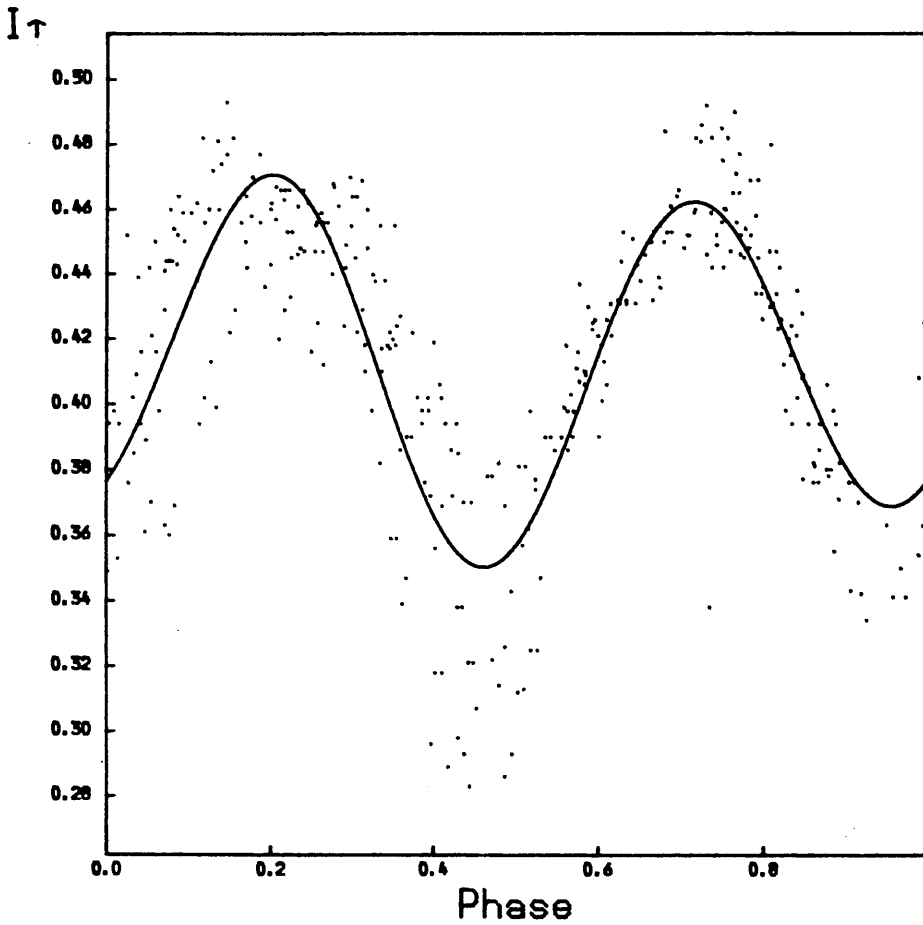


Fig. 4.3.2(a) U-band : J.D. 2442239.3252 - J.D. 2442283.5656

The curves are the best fit of a SORM to UBV data on EM Cep recorded by Rachkovskaya (1975,1976). The arrow shows the direction of increasing brightness, the divisions being in magnitude. Phase is with respect to the time of measurement of the first data point in each set.

Table 4.3.2

The results of fitting a SORM to UBV photometric data of EM Cep recorded by Rachkovskaya (1975, 1976). The most significant period from the interval 0d.803(0d.00001)0d.8072 is also shown. Phase is w.r.t. the first data point in the appropriate measurement set.

<u>Filter</u>	<u>Time Interval (JD)</u>	<u>No. of Points</u>	<u>Period (dys)</u>	<u>DC</u>	<u>Fundamental</u>	<u>Harmonic</u>	<u>R²</u>
U	2442239.3252 →2442283.5656	345	0.80546	0.413±0.001 [*]	Amp* =0.010±0.002 Phase= 170°±11°	0.053±0.002 105°±1°	0.6727
B	2442239.3259 →2442283.5663	355	0.80575	0.386±0.001	0.007±0.002 175°±14°	0.055±0.002 108°±1°	0.7355
B	2441206.233 →2441527.554	2353	0.80615	0.341±0.001	0.002±0.001 58°±40°	0.058±0.001 127°±0°5	0.5974
B	2441206.233 →2442283.5663	2708	0.80618	0.345±0.001	0.005±0.001 74°±14°	0.055±0.001 129°±0°6	0.4918
V	2442239.3266 →2442283.5673	348	0.80591	0.361±0.001	0.007±0.002 185°±13°	0.055±0.002 110°±0°9	0.7613

* units are magnitude

parameters that could match the requirements are $i = 60^\circ-90^\circ$, $\theta \sim 90^\circ$, $T_s \sim 45000^\circ\text{K}$ and spot size equivalent to $\sim 25\%$ of the stellar disk in area. The only deviation between the model and the observations is that the colour indices of the model parameters are a little larger than those recorded.

(c) Fitting the SORM Here the fitted equation took the form (cf. Equations (4.2.5) and (4.2.7)):

$$I_i = d_0 - d_1 \cos \omega t_i + d_2 \sin \omega t_i + d_3 \cos 2\omega t_i - d_4 \sin 2\omega t_i \quad (4.3.2)$$

i.e. a dc and the amplitudes and phases of the fundamental and harmonic contributions. The method of least squares was invoked for data reduction, the procedure being analogous to that shown in Appendix C. According to H, various periods have been derived ranging from $0^d.806179$ to $0^d.807187$. The form of Equation (4.3.2) allows a grid of frequencies to be applied relatively easily, compared to that of Equation (4.3.1). After experimentation, the stepsize was taken as $0^d.00001$ rather than $0^d.000001$ as the finer mesh does not appear to reveal any greater significant results than the coarser one.

Table 4.3.2 shows the consequence of fitting a grid of periods, $0^d.803(0^d.00001)0^d.8072$, to the said UBV data and Fig. 4.3.2(a)-(e) displays the results in a pictorial fashion.

The shorter data sets imply that better fits emerge with increasing wavelength and that the period of co-rotation is less than that generally accepted - although the extended B run would argue this latter result. The fundamental amplitude is consistently (in colour) barely significant and for the longest individual observing run is essentially non-existent, implying that the variations are due to equatorially located events. For Thomson scattering the amplitudes would be expected to be colour independent and this is what is seen.

As in the PSM treatment, the measurements were each similarly

subdivided into two classes. For the brief data sets no changes in the fundamental and harmonic amplitudes were cited. The phase of the fundamental varies for B and V, whilst the harmonic phases remain constant; only for B does the dc level fluctuate. In common with the PSM analysis, the former halves of the data consistently appear to give more significant fits than the latter halves. Investigation of the extended B measurements reveals that all the examined parameters (not period), except the phase of the harmonic, are subject to temporal change.

For equatorial zone events, it is impossible to derive a value of i . It is also impractical to estimate τ_0 since when $\theta \sim 90^\circ$, i also acts as a scaling factor. If $i \sim 90^\circ$ then, to observe a peak to trough amplitude of about $0^m.1$, τ_0 needs to be around 0.1, which still allows the assumption of optical thinness. The phase changes often found for the fundamental contributions, though little, may imply that scattering material is moving perpendicularly or parallel to the stellar equatorial plane.

(d) Conclusion Both the PSM and SORM were applied to UBV data of EM Cep recorded by R. For the PSM, a period of $0^d.806196$ was assumed and typical colour independent amplitudes of variation of $0^m.13$ were found, implying that the two diametrically opposed spots are about each 25% of the area of the apparent disk, and $\sim 18000^\circ\text{K}$ hotter than the surrounding photosphere. The implied geometry is that the stellar inclination is of the order of 90° , and the spots are at equatorial latitudes.

In fitting a SORM, derived periods ranged from $0^d.80546$ to $0^d.80618$. The scattering material seems to be zonal to the equatorial regions of the star as the fundamental contributions to the observed variations were found to be small relative to the harmonic dominance. The amplitude of the harmonic fluctuations were wavelength independent

and exhibited amplitudes of $\sim 0^m.055$. It was not possible to derive an inclination, but the scattering optical depth was estimated to be ~ 0.1 . In common with the PSM exercise, temporal changes were apparent over intervals of days. Both models give approximately the same significance of fit, but a complication for the PSM is that non-zero colour indices would be expected and none are observed.

The lack of strong fundamental variations makes it difficult to disentangle the two model types and it is suggested that further spectroscopic and polarimetric observations should be undertaken to help in distinction. Line profiles and equivalent widths are particularly sensitive to the presence of spots and it is strange that the measurements of Rachkovskaya (1980) did not show any apparent phase-dependence. A plausible explanation could be that as one spot moves out of view the other is moving in, so it appears as if the disk is always spotted - this being particularly noticeable with lower inclinations. Spots would not be expected to cause photospheric lines to exhibit changes, as the actual speed of rotation is not varying.

CHAPTER 5. CONCLUSIONS

5.1 Conclusions

5.2 Suggestions for Future Work and Discussion

CHAPTER 5. Conclusions

5.1 Conclusions

The development of a simple polarimetric stochastic scattering model has made it possible to offer an explanation for the variety of scatter diagrams displayed in the normalized Stokes parameter plane by some early-type stars. The model allows analysis of data either as a density distribution, a time-series or both. It was noted that scatter diagrams, or loci, should always exhibit at least one axis of symmetry, this being related to the projection of the stellar equatorial plane onto the sky.

Several means of investigating polarimetric data were also constructed and taken all together allow correction for experimental noise, the overcoming of secular variations (say from the general extended atmosphere) and the estimation of the model parameters, *viz.* periodicity, sense of rotation, inclination of the stellar rotation axis to the line of sight, co-latitude of the scattering region and its optical depth. Some of the procedures facilitate data weighting. It was made clear that obtaining a good appraisal of any interstellar contribution can simplify the model fitting procedures. Several computer programs were necessary for model to data application and consequently designed. It was not always possible to treat measurements in terms of a model, because perhaps of data paucity, but methods for searching for variations within the available data after consideration of instrumental induced effects were put forward.

It was reconfirmed that the Be stars ζ Tau, γ Cas and 28 ω CMa are polarimetric variables. Both ζ Tau and γ Cas were observed in H β and Ca II K. ζ Tau exhibited no changes from hour to hour, but night to night fluctuations were apparent, these being stronger in H β than in Ca II K. γ Cas was found to display irregular hourly variations as well as changes on timescales similar to that of ζ Tau, but of the same

power at both wavelengths. The several colour measures of 28ω CMa revealed a coherence to its fluctuations over the period of at least 2 years.

Comprehensive V wide-band polarimetric data were available for the star X Persei, the behaviour of the measurements being matched by the above-mentioned model in the guise of an oblique rotator. A newly found period ($23^{\text{h}}.95$) was uncovered and it was assumed to be due to co-rotation of scattering material.

The oblique rotator model was also applied to σ Ori E and was found to explain the form of its polarimetric, photometric and magnetometric display brilliantly, with the three facets varying in the required synchronous manner.

It was thought possible that for any polarimetric model the relevant light curve should also be predictable. It was found that the point source/point scattering model used in explaining polarimetric traits needed to be enhanced a little to a point (or extended) source/extended scatterer to describe more completely photometric double-wave forms with unequal minima and/or maxima (the minima often being found not to be evenly spaced within the phase of any one period). The simpler model still gave a better description of such light curves than any other proposals, which usually involve various degrees of contrivance.

Photometrically, under particular geometries, photosphere spot and oblique rotator models can give essentially identical predictions. Both scenarios were fitted to readily available extended UVB data on EM Cep. Each gave equal significance of fit to the measurements for the respective models. EM Cep as well as exhibiting cyclic variations also displayed longer (several days) temporal fluctuations.

5.2 Suggestions for Future Work and Discussion

For a star to have locally enhanced scattering regions there must

Table 5.2.1

Stars worthy of polarimetric, photometric and magnetometric study.

<u>HD</u>	<u>Name</u>	<u>Spec. Type</u>
members of NGC 3766	Ahmed 1 Ahmed 7 Ahmed 15 Ahmed 36 Ahmed 63 Ahmed 88	B2 IVp(e) B2 V B2 III B4 Vne B1.5 Vn B3npe
37479 208392 24534	σ Ori E EM Cep X Per	B2 V B1 IVe Bone
224559 217675-6 109387 5394 217050 56139 33328	LQ And \circ And κ Dra γ Cas EW Lac 28 ω CMa λ Eri	B3-4 IV-Ve B5 + A2p B5p B0.5 Ive B3 B2-3 IV-Ve B2
184927	-	B2 V
5737 125823 142301 142990 175362	α Scl a Cen 3 Sco - "	B5 B2.5 B3-4 B3 B2.5

be a disturbing or controlling mechanism. One possibility is an interactive (say with the stellar wind) magnetic field (fossil or dynamo generated). The star σ Ori E is already known to have a dipole magnetic field as have most other helium strong stars. An immediate proposal would be to search for magnetic variability in X Persei and EM Cep.

As already mentioned an oblique rotator, or more descriptively a scattering dipole-oblique rotator model (SDORM), is successful in explaining the photometric double-wave forms observed for many Be stars hence such objects suggest themselves for polarimetric and magnetometric study and *vice versa*.

It is common in astronomy for theories to be subject to vogue and at the moment the oblique model, and possibly now SDORM, is favoured for explaining the behaviour of helium rich, helium weak and Ap stars. Table 5.2.1 lists possible candidates for some combination of polarimetric, photometric and magnetometric study because of their known particular facet of variability.

There is scope for improvement to the simple point source/point scattering model that has been proposed, as has already been done to a small extent in Chapter 4. For example, it can be enhanced to ponder specific geometrical extended scattering zones and more consideration of absorption with increased optical depth to cover possible eclipsing aspects. Techniques for analysing photometric (and magnetometric) data may also need to be investigated or reassessed along similar lines to those of Simmons *et al.* (1980) for polarimetry, to check if model parameters derived from studies are in any way biased estimates. Incidentally, the paper by Aspin *et al.* (1981) which considers the accuracy needed to determine the inclination of a binary's orbital plane to within $\pm 5^\circ$ from polarization measurements would also be applicable to single star cases. Obviously more exact

observations are needed for systems whose geometry gives rise to the lowest amplitudes of variations.

The armoury of spectrometry, polarimetry, photometry and magnetometry can now be used on any program star to determine if it is a SDORM candidate. Spectrometry may be invoked to measure the expected small radial velocities of relevant lines, e.g. helium lines if the star is helium rich. Polarimetry may be used to define the geometry of the system under study, although care should be taken in interpreting some of the derived parameters, e.g. the co-latitude of the scattering bulge may not necessarily be the co-latitude of the magnetic pole as it is thought that for a star which shows excess helium abundance, the region of localisation moves away from the magnetic pole to the magnetic equator with increasing temperature. Photometry can be used to check if the light curve is exhibiting the predicted cyclic double-wave form, and similarly for magnetometry to examine the magnetic field variations - if any. All four facets should be tested for synchrony of fluctuations. Other interesting traits may also be investigated, e.g. the UV C IV line for rotational modulation to reveal if the stellar wind is being influenced by the magnetic field. Spectropolarimetric studies may reveal something about the magnetic geometry giving possibilities of consistency checking. Some lines might be found to vary in antiphase, e.g. the maximum abundance of rare earths would be expected to occur near the negative magnetic pole. The boundary of the magnetosphere, i.e. the height at which the energy density of the field is approximately equal to the kinetic energy density of the trapped gas, should give the maximum level above the photosphere at which the scattering takes place.

Appendix A

Correlation Coefficient Percentage Levels

APPENDIX A - Correlation Coefficient Percentage Levels

Whilst correlation tables are available in various publications, none was found to be comprehensive enough for use in the work contained in this thesis. Another reason for their production was simply for a convenient source of reference. The sample linear correlation coefficient (r) can be determined from the relation $r = \sqrt{b_1 b_2}$, where b_1 is the measured gradient in a "(x,y)" plane and b_2 in a "(y,x)" plane.

Since r is evaluated from a finite set of data points, a spread of possible values exists around the true correlation. For a determined value of r , based on N pairs of observations, to test against the null hypothesis that there is no relation between the two variables "y" and "x" the familiar statistic

$$r \sqrt{\frac{N-2}{1-r^2}}$$

may be used, which has a Student's t -distribution with $N-2$ degrees of freedom.

The presented table shows the associated confidence intervals for a true correlation of zero at the 67%, 90%, 95%, 99% and 99.9% levels.

If the absolute value of r is less than the correlation coefficient at the approximate confidence level, then the two variables are unrelated. This is usually taken as the 95% level.

Introduced is a table of sample size (i.e. corrected for degrees of freedom) versus absolute value of the correlation coefficient at the prescribed confidence levels and for sample sizes of 3(1)200(10)500 → (50)1000(500)10,000(10,000)100,000(100,000)1,000,000.

PERCENTAGE LEVELS FOR CORRELATION COEFFICIENTS

No. of samples	67%	90%	95%	99%	99.9%
3	0.869	0.988	0.997	1.000	1.000
4	0.670	0.900	0.950	0.990	0.999
5	0.556	0.805	0.878	0.959	0.991
6	0.485	0.729	0.811	0.917	0.974
7	0.434	0.669	0.754	0.875	0.951
8	0.397	0.621	0.707	0.834	0.925
9	0.368	0.582	0.666	0.798	0.898
10	0.344	0.549	0.632	0.765	0.872
11	0.325	0.521	0.602	0.735	0.847
12	0.308	0.497	0.576	0.708	0.823
13	0.294	0.476	0.553	0.684	0.801
14	0.281	0.458	0.532	0.661	0.780
15	0.270	0.441	0.514	0.641	0.760
16	0.260	0.426	0.497	0.623	0.742
17	0.252	0.412	0.482	0.606	0.725
18	0.244	0.400	0.468	0.590	0.708
19	0.236	0.389	0.456	0.575	0.693
20	0.230	0.378	0.444	0.561	0.679
21	0.224	0.369	0.433	0.549	0.665
22	0.218	0.360	0.423	0.537	0.652
23	0.213	0.352	0.413	0.526	0.640
24	0.208	0.344	0.404	0.515	0.629
25	0.203	0.337	0.396	0.505	0.618
26	0.199	0.330	0.388	0.496	0.607
27	0.195	0.323	0.381	0.487	0.597
28	0.191	0.317	0.374	0.479	0.588
29	0.188	0.311	0.367	0.471	0.579
30	0.184	0.306	0.361	0.463	0.570
31	0.181	0.301	0.355	0.456	0.562
32	0.178	0.296	0.349	0.449	0.554
33	0.175	0.291	0.344	0.442	0.547
34	0.172	0.287	0.339	0.436	0.539
35	0.170	0.283	0.334	0.430	0.532
36	0.167	0.279	0.329	0.424	0.525
37	0.165	0.275	0.325	0.418	0.519
38	0.162	0.271	0.320	0.413	0.513
39	0.160	0.267	0.316	0.406	0.507
40	0.158	0.264	0.312	0.403	0.501

No. of samples	67%	90%	95%	99%	99.9%
41	0.156	0.260	0.308	0.398	0.495
42	0.154	0.257	0.304	0.393	0.490
43	0.152	0.254	0.301	0.389	0.484
44	0.150	0.251	0.297	0.384	0.479
45	0.149	0.248	0.294	0.380	0.474
46	0.147	0.246	0.291	0.376	0.469
47	0.145	0.243	0.288	0.372	0.465
48	0.144	0.240	0.285	0.368	0.460
49	0.142	0.238	0.282	0.365	0.456
50	0.141	0.235	0.279	0.361	0.451
51	0.139	0.233	0.276	0.358	0.447
52	0.138	0.231	0.273	0.354	0.443
53	0.136	0.228	0.271	0.351	0.439
54	0.135	0.226	0.268	0.348	0.435
55	0.134	0.224	0.266	0.345	0.432
56	0.133	0.222	0.263	0.341	0.428
57	0.131	0.220	0.261	0.339	0.424
58	0.130	0.218	0.259	0.336	0.421
59	0.129	0.216	0.256	0.333	0.418
60	0.128	0.214	0.254	0.330	0.414
61	0.127	0.213	0.252	0.327	0.411
62	0.126	0.211	0.250	0.325	0.408
63	0.125	0.209	0.248	0.322	0.405
64	0.124	0.207	0.246	0.320	0.402
65	0.123	0.206	0.244	0.317	0.399
66	0.122	0.204	0.242	0.315	0.396
67	0.121	0.203	0.240	0.313	0.393
68	0.120	0.201	0.239	0.310	0.390
69	0.119	0.200	0.237	0.308	0.388
70	0.118	0.198	0.235	0.306	0.385
71	0.117	0.197	0.234	0.304	0.382
72	0.116	0.195	0.232	0.302	0.380
73	0.116	0.194	0.230	0.300	0.377
74	0.115	0.193	0.229	0.298	0.375
75	0.114	0.191	0.227	0.296	0.372
76	0.113	0.190	0.226	0.294	0.370
77	0.112	0.189	0.224	0.292	0.368
78	0.112	0.188	0.223	0.290	0.365
79	0.111	0.186	0.221	0.288	0.363
80	0.110	0.185	0.220	0.286	0.361

No. of samples	67%	90%	95%	99%	99.9%
81	0.110	0.184	0.219	0.285	0.359
82	0.109	0.183	0.217	0.283	0.357
83	0.108	0.182	0.216	0.281	0.355
84	0.108	0.181	0.215	0.280	0.353
85	0.107	0.180	0.213	0.278	0.351
86	0.106	0.179	0.212	0.276	0.349
87	0.106	0.178	0.211	0.275	0.347
88	0.105	0.176	0.210	0.273	0.345
89	0.104	0.175	0.208	0.272	0.343
90	0.104	0.174	0.207	0.270	0.341
91	0.103	0.174	0.206	0.269	0.339
92	0.103	0.173	0.205	0.267	0.338
93	0.102	0.172	0.204	0.266	0.336
94	0.102	0.171	0.203	0.264	0.334
95	0.101	0.170	0.202	0.263	0.332
96	0.100	0.169	0.201	0.262	0.331
97	0.100	0.168	0.200	0.260	0.329
98	0.099	0.167	0.199	0.259	0.327
99	0.099	0.166	0.198	0.258	0.326
100	0.098	0.165	0.197	0.256	0.324
101	0.098	0.165	0.196	0.255	0.323
102	0.097	0.164	0.195	0.254	0.321
103	0.097	0.163	0.194	0.253	0.320
104	0.096	0.162	0.193	0.252	0.318
105	0.096	0.161	0.192	0.250	0.317
106	0.096	0.161	0.191	0.249	0.315
107	0.095	0.160	0.190	0.248	0.314
108	0.095	0.159	0.189	0.247	0.312
109	0.094	0.158	0.188	0.246	0.311
110	0.094	0.158	0.187	0.245	0.310
111	0.093	0.157	0.187	0.244	0.308
112	0.093	0.156	0.186	0.242	0.307
113	0.092	0.156	0.185	0.241	0.306
114	0.092	0.155	0.184	0.240	0.304
115	0.092	0.154	0.183	0.239	0.303
116	0.091	0.153	0.182	0.238	0.302
117	0.091	0.153	0.182	0.237	0.300
118	0.090	0.152	0.181	0.236	0.299
119	0.090	0.152	0.180	0.235	0.298
120	0.090	0.151	0.179	0.234	0.297

No. of samples	67%	90%	95%	99%	99.9%
121	0.089	0.150	0.179	0.233	0.295
122	0.089	0.150	0.178	0.232	0.294
123	0.089	0.149	0.177	0.231	0.293
124	0.088	0.148	0.176	0.231	0.292
125	0.088	0.148	0.176	0.230	0.291
126	0.087	0.147	0.175	0.229	0.290
127	0.087	0.147	0.174	0.228	0.289
128	0.087	0.146	0.174	0.227	0.287
129	0.086	0.145	0.173	0.226	0.286
130	0.086	0.145	0.172	0.225	0.285
131	0.086	0.144	0.172	0.224	0.284
132	0.085	0.144	0.171	0.223	0.283
133	0.085	0.143	0.170	0.223	0.282
134	0.085	0.143	0.170	0.222	0.281
135	0.084	0.142	0.169	0.221	0.280
136	0.084	0.142	0.168	0.220	0.279
137	0.084	0.141	0.168	0.219	0.278
138	0.084	0.141	0.167	0.219	0.277
139	0.083	0.140	0.167	0.218	0.276
140	0.083	0.140	0.166	0.217	0.275
141	0.083	0.139	0.165	0.216	0.274
142	0.082	0.139	0.165	0.216	0.273
143	0.082	0.138	0.164	0.215	0.272
144	0.082	0.138	0.164	0.214	0.271
145	0.081	0.137	0.163	0.213	0.270
146	0.081	0.137	0.163	0.213	0.270
147	0.081	0.136	0.162	0.212	0.269
148	0.081	0.136	0.161	0.211	0.268
149	0.080	0.135	0.161	0.210	0.267
150	0.080	0.135	0.160	0.210	0.266
151	0.080	0.134	0.160	0.209	0.265
152	0.080	0.134	0.159	0.208	0.264
153	0.079	0.133	0.159	0.208	0.263
154	0.079	0.133	0.158	0.207	0.263
155	0.079	0.133	0.158	0.206	0.262
156	0.079	0.132	0.157	0.206	0.261
157	0.078	0.132	0.157	0.205	0.260
158	0.078	0.131	0.156	0.204	0.259
159	0.078	0.131	0.156	0.204	0.259
160	0.078	0.131	0.155	0.203	0.258

No. of samples	67%	90%	95%	99%	99.9%
161	0.077	0.130	0.155	0.202	0.257
162	0.077	0.130	0.154	0.202	0.256
163	0.077	0.129	0.154	0.201	0.255
164	0.077	0.129	0.153	0.201	0.255
165	0.076	0.128	0.153	0.200	0.254
166	0.076	0.128	0.152	0.199	0.253
167	0.076	0.128	0.152	0.199	0.252
168	0.076	0.127	0.151	0.198	0.252
169	0.075	0.127	0.151	0.198	0.251
170	0.075	0.127	0.151	0.197	0.250
171	0.075	0.126	0.150	0.196	0.249
172	0.075	0.126	0.150	0.196	0.249
173	0.074	0.125	0.149	0.195	0.248
174	0.074	0.125	0.149	0.195	0.247
175	0.074	0.125	0.148	0.194	0.247
176	0.074	0.124	0.148	0.194	0.246
177	0.074	0.124	0.148	0.193	0.245
178	0.073	0.124	0.147	0.193	0.245
179	0.073	0.123	0.147	0.192	0.244
180	0.073	0.123	0.146	0.192	0.243
181	0.073	0.123	0.146	0.191	0.243
182	0.073	0.122	0.146	0.190	0.242
183	0.072	0.122	0.145	0.190	0.241
184	0.072	0.122	0.145	0.189	0.241
185	0.072	0.121	0.144	0.189	0.240
186	0.072	0.121	0.144	0.188	0.239
187	0.072	0.121	0.144	0.188	0.239
188	0.071	0.120	0.143	0.187	0.238
189	0.071	0.120	0.143	0.187	0.237
190	0.071	0.120	0.142	0.186	0.237
191	0.071	0.119	0.142	0.186	0.236
192	0.071	0.119	0.142	0.185	0.236
193	0.070	0.119	0.141	0.185	0.235
194	0.070	0.118	0.141	0.185	0.234
195	0.070	0.118	0.141	0.184	0.234
196	0.070	0.118	0.140	0.184	0.233
197	0.070	0.118	0.140	0.183	0.233
198	0.070	0.117	0.139	0.183	0.232
199	0.069	0.117	0.139	0.182	0.232
200	0.069	0.117	0.139	0.182	0.231

No. of samples	67%	90%	95%	99%	99.9%
210	0.068	0.114	0.135	0.177	0.225
220	0.066	0.111	0.132	0.173	0.220
230	0.065	0.109	0.129	0.170	0.216
240	0.063	0.106	0.127	0.166	0.211
250	0.062	0.104	0.124	0.163	0.207
260	0.061	0.102	0.122	0.159	0.203
270	0.060	0.100	0.119	0.157	0.199
280	0.058	0.099	0.117	0.154	0.196
290	0.057	0.097	0.115	0.151	0.192
300	0.056	0.095	0.113	0.149	0.189
310	0.056	0.094	0.111	0.146	0.186
320	0.055	0.092	0.110	0.144	0.183
330	0.054	0.091	0.108	0.142	0.180
340	0.053	0.089	0.106	0.140	0.178
350	0.052	0.088	0.105	0.138	0.175
360	0.051	0.087	0.103	0.136	0.173
370	0.051	0.086	0.102	0.134	0.170
380	0.050	0.085	0.101	0.132	0.168
390	0.049	0.083	0.099	0.130	0.166
400	0.049	0.082	0.098	0.129	0.164
410	0.048	0.081	0.097	0.127	0.162
420	0.048	0.080	0.096	0.126	0.160
430	0.047	0.079	0.095	0.124	0.158
440	0.047	0.079	0.093	0.123	0.156
450	0.046	0.078	0.092	0.121	0.155
460	0.046	0.077	0.091	0.120	0.153
470	0.045	0.076	0.090	0.119	0.151
480	0.045	0.075	0.090	0.117	0.150
490	0.044	0.074	0.089	0.116	0.148
500	0.044	0.074	0.088	0.115	0.147
550	0.042	0.070	0.084	0.110	0.140
600	0.040	0.067	0.080	0.105	0.134
650	0.038	0.065	0.077	0.101	0.129
700	0.037	0.062	0.074	0.097	0.124
750	0.036	0.060	0.072	0.094	0.120
800	0.034	0.058	0.069	0.091	0.116
850	0.033	0.056	0.067	0.088	0.113
900	0.033	0.055	0.065	0.086	0.110
950	0.032	0.053	0.064	0.084	0.107
1000	0.031	0.052	0.062	0.081	0.104

No. of samples	67%	90%	95%	99%	99.9%
1500	0.025	0.042	0.051	0.066	0.085
2000	0.022	0.037	0.044	0.058	0.074
2500	0.019	0.033	0.039	0.052	0.066
3000	0.018	0.030	0.036	0.047	0.060
3500	0.016	0.028	0.033	0.044	0.056
4000	0.015	0.026	0.031	0.041	0.052
4500	0.015	0.025	0.029	0.038	0.049
5000	0.014	0.023	0.028	0.036	0.047
5500	0.013	0.022	0.026	0.035	0.044
6000	0.013	0.021	0.025	0.033	0.042
6500	0.012	0.020	0.024	0.032	0.041
7000	0.012	0.020	0.023	0.031	0.039
7500	0.011	0.019	0.023	0.030	0.038
8000	0.011	0.018	0.022	0.029	0.037
8500	0.011	0.018	0.021	0.028	0.036
9000	0.010	0.017	0.021	0.027	0.035
9500	0.010	0.017	0.020	0.026	0.034
10000	0.010	0.016	0.020	0.026	0.033
20000	0.007	0.012	0.014	0.018	0.023
30000	0.006	0.009	0.011	0.015	0.019
40000	0.005	0.008	0.010	0.013	0.016
50000	0.004	0.007	0.009	0.012	0.015
60000	0.004	0.007	0.008	0.011	0.013
70000	0.004	0.006	0.007	0.010	0.012
80000	0.003	0.006	0.007	0.009	0.012
90000	0.003	0.005	0.007	0.009	0.011
100000	0.003	0.005	0.006	0.008	0.010
200000	0.002	0.004	0.004	0.006	0.007
300000	0.002	0.003	0.004	0.005	0.006
400000	0.002	0.003	0.003	0.004	0.005
500000	0.001	0.002	0.003	0.004	0.005
600000	0.001	0.002	0.003	0.003	0.004
700000	0.001	0.002	0.002	0.003	0.004
800000	0.001	0.002	0.002	0.003	0.004
900000	0.001	0.002	0.002	0.003	0.003
1000000	0.001	0.002	0.002	0.003	0.003

Appendix B

Moments

APPENDIX B - Moments

A moment m_k ($k \in \mathbb{Z}^+$) can be defined as

$$m_k = \frac{1}{N} \sum_{j=1}^N (x_j - \bar{x})^k \quad (\text{B1})$$

where N = number of measurements

x_j = j^{th} measurement

\bar{x} = the mean value of all the measurements.

Now from Equations (2.11.2) the measured Stokes parameters rotated through an angle α , are represented by:

$$\begin{aligned} q_{x_j} &= q_I \cos 2\alpha + u_I \sin 2\alpha + n_{q_j} \cos 2\alpha + n_{u_j} \sin 2\alpha + q_j' \cos 2(\Omega - \alpha) \\ &\quad - u_j' \sin 2(\Omega - \alpha) \\ u_{x_j} &= -q_I \sin 2\alpha + u_I \cos 2\alpha - n_{q_j} \sin 2\alpha + n_{u_j} \cos 2\alpha + q_j' \sin 2(\Omega - \alpha) \\ &\quad + u_j' \cos 2(\Omega - \alpha) \end{aligned} \quad (\text{B2})$$

where $q_j' = q_A + \tau_o (a_o + a_1 \cos \phi_j + a_2 \cos 2\phi_j)$

$u_j' = \tau_o (b_1 \sin \phi_j + b_2 \sin 2\phi_j)$

remembering that q_I , u_I are the interstellar contributions and 2Ω is the orientation of the stellar equatorial co-ordinates relative to the instrumental frame. As n_{q_j} and n_{u_j} , the experimental noises of q and u respectively, have means equal to zero, then for a large sample:

$$\sum_j n_{q_j} = \sum_j n_{u_j} = 0$$

If ϕ is uniformly distributed then the probability density function, $f(\phi)$, of ϕ is:

$$f(\phi) = \frac{1}{2\pi} \quad (\text{B3})$$

The moments of q_* and u_* are to be taken about the expectation values $\langle q_* \rangle$ and $\langle u_* \rangle$ respectively. So for large N :

$$\begin{aligned} \langle q_* \rangle &= \frac{1}{2\pi} \int_0^{2\pi} q_* \, d\phi = q_I \cos 2\alpha + u_I \sin 2\alpha + (\tau_o a_o + q_A) \cos 2(\Omega - \alpha) \\ \langle u_* \rangle &= \frac{1}{2\pi} \int_0^{2\pi} u_* \, d\phi = -q_I \sin 2\alpha + u_I \cos 2\alpha + (\tau_o a_o + q_A) \sin 2(\Omega - \alpha) \end{aligned} \quad (\text{B4})$$

Hence $\langle q_* \rangle$ and $\langle u_* \rangle$ are the co-ordinates of the centre of gravity of the measurements. So it is possible to define q_* and u_* in a centre of gravity (CG) frame, i.e.

$$\begin{aligned}
 q_{(CG)j} &= n_{qj} \cos 2\alpha + n_{uj} \sin 2\alpha + \tau_o (a_1 \cos \phi_j + a_2 \cos 2\phi_j) \cos 2(\Omega - \alpha) \\
 &\quad - \tau_o (b_1 \sin \phi_j + b_2 \sin 2\phi_j) \sin 2(\Omega - \alpha) \\
 u_{(CG)j} &= -n_{qj} \sin 2\alpha + n_{uj} \cos 2\alpha + \tau_o (a_1 \cos \phi_j + a_2 \cos 2\phi_j) \sin 2(\Omega - \alpha) \\
 &\quad + \tau_o (b_1 \sin \phi_j + b_2 \sin 2\phi_j) \cos 2(\Omega - \alpha)
 \end{aligned} \tag{B5}$$

Allowing the moments to be represented by:

$$\begin{aligned}
 m_{kq} &= \frac{1}{N} \sum_{j=1}^N q_{(CG)j}^k \\
 m_{ku} &= \frac{1}{N} \sum_{j=1}^N u_{(CG)j}^k
 \end{aligned} \tag{B6}$$

First Moment

For q :

$$m_{(1)q\alpha} = \frac{1}{N} \sum_{j=1}^N q_{(CG)j}$$

If N is large then $\frac{1}{N} \sum_{j=1}^N$ can be approximated to $\frac{1}{2\pi} \int_0^{2\pi}$ so,

$$\frac{1}{2\pi} \int_0^{2\pi} \tau_o (a_1 \cos \phi + a_2 \cos 2\phi) \cos 2(\Omega - \alpha) d\phi = 0$$

$$\frac{1}{2\pi} \int_0^{2\pi} \tau_o (b_1 \sin \phi + b_2 \sin 2\phi) \sin 2(\Omega - \alpha) d\phi = 0$$

$$\therefore m_{(1)q\alpha} = 0 \tag{B7}$$

For u : By analogy with q

$$m_{(1)u\alpha} = 0 \tag{B8}$$

Second Moment

For q :

$$m_{(2)q\alpha} = \frac{1}{N} \sum_{j=1}^N q_{(CG)j}^2$$

Again using the large N approximation, the important (i.e. non-zero) integrals are:

$$\frac{1}{2\pi} \int_0^{2\pi} (a_1 \cos\phi + a_2 \cos 2\phi)^2 d\phi = \frac{1}{2}(a_1^2 + a_2^2)$$

$$\frac{1}{2\pi} \int_0^{2\pi} (b_1 \sin\phi + b_2 \sin 2\phi)^2 d\phi = \frac{1}{2}(b_1^2 + b_2^2)$$

and noting that $\frac{1}{N} \sum_j n_{qj}^2 = \sigma_q^2$ and similarly $\frac{1}{N} \sum_j n_{uj}^2 = \sigma_u^2$ the summation gives:

$$\begin{aligned} m^{(2)}_{q\alpha} = \frac{\tau_0^2}{2} [(a_1^2 + a_2^2)\cos^2 2(\Omega-\alpha) + (b_1^2 + b_2^2)\sin^2 2(\Omega-\alpha)] \\ + \sigma_q^2 \cos^2 2\alpha + \sigma_u^2 \sin^2 2\alpha \end{aligned} \quad (B9)$$

For u: By analogy with q

$$\begin{aligned} m^{(2)}_{u\alpha} = \frac{\tau_0^2}{2} [(a_1^2 + a_2^2)\sin^2 2(\Omega-\alpha) + (b_1^2 + b_2^2)\cos^2 2(\Omega-\alpha)] \\ + \sigma_q^2 \sin^2 2\alpha + \sigma_u^2 \cos^2 2\alpha \end{aligned} \quad (B10)$$

It can be noted that the sum of the moments $m^{(2)}_{q\alpha}$ and $m^{(2)}_{u\alpha}$ are independent of α whereas their difference $\Delta m^{(2)} = m^{(2)}_{q\alpha} - m^{(2)}_{u\alpha}$ is not. Unfortunately this dependence does not help in determining Ω , as an ambiguity, demonstrated below, exists.

Assume for simplicity that $\sigma_q = \sigma_u$ then:

$$\frac{d\Delta m^{(2)}}{d\alpha} = -2\tau_0^2 [a_1^2 + a_2^2 - b_1^2 - b_2^2] \sin 4(\Omega-\alpha) \quad (B11)$$

$$\begin{aligned} \text{The critical values are therefore: } \quad \Omega = \alpha \quad \Omega = \alpha + \frac{\pi}{2} \\ \Omega = \alpha + \frac{\pi}{4} \quad \Omega = \alpha + \frac{3\pi}{4} \end{aligned} \quad (B12)$$

Depending on the sign of $[a_1^2 + a_2^2 - b_1^2 - b_2^2]$, the individual critical values (B12) could be either a maximum or a minimum. Using the second derivative to investigate concavity:

$$\frac{d^2 \Delta m^{(2)}}{d\alpha^2} = -8\tau_0^2 [a_1^2 + a_2^2 - b_1^2 - b_2^2] \cos 4(\Omega-\alpha) \quad (B13)$$

greatest is also the course of significant non-skewness, the q axis of the stellar equatorial frame has been found.

Appendix C

Least Squares Treatment of a Co-rotating Globule

APPENDIX C - Least Squares Treatment of a Co-rotating Globule

In the stellar equatorial frame, the equations describing the polarimetric effect of a co-rotating globule at co-latitude θ , about a star at inclination i , and of angular velocity ω , can be written as:

$$q_{*j} = q_A + q_0 + a_1 \cos(\omega t_j + \epsilon) + a_2 \cos 2(\omega t_j + \epsilon)$$

$$u_{*j} = b_1 \sin(\omega t_j + \epsilon) + b_2 \sin 2(\omega t_j + \epsilon)$$
(C1)

where q_A is the contribution of the axisymmetric envelope

$$a_0 = \frac{\sigma_0 n}{r^2} \sin^2 i \left(\frac{3}{2} \sin^2 \theta - 1 \right) \quad \frac{\sigma_0 n}{r^2} \equiv \text{scattering optical depth} = \tau_0$$

$$a_1 = \frac{-\sigma_0 n}{2r^2} \sin 2\theta \sin 2i \quad b_1 = \frac{\sigma_0 n}{r^2} \sin 2\theta \sin i$$

$$a_2 = \frac{-\sigma_0 n}{2r^2} \sin^2 \theta (1 + \cos^2 i) \quad b_2 = \frac{\sigma_0 n}{r^2} \sin^2 \theta \cos i$$
(C2)

ϵ = arbitrary phase.

Now the plane of the equator of the star may be tilted at an angle Ω (about the plane in which i is measured). In the instrumental (q , u) plane, this angle will be seen as 2Ω , further there may be an interstellar offset to (q_I , u_I). So:

$$q_j = q_{*j} \cos 2\Omega - u_{*j} \sin 2\Omega + q_I$$

$$u_j = q_{*j} \sin 2\Omega + u_{*j} \cos 2\Omega + u_I$$
(C3)

By least squares (LS) via linear regression, ϵ , Ω , i , θ , τ_0 , and a_0 , can be derived by applying a grid of ω 's (q_I , u_I and q_A are indeterminate by this method) and on expanding Equations (C3):-

$$q_j = q_0 + q_1 \cos \omega t_j + q_2 \sin \omega t_j + q_3 \cos 2\omega t_j + q_4 \sin 2\omega t_j$$

$$u_j = u_0 + u_1 \cos \omega t_j + u_2 \sin \omega t_j + u_3 \cos 2\omega t_j + u_4 \sin 2\omega t_j$$
(C4)

where

$$\begin{aligned}
 q_0 &= q_1 + q_A \cos 2\Omega + a_0 \cos 2\Omega & u_0 &= u_1 + q_A \sin 2\Omega + a_0 \sin 2\Omega \\
 q_1 &= a_1 \cos 2\Omega \cos \epsilon - b_1 \sin 2\Omega \sin \epsilon & u_1 &= a_1 \sin 2\Omega \cos \epsilon + b_1 \cos 2\Omega \sin \epsilon \\
 q_2 &= -a_1 \cos 2\Omega \sin \epsilon - b_1 \sin 2\Omega \cos \epsilon & u_2 &= -a_1 \sin 2\Omega \sin \epsilon + b_1 \cos 2\Omega \cos \epsilon \\
 q_3 &= a_2 \cos 2\Omega \cos 2\epsilon - b_2 \sin 2\Omega \sin 2\epsilon & u_3 &= a_2 \sin 2\Omega \cos 2\epsilon + b_2 \cos 2\Omega \sin 2\epsilon \\
 q_4 &= -a_2 \cos 2\Omega \sin 2\epsilon - b_2 \sin 2\Omega \cos 2\epsilon & u_4 &= -a_2 \sin 2\Omega \sin 2\epsilon + b_2 \cos 2\Omega \cos 2\epsilon
 \end{aligned} \tag{C5}$$

Hence the estimated equation takes the form (adapted from Daniel and Wood (1980))

$$Y = b_0 + b_1 x_1 + b_2 x_2 + b_3 x_3 + b_4 x_4 \tag{C6}$$

which can be re-written as

$$Y - \bar{y} = b_1 (x_1 - \bar{x}_1) + b_2 (x_2 - \bar{x}_2) + b_3 (x_3 - \bar{x}_3) + b_4 (x_4 - \bar{x}_4) \tag{C7}$$

where \bar{y} , \bar{x}_1 , \bar{x}_2 , \bar{x}_3 , \bar{x}_4 are the means of the variables for the set of N observations. This takes advantage of the fact that for any LS fit, the constant b_0 takes the form

$$b_0 = \bar{y} - \sum_{\ell=1}^K b_{\ell} \bar{x}_{\ell}, \text{ for } K \text{ constants fitted (} K = 4 \text{ here).}$$

Thus only the coefficients b_1 , b_2 , b_3 and b_4 need to be found. As usual, the LS solutions for the coefficients are obtained by minimizing the sum of squares of the residuals $[rr]$ where

$$[rr] = \sum_{j=1}^N ((y_j - \bar{y}) - b_1 (x_{1j} - \bar{x}_1) - b_2 (x_{2j} - \bar{x}_2) - b_3 (x_{3j} - \bar{x}_3) - b_4 (x_{4j} - \bar{x}_4))^2 \tag{C8}$$

On differentiating Equation (C8) w.r.t. each b_i and setting the resultant equations equal to zero, the "normal equations" ensue:

$$\begin{aligned}
 b_1[11] + b_2[12] + b_3[13] + b_4[14] &= [1y] \\
 b_1[12] + b_2[22] + b_3[23] + b_4[24] &= [2y] \\
 b_3[13] + b_2[23] + b_3[33] + b_4[34] &= [3y] \\
 b_4[14] + b_4[24] + b_4[34] + b_4[44] &= [4y]
 \end{aligned} \tag{C9}$$

Using the notation

$$[21] \equiv [12] \equiv \sum_{j=1}^N (x_{1j} - \bar{x}_1)(x_{2j} - \bar{x}_2) ; \text{ etc.}$$

the b's can be solved by the determinant method, i.e. using Cramer's Rule.

Let

$$\Delta = \begin{vmatrix} [11] & [12] & [13] & [14] \\ [12] & [22] & [23] & [24] \\ [13] & [23] & [33] & [34] \\ [14] & [24] & [34] & [44] \end{vmatrix}$$

$$\Delta b_1 = \begin{vmatrix} [1y] & [12] & [13] & [14] \\ [2y] & [22] & [23] & [24] \\ [3y] & [23] & [33] & [34] \\ [4y] & [24] & [34] & [44] \end{vmatrix}$$

$$\Delta b_2 = \begin{vmatrix} [11] & [1y] & [13] & [14] \\ [12] & [2y] & [23] & [24] \\ [13] & [3y] & [33] & [34] \\ [14] & [4y] & [34] & [44] \end{vmatrix} \tag{C10}$$

$$\Delta b_3 = \begin{vmatrix} [11] & [12] & [1y] & [14] \\ [12] & [22] & [2y] & [24] \\ [13] & [23] & [3y] & [34] \\ [14] & [24] & [4y] & [44] \end{vmatrix}$$

$$\Delta b_4 = \begin{vmatrix} [11] & [12] & [13] & [1y] \\ [12] & [22] & [23] & [2y] \\ [13] & [23] & [33] & [3y] \\ [14] & [24] & [34] & [4y] \end{vmatrix}$$

So the coefficients are then easily calculated from

$$b_1 = \frac{\Delta b_1}{\Delta} ; b_2 = \frac{\Delta b_2}{\Delta} ; b_3 = \frac{\Delta b_3}{\Delta} ; b_4 = \frac{\Delta b_4}{\Delta} \tag{C11}$$

The numerators of Equations (C11) can be expanded by using the column

vector $\begin{pmatrix} [1y] \\ [2y] \\ [3y] \\ [4y] \end{pmatrix}$ as the minors. Hence, Equations (C11) become:

$$b_1 = \frac{1}{\Delta} \left\{ [1y] \begin{vmatrix} [22][23][24] \\ [23][33][34] \\ [24][34][44] \end{vmatrix} - [2y] \begin{vmatrix} [12][13][14] \\ [23][33][34] \\ [24][34][44] \end{vmatrix} + [3y] \begin{vmatrix} [12][13][14] \\ [22][23][24] \\ [24][34][44] \end{vmatrix} - [4y] \begin{vmatrix} [12][13][14] \\ [22][23][24] \\ [24][33][34] \end{vmatrix} \right\}$$

$$b_2 = \frac{1}{\Delta} \left\{ [1y] \begin{vmatrix} [12][23][24] \\ [13][33][34] \\ [14][34][44] \end{vmatrix} + [2y] \begin{vmatrix} [11][13][14] \\ [13][33][34] \\ [14][34][44] \end{vmatrix} - [3y] \begin{vmatrix} [11][13][14] \\ [12][23][24] \\ [14][34][44] \end{vmatrix} + [4y] \begin{vmatrix} [11][13][14] \\ [12][23][24] \\ [13][33][34] \end{vmatrix} \right\} \quad (C12)$$

$$b_3 = \frac{1}{\Delta} \left\{ [1y] \begin{vmatrix} [12][22][24] \\ [13][23][34] \\ [14][24][44] \end{vmatrix} - [2y] \begin{vmatrix} [11][12][14] \\ [13][23][34] \\ [14][24][44] \end{vmatrix} + [3y] \begin{vmatrix} [11][12][14] \\ [12][22][24] \\ [14][24][44] \end{vmatrix} - [4y] \begin{vmatrix} [11][12][14] \\ [12][22][24] \\ [13][23][34] \end{vmatrix} \right\}$$

$$b_4 = \frac{1}{\Delta} \left\{ [1y] \begin{vmatrix} [12][22][23] \\ [13][23][33] \\ [14][24][34] \end{vmatrix} + [2y] \begin{vmatrix} [11][12][13] \\ [13][23][33] \\ [14][24][34] \end{vmatrix} - [3y] \begin{vmatrix} [11][12][13] \\ [12][22][23] \\ [14][24][34] \end{vmatrix} + [4y] \begin{vmatrix} [11][12][13] \\ [12][22][23] \\ [13][23][33] \end{vmatrix} \right\}$$

The solutions may be written as:

$$\begin{aligned} b_1 &= C_{11}[1y] + C_{12}[2y] + C_{13}[3y] + C_{14}[4y] \\ b_2 &= C_{21}[1y] + C_{22}[2y] + C_{23}[3y] + C_{24}[4y] \\ b_3 &= C_{31}[1y] + C_{32}[2y] + C_{33}[3y] + C_{34}[4y] \\ b_4 &= C_{41}[1y] + C_{42}[2y] + C_{43}[3y] + C_{44}[4y] \end{aligned} \quad (C13)$$

where, e.g.

$$C_{31} = \frac{(-1)^{r+c}}{\Delta} \begin{vmatrix} [12][22][24] \\ [13][23][34] \\ [14][24][44] \end{vmatrix} = C_{13} \quad ; \quad \text{here } r=3, c=1$$

The standard errors of the coefficients are:

$$s(b_i) = s(y)C_{ii}^{\frac{1}{2}} \quad ; \quad s(y) = \left(\frac{[rr]}{(N-K-1)} \right)^{\frac{1}{2}} \quad (C14)$$

and the standard error of b_0 is $s(b_0) = \frac{s(y)}{N^{\frac{1}{2}}}$

Relating the Estimated Coefficients to ϵ , Ω , i , τ_0 and a_0

Consider

$$\begin{aligned}
 u_1 + q_2 &= a_1 \sin(2\Omega - \epsilon) - b_1 \sin(2\Omega - \epsilon) \\
 q_1 - u_2 &= a_1 \cos(2\Omega - \epsilon) - b_1 \cos(2\Omega - \epsilon) \\
 u_1 - q_2 &= a_1 \sin(2\Omega + \epsilon) + b_1 \sin(2\Omega + \epsilon) \\
 u_2 + q_1 &= a_1 \cos(2\Omega + \epsilon) + b_1 \cos(2\Omega + \epsilon) \\
 u_3 + q_4 &= a_2 \sin(2\Omega - 2\epsilon) - b_2 \sin(2\Omega - 2\epsilon) \\
 q_3 - u_4 &= a_2 \cos(2\Omega - 2\epsilon) - b_2 \cos(2\Omega - 2\epsilon) \\
 u_3 - q_4 &= a_2 \sin(2\Omega + 2\epsilon) + b_2 \sin(2\Omega + 2\epsilon) \\
 u_4 + q_3 &= a_2 \cos(2\Omega + 2\epsilon) + b_2 \cos(2\Omega + 2\epsilon)
 \end{aligned} \tag{C15}$$

Then it is obvious that (cf. Brown *et al.*, 1978):

$$\epsilon = \frac{1}{2} \left[\tan^{-1} \left(\frac{u_1 - q_2}{u_2 + q_1} \right) - \tan^{-1} \left(\frac{u_1 + q_2}{q_1 - u_2} \right) \right] \text{ by fundamental}$$

or

$$\epsilon = \frac{1}{4} \left[\tan^{-1} \left(\frac{u_3 - q_4}{u_4 + q_3} \right) - \tan^{-1} \left(\frac{u_3 + q_4}{q_3 - u_4} \right) \right] \text{ by harmonic} \tag{C16}$$

and

$$2\Omega = \frac{1}{2} \left[\tan^{-1} \left(\frac{u_1 - q_2}{u_2 + q_1} \right) + \tan^{-1} \left(\frac{u_1 + q_2}{q_1 - u_2} \right) \right] \text{ by fundamental}$$

or

$$2\Omega = \frac{1}{2} \left[\tan^{-1} \left(\frac{u_3 - q_4}{u_4 + q_3} \right) + \tan^{-1} \left(\frac{u_3 + q_4}{q_3 - u_4} \right) \right] \text{ by harmonic} \tag{C17}$$

Also, let

$$\begin{aligned}
 D^2 &= (u_1 + q_2)^2 + (q_1 - u_2)^2 \\
 E^2 &= (u_1 - q_2)^2 + (u_2 + q_1)^2 \\
 F^2 &= (u_3 + q_4)^2 + (q_3 - u_4)^2 \\
 G^2 &= (u_3 - q_4)^2 + (u_4 + q_3)^2
 \end{aligned} \tag{C18}$$

Then Equations (C18) give:

$$\begin{aligned}
 a_1 &= \frac{D + E}{2} \quad ; \quad b_1 = \frac{E - D}{2} \\
 a_2 &= \frac{F + G}{2} \quad ; \quad b_2 = \frac{G - F}{2}
 \end{aligned}
 \tag{C19}$$

Combining Equations (C19) and (C2), the signs of a_1 and a_2 can be neglected, gives:

$$i = \cos^{-1} \left[\frac{a_1}{b_1} \right] \quad \text{by fundamental}$$

$$i = \cos^{-1} \left[\frac{a_2}{b_2} - \left(\left(\frac{a_2}{b_2} \right)^2 - 1 \right)^{\frac{1}{2}} \right] \quad \text{by harmonic}$$

Allowing

$$\theta = \tan^{-1} \left[\frac{2a_2 \sin 2i}{a_1(1 + \cos^2 i)} \right] \quad \text{by components of } q_* \tag{C20}$$

$$\theta = \tan^{-1} \left[\frac{2b_2 \tan i}{b_1} \right] \quad \text{by components of } u_*$$

which in turn permits

$$\tau_o = \frac{2a_1}{\sin 2\theta \sin 2i} \quad ; \quad \text{or} \quad \tau_o = \frac{2a_2}{\sin^2 \theta (1 + \cos^2 i)}$$

$$\text{or} \quad \tau_o = \frac{b_1}{\sin 2\theta \sin i} \quad \tau_o = \frac{b_2}{\sin^2 \theta \cos i}$$

$$\therefore a_o = \tau_o \sin^2 i \left(\frac{3}{2} \sin^2 \theta - 1 \right)$$

Noting that

$$q_o = q_I + (q_A + a_o) \cos 2\Omega$$

$$u_o = u_I + (q_A + a_o) \sin 2\Omega$$

$$\therefore q_I, u_I \text{ and } q_A \text{ are indeterminate}$$

as there are 3 unknowns and only

2 equations.

The Standard Errors of ϵ , Ω , i , θ , τ_0 and a_0

The standard errors of the coefficients $q_0 \rightarrow u_4$, $\Delta q_0 \rightarrow \Delta u_4$ that the least squares analysis provides, need to be transferred to standard errors of ϵ , Ω , i , θ , τ_0 and a_0 .

Standard Error of ϵ

$$\text{Let } A_{M,N}^2 = \frac{\left(\frac{u_M - q_N}{u_N + q_M}\right)^2 \left[\left(\frac{\Delta u_M^2 + \Delta q_N^2}{(u_M - q_N)^2}\right) + \left(\frac{\Delta u_N^2 + \Delta q_M^2}{(u_N + q_M)^2}\right) \right]}{\left[1 + \left(\frac{u_M - q_N}{u_N + q_M}\right)^2 \right]^2} \quad (\text{C21})$$

$$+ \frac{\left(\frac{u_M + q_N}{q_M - u_N}\right)^2 \left[\left(\frac{\Delta u_M^2 + \Delta q_N^2}{(u_M + q_N)^2}\right) + \left(\frac{\Delta q_M^2 + \Delta u_N^2}{(q_M - u_N)^2}\right) \right]}{\left[1 + \left(\frac{u_M + q_N}{q_M - u_N}\right)^2 \right]^2}$$

$$\text{Determined by the fundamental: } \Delta \epsilon = \frac{A_{1,2}}{2} \quad (\text{C22})$$

$$\text{harmonic: } \Delta \epsilon = \frac{A_{3,4}}{4}$$

Standard Error of Ω

$$\text{Determined by the fundamental: } \Delta \Omega = \frac{A_{1,2}}{2} \quad (\text{C23})$$

$$\text{harmonic: } \Delta \Omega = \frac{A_{3,4}}{4}$$

Standard Errors of a_1 , a_2 , b_1 and b_2

Let

$$B_{M,N} = \left[\frac{(u_M + q_N)^2 (\Delta u_M^2 + \Delta q_N^2) + (q_M - u_N)^2 (\Delta q_M^2 + \Delta u_N^2)}{(u_M + q_N)^2 + (q_M - u_N)^2} \right]^{\frac{1}{2}} \quad (C24)$$

$$H_{M,N} = \left[\frac{(u_M - q_N)^2 (\Delta u_M^2 + \Delta q_N^2) + (u_N + q_M)^2 (\Delta u_N^2 + \Delta q_M^2)}{(u_M - q_N)^2 + (u_N + q_M)^2} \right]^{\frac{1}{2}}$$

Then

$$\begin{aligned} \Delta a_1 &= \frac{(B_{1,2}^2 + H_{1,2}^2)^{\frac{1}{2}}}{2} \\ \Delta a_2 &= \frac{(B_{3,4}^2 + H_{3,4}^2)^{\frac{1}{2}}}{2} \\ \Delta b_1 &= \frac{(B_{1,2}^2 + H_{1,2}^2)^{\frac{1}{2}}}{2} \\ \Delta b_2 &= \frac{(B_{3,4}^2 + H_{3,4}^2)^{\frac{1}{2}}}{2} \end{aligned} \quad (C25)$$

Standard Error of i

If derived by fundamental then:

$$\Delta i = \frac{1}{\left[1 - \left(\frac{a_1}{b_1} \right)^2 \right]^{\frac{1}{2}}} \frac{a_1}{b_1} \left[\frac{\Delta a_1^2}{a_1^2} + \frac{\Delta b_1^2}{b_1^2} \right]^{\frac{1}{2}}$$

harmonic then: Let $I = \left[\left(\frac{a_2}{b_2} \right)^2 - 1 \right]$

$$\Delta i = \frac{1}{\left[1 - \left(\frac{a_2}{b_2} - I^{\frac{1}{2}} \right)^2 \right]^{\frac{1}{2}}} \left[\left(\frac{1}{b_2} - \frac{a_2}{b_2^2 I^{\frac{1}{2}}} \right)^2 \Delta a_2^2 + \left(\frac{-a_2}{b_2^2} + \frac{a_2^2}{b_2^3 I^{\frac{1}{2}}} \right)^2 \Delta b_2^2 \right]^{\frac{1}{2}}$$

- (C26)

Standard Error of θ

If derived by q_* then:

$$\Delta\theta = \frac{1}{1 + \left(\frac{2a_2 \sin 2i}{a_1(1+\cos^2 i)}\right)^2} \left[\frac{4\sin^2 2i \Delta a_2^2}{a_1^2(1+\cos^2 i)^2} + \frac{4a_2^2 \sin^2 2i \Delta a_1^2}{a_1^4(1+\cos^2 i)^2} + \frac{4a_2^2(1+3\cos 2i - \sin 2i)^2 \Delta i^2}{a_1^2(1+\cos 2i)^4} \right]^{\frac{1}{2}}$$

by u_* then:

$$\Delta\theta = \frac{1}{1 + \left(\frac{2b_2 \tan i}{b_1}\right)^2} \left[\frac{4\tan^2 i \Delta b_2^2}{b_1^2} + \frac{4b_2^2 \tan^2 i \Delta b_1^2}{b_1^4} + \frac{4b_2^2 \Delta i^2}{b_1^2 \cos^4 i} \right]^{\frac{1}{2}}$$

- (C27)

Standard Error of τ_0

If derived by a_1 then:

$$\Delta\tau_0 = \frac{1}{\sin 2\theta \sin 2i} \left[4\Delta a_1^2 + \frac{16a_1^2 \Delta\theta^2}{\tan^2 2\theta} + \frac{16a_1^2 \Delta i^2}{\tan^2 2i} \right]^{\frac{1}{2}}$$

by a_2 then:

$$\Delta\tau_0 = \frac{2\operatorname{cosec}^2 \theta}{(1+\cos^2 i)} \left[\Delta a_2^2 + 4a_2^2 \cot^2 \theta \Delta\theta^2 + \frac{a_2^2 \sin^2 2i \Delta i^2}{(1+\cos^2 i)^2} \right]^{\frac{1}{2}}$$

by b_1 then:

$$\Delta\tau_0 = \frac{1}{\sin 2\theta \sin i} \left[\Delta b_1^2 + \frac{4b_1^2 \Delta\theta^2}{\tan^2 2\theta} + \frac{b_1^2 \Delta i^2}{\tan^2 i} \right]^{\frac{1}{2}}$$

by b_2 then:

$$\Delta\tau_0 = \frac{1}{\sin^2 \theta \cos i} \left[\Delta b_2^2 + \frac{4b_2^2 \Delta\theta^2}{\tan^2 \theta} + b_2^2 \tan^2 i \Delta i^2 \right]^{\frac{1}{2}}$$

- (C28)

Standard Error of a_0

$$\Delta a_0 = \left[\sin^4 i \left(\frac{3}{2} \sin^2 \theta - 1 \right)^2 \Delta \tau_0^2 + \tau_0^2 \left(\frac{3}{2} \sin^2 \theta - 1 \right)^2 \sin^2 2i \Delta i^2 + \frac{9}{4} \tau_0^2 \sin^4 i \sin^2 2\theta \Delta \theta^2 \right]^{\frac{1}{2}} \quad (C29)$$

It is important to note that the above analysis on the uncertainties $\Delta \epsilon \rightarrow \Delta a_0$ was a formal error treatment. In the presence of a small signal to noise ratio, the confidence interval for a given parameter may therefore be an optimistic one (see Simmons *et al.* (1982)). However, as seen above, there was superfluity in deriving most of the parameters. A rule of thumb that might be used to check for biasing is that the redundant equations give inconsistent results. The deduction of a low inclination is an encouraging sign, regarding the apparent effect of noise, as the LS method is biased towards high inclinations in the company of excessive noise.

Appendix D

Polarimetric Data on HDE 226868 and σ Ori E

The data presented here were recorded by Kemp's group on the 61cm telescope at Pine Mountain Observatory.

(Data kindly provided by Professor Kemp)

V wide-band normalized Stokes parameters (equatorial co-ordinates)
of HDE 226868

J.D.	q(%)	u(%)	J.D.	q(%)	u(%)
2442572.900	0.791	-4.603	2442660.800	0.611	-5.193
2442573.900	0.583	-4.974	2442661.800	0.784	-4.502
2442574.900	0.684	-4.571	2442662.800	0.848	-4.694
2442575.900	0.631	-5.189	2442663.800	0.495	-4.394
2442577.900	1.207	-5.118	2442664.800	0.471	-4.517
2442578.900	1.858	-5.125	2442666.800	1.337	-4.933
2442579.900	0.191	-5.460	2442668.800	0.716	-4.870
2442584.900	0.720	-5.295	2442670.800	0.686	-4.641
2442592.900	0.984	-4.772	2442672.800	0.687	-5.108
2442595.900	0.968	-4.744	2442673.800	0.331	-4.755
2442596.900	0.614	-4.461	2442674.800	0.645	-3.948
2442597.900	0.426	-4.545	2442675.800	0.784	-4.736
2442599.900	0.916	-4.448	2442676.800	0.575	-4.874
2442600.900	0.108	-4.530	2442677.800	0.590	-5.014
2442601.900	0.398	-5.139	2442678.800	0.653	-4.282
2442602.900	0.801	-4.540	2442679.800	0.774	-4.849
2442604.900	0.700	-4.720	2442680.800	0.260	-5.102
2442607.800	0.405	-4.945	2442681.700	0.949	-4.636
2442609.800	0.557	-4.888	2442682.700	0.482	-4.748
2442623.800	1.603	-4.195	2442684.700	0.609	-4.604
2442624.800	1.154	-4.762	2442685.700	0.739	-4.825
2442626.800	0.461	-4.458	2442686.700	0.844	-4.268
2442627.800	0.706	-4.810	2442687.700	0.762	-4.608
2442628.800	0.823	-4.495	2442690.700	0.832	-4.717
2442629.800	0.595	-4.698	2442692.800	0.535	-4.648
2442630.800	0.598	-4.657	2442693.700	0.664	-4.859
2442631.800	0.713	-4.850	2442693.800	0.650	-5.013
2442632.800	0.755	-4.802	2442694.800	0.637	-4.995
2442633.800	1.462	-4.373	2442716.700	0.460	-4.854
2442634.800	0.565	-4.470	2442717.700	0.584	-4.406
2442635.800	0.615	-4.583	2442728.600	0.663	-4.564
2442636.800	0.999	-4.800	2442749.600	0.655	-4.637
2442639.800	0.398	-4.733	2442750.600	0.940	-4.526
2442648.800	0.950	-5.042	2442755.600	0.875	-4.618
2442649.800	0.869	-4.640	2442757.600	0.465	-5.056
2442650.800	0.919	-4.925	2442767.600	0.617	-4.765
2442651.800	0.496	-4.888	2443318.800	0.105	-4.669
2442654.800	0.666	-4.584	2443320.900	-0.061	-5.195
2442657.800	0.623	-4.744	2443321.700	0.368	-4.785
2442658.800	0.543	-4.291	2443322.700	0.740	-5.437
2442659.800	0.970	-4.813	2443323.757	0.864	-4.752
			2443324.771	0.899	-4.860
			2443325.785	0.951	-4.970
			2443329.731	0.662	-4.802
			2443330.729	0.597	-4.846
			2443331.815	0.862	-4.841
			2443332.941	0.578	-4.818
			2443335.896	0.678	-4.960

J.D.	q(%)	u(%)	J.D.	q(%)	u(%)
2443336.849	0.639	-5.010	2443395.771	0.740	-4.701
2443337.844	0.621	-4.906	2443395.898	0.743	-4.745
2443338.962	0.573	-4.904	2443396.785	0.716	-5.170
2443339.923	0.945	-4.714	2443396.895	0.687	-4.986
2443340.925	0.767	-4.846	2443397.902	0.527	-4.733
2443344.833	0.772	-4.904	2443398.762	0.835	-5.093
2443345.863	0.835	-5.104	2443399.812	0.367	-4.984
2443346.755	0.649	-4.928	2443399.851	0.529	-4.918
2443349.759	0.812	-5.115	2443400.715	0.614	-5.223
2443351.906	0.498	-4.745	2443403.700	0.561	-4.752
2443353.865	0.654	-4.878	2443409.749	1.109	-4.765
2443354.719	0.712	-5.093	2443412.690	0.887	-4.595
2443355.851	0.793	-5.036	2443413.771	0.481	-5.249
2443356.921	0.645	-5.370	2443415.962	0.724	-4.645
2443358.972	0.902	-4.598	2443418.867	0.258	-4.625
2443359.684	0.917	-4.545	2443420.731	0.747	-4.417
2443359.862	1.028	-4.983	2443421.688	0.772	-4.666
2443360.846	0.342	-4.895	2443422.719	0.233	-5.054
2443361.838	0.834	-4.775	2443424.816	0.318	-4.962
2443357.750	0.725	-4.632	2443425.639	0.592	-4.663
2443362.792	0.637	-4.972	2443425.709	0.636	-5.309
2443364.713	0.980	-4.761	2443426.730	0.633	-4.912
2443364.849	0.903	-4.725	2443426.832	0.913	-4.827
2443365.913	0.410	-4.992	2443427.643	0.694	-4.988
2443366.872	0.692	-4.840	2443427.797	0.408	-5.212
2443367.764	0.901	-4.988	2443428.651	0.499	-4.630
2443367.889	0.939	-4.705	2443428.793	0.614	-4.720
2443368.786	0.815	-5.314	2443429.709	0.599	-4.843
2443368.921	0.661	-5.155	2443429.817	0.707	-5.074
2443370.719	0.611	-5.007	2443430.647	0.591	-5.046
2443370.948	0.559	-5.379	2443430.808	0.476	-4.838
2443371.969	0.544	-4.979	2443431.787	0.501	-4.657
2443372.747	0.712	-4.959	2443433.729	0.613	-5.008
2443372.927	0.865	-4.919	2443434.644	0.601	-4.889
2443373.760	0.944	-4.943	2443434.791	0.505	-5.059
2443375.726	0.595	-4.552	2443435.647	1.134	-5.043
2443375.931	0.691	-4.797	2443436.653	0.610	-5.033
2443377.750	0.559	-4.544	2443438.651	0.552	-5.199
2443378.705	0.681	-5.177	2443443.697	1.046	-4.895
2443378.910	0.641	-4.822	2443444.788	0.248	-5.440
2443386.743	0.624	-4.768	2443450.732	0.145	-5.065
2443387.729	0.711	-4.800	2443451.772	1.199	-4.877
2443388.802	0.569	-5.123	2443455.672	0.381	-4.850
2443390.760	0.769	-4.890	2443459.649	0.739	-4.700
2443391.718	0.664	-4.976	2443463.657	0.556	-4.905
2443392.793	0.690	-4.643	2443467.700	0.359	-4.724
2443393.795	0.632	-4.824	2443477.694	0.066	-4.483
2443394.847	0.382	-4.616	2443481.653	0.585	-4.659

J.D.	q(%)	u(%)	J.D.	q(%)	u(%)
2443482.611	0.811	-4.321	2443660.815	0.352	-4.906
2443486.622	0.956	-4.747	2443661.795	0.743	-5.030
2443489.594	0.793	-4.825	2443662.834	0.620	-5.061
2443496.692	0.987	-4.926	2443663.867	0.744	-4.863
2443497.632	0.654	-4.893	2443664.777	0.867	-5.100
2443568.924	0.624	-5.043	2443664.937	0.807	-4.959
2443569.101	0.647	-4.854	2443665.795	0.626	-5.086
2443574.000	0.551	-4.720	2443666.788	0.624	-5.008
2443577.984	0.580	-4.970	2443667.802	0.692	-4.870
2443583.022	0.708	-4.974	2443668.805	0.624	-4.952
2443584.003	0.712	-4.748	2443670.794	0.579	-4.736
2443585.000	0.643	-5.174	2443671.892	0.220	-4.918
2443585.984	0.799	-4.739	2443674.841	0.413	-5.019
2443586.997	0.779	-5.120	2443675.829	0.570	-5.000
2443587.988	0.733	-4.755	2443676.806	0.781	-4.879
2443593.999	0.758	-4.840	2443677.793	0.617	-4.846
2443595.029	0.324	-4.663	2443678.833	0.763	-4.829
2443596.996	0.731	-5.086	2443680.824	0.694	-4.860
2443598.971	0.522	-4.756	2443681.789	0.557	-4.845
2443603.992	0.932	-5.446	2443682.850	0.726	-4.982
2443606.960	0.600	-4.756	2443684.934	0.497	-4.956
2443607.922	0.773	-4.898	2443685.844	0.867	-4.778
2443608.922	0.924	-4.672	2443686.840	0.714	-4.940
2443609.936	0.762	-5.159	2443687.843	0.733	-4.947
2443610.921	0.519	-4.911	2443689.873	0.766	-4.745
2443611.934	0.643	-4.908	2443690.810	0.622	-4.814
2443615.956	0.372	-4.772	2443694.882	0.670	-5.149
2443619.956	0.577	-4.734	2443695.865	0.753	-4.914
2443621.979	0.595	-4.772	2443696.875	0.709	-4.997
2443626.873	0.571	-4.903	2443697.862	1.112	-4.627
2443627.968	0.878	-4.755	2443698.782	0.630	-4.865
2443630.858	0.654	-5.182	2443699.840	0.450	-4.823
2443631.870	0.570	-4.817	2443700.747	0.428	-4.757
2443632.871	0.775	-5.091	2443700.944	0.750	-4.886
2443634.932	0.739	-4.849	2443701.745	0.710	-5.087
2443635.874	0.826	-5.282	2443701.932	0.601	-5.033
2443636.849	1.135	-5.030	2443702.774	0.545	-4.863
2443637.859	0.489	-5.198	2443703.753	0.666	-4.892
2443640.842	0.528	-4.965	2443703.961	0.726	-4.854
2443642.908	0.600	-5.339	2443704.751	0.717	-5.031
2443646.891	0.583	-5.308	2443704.964	0.784	-4.855
2443648.872	0.954	-4.901	2443705.922	0.679	-4.962
2443652.855	0.689	-4.712	2443706.883	0.643	-4.781
2443653.897	0.645	-4.906	2443707.799	0.589	-4.914
2443655.934	0.735	-4.666	2443708.801	0.717	-4.882
2443657.826	0.662	-4.912	2443709.949	0.752	-5.007
2443658.810	0.676	-4.792	2443710.770	0.607	-4.855
2443659.816	0.702	-5.157	2443711.770	0.693	-4.833

J.D.	q(%)	u(%)	J.D.	q(%)	u(%)
2443712.768	0.852	-4.744	2443781.775	0.889	-4.753
2443712.951	0.754	-4.908	2443782.845	0.901	-4.916
2443713.787	0.753	-4.893	2443783.727	0.705	-4.828
2443714.826	0.764	-4.852	2443784.767	1.006	-4.654
2443716.964	0.658	-4.992	2443785.746	0.541	-4.886
2443717.810	0.686	-5.085	2443786.785	0.572	-4.845
2443718.804	0.641	-4.961	2443787.689	0.436	-5.050
2443719.741	0.676	-4.733	2443788.739	0.565	-4.999
2443719.887	0.745	-4.757	2443790.646	0.632	-4.722
2443720.826	0.682	-4.853	2443791.674	0.691	-5.262
2443721.794	0.617	-5.009	2443792.752	0.355	-4.581
2443722.850	0.615	-4.875	2443793.629	0.530	-4.633
2443723.846	0.586	-4.924	2443794.738	0.907	-5.306
2443724.744	0.482	-4.960	2443795.646	0.466	-4.788
2443724.909	0.645	-4.787	2443796.782	0.664	-5.233
2443725.798	0.843	-4.948	2443798.794	0.566	-4.972
2443726.756	0.599	-4.881	2443799.620	0.722	-4.929
2443727.751	0.717	-4.734	2443800.747	0.632	-4.651
2443728.752	0.516	-4.842	2443803.739	0.577	-4.629
2443729.753	0.649	-5.064	2443804.638	0.641	-5.066
2443730.790	0.353	-4.757	2443806.729	0.706	-4.698
2443731.839	0.855	-4.908	2443807.766	0.511	-4.924
2443732.737	0.759	-4.946	2443808.640	0.626	-4.821
2443733.796	0.760	-4.842	2443809.722	0.494	-4.850
2443734.798	0.767	-4.725	2443811.707	0.383	-4.841
2443735.753	0.621	-4.961	2443812.634	0.482	-5.079
2443737.925	0.640	-4.683	2443813.741	0.582	-5.041
2443738.733	0.286	-4.813	2443814.725	0.674	-4.864
2443739.725	0.574	-4.934	2443816.640	0.826	-4.539
2443740.826	0.660	-5.027	2443819.726	0.348	-4.730
2443746.746	0.535	-4.914	2443822.728	0.881	-5.156
2443747.930	0.765	-4.941	2443824.750	0.485	-5.229
2443748.907	0.532	-5.026	2443826.697	0.840	-5.165
2443749.744	0.613	-4.868	2443827.696	0.644	-4.716
2443750.696	0.451	-5.003	2443829.691	0.756	-4.933
2443751.896	0.524	-4.821	2443830.621	0.635	-5.031
2443752.716	0.508	-4.824	2443835.755	1.008	-4.782
2443753.876	0.799	-4.861	2443839.701	0.413	-4.988
2443754.704	0.861	-5.164	2443844.693	0.669	-5.109
2443755.816	0.450	-4.842	2443845.718	0.815	-4.916
2443764.771	0.424	-4.528	2443847.731	0.341	-4.834
2443766.752	0.379	-5.304	2443848.673	0.364	-4.654
2443770.917	0.232	-4.901	2443850.684	0.461	-5.195
2443771.760	0.300	-5.361	2443852.732	0.665	-4.898
2443772.770	0.758	-4.749	2443858.675	0.548	-4.696
2443374.863	0.870	-4.925	2443862.639	0.545	-5.013
2443779.664	0.729	-4.925	2443864.658	0.562	-5.009
2443780.746	0.414	-4.942	2443867.657	0.532	-4.958
			2443868.608	0.670	-4.787

B wide-band normalized Stokes parameters (equatorial co-ordinates)

of σ Ori E

J.D.	q(%)	u(%)
2443150.830	-0.285	-0.079
2443154.730	-0.337	-0.082
2443156.690	-0.321	0.065
2443163.610	-0.303	0.000
2443163.870	-0.251	0.036
2443166.620	-0.322	-0.078
2443167.676	-0.338	0.065
2443167.802	-0.319	0.032
2443167.868	-0.303	-0.094
2443172.678	-0.275	-0.030
2443172.718	-0.315	-0.029
2443172.804	-0.361	0.053
2443176.629	-0.261	-0.050
2443168.708	-0.295	0.051
2443169.625	-0.270	-0.005
2443169.665	-0.260	-0.028
2443169.814	-0.353	-0.037
2443169.860	-0.351	0.053
2443170.610	-0.360	0.038
2443170.650	-0.287	-0.093
2443170.697	-0.281	0.037
2443170.738	-0.327	-0.010
2443170.802	-0.324	-0.103
2443170.845	-0.304	-0.046
2443171.635	-0.278	0.008
2443171.685	-0.318	0.043
2443171.726	-0.322	0.011
2443171.802	-0.329	0.012
2443171.860	-0.312	-0.052
2443174.721	-0.347	0.052
2443179.625	-0.351	0.057
2443176.633	-0.348	-0.009
2443176.734	-0.294	-0.039
2443177.712	-0.310	0.047
2443176.833	-0.296	-0.011
2443177.617	-0.319	-0.055
2443178.713	-0.325	-0.046
2443178.817	-0.326	-0.004
2443178.619	-0.292	-0.089
2443184.627	-0.323	0.063
2443183.795	-0.264	-0.049
2443183.703	-0.363	0.020
2443185.640	-0.271	0.017
2443185.810	-0.257	-0.014
2443187.790	-0.321	0.069
2443208.679	-0.399	-0.043
2443208.722	-0.408	0.009
2443209.671	-0.239	0.024
2443209.724	-0.287	-0.011
2443213.680	-0.333	-0.136
2443213.708	-0.298	-0.043
2443214.708	-0.397	-0.062
2443214.750	-0.333	0.006
2443215.653	-0.367	-0.050
2443215.732	-0.297	0.076
2443216.692	-0.247	0.002
2443218.650	-0.299	0.079
2443218.676	-0.293	0.071
2443218.703	-0.324	0.087
2443219.734	-0.248	0.015

Appendix E

Two FORTRAN77 Program Listings

Two programs that were composed for application of methods 2.14(c) and 2.14(d), *viz.* the correlation of polarization position angle and correlation of the sign of u .

- * Program carries out the method of correlation of polarization position angle as outlined in Clarke and McGale (1986) (submitted to Astron. & Astrophys.). The object is to derive the best period and phase from a fit of the data under study to the canonical scattering model. The value of stellar inclination may be varied as can also the co-latitude of the scattering material, to give the best model match.
- * Program allows particular intervals of data to be put through a grid of chosen periods and phases.

```

PROGRAM FPAP
CHARACTER IN*10,ANS
DIMENSION T(400),AE(400),AO(400)
PI=4.0*ATAN(1.0)

```

- * Get input parameters for particular run.

```

70 PRINT ('Give filename:')
READ(*,*) IN
60 PRINT ('Give start and finishing times(inclusive):')
READ(*,*) ST,FT
PRINT ('Give upper,lower and stepsize for period(hrs):')
READ(*,*) PU,PL,PS
PRINT ('Give delta phase(hrs):')
READ(*,*) DP
PRINT ('Give inclination and theta(deg):')
READ(*,*) INCL,TH

```

- * Convert degrees to radians, open file for analysis, and calculate the position of the centre of gravity of the points.

```

RI=INCL*PI/180.0
RT=TH*PI/180.0
OPEN(1,FILE=IN,STATUS='OLD')
QS=0.0
US=0.0
I=1
5 READ(1, '(F8.3,1X,F8.5,1X,F8.5)',END=6) D,Q,U
IF(C.LT.ST) GOTO 5
IF(D.GT.FT) GOTO 6
QS=QS+Q
US=US+U
I=I+1
GOTO 5
6 NL=I-1
QB=QS/NL
UB=US/NL

```

- * Round to five decimal places.

```

QB=INT(QB*100000)/100000.0
UB=INT(UB*100000)/100000.0
REWIND 1

```

- * Read in measurements again but translate them to a centre of gravity frame. Ensure that position angle is described in the same sense as positive phi in the canonical model.

```

I=1
10 READ(1, '(F8.3,1X,F8.5,1X,F8.5)',END=20) T(I),Q,U
IF(T(I).LT.ST) GOTO 10
IF(T(I).GT.FT) GOTO 20

```

```

Q=Q-QB
U=U-UB
AO(I)=ATAN2(L,Q)
IF(AC(I).LT.C.0) AO(I)=AO(I)+2*PI
IF(AO(I).LE.FI) AO(I)=PI-AC(I)
IF(AO(I).GT.PI) AO(I)=3*PI-AO(I)
I=I+1
GOTO 10
20 NL=I-1
CLOSE(1)
*
* Call NAG routine to get critical values of the correlation co-eff
* 95% & 99% confidence intervals.
*
IDF=NL-2
V95=GO1CAF(0.025,IDF,0)
V99=GO1CAF(0.005,IDF,0)
C95=SQRT(V95**2/((V95**2)+IDF))
C99=SQRT(V99**2/((V99**2)+IDF))
*
* Write out header.
*
WRITE(*,'(//)')
IT=INT(TH)
WRITE(*,'(''QB = '' ,F8.5,''' UB = '' ,F8.5)'') QB,UB
WRITE(*,'(''Inclination = '' ,I3,''' Theta = '' ,I3)'') INCL,IT
WRITE(*,'(''Start time: '' ,F8.3,''' Finish time: '' ,F8.3)'') ST,FT
WRITE(*,'(''No. of points: '' ,I4,''' C95 = '' ,F6.4,''' C99 = '' ,F6.4
+)'') NL,C95,C99
WRITE(*,'('' Gradient error Inter. error TO Perio
+d CV'')'')
WRITE(*,'(65(1H-))')
*
* Run through the chosen mesh of periods and phases.
*
DO 30,PER=PL,PU,PS
PR=PER/24.0
DO 40,PH=0,PER,DP
PHA=PH/24.0
TO=T(1)+PHA
*
* Call subroutines to find model position angle and to perform
* the two sample linear regressions needed to give the sample
* correlation co-efficient.
*
CALL SFPAP(RI,RT,NL,T,TC,PR,AE)
CALL SUBGI(AC,AE,NL,AXY,EAXY,BXY,EEXY)
CALL SUBGI(AE,AO,NL,AYX,EAYX,BYX,EEYX)
SCC=SQRT(AXY*AYX)
*
* Result worth outputting?
*
IF(SCC.GE.C95.AND.AXY.GT.0.3) THEN
WRITE(*,'(3X,4(F6.4,3X),F8.3,2X,F6.3,2X,F6.4)'') AXY,EAXY,BXY,EBXY,
+TO,PER,SCC
END IF
40 CONTINUE
30 CONTINUE
*
* Option for another run with the same data file or a new data
* set before terminating program.

```

```

WRITE(*, '(//)')
PRINT '( "Another run with same file?" )'
READ(*, '(A1)') ANS
IF(ANS.EQ.'Y') GOTO 60
PRINT '( "Another run?" )'
READ(*, '(A1)') ANS
IF(ANS.EQ.'Y') GOTO 70
STOP
END

```

*
 * Subroutine calculates model polarization position angles
 * given an inclination, co-latitude of scattering material
 * and period and phase.
 *

```

SUBROUTINE SFPAP(RI,RT,NL,I,T0,PR,AE)
DIMENSION AE(*),T(*)
PI=4.0*ATAN(1.0)

```

*
 *
 * Get fundamental and harmonic amplitudes of q & u.
 *

```

A1=-0.5*SIN(2*RT)*SIN(2*RI)
A2=-0.5*SIN(RT)*SIN(RT)*(1.+COS(RI)*COS(RI))
B1=SIN(2*RT)*SIN(RI)
B2=SIN(RT)*SIN(RT)*COS(RI)

```

*
 * Calculate as many position angles as there are points in the
 * data set under study.
 *

```

DO 10, I=1,NL
P=2*PI*(T(I)-T0)/PR
QD=A1*COS(P)+A2*COS(2*P)
UD=B1*SIN(P)+B2*SIN(2*P)
AE(I)=ATAN2(UD,QD)
IF(AE(I).LT.(.0) AE(I)=AE(I)+2*PI
IF(AE(I).LE.(PI) AE(I)=PI-AE(I)
IF(AE(I).GT.(PI) AE(I)=3*PI-AE(I)
10 CONTINUE

```

*
 * Return to main program.
 *

```

RETURN
END

```

```

*
* Subroutine performs a linear regression. The sample gradient
* sample intercept and their errors are derived by the method
* of least squares.
*
  SUBROUTINE SUBGI(Y,X,NP,A,SEA,B,SEB)
  DIMENSION X(*),Y(*)
*
* Initialise summations.
*
  SUMX=0.0
  SUMX2=0.0
  SUMXY=0.0
  SUMY=0.0
  SUMY2=0.0
*
* Do summations for the total number of data points involved.
*
  DO 10,K=1,NP
  SUMX=SUMX+X(K)
  SUMX2=SUMX2+X(K)*X(K)
  SUMXY=SUMXY+X(K)*Y(K)
  SUMY=SUMY+Y(K)
  SUMY2=SUMY2+Y(K)*Y(K)
10  CONTINUE
  D=NP*SUMX2-SUMX**2
  AN=NP*SUMXY-SUMX*SUMY
  BN=SUMX2*SUMY-SUMX*SUMXY
  SD2=NP*SUMY2-SUMY**2-(AN**2)/D
  SD=SQRT(SD2)/NP
*
* Calculate the sample gradient and intercept and their standard errors.
*
  A=AN/D
  SEA=NP*SD/SQRT((NP-2)*D)
  B=BN/D
  SEB=NP*SD*SQRT(SUMX2)/SQRT(NP*(NP-2)*D)
*
* Return to main program.
*
  RETURN
  END

```

*
 * Program finds the period and phase by comparing the sign
 * of the u parameter of real data with the sign got by
 * use of the phi-time relation.
 * The method, known as the correlation of the sign of u, has been
 * described by Clarke and McGale (1986)(submitted to Astron. &
 * Astrophys.).
 * Program allows particular intervals of data to be put through a grid
 * of chosen periods and phases.
 *

```
PROGRAM FPAP3
CHARACTER IA*10,ANS,SIGN0(400),SIGNE
DIMENSION T(400),S(10000),PERIOD(10000),PHASE(10000)
+,DUM(10000),IND(10000),INDW(10000)
PI=4.0*ATAN(1.0)
```

*
 * Get input parameters for particular run.
 *

```
70 PRINT ('Give filename:')
READ(*,*) IN
60 PRINT ('Give start and finishing times(inclusive):')
READ(*,*) ST,FT
PRINT ('Give upper,lower and stepsize for period(hrs):')
READ(*,*) PU,PL,PS
PRINT ('Give delta phase(hrs):')
READ(*,*) DP
PRINT ('Give inclination and theta(deg):')
READ(*,*) INCL,TH
```

*
 * Convert degrees to radians, open file for analysis, and calculate
 * the position of the centre of gravity of the points.
 *

```
IT=INT(TH)
RI=INCL*PI/180.0
RT=TH*PI/180.0
```

*
 * Also get the critical u value below which measurements are to be
 * ignored for this run.
 *

```
PRINT ('Give critical u value:')
READ(*,*) CUV
OPEN(1,FILE=IN,STATUS='OLD')
QS=0.0
US=0.0
I=1
5 READ(1,'(F8.3,1X,F8.5,1X,F8.5)',END=6) D,Q,U
IF(D.LT.ST) GOTC 5
IF(D.GT.FT) GOTC 6
QS=QS+Q
US=US+U
I=I+1
GOTC 5
6 NL=I-1
QB=QS/NL
UB=US/NL
```

*
 * Round to five decimal places.
 *

```
QB=INT(QB*100000)/100000.0
UB=INT(UB*100000)/100000.0
REWIND 1
```

```

*
* Read in points and translate them to a centre of gravity frame, q
* can be ignored.
*
      I=1
10  READ(1, '(F8.3,1X,F8.5,1X,F8.5)', END=20) D,Q,U
      IF(D.LT.ST) GOTO 10
      IF(D.GT.FT) GOTO 20
      U=U-UB
      IF(ABS(U).GT.CUV) THEN
          T(I)=D
*
* Note the sign of the observed u value.
*
      IF(U.GT.0.0) SIGNO(I)='P'
      IF(U.LT.0.0) SIGNO(I)='N'
      I=I+1
      END IF
      GOTO 10
20  NL=I-1
      CLOSE(1)
      B1=SIN(2*RT)*SIN(RI)
      B2=SIN(RT)*SIN(RT)*COS(RI)
      J=1
*
* Run through the grid of chosen periods and phases. The stepsizes
* must be allow not more than 10000 combinations of period and phase.
*
      DO 30, PER=PL,PU,PS
          PR=PER/24.0
          DO 40, PH=0,PER,DP
              PHA=PH/24.0
              TO=ST+PHA
              IR=0
              DO 50, I=1,NL
                  PHI=2*PI*(T(I)-TO)/PR
*
* Get the sign of the model u value and note it.
*
                  U=B1*SIN(PHI)+B2*SIN(2*PHI)
                  IF(U.GE.0.0) SIGNE='P'
                  IF(U.LT.0.0) SIGNE='N'
*
* Compare the observed and model signs of u.
*
                  IF(SIGNE.EQ.SIGNO(I)) IR=IR+1
50  CONTINUE
          S(J)=IR*1.0
          PERIOD(J)=PER
          PHASE(J)=PH
          J=J+1
40  CONTINUE
30  CONTINUE
      J=J-1
*
* Sort results to look for the biggest success rate, using
* the NAG routine NC1AKF.
*
      CALL NC1AKF(S,DUM,IND,INDW,J,1000,0)
*
* Output a header.
*

```

```

WRITE(*, '(//)')
WRITE(*, ('QB = ', F8.5, ' UB = ', F8.5)) QB, UB
WRITE(*, ('Inclination = ', I3, ' Theta = ', I3)) INCL, IT
WRITE(*, ('Start Time : ', F8.3, ' Finish Time : ', F8.3)) ST, FT
WRITE(*, ('Critical u value = ', F8.5)) CUV
WRITE(*, ('Period Phase NoP NS'))
WRITE(*, '(28(1H-))')

```

*
* List the top twenty matches and the worst match.
*

```

DO 80, I=1,20
WRITE(*, '(1X, F6.3, 1X, F8.3, 2X, I3, 2X, F4.0)') PERIOD(IND(I)),
+PHASE(IND(I)), NL, S(I)
80 CONTINUE
WRITE(*, '(/, 1X, F6.3, 1X, F8.3, 2X, I3, 2X, F4.0)') PERIOD(IND(J)),
+PHASE(IND(J)), NL, S(J)

```

*
* Option for another run with the same data file or a new data set
* otherwise terminate program.
*

```

WRITE(*, '(//)')
PRINT ('Another run with same file?')
READ(*, '(A1)') ANS
IF(ANS.EQ.'Y') GOTO 60
PRINT ('Another run?')
READ(*, '(A1)') ANS
IF(ANS.EQ.'Y') GOTO 70
STOP
END

```

REFERENCES

- ALLEN, C.W., "Astrophysical Quantities", ATHLONE PRESS, Univ. London, (1955)
- ASPIN, C., SIMMONS, J.F.L., BROWN, J.C., M. N. R. A. S., **194**, 283, (1981)
- ASPIN, C., Ph. D. Thesis, University of Glasgow, (1981)
- AVERY, R.W., MICHALSKY, J.J., STOKES, R.A., Ap. J., **180**, L127, (1973)
- BAADE, D., A. & A., **110**, L15, (1982b)
- BAADE, D., A. & A., **105**, 65, (1982a)
- BALONA, L.A., ENGELBRECHT, C.A., M.N.R.A.S., **219**, 131, (1986)
- BARFORD, N.C., "Experimental Measurements: Precision Error and Truth", ADDISON-WESLEY PUB., (1967)
- BATTEN, A.H., "Binary and Multiple Systems of Stars", PERGAMON PRESS LTD, 1st. ed., (1973)
- BAUD, B., TINBERGEN, J., Nature, **227**, 29, (1972)
- BEALS, C.S., Publ. Dom. Astrophys. Obs. Victoria, **9**, 1, (1951)
- BEHR, A., Veroff, zu Gottingen, No. 126, (1959)
- BOLTON, C.T., Nature, **235**, 271, (1972)
- BOLTON, C.T., Ap. J., **192**, L7, (1974)
- BOLTON, C.T., Bull. AAS, **3**, 458, (1971)
- BROOKS, A., Biometrika, submitted, (1984)
- BROWN, J.C., MCLEAN, I.S., EMSLIE, A.G., A. & A., **68**, 415, (1978)
- * BROWN, J.C., MCLEAN, I.S., A. & A., **57**, 141, (1977)
- BUERGER, P.F., COLLINS II, G.W., Ap J., **161**, 1025, (1970)
- CAPPS, R.W., COYNE, G.V., DYCK, H.M., Ap. J., **184**, 173, (1973)
- CLARKE D., MCLEAN. I.S., M.N.R.A.S., **174**, 335, (1976)
- CLARKE, D., MCGALE, P.A., A. & A., in press, (1986a)
- CLARKE, D., MCGALE, P.A., A. & A., submitted, (1986b)
- CLARKE, D., MCGALE, P.A., IAU Coll. 92, "Physics of Be Stars", in press, (1986d)
- CLARKE, D.C., MCGALE, P.A., A. & A., submitted, (1986c)
- CLARKE, D., MCLEAN, I.S., M.N.R.A.S., **173**, 21P, (1975)
- CLARKE, D., STEWART, B.G., Vistas in Astronomy, **29**, 27, (1986)
- CLARKE, D., BROOKS, A., M.N.R.A.S., **211**, 737, (1984)
- CLARKE, D., GRAINGER, J.F., "Polarized Light and Optical Measurement" PERGAMON PRESS, OXFORD, (1971)
- COCHRAN, W.G., Annals of Math. Stat., **23**, 315, (1952)
- COWELY, A.P., MCLAUGHLIN, D.B., TONEY, J., MACCONNELL, D.J., P.A.S.P., **84**, 834, (1972)
- COYNE, G.V., Ricerche Astronomiche, **8(28)**, 533, (1975)
- COYNE, G.V., MCLEAN, I.S., Astron. J., **80(9)**, 702, (1975)
- COYNE, G.V., KRUCZEWSKI, A., Astron. J., **74**, 528, (1969)
- DANIEL, C., WOOD, F.S., "Fitting Equations to Data" 2nd. ed. J. WILEY and SONS, NEW YORK, (1980)
- DOAZAN, V., THOMAS, R.N. Hvar Obs. Bull., **7(1)**, 97, (1983)
- DOAZAN, V., PETON, A., A. & A., **9**, 245, (1970)
- EVANS, D.S., M.N.R.A.S., **154**, 329, (1971)
- GEHRELS, T., Ap. J., **173**, L23, (1972)
- GROOTE, D., HUNGER, K., A. & A., **56**, 129, (1977)
- * BROWN, M.B., FORSYTHE, A.B., Technometrics, **16(1)**, 129, (1974)

- HALL, J.S., Pub. US Naval Obs., **XVII**(vi), (1958)
 HARMANEC, P., Bull. Astron. Inst. Czechosl., **35**, 193, (1984)
 HARMANEC, P., Hvar. Obs. Bull., **7**(1), 55, (1983)
 HARPER, W.E., Publ. Dom. Astrophys. Obs. Victoria, **7**, 1, (1937)
 HAYES, D.P., GUINAN, E., Ap. J., **279**, 721, (1984)
 HAYES, D.P., P. A. S. P., **92**, 661, (1980)
 HAYES, D.P., Astron. J., **89**(8), 1219, (1984)
 HENRICHS, H.F., van den HUVAL, E.P.J., A. & A., **54**, 817, (1977)
 HERMAN, R., BARIN, M.T., PENDZEL, M., Ann. Astrophys., **22**, 540, (1959)
 HESSER, J.E., WALBORN, N.R., UGARTE. P., Nature, **262**, 116, (1976)
 HILDITCH, R.W., MCLEAN, B.J., REID, I.N., M.N.R.A.S., **200**, 1153,
 (1982)
 HILTNER, W.A., Ap. J., **120**, 454, (1954)
 HSU, J., BREGER, M., Ap. J., **262**, 732, (1982)
 HUBERT-DEPLAPLACE, A.-M., HUBERT, H., "An Atlas of Be Stars",
 PARIS-MEUDON AND HAUTE PROVENCE OBS., FRANCE, (1979)
 HUTCHINGS, J.B., M.N.R.A.S., **181**, 619, (1977)
 HUTCHINGS, J.B., CRAMPTON, A.P., REDMAN, R.O., M.N.R.A.S., **170**, 313,
 (1975)
 HUTCHINGS, J.B., COWLEY, A.P., CRAMPTON, D., REDMAN, R.O., Ap. J.,
191, L101, (1974)
- JONES, T.A., J. Sedimentary Petrology, **39**, 1622, (1969)
- KEMP, J.C., HERMAN, L.C., Ap. J., **218**, 770, (1977)
 KEMP, J.C., BARBOUR, M.S., HERMAN, L.C., RUDY, R.J., Ap. J., **220**,
 L123, (1978)
 KEMP, J.C., SOUTHWICK, R.G., RUDY, R.J., Ap. J., **210**, 239, (1976)
 KEMP, J.C., BARBOUR, M.S., PARKER, T.E., HERMAN, L.C., Ap. J., **228**,
 L23, (1979)
 KEMP, J.C., WOLSTENCROFT, R.D., Ap. J., **182**, L43, (1973)
 KEMP, J.C., BARBOUR, M.S., Ap. J., **264**, 237, (1983)
 KLARE, G., NECKEL, Th., A. & A. Supp. Ser., **27**, 215, (1980)
 KOPAL, Z., "Close Binary Systems", CHAPMAN AND HALL LTD., (1959)
 KRAUTTER, J., A. & A. Supp. Ser., **39**, 167, (1980)
- LANDSTREET, J.D., BORRA, E.F., Ap. J., **224**, L5, (1978)
 LANDSTREET, J.D., Ap. J., **258**, 639, (1982)
 LESH, J.R., AIZENMAN, M.L., A. & A., **34**, 203, (1974)
 LILLER, W., IAU Circular No. 2888, (1975)
 LUPIE, O.L., Ph. D. Thesis, University of Wisconsin, MADISON, (1983)
 LYND, C.R., Ap. J., **130**, 577, (1959a)
 LYND, C.R., Ap. J., **130**, 603, (1959b)
- MARGON, B., BOWYER, S., PENEGOR, G., M.N.R.A.S., **176**, 217, (1976)
 MATHEWSON, D.S., FORD, V.L., Mem. R.A.S., **74**, 139, (1970)
 MAZEH, T., TREFFERS, R.R., VOGT, S.S., Ap. J., **256**, L13, (1982)
 MCLEAN, I.S., CLARKE, D., IAU SYMP. 70, "Be and Shell Stars" ed. A.
 Slettebak, Riedel, Dordrecht, (1976)
 MCLEAN, I.S., CLARKE, D., M. N. R. A. S., **186**, 245, (1979)
 MERRILL, P.W., Ap. J., **72**, 109, (1930)
 MOFFAT, A.F.J., HAUPT, W., SCHMIDT-KALER, T., A. & A., **23**, 433, (1973)
- NOLT, I.G., KEMP, J.C., RUDY, R.J., SOUTHWICK, R.G., RADOSTITZ, J.V.,
 CAROFF, L.J., Ap. J., **199**, L27, (1975)

- PAVLOVSKI, K., Hvar Obs. Bull. 7(1), 133, (1983)
 PENROD, G.D., VOGT, S.S., Ap. J., 299, 653, (1985)
 PERCY, J.R., Bull. AAS, 14, 879, (1982)
 PETERS, G.J., IAU SYMP. 70, "Be and Shell Stars" p.69, Ed. SLETTEBAK, REIDEL, DORDRECHT, (1976)
 PICKERING, E.C., Proc. Amer. Acad. Arts. Sci., 16, 257, (1880)
 PIIROLA, V., A. ' A. Suppl. Ser., 38, 193, (1979)
 POECKERT, R., MARLBOROUGH, J.M., Ap. J. 218, 220, (1977)
 POECKERT, R., MARLBOROUGH, J.M., Ap. J. Suppl., 38, 229, (1978b)
 POECKERT, R., MARLBOROUGH, J.M., Ap. J., 220, 940, (1978a)
 POLIDAN, R.S., IAU SYMP. 70, p401, (1976)
- RACHKOVSKAYA, T.M., Thesis, Inst. Astrophys. & Physics of the Atmosphere TARTU, ESTONIAN, SSR, USSR, (1980)
 RACHKOVSKAYA, T.M., Izv. Krym. Astrophys. Obs., 53, 168, (1975)
 RACHKOVSKAYA, T.M., Izv. Krym. Astrophys. Obs., 55, 100, (1976)
 RUDY, R.J., KEMP, J.C., Ap. J., 221, 200, (1978)
 RUDY, R.J., KEMP, J.C., Ap. J., 207, L125, (1976)
- SCHMIDT-KALER, T., P. A. S. P., 79, 181, (1967)
 SERKOWSKI, K., MATHEWSON, D.S., FORD, V.L., Ap. J., 196, 261, (1975)
 SERKOWSKI, K., "PLANETS, STARS and NEBULAE studied with photopolarimetry." pp135-174, ed. GEHELRS, UAP, (1974)
 SHAKHOVSKOI, N.M., Soviet Astron. 8, 83, (1964)
 SHAKHOVSKOI, N.M., Soviet Astron. 8, 833, (1965)
 SIMMONS, J.F.L., ASPIN, C., BROWN, J.C., M.N.R.A.S., 198, 45, (1982)
 SIMMONS, J.F.L., ASPIN, C., BROWN, J.C., A. & A., 91, 97, (1980)
 SNEDECOR, G.W., COCHRAN, W.G., "Statistical Methods" 7ed., IOWA STATE UNIV. PRESS, (1980)
 STEWART, B.G., Ph. D. Thesis, University of Glasgow, (1984)
 STIBBS, D.W.N., M.N.R.A.S., 110, 395, (1950)
 SWINGS, P., STRUVE, O., Ap. J., 91, 590, (1940)
- TORRES, C.A.O., FERRAZ MELLO, S., A. & A., 27, 231, (1973)
- UNDERHILL, A.B., DOAZAN, V. "B STARS with and without Emission Lines" p404, NASA DOC. SP-456, (1983)
 UNDERHILL, A.B., Hvar Obs. Bull., 7(1), 345, (1983)
- WALKER, M.F., Ap. J., 118, 481, (1953)
 WEBSTER, B.L., MURDIN, P., Nature, 235, 37, (1972)
 WEISSKOPF, M.C., ELSNER, R.F., DARBO, W., NARANAN, S., WEISSKOPF, V.J., WILLIAMS, A., WHITE, N.E., GRINDLEY, J.E., SUTHERLAND, P.G., Ap. J., 278, 711, (1984)
 WHITE, N.E., SANDFORD, P.W., M.N.R.A.S., 176, 201, (1976)
 WOLF, G.W., Astron. J., 77, 576, (1972)

